A molecular genetic investigation of pivotal ABC-transporters involved in mycobacterial cell envelope biosynthesis

By

Stephen A. Bethell

A thesis submitted to the University of Birmingham for the degree of Doctor of Philosophy

Institute of Microbiology and Infection

School of Biosciences

Life and Environmental Sciences

University of Birmingham

September 2019

Abstract:

Mycobacterium tuberculosis (*Mtb*), the causative agent of tuberculosis (TB), is responsible for approximately 1.6 million deaths per annum. *Mtb* has a complex cell envelope that contains unique polysaccharide structures that include arabinogalactan, phosphatidyl-myo-inositol mannosides (PIMs), lipomannan and lipoarabinomannan. These glycoconjugates appear throughout Corynebacteria mycobacteria nocardia (CMN) group of bacterial organisms. However, the mechanism by which these key cell envelope components are translocated across the cytoplasmic membrane, remain to be elucidated. The ABC transporter superfamily of proteins are responsible for the movement of a wide variety of molecular species across membranes and require hydrolysis of ATP to provide energy to facilitate movement. Here I investigated two ABC transporter systems involved in galactan and PIM translocation in *Corynebacteriaceae*. Using phenotypic analysis of deletion mutants in *C. glutamicum,* I provide evidence to support that Rv1272c/Rv1273c are directly involved in PIM translocation as the deletion of the *C. glutamicum* orthologs results in a depletion of PIM species on the cell surface. Through characterising protein-ligand interactions between the M. smegmatis Rv3781 ortholog and immature galactan analogues, I present evidence to support the prediction that Rv3781/Rv3783 may be involved in galactan translocation

. Finally, this study explores the effect of point mutations linked to Ethambutol (EMB) resistance in the key arabinosyltransferase (Emb) on the *C. glutamicum* cell envelope, through phenotypic characterisation of the effect on component cell envelope compounds.

This thesis is dedicated to Claire.

Acknowledgements:

I would like to thank my supervisors, Luke Alderwick and Del Besra, for their guidance and support throughout this project. I would not have been able to reach this point without their experience, patience and wisdom. I would also like to thank everyone in E106 who made this experience an enjoyable one, even in the difficult times.

The work presented would not have been possible without the assistance of our collaborators. I would like to thank Tom Bernhardt, and Jan Marienhagen's groups for the provision of *C. glutamicum* strains. I would also like to thank Helen Cooper's group, in particular Todd Mize, for the training on and use of the Mass Spec facilities, and Todd Lowry's group for the synthesis of ligands. I would also like to thank Sam Benedict for his assistance conducting experiments in Chapter 3.

While many people helped me during my time in the lab, and during the process of writing my thesis I would like to give special thanks to: Alice Darbyshire, Kat Abrahams, Patrick Moynihan, Natacha Veerapen, Chris Burke, Anja Dokic, Alice Lanne, Alice Moorey, Helen Clayton.

I could never have done this without the love and support of my partner Claire, who always believed in me even when I did not. Since we met time with you has been the best part of my day. Another constant source of support has been my parents, whose love and advice is always appreciated. Your understanding and experience helped me so much and knowing that you had the same fears as me throughout your own studies was immensely reassuring.

Perhaps most importantly I would like to thank Pebbles. I would also like to thank the cast of Critical Role for inspiring me throughout my work, giving me space from my project when I needed it most, and always cheering me up.

Finally, I would like to thank my funding body, the BBSRC through the MIBTP program, for funding this project.

Table of contents:

List of Figures:

List of Tables:

List of abbreviations:

ABC-transporter: ATP binding cassette transporter

ADP: Adenosine di-phosphate

AG: Arabinogalactan

Ag85: Antigen 85

Amp: Ampicillin

ANOVA: Analysis of variance

AOT: Sodium docusate

Ara: Arabinose

Ara*f*: Arabinofuranose

AraT: Arabinosyl tranferase

ATP: Adenosine tri-phosphate

BCIP: 5-Bromo-4-chloro-3-indolyl-phosphate

BHI: Brain heart infusion

BLAST: Basic local alignment search tool

BSA: Bovine serum albumin

C_{50}-P: Decaprenylphosphate

CDP: Cytosine di-phosphate

CFU: Colony forming unit

Cg: *Corynebacterium glutamicum*

CH_3OH: Methanol

$CHCl_3$: Chloroform

CL: Cardiolipin

cMAME: Corynemycolic acid methyl ester

CMN group: Corynebacteria mycobacteria nocardia

D-Ala: D-Alanine

D-isoGlu: D-isoglutamate

DAG: Diacyl glycerol

DMSO: Dimethyl sulfoxide

DNA: Deoxyribonucleic acid

DOTS course: Directly observed treatment short course

DPA: Decaprenyl arabinose

DPH: 1,6-diphenyl-1,3,5-hexatriene

DPM: Decaprenyl mannose

DPR: Decaprenyl ribose

EDTA: Ethylene diamine tetraacetic acid

EMB: Ethambutol

FAME: Fatty acid methyl ester

FAS-I: Fatty acid synthase I

FAS-II: Fatty acid synthase II

FFA: Free fatty acid

FMA: Free mycolic acid

FMM: Functional membrane microdomain

G: Gravity

Gal*f*: Galactofuranose

Galf_n: Polygalactofuranose chain containing n residues

GC: Gas Chromatography

GDP: Guanosine di-phosphate

GDP-Man: Guanosine di-phospho mannose

Gl-A: Glucuronic acid (1→3) glycerol

GlcNAc: N-acetyl glucosamine

HIV: Human immunodeficiency virus

Hyg: Hygromycin B

IL-12: Interleukin 12

INH: Isoniazid

Ino: Inositol

IPTG: Isopropyl-beta-D-thiogalactoside

ITF: Intrinsic tryptophan fluoresence

Kan: Kanamycin

K_d: Dissociation constant

kDa: KiloDaltons

L: Litre

LAM: Lipoarabinomannan

LB: Lysogeny broth

LM: Lipomannan

M: Molar

m: Meter

m-DAP: Meso-diaminopimelate

mAGP complex: Mycolyl arabinogalactan peptidoglycan complex

mAmp: Milliamps

Man: Mannose

ManLAM: Mannosylated lipoarabinomannan

Man*p*: Mannopyranose

MAPK: Mitogen activated protein kinase

MBP: Maltose binding protein

MDR-TB: Multi-drug resistant tuberculosis

mg/ml: Milligrams per millilitre

MIC_{99}: Minimum inhibitory concentration 99%

min: Minute

ml: Millilitre

mM: Millimolar

mm: Millimeter

MPA: Phosphomolybdic acid

MSD: Membrane spanning domain

Mtb: Mycobacterium tuberculosis

MTX: 5-deoxy-5-methyl-thio-xylofuranose

MurNAc: N-acetyl muramic acid

MurNGlyc: N-glycolyl muramic acid

NAD^+: Nicotinamide adenine dinucleotide, oxidized

NADH: Nicotinamide adenine dinucleotide, reduced

NADPH: Nicotinamide adenine dinucleotide phosphate, reduced

NBD: Nucleotide binding domain

nm: Nanometer

OD: Optical density

PBS: phosphate buffered saline

PCR: Polymerase chain reaction

PE: Phosphatidyl ethanolamine

PE60: Petroleum Ether 60-80

PG: Peptidoglycan

PI: Phosphatidyl inositol

PI_3P: Phosphatidyl inositol-3-phosphate

PIM: Phosphatidyl-*myo*-insitol mannoside

PPM: Polyprenyl mannose

pRpp: Phospho-α-D-ribosyl-1-pyrophosphate

PYR: Pyrazinamide

Rf: Retention factor

Rha: Rhamnose

RIF: Rifampicin

RNA: Ribonucleic acid

rpm: Revolutions per minute

RR-TB: Rifamicin resistant tuberculosis

RT: Room temperature

SBP: Substrate binding protein

SDS: Sodium dodecyl sulphate

SDS-PAGE: Sodium dodecyl sulphate polyacrylamide gel electrophoresis

TB: Tuberculosis

TDM: Trehalose dimycolate

TDP-Rha: Thymidine di-phospho rhamnose

TLC: Thin layer chromatography

TMcM: Trehalose mono-corynemycolate

TMHMM: Transmembrane hidden markov model

TMM: Trahalose monomycolate

UDP: Uracil di-phosphate

UDP-MurNAc: urasil diphospho N-acetyl muramic acid

UDP-MurNGlyc: urasil diphospho N-glycolyl muramic acid

μg: Micrograms

μl: Microliters

μM: Micromolar

μV: Microvolts

V: Volts

v/v: Volume by volume

w/v: Weight by volume

WHO: World Health Organisation

WT: Wild Type

XDR-TB: Extensively drug resistant tuberculosis

Chapter 1:

General introduction

1.1.1: *Mycobacterium tuberculosis* and related species:

Mycobacterium tuberculosis (*Mtb*), is an aerobic, rod shaped bacillus belonging to the order *Actinomycetales* (Guglielmetti et al., 2015). *Mtb* was first identified as the agent responsible for TB by Robert Koch in 1882 (Murray et al., 2015). *Mtb,* is responsible for an estimated 10 million infections, and 1.6 million deaths globally in 2017 (World Health Organization, 2018).

The primary site of infection for TB are the lungs (referred to as pulmonary TB), with transmission being largely airborne (Escombe et al., 2008). However, the infection can also affect other organs, then it is referred to as extrapulmonary TB (Singer-Leshinsky, 2016). Pulmonary TB is characterised by a chronic cough, fever, fatigue, and weight loss (Singer-Leshinsky, 2016).

In addition to causing active infections, TB is also known for its ability to infect a host and remain in a non-proliferative, non-symptomatic state within host macrophages (known as latent infection). *Mtb* can remain in this state until the host immune system is unable to defend itself before causing an active infection (Haley, 2019; Piccazzo et al., 2014; Tang and Johnston, 2017). As individuals who are infected with latent TB do not show symptoms the estimated prevalence of latent TB, is a cause for some debate. Studies of the global prevalence of infection using different methods for the determining the incidence give a range from 25- 33 % of the global population currently being infected (Houben and Dodd, 2016; Matteelli et al., 2017).

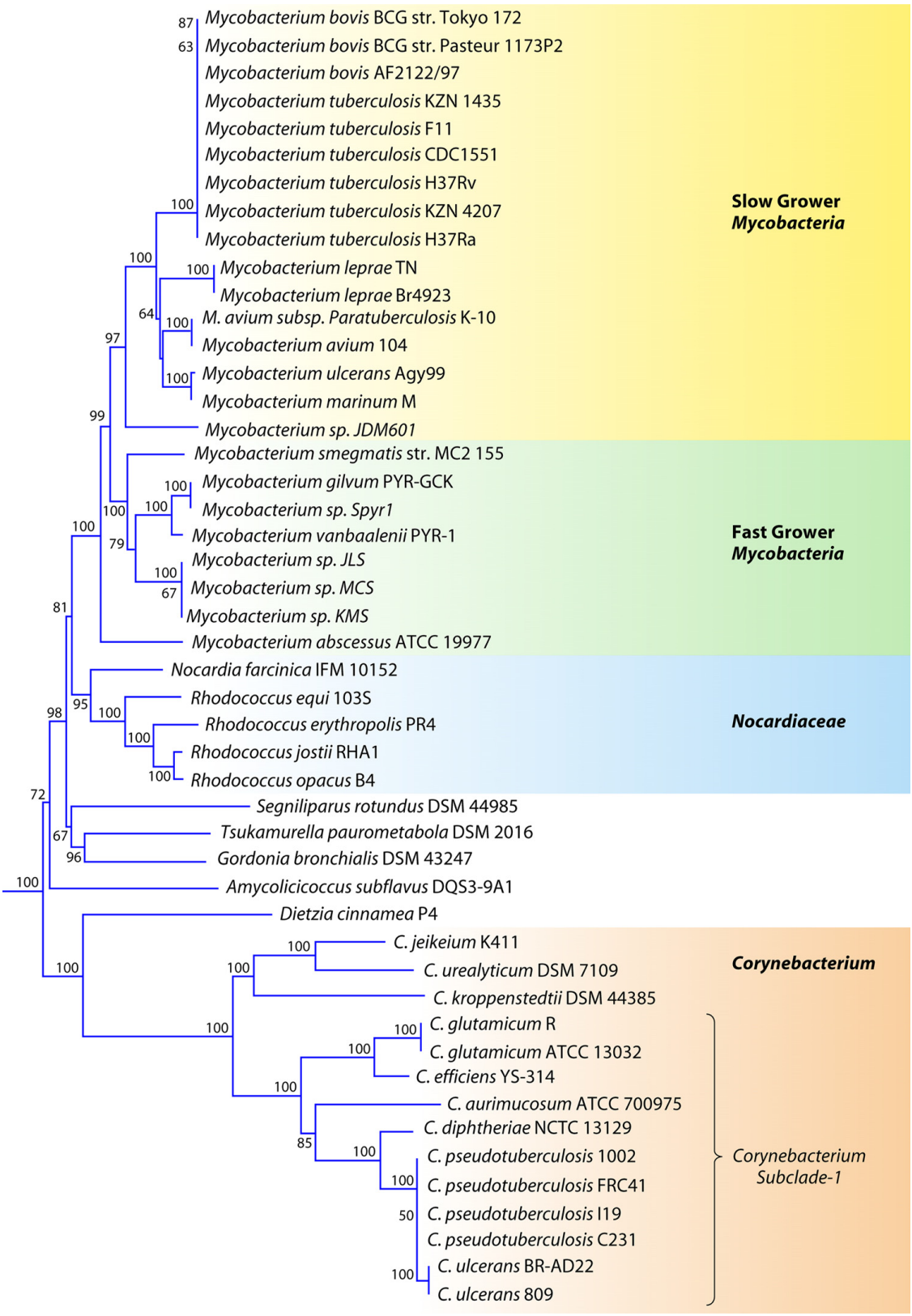

Figure 1.1: Phylogenetic tree of species from the suborder corynebacteriales. Showing the various pathogenic and non-pathogenic species within the suborder, and their relative divergence. Figure reproduced with permission from Gao and Gupta, 2012.

1.1.2: Clinical manifestations of the *Corynebacterineae*:

The suborder *Corynebacterineae* contains many pathogenic agents, not limited to *Mycobacteria*, such as *Corynebacterium pseudotuberculosis*, and *Corynebacterium diphtheriae* (Figure 1.1) (Gao and Gupta, 2012). However, the most prevalent diseases such as TB and leprosy, are caused by mycobacterial species.

Pathogenic mycobacteria are classified into: tuberculous, nontuberculous, or leprotic mycobacteria. Tuberculous mycobacteria include: *Mtb*, *Mycobacterium bovis*, and *Mycobacterium africanum* (Addo et al., 2010). While nontuberculous mycobacteria include *Mycobacterium absessus*, *Mycobacterium ulcerans*, *Mycobacterium gordonae*, and *Mycobacterium marinum* (Porvaznik et al., 2016). The major causative agent of mycobacterial leprosy are *Mycobacterium leprae* and *Mycobacterium lepromatosis* (Franco-Paredes et al., 2018).

Mycobacteria are unusual in that they do not stain as either Gram positive or negative but instead as between the two, leading to them being classified as Gram indeterminate. This has led to alternate staining methods to better visualize the bacteria, resulting in further classification as acid-fast bacteria, a status shared only with some *Nocardia* species (Brennan and Nikaido, 1995). The cause of this unique staining phenotype is the unusual structure of the cell wall they produce, which results in a thick, waxy outer pseudo-membrane referred to as the myco-membrane. While there are differences in the cell wall and lipid composition between species within the corynebacteria mycobacteria nocardia (CMN) group, much of the structure of the cell wall and the biosynthetic pathways are very similar (Besra et al., 1995).

1.1.3: Mechanism of infection by *Mycobacterium tuberculosis*:

Mtb is recognised by the macrophages of the host immune system, by a variety of receptors. Upon recognition it is engulfed and contained within the macrophage in a phagosome. The receptor that recognises the bacillum is important for the outcome of the phagocytosis process, as there have been different responses shown when particles are captured through different receptors (Pieters, 2008). With some receptors (such as CR3 mediated uptake), being beneficial to the bacteria. Uptake mediated by CR3 (which is involved in uptake of cholesterol), leads to improved prevention of phagosome fusion with the lysosome, allowing for increased bacterial survival within the macrophage (Gatfield and Pieters, 2000).

Phagosome-lysosome fusion is inhibited by the degradation of the phosphatidylinositol-3-phosphate (PI3P) that is produced to phosphatidyl inositol and inorganic phosphate, as *Mtb* secretes SapM, a phosphatase which hydrolyses PI3P. The inhibition of hVP34 results in insufficient PI3P for phagolysosome formation, increasing bacterial survival within the macrophage (Saleh and Belisle, 2000; Vergne et al., 2005, 2003). *Mtb* also prevents phagolysosome formation by secretion of PknG, a membrane embedded protein kinase released by mycobacteria upon entry to the phagosome, whereby it gains access to the cytosol of the macrophage, and inhibits the activity of protein kinase C-α (Chaurasiya and Srivastava, 2009; Walburger, 2004).

Additional to survival within the macrophage, *Mtb* triggers formation of granuloma, structures of infected macrophages, surrounded by un-infected immune cells. The interactions between the infected and un-infected cells maintains an immune presence at the site of infection, allowing for the bacteria to determine if the host immune system is functional. While in the

granuloma, there has been no conclusive evidence on whether the bacteria are dividing or in a non-replicative state, however during this stage of infection, the host shows no symptoms of active TB, and is defined as having latent TB (Karakousis et al., 2004; Pieters, 2008).

1.1.4 Global prevalence of TB:

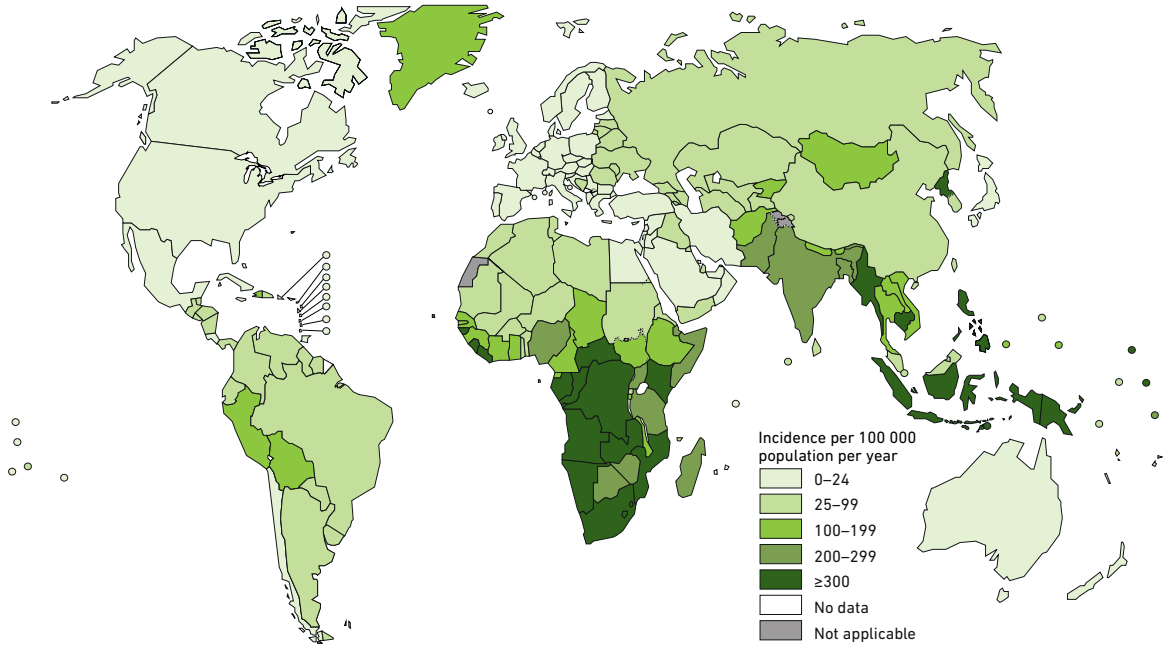

Figure 1.2: Reported incidence of TB globally per 100,000 population. Showing the major burden of TB is in sub-saharan Africa. Figure reproduced from World Health Organization, 2018.

TB is the leading cause of death by a single infectious agent, with 1.6 million deaths attributed to *Mtb* in 2017 (World Health Organization, 2018). While cases of *Mtb* are found worldwide, 66 % of confirmed cases are found within eight high burden countries, the most affected of which is India, accounting for 27 % of global cases (World Health Organization, 2018). *Mtb* infections affect all ages groups, though 90 % of reported cases are seen in adults over the age of 15.

Globally the incidence of TB is falling by 2 % per year, and mortality is falling at a rate of 4 % per year, with a decrease of 42 % between 2000 and 2017, although the rate of new and relapse cases of *Mtb* (Figure 1.3) (World Health Organization, 2018).

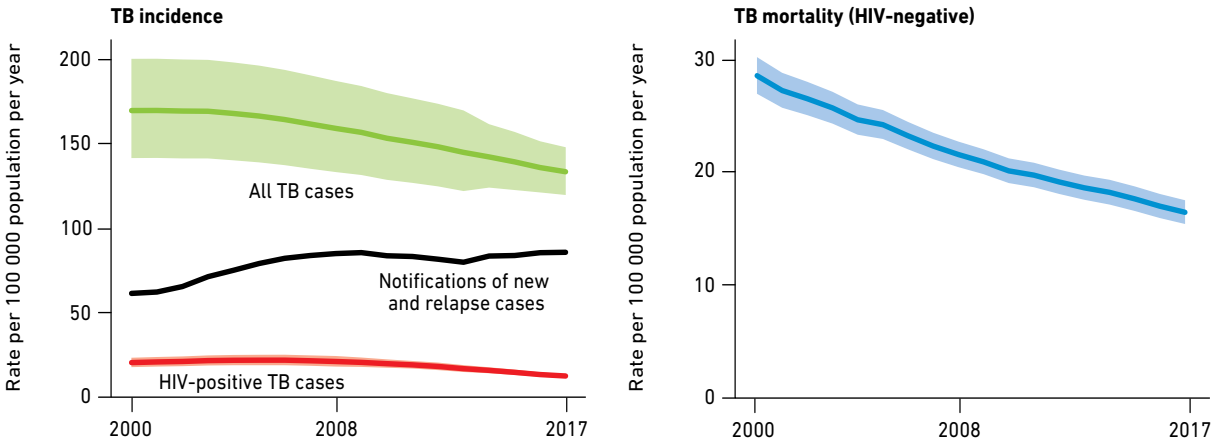

Figure 1.3: Global incidence of TB. Global incidence of TB showing 95 % confidence interval from 2000-2017, including incidence of HIV-positive patients and mortality rate of TB from HIV-negative patients. Figure reproduced from World Health Organization, 2018.

1.2.1: Treatment of TB:

Mtb has been the subject of intense research for decades, due to the high burden of infection and the difficulty in treating the disease. This research has led to the development of effective antimycobacterial molecules which have been instrumental in the improvements in the outcome of infection (Zumla et al., 2013). The World Health Organisation (WHO) credits the implementation of the Directly Observed Treatment Short (DOTS) course, where patients are treated with Rifampicin, Isoniazid, Pyranzinamide, and Ethambutol for two months, with continued treatment with Rifampicin and Isoniazid for a further four months. The DOTS course treatment regimens require dosage either daily or three times a week for the duration,

depending on a variety of factors, including: HIV status, kidney disease, and if the infection is disseminated (Thwaites, 2014; World Health Organization, 2018).

Due to the severity of the TB epidemic, the World Health Organisation, has made it a priority to reduce both the incidence and mortality associated with TB by 95 % by 2035 (Figure 1.4). This would require significant technological advancement in preventing the development of active TB from the reservoir of latent TB in the global population, as well as an improvement in the availability of high quality treatment, especially to those in the developing world (World Health Organization, 2018).

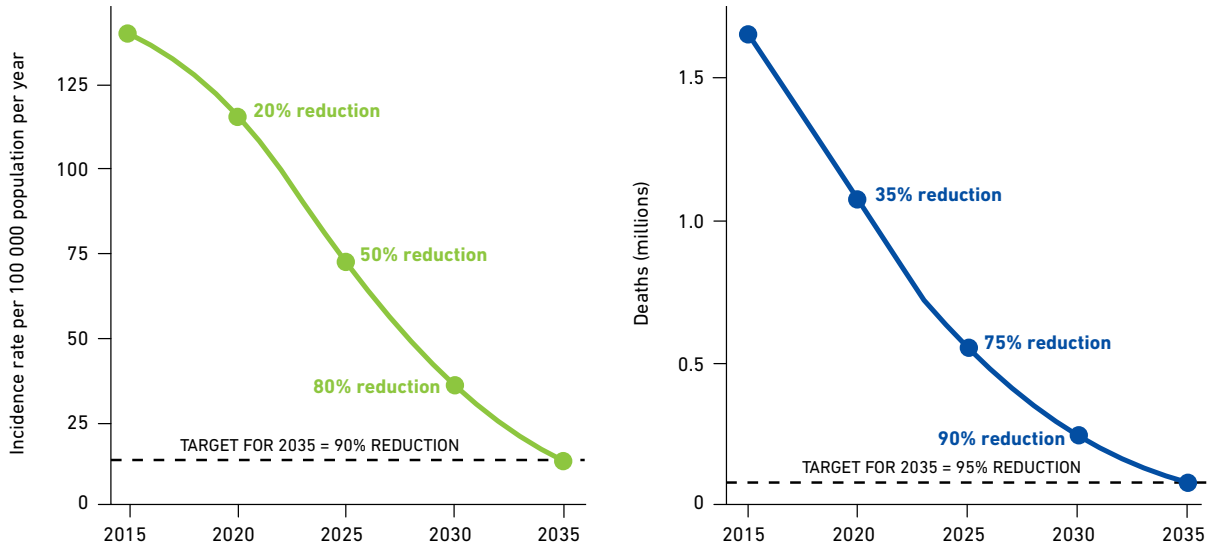

Figure 1.4: World Health Organisation targets for global TB incidence and death rates. Showing the target global incidence and mortality rates along with projected milestones. Figure reproduced from World Health Organization, 2018.

The cell wall of bacteria is an attractive target for antimicrobial compounds, with perhaps the most well-known antibiotic, Penicillin, which inhibits cell wall synthesis. While Penicillin is widely used to treat many bacterial infections, the expression an extended spectrum beta-lactamase renders Penicillin ineffective against *Mtb* (Abrahams and Besra, 2016; Tassoni et

al., 2019). Due to the essentiality of the cell wall, and the lack of an orthologous structure in mammalian cells, disruption of many of the processes in the synthesis and maintenance of the bacterial cell wall is an inviting target for the development of novel antibacterial agents. As such the processes involved in the biosynthesis, and maintenance of the cell wall have been a topic of study for decades, with many anti-tubercular drugs, such as Ethambutol, Isoniazid, and Ethionamide inhibiting cell wall processes (Table 1.1) (Takeya K. and Hisatsune K., 1963).

Table 1.1: Antimycobacterial drugs. Detailing the year of discovery, and mechanism of action of first and second line antimycobacterial drugs. Table reproduced from Zumla et. al., 2013

Drug (year of discovery)	Target	Effect
First-line drugs		
Isoniazid (1952)	Enoyl-[acyl-carrier-protein] reductase	Inhibits mycolic acid synthesis
Rifampicin (1963)	RNA polymerase, beta subunit	Inhibits transcription
Pyrazinamide (1954)	S1 component of 30S ribosomal subunit	Inhibits translation and *trans*-translation, acidifies cytoplasm
Ethambutol (1961)	Arabinosyl transferases	Inhibits arabinogalactan biosynthesis
Second-line drugs		
Para-amino salicylic acid (1948)	Dihydropteroate synthase	Inhibits folate biosynthesis
Streptomycin (1944)	S12 and 16S rRNA components of 30S ribosomal subunit	Inhibits protein synthesis
Ethionamide (1961)	Enoyl-[acyl-carrier-protein] reductase	Inhibits mycolic acid biosynthesis
Ofloxacin (1980)	DNA gyrase and DNA topoisomerase	Inhibits DNA supercoiling
Capreomycin (1963)	Interbridge B2a between 30S and 50S ribosomal subunits	Inhibits protein synthesis
Kanamycin (1957)	30S ribosomal subunit	Inhibits protein synthesis
Amikacin (1972)	30S ribosomal subunit	Inhibits protein synthesis
Cycloserine (1955)	D-alanine racemase and ligase	Inhibits peptidoglycan synthesis

1.2.2: Rifampicin:

Rifampicin (RIF, Table 1.1, Figure 1.5), is a semisynthetic rifamycin belonging to the antibiotic family ansamycins. RIF is used to treat a variety of bacterial infections, but most notably TB. The first rifamycin was discovered after the bacterium responsible for producing it, *Amycolatopsis mediterranei*, was isolated from a soil sample in southern France. This molecule was then modified to improve the antibiotic potency and bioavailability to produce RIF (Alifano et al., 2015).

RIF functions by inhibiting RNA polymerase, preventing the elongation of the transcript after the initiation by blocking the path of the 5' transcript (Campbell et al., 2001). Mutations have been found increasingly frequently where an amino acid change in the fork domain by the catalytic site, or in domains 1 and 2 of the β-subunit result in an change in the binding pocket and therefore a reduced affinity for rifampicin resulting in resistance (Alifano et al., 2015).

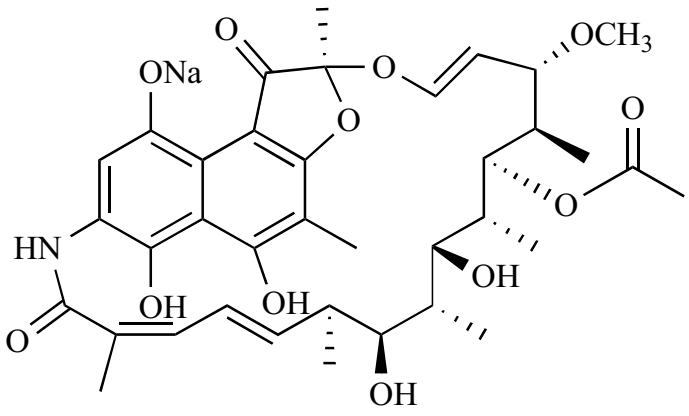

Figure 1.5: Chemical structure of Rifampicin.

1.2.3: Ethambutol:

Ethambutol (EMB, Table 1.1, Figure 1.6) is a small molecular inhibitor of arabinosyltransferases, it has been shown to cause an accumulation of the arabinofuranose donor, β-D-arabinofuranosyl-1-monophophodecaprenol (DPA) (Takayama and Kilburn, 1989). This finding suggests that the primary target of EMB is the incorporation of arabinose into the cell wall, either as part of the arabinogalactan, or as part of the lipoarabinomannan.

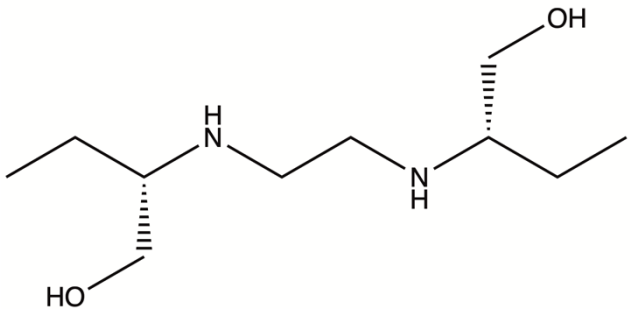

Figure 1.6: Chemical structure of Ethambutol.

Resistant mutants generated to EMB have been shown to possess point mutations in the *embCAB* genes, associated with the synthesis of the arabinan domain in arabinogalactan (AG) and LAM. However, many of the most common mutations in resistant *Mtb* strains have also been seen in sensitive strains, and the overexpression of EmbC does result in mild resistance to EMB suggesting that the target of EMB is EmbA and or EmbB (Goude et al., 2009; D. Shi et al., 2011). The most common resistance conferring mutation to EMB is EmbB306, with the wild type methionine being replaced with leucine, isoleucine, or valine (Safi et al., 2008; Shi et al., 201; Srivastava et al., 2009)

1.2.4: Pyrazinamide:

Pyrazinamide (PYR, Table 1.1, Figure 1.7), is a prodrug based on a nicotinamide which requires acidic conditions to function (Chakraborty and Rhee, 2015). PYR is activated by an amidase, encoded by *pncA*, to form pyrazinoic acid. Pyrazinoic acid binds strongly to the RpsA subunit of the 30S ribosome, which rescues stalled ribosomes in a process called trans-translation, the accumulation of pyrazinoic acid also results in disruption of the membrane potential (W. Shi et al., 2011; Zhang, 2003). Resistance to PYR is seen in the mutation of *pncA* to prevent activation of PYR rather than in changes to the target enzyme. This coupled to the fact that the compound requires acidic conditions to function has led to difficulties in the determination of the target for PYR (Chakraborty and Rhee, 2015).

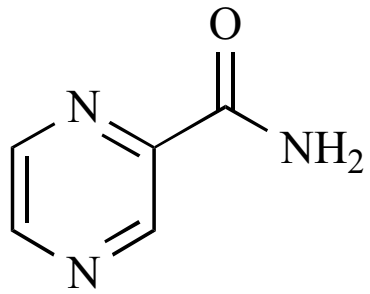

Figure 1.7: Chemical structure of Pyrazinamide

1.2.5: Isoniazid:

Isoniazid (INH, Table 1.1, Figure 1.8), is also a nicotinic acid derivative, was first synthesised in 1912, though the anti-mycobacterial properties were not discovered until 1952 (Chakraborty and Rhee, 2015; Zumla et al., 2013). Isolates that were found to be resistant to INH resulted in inactivation of the catalase, KatG. This resulted in the determination that INH was a prodrug, as sensitivity could restored by the transformation of *katG* into resistant strains (Chakraborty and Rhee, 2015).

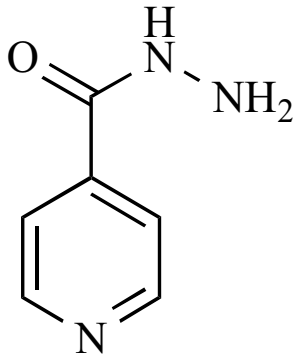

Figure 1.8: Chemical structure of Isoniazid

1.2.6: Antibiotic resistance in *Mtb*:

Resistance to antimycobacterial agents is significantly linked to compliance issues caused in part by the length of the treatment regimen. This led to issues with patient compliance and therefore rising levels of resistance to frontline drugs such as rifampicin, as well a rise in multi-drug resistant TB (MDR-TB) and extensively drug resistant TB (XDR-TB).

MDR-TB is classified as a strain of *Mtb* that is resistant to both Rifampicin and Isoniazid, while XDR-TB is a strain of MDR-TB that has an additional resistance to at least one Fluoroquinolone and one of the second-line injectable antimycobacterial agent such as

Kanamycin. The global estimate for the incidence of MDR-TB, or Rifampicin resistant TB (RR-TB) in new infections is 3.5 %, and 18 % in previously treated cases respectively, with 8.5 % of MDR-TB cases being classified as XDR-TB (World Health Organization, 2018).

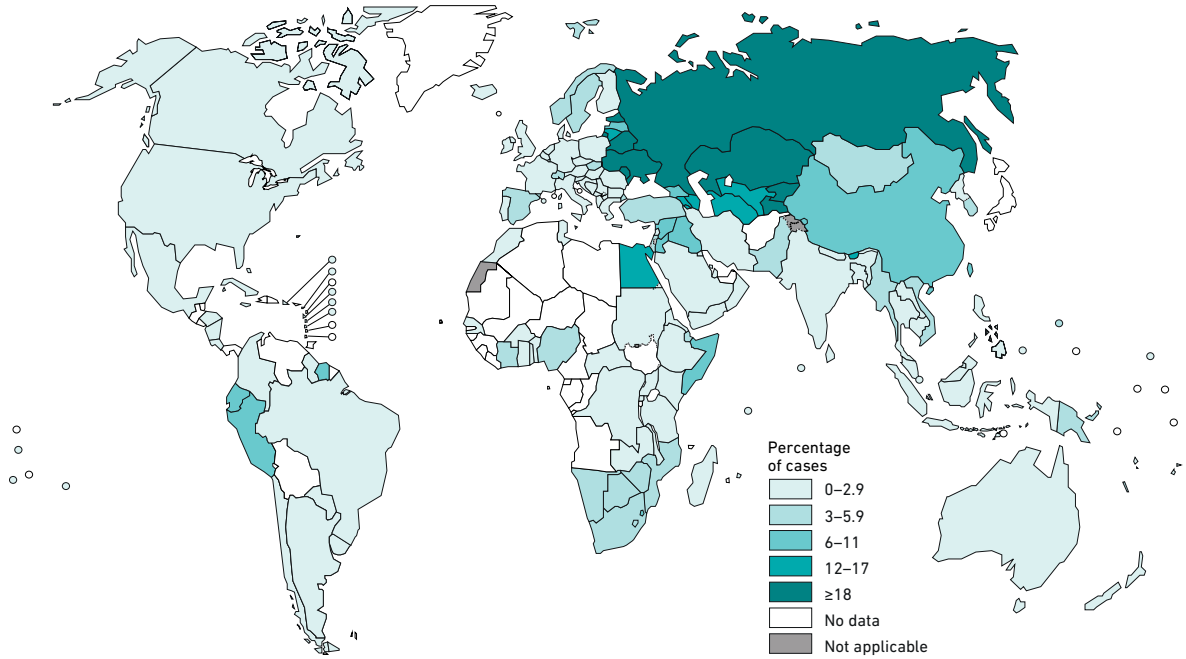

Figure 1.9: Reported rate of MDR-TB in new cases reported to the World Health Organisation. Figure reproduced from World Health Organization, 2018.

1.3.1: Mycobacterial cell envelope:

The mycobacterial cell envelope is a highly specialised, layered, structure (Figure 1.10) (Abrahams and Besra, 2016). The innermost layer is the cytoplasmic membrane, a phospholipid bilayer that surrounds the cell. The second layer is the peptidoglycan (PG), a structural layer formed of glycan chains cross-linked with short peptide chains (Jankute et al., 2015; Moynihan et al., 2019). The PG structure is the base upon which the AG is built, AG is a polysaccharide structure made of a galactofuranose residues, the galactan chain is then decorated with a branching arabinofuranose polysaccharide (Alderwick et al., 2005; Besra et al., 1995; Birch et al., 2008).

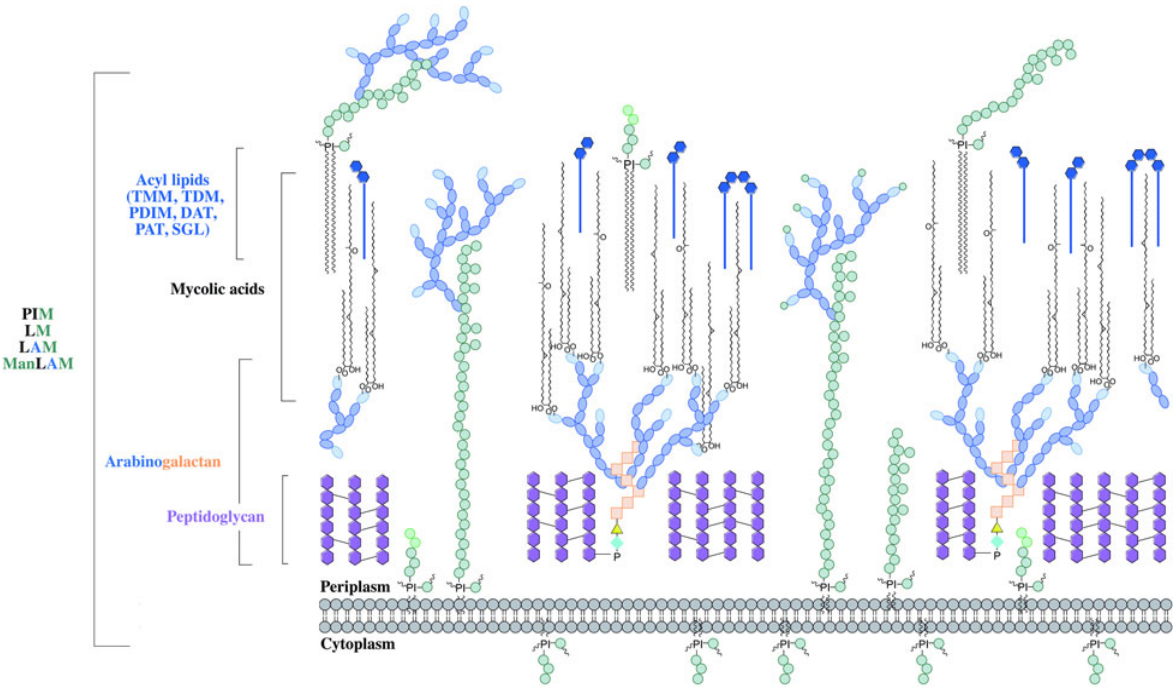

Figure 1.10: Representative model of a cross-section of the mycobacterial cell wall. *Mtb* cell wall model showing; the peptidoglycan, arabinogalactan, mycolic acids, lipomannan, lipoarabinomannan and mannosylated lipoarabinomannan, and surface glycolipids. Figure reproduced, with permission, from Abrahams and Besra, 2016.

The AG layer is decorated with an additional layer of lipids, termed the mycomembrane (Chiaradia et al., 2017). The inner leaflet of this membrane is composed of mycolic acids, and fatty acids covalently bound to the AG. While the outer leaflet is composed of various different species of mycolic acid derivatives (Bansal-Mutalik and Nikaido, 2014, 2011; Touchette and Seeliger, 2017) and the lipoglycans: lipomannan (LM), and lipoarabinomannan (LAM), intercalated with the inner leaflet. LM and LAM are lipid anchored polysaccharides built from a phosphatidylinositol decorated with mannose to form LM, which is further decorated with arabinose to form LAM. Additionally both LM and LAM are found in the inner membrane. Although the presence of LM and LAM may be as an intermediate before transport to the cell surface (Cashmore et al., 2017; Mishra et al., 2007; Pitarque et al., 2005; Touchette and Seeliger, 2017).

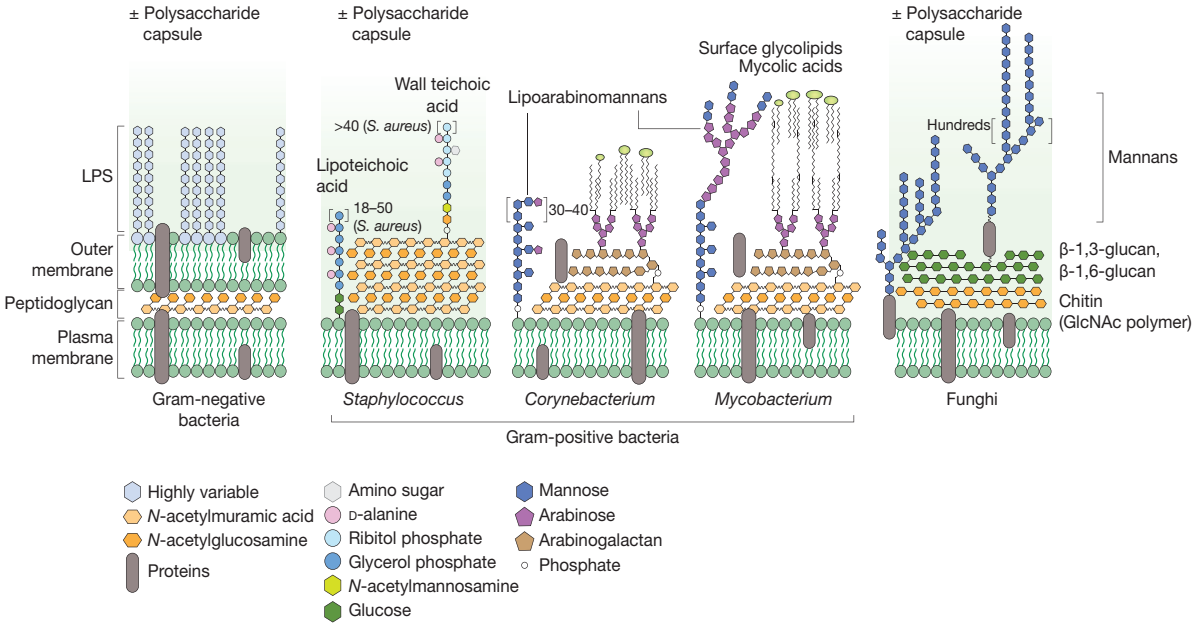

Figure 1.11: Cross sectional models of bacterial and fungal cell surfaces. Cell wall models highlighting the differences between the cell surfaces of the Corynebacteriales and both other Gram-positive as well as Gram-negative bacterial cell surfaces, as well as highlighting the similarities between the Corynebacterial and Mycobacterial cell wall structures. Figure reproduced, with permission from Chen et al. 2018.

The outermost layer of the mycobacterial cell envelope is the capsule, a loosely associated structure primarily comprised of polysaccharides such as alpha-glucan, arabinomannan, and mannan, as well as secreted proteins and lipids (Kalscheuer et al., 2019; Koliwer-Brandl et al., 2016; Ortalo-Magne et al., 1995, 1995).

While the general architecture of the cell wall is conserved between mycobacteria and corynebacteria, there are some differences in the overall structure, as shown in Figure 1.11 (Chen et al., 2018). The most notable differences in the cell wall structure are that the mycolic acids in corynebacterial species are shorter, containing 20- 36 carbon atoms, while mycobacterial mycolic acids contain 60- 90 carbon atoms (Butler and Ahearn, 1986), and changes in the structure of LAM, with the arabinan domains of corynebacterial LAM (Cg-LAM) being less elaborate than mycobacterial LAM (Briken et al., 2004; Chen et al., 2018; Kaur et al., 2008).

1.3.2: The cytoplasmic membrane:

While all bacteria have a cytoplasmic membrane, the component phospholipids, and the ratios of phospholipids, vary from species to species (Bansal-Mutalik and Nikaido, 2014; Kawai et al., 2004; Sathappa and Alder, 2016). These differences in membrane composition lead to differing membrane fluidity. With changes in the phospholipid composition of the membrane, and the acyl chain length both reacting dynamically to changes in the environment (De Siervo, 1969; Russell and Sandercock, 1980).

In mycobacteria, the cytoplasmic membrane is an asymmetric structure, made up of cardiolipin (CL), phosphatidylinositol (PI), phosphotidylethanolamine (PE), and various species of

phosphotidyl-*myo*-inositol mannosides (PIMs) (Figure 1.12) (Bansal-Mutalik and Nikaido, 2014, 2011; Chiaradia et al., 2017).

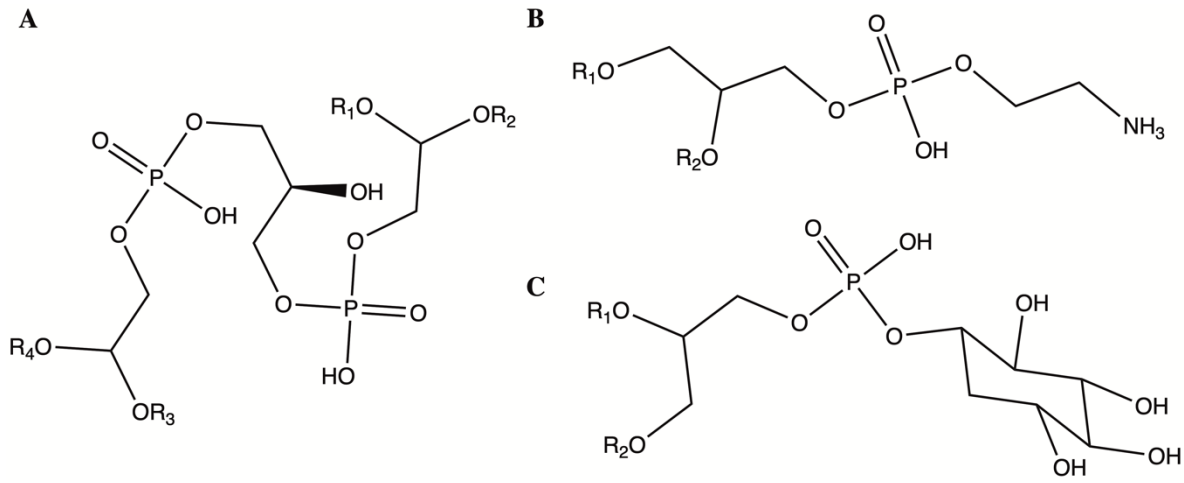

Figure 1.12: Structural representation of mycobacterial phospholipid head groups. A: cardiolipin, B: phosphotidylethanolamine, C: phosphatidylinositol. R denotes the site of fatty acids attachment through esterification.

The most abundant of the PIM species is diacyl-phosphotidyl-*myo*-inositol-dimannoside (Ac_2PIM_2), which along with the other PIM species, can account for up to 42 % of the dry lipid mass in *M. smegmatis* (Bansal-Mutalik and Nikaido, 2014). The outer leaflet of the mycobacterial cytoplasmic membrane is thought to be composed of a majority of PIMs, with the PIMs acting as the anchor for the external glycoconjugates LM, and LAM (Abrahams and Besra, 2016; Bansal-Mutalik and Nikaido, 2014; Mishra et al., 2007, 2008a).

It has been shown that, similar to other bacteria such as *Bacillus subtalis* and *Escherichia coli*, the mycobacterial membrane contains Functional Membrane Microdomains (FMMs) (Hayashi et al., 2016; Kawai et al., 2004; Maloney et al., 2011; Wagner et al., 2017). One such FMM in mycobacteria is CL localization to the poles of the cell, as well as the centre of the cell in actively dividing cells (Maloney et al., 2011). Due to the ability of CL to form non-bilayer

formations this would allow for the formation of the septum in division, while also potentially allowing for the curvature of the membrane at the poles (Maloney et al., 2011; Renner and Weibel, 2011).

Simulations of membranes containing proteins show that the various proteins have a different affinity for CL, this could also aid in the localisation of proteins to correct cellular position (Renner and Weibel, 2011; Wagner et al., 2017). As this has been shown for CL, there is a distinct possibility that a similar phenomenon could occur in other FMMs with different phospholipid composition, resulting in localisation of different proteins into separate microdomains (Heinkel et al., 2019). Protein localisation into FMMs allows for improved signalling, as FMMs tend to cause the accumulation of a group of proteins related to various functions into the same microdomain, which has been seen in various regulated cell functions (Wagner et al., 2017).

Another factor in the variability of the cytoplasmic membrane between bacteria is the number and lengths of the acyl chains within the phospholipid components. Depending on the species of phospholipid the number of acyl chains can vary between 2- 4 acyl chains per molecule (Maloney et al., 2011). It has been shown that certain phospholipids have a tendancy to be synthesised using specific acyl chains. In mycobacterial species the two fatty acid tails of PI tend to be one palmitic acid ($C_{16:0}$) and one tuberculosteric acid (10-methyloctadecanoate, $C_{19:0}$) acyl chains (Morita et al., 2011). However, under some stress conditions PI is converted to PI3P. PI3P has a substantially different acyl profile, with the palmitic acid of PI being replaced with an oleic acid ($C_{18:1}$). PI3P has been suggested to act as a signalling molecule when the cell undergoes high salt stress (Morita et al., 2010).

The various PIM species found in the mycobacterial cytoplasmic membrane have been shown to have differing acyl chain lengths depending on both the mannosylation state as well as the acylation state (Sancho-Vaello et al., 2017). This is in part due to the different numbers of acyl chains attached to the causing the acyl profiles to be different. However, this would not account for all of the differences between the acyl chains found the different mannosylation states. The tri-acylated PIMs, $AcPIM_2$ and $AcPIM_6$, have been shown to have the same acyl chain profile: $C_{16:0}$ and $C_{19:0}$. The tetra-acylated forms of the PIMs, Ac_2PIM_2 and Ac_2PIM_6, are split into 2 populations, either with three $C_{16:0}$ and one $C_{19:0}$, or two $C_{16:0}$ and two $C_{19:0}$ (Gilleron et al., 2003, 2001; Sancho-Vaello et al., 2017).

The acylation positions for Ac_1PIM and Ac_2PIM species have been determined in both the tri-acyl and tetra-acyl forms: two acyl chains are on the glycerol moiety, with the additional acyl chains being on carbon 3 of the inositol ring, and on carbon 6 of the mannose attached to carbon 2 of the inositol ring (Gilleron et al., 2003, 2001; Sancho-Vaello et al., 2017).

PI is found in a variety of living organisms, and is produced from glucose-6-phosphate in *Mtb* by the action of the D-*myo*-inositol 3-phosphate synthase (MIPS) encoded by *Rv0046c*, which catalyses the conversion to inositol-1-phosphate, this is then dephosphorylated to produce inositol (Bachhawat, 1999; Jackson et al., 2000; Morita et al., 2011). *Rv0046c* is essential in mycobacteria, with complementation possible by the addition of inositol into the media (Movahedzadeh et al., 2004). Three genes in the *Mtb* genome have been hypothesised as the phosphatase responsible for the removal of the phosphate from the inositol-1-phosphate, however each one of them is individually non-essential, suggesting that there is some redundancy in the genome. This redundancy reduces the phenotype of the deletion mutants, as such the primary inositol phosphatase remains unknown (Morita et al., 2011). The final step of

PI biosynthesis is catalysed by the action of PgsA1, which catalyses the addition of inositol to CDP-diacyl glycerol to produce PI (Figure 1.13) (Jackson et al., 2000; Salman et al., 1999).

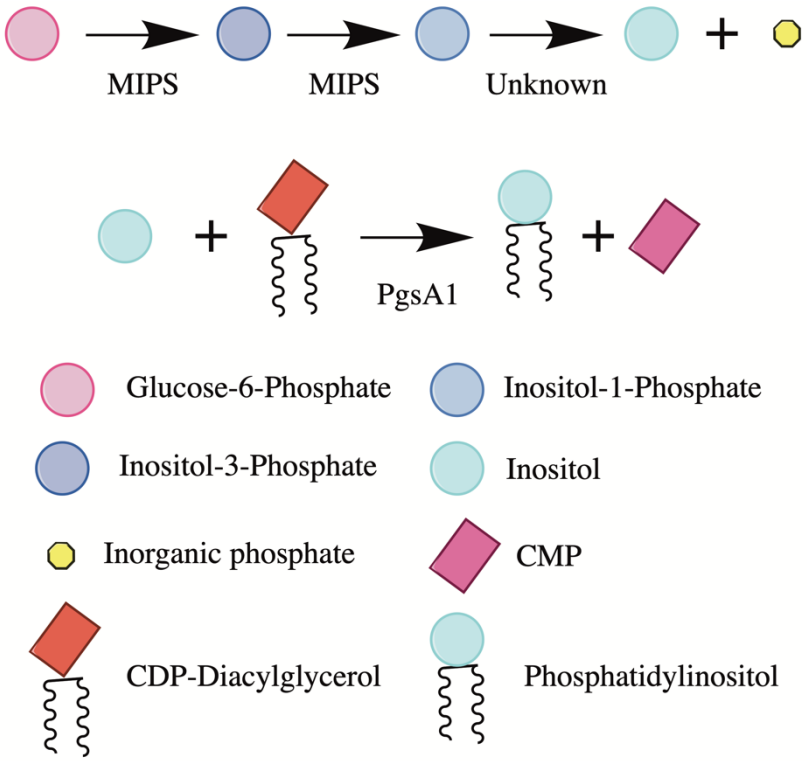

Figure 1.13: Schematic representation of phosphatidylinositol biosynthesis. Showing the conversion of glucose-6-phosphate to inositol-1-phosphate by MIPS, through inositol-3-phosphate, followed by dephosphorylation of inositol. PI synthesis is the completed by PgsA1, converting and CDP-diacylglycerol into PI, and CMP.

Certain lipids are further elaborated upon as well as being present in their 'base' form in the cytoplasmic membrane. PI is found in the membrane both as PI, but more often it has been mannosylated to form the PIMs, the different species of PIM are annotated based on the extent of their mannosylation, and their acylation state. The major PIMs in mycobacteria are $AcPIM_2$, Ac_2PIM_2, $AcPIM_6$, and Ac_2PIM_6 (Figure 1.14) (Brennan and Nikaido, 1995), with other CMN bacteria such as *C. glutamicum* possessing many of the PIM species but not the "higher PIMs" ($AcPIM_6$ and Ac_2PIM_6) (Bansal-Mutalik and Nikaido, 2011).

There are two mannose sources for biosynthetic pathways requiring the mannosylation of substrates: GDP-Mannose (GDP-Man), and polyprenylmannose (PPM) (Kremer et al., 2002; Sancho-Vaello et al., 2017).

GDP-Man acts as the cytoplasmic source for the initial two additions of mannose to the PI, these reactions are catalysed by: PimA and PimB'. PimA catalyses the conversion of PI to PIM_1, where the initial mannose is attached to carbon 2 of the inositol ring (Korduláková et al., 2002). The biosynthetic pathway of PIMs is shown in Figure 1.14. The path branches briefly with PIM_1 either being acylated or mannosylated by AcylT or PimB' respectively. The acylation results in the production of $AcPIM_1$, which can then be converted into $AcPIM_2$ by the action of PimB' (Morita et al., 2011; Schaeffer et al., 1999). If PIM_1 is mannosylated by PimB' the second mannose is attached at the carbon 6 position, to form PIM_2, which can be acylated by AcylT to form $AcPIM_2$, the acyl chain is attached to the mannose on the carbon 2 of the inositol. $AcPIM_2$ can then be further acylated by an unknown acyltransferase, which attaches an additional acyl chain to the carbon 3 of the inositol ring to the form Ac_2PIM_2 (Kremer et al., 2002). The Ac-/Ac_2- PIM_2 can then be further mannosylated by PimC to

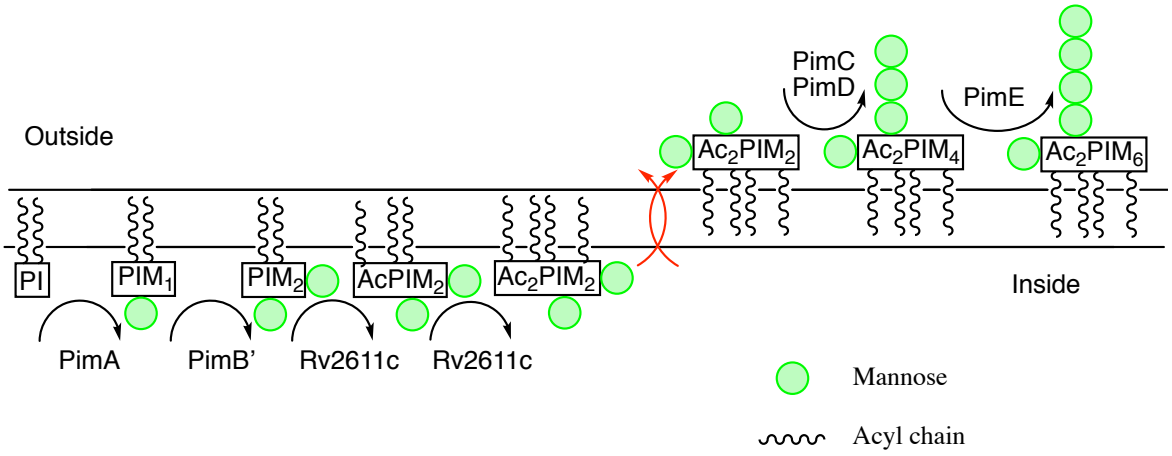

Figure 1.14: Biosynthetic pathway of PIM species in *Mtb*. Biosynthesis of PIMs, showing the enzymes responsible for the biosynthetic step. Unknown processes highlighted in red.

produce Ac/Ac_2-PIM_3 (Kremer et al., 2002; Morita et al., 2011). The enzyme responsible for the additional mannosylation to form Ac-/Ac_2- PIM_4 is as yet unknown (Morita et al., 2011).

During the synthesis of PIMs beyond Ac-/Ac_2- PIM_2, there is a branch point after translocation to the outer leaflet of the plasma membrane, this is proposed to be Ac-/Ac_2- PIM_4. From this point the synthesis can either lead to the production of the higher PIMs (Ac-/Ac_2 -PIM_6), or lead into the production or LM and LAM. (Sancho-Vaello et al., 2017).

1.3.3: Peptidoglycan:

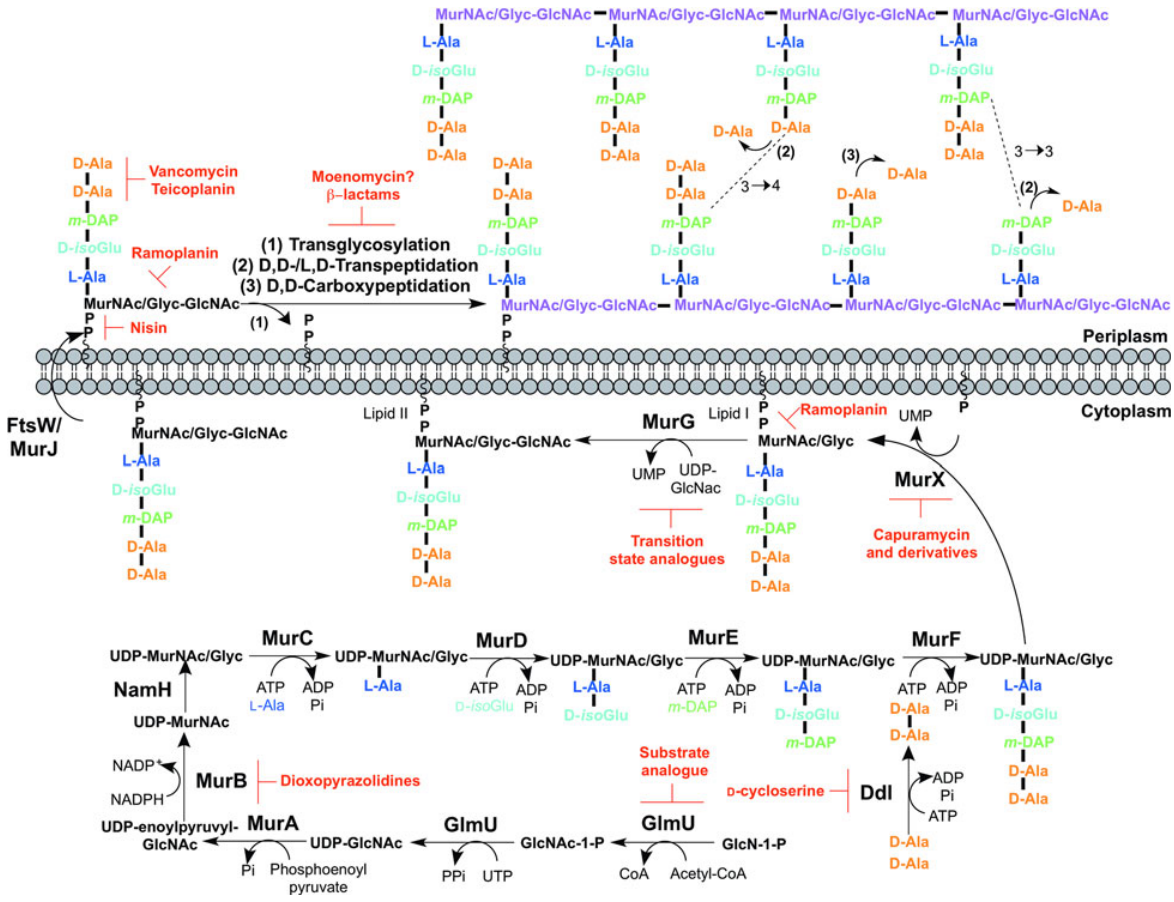

Figure 1.15: Biosynthesis schematic of mycobacterial peptidoglycan. Peptidoglycan synthesis showing the enzymes or processes that drugs used to prevent the biogenesis of peptidoglycan. Figure reproduced, with permission, from Abrahams and Besra, 2016.

Peptidoglycan is found in almost every species of bacteria, forming a protective layer surrounding the cytoplasmic membrane of the bacteria. The thickness of the peptidoglycan and the amount of cross-linking between the glycan strands affects the rigidity and shape of the bacteria (Egan et al., 2017; Kim et al., 2015; Loskill et al., 2014). Peptidoglycan also resists the turgor pressure of the cell, caused by the osmotic difference between the cytoplasm of the bacteria and that of the surrounding media (Moynihan et al., 2019).

Gram-positive have a thicker layer of peptidoglycan then Gram-negative bacteria (Chen et al., 2018). Mycobacterial species have peptidoglycan much more similar to that of Gram-positive bacteria than Gram-negative bacteria (Figure 1.11) (Chen et al., 2018; Jankute et al., 2015).

Peptidoglycan is formed from strands of polysaccharide, composed of alternating N-acetyl-glucosamine (GlcNAc) and N-acetyl-muramic acid (MurNAc) residues (Figure 1.15) (Moynihan et al., 2019). Mycobacterial PG is differentiated from the PG of other bacteria, due to the fact that the MurNAc can instead be N-glycolylmuramic acid (MurNGlyc) (Abrahams and Besra, 2016; Alderwick et al., 2015; Mahapatra et al., 2005, 2000). These strands are cross-linked by a linking unit. While the structure of the polysaccharide chains is conserved between bacteria the peptide cross-linking unit sequence and the position of the cross-links vary (Vollmer et al., 2008). In mycobacteria the crosslinking pentapeptide is built from: L-alanine (L-Ala), D-isoglutamate (D-isoGlu), meso-diaminopimelate (m-DAP), D-alaline (D-Ala) and a final D-Ala (Figure 1.15) (Kurosu et al., 2007). This pentapeptide is built upon either UDP-MurNAc, or UDP-MurNGlyc, and when fully synthesised is referred to as Park's nucleotide (Kurosu et al., 2007). Park's nucleotide is then transferred onto decaprenylphosphate (C_{50}-P) by MurX, followed by the addition of GlcNAc by MurG to form the mature lipid II.

Once lipid II is synthesised it must be translocated to the outer face of the membrane for incorporation into the PG. Lipid II is translocated across the inner membrane to the outer leaflet by FtsW/MurJ (Mohammadi et al., 2014; Ruiz, 2016, 2008; Sham et al., 2014). The polysaccharide is then built from this subunit by various enzymes with transglycosylase activity (Sauvage et al., 2008). These enzymes can either solely have transglycosylase activity, or have both transglycosylase and transpeptidase activity (Sauvage et al., 2008). The transglycosylation step releases the C_{50}-P for translocation back to the inner leaflet of the plasma membrane for further use in cell wall biosynthesis, as C_{50}-P acts as the anchor for many cell wall biosynthetic intermediates (Figure 1.14, Table 1.2).

The strand of polymerised GlcNAc-MurNAc/Glyc are crosslinked by the action of transpeptidases, these links can be either between the m-DAP and the D-Ala in the fourth position (3→4), or two m-DAP residues on separate peptide chains (3→3) (Kumar et al., 2012; Lavollay et al., 2008; Sanders et al., 2014). The ratio of 3→4 and 3→3 linkages has been shown to vary between bacteria (Pandey et al., 2018; Pisabarro et al., 1985). Mycobacterial species have a higher ratio of 3→3 linkages, between 60- 80 %, when compared to other bacteria (Sanders et al., 2014). This change in the crosslinking structure of PG is thought to lead to less flexible peptidoglycan (Pandey et al., 2018; Sanders et al., 2014).

1.3.4: Arabinogalactan:

One of the unique features of the *Mtb* cell wall is that the peptidoglycan is decorated with additional polysaccharide structures only found within the sub-order of Corynebacteriales. One of these structures is arabinogalactan (AG), a branched polysaccharide comprised of a galactan core formed linear polygalactofuranose, elaborated with 3 branched chains of polyarabinofuranose which is found attached covalently onto the PG (Abrahams and Besra, 2016; Jankute et al., 2015). The biosynthesis of this structure is separated into two phases; the synthesis of the galactan core on the inner leaflet of the plasma membrane, and the decoration of the galactan with arabinose in the periplasm.

Synthesis of galactan is initiated by WecA, which catalyses the transfer of GlcNAc from UDP-GlcNAc onto C_{50}-P, resulting in the formation of: C_{50}-P-P-GlcNAc (Jin et al., 2010). The resulting molecule is then rhamnoslylated by WbbL, using dTDP-L-rhamnose as a substrate, completing the linking unit that connects the PG and the galactan backbone (McNeil et al., 1990; Mills et al., 2004). The linking unit is then built upon by the action of galactofuranosyltransferases, GlfT1 and GlfT2 (Alderwick et al., 2008). GlfT1 attaches the initial galactofuranose (Gal*f*) from a UDP carrier onto the carbon 4 of the rhamnose, and an additional Gal*f* onto the carbon 5 of the first Gal*f* residue (Alderwick et al., 2008; Belanova et al., 2008; Mikusova et al., 2006). The resulting C_{50}-P-P-GlcNAc-L-Rha-Galf_2, is further built upon by GlfT2 which catalyses the elongation of the galactan to contain 25- 30 Gal*f* residues, which are linked with alternating β(1→5) and β(1→6) glycosidic bonds (Figure 1.15) (Kremer et al., 2001a; Rose et al., 2006).

Once the synthesis of the galactan core is complete it is translocated to the outer leaflet of the plasma membrane. This translocation has been predicted that this translocation is carried out by Rv3781 and Rv3783 in *Mtb* (Dianišková et al., 2011). Rv3783 is predicted to be a transmembrane domain of an ABC-transporter, while Rv3781 is predicted to form the corresponding nucleotide binding domain, however these have not been confirmed in the literature (Dianišková et al., 2011).

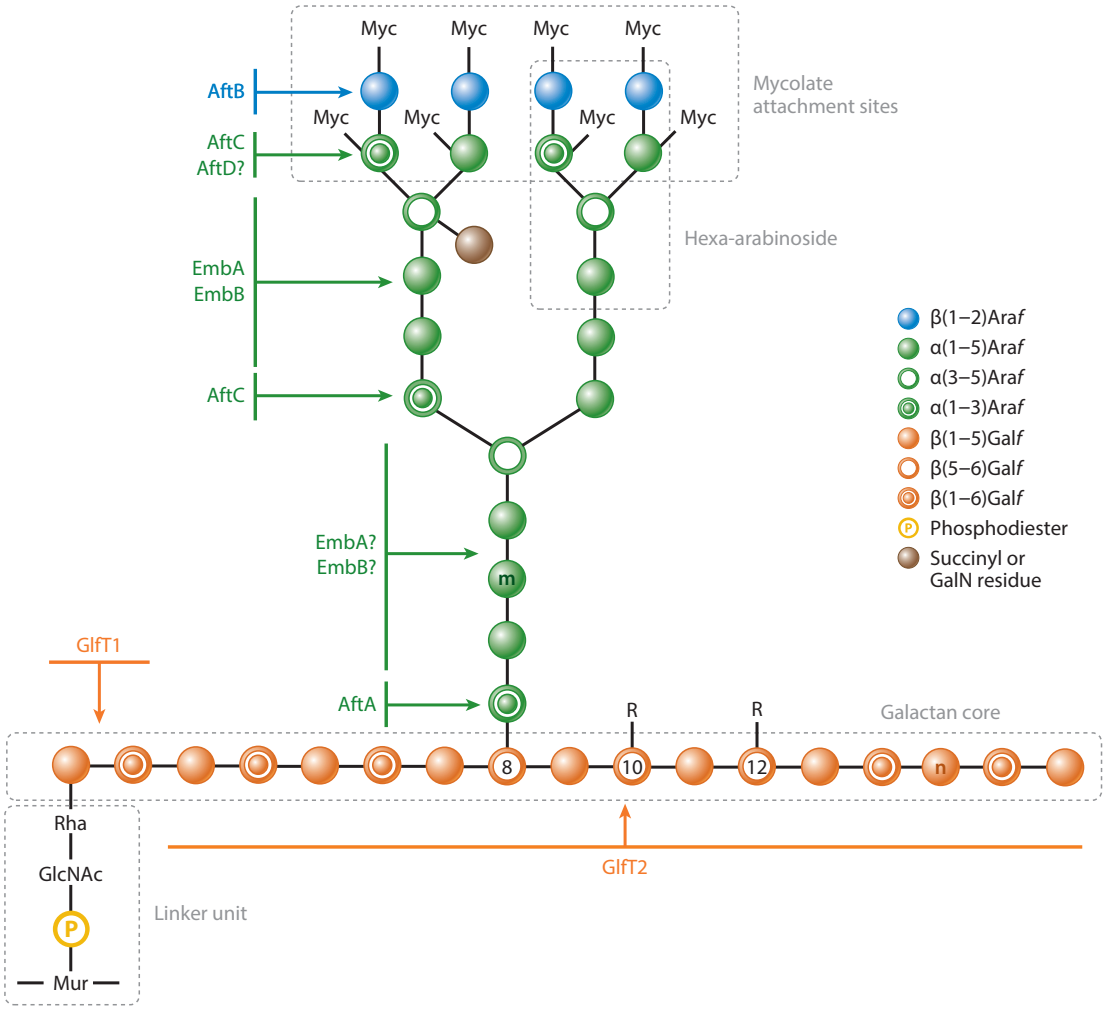

Figure 1.16: Biosynthesis of arabinogalactan in *Mtb*. Arabinogalactan biosynthetic pathway annotated with enzymes responsible for biosynthesis. Figure reproduced, with permission from Jankute et al. 2015.

Once the galactan is transported to the external face of the cell, the galactan is decorated with arabinofuranose (Ara*f*). The source of the Ara*f* is DPA, which is synthesised cytoplasmicly from phospho-α-D-ribosyl-1-pyrophosphate (pRpp). pRpp is attached to C_{50}-P by UbiA to form decaprenol-1-phosphate-5-phosphoribose (Alderwick et al., 2005; Huang et al., 2008, 2005). Decaprenol-1-phosphate-5-phosphoribose is dephosphorylated by Rv3807c to form decaprenol-1-phosphoribose (DPR) (Jiang et al., 2011). DPR is then epimerised into DPA, the sole known source of arabinose for the mycobacterial cell wall, by DprE1 and DprE2 (Kolly et al., 2014; Mikusova et al., 2005). The process of the translocation of the DPA to the external face of the membrane is not yet understood, it has been hypothesised that Rv3789 is responsible for the translocation. However, there is evidence to support a different role that of the anchor protein which aids in the recruitment of AftA (Kolly et al., 2014).

Arabinose is attached to the galactan chain at three specific residues: residues 8, 10, and 12 (Alderwick et al., 2006, 2005). The enzyme responsible for this transfer is AftA which catalyses the synthesis of a β(1→6) bond, adding a priming Ara*f* onto the galactan core. Once the priming Ara*f* residue is attached the arabinan domains of the AG are extended by EmbA and EmbB in α(1→5) linkages (Alderwick et al., 2005; Jankute et al., 2018). The extended arabinan chain is then branched by the action of AftC and AftD through α(1→3) linkages, with AftD providing the same for the branching of the arabinose domains in mycobacterial LAM (Birch et al., 2008; Škovierová et al., 2009). The terminal domain of the arabinan is well characterised, forming a [β-D-Ara*f*-(1→2)-α-D-Ara*f*]$_2$-3,5-α-D-Ara*f*-(1→5)-α-D-Ara*f* domain. This domain is synthesised by the action of EmbA, EmbB, AftB, AftC, and AftD (Alderwick et al., 2005; Birch et al., 2010, 2008; Escuyer et al., 2001; Jankute et al., 2017; Škovierová et al., 2009).

Table 1.2: Biosynthetic genes involved in the synthesis of arabinogalactan in *Mtb*. Showing the gene name where given, the *Mtb* H37Rv gene accession number, the function of the gene, and the first available reference describing gene function.

Gene name	*Mtb* H37Rv accession number	Gene function	Reference
WecA	Rv1302	Addition of GlcNAc-1-P to decaprenol phosphate	Jin et al., 2010
Wbbl	Rv3265c	Addition of rhamnose to decaprenyl-GlcNAc-1-P α(1→3)	McNeil et al., 1990
GlfT1	Rv3782	Addition of 2 Gal*f* to linker unit, β(1→4) α(1→5)	Mikusova et al., 2006
GlfT2	Rv3808c	Elongation of the galactan chain with alternating β(1→5) β(1→6)	Alderwick et al., 2008
AftA	Rv3792	Addition of arabinofuranose to the galactan core, α(1→5) bonds	Alderwick et al., 2006
EmbA	Rv3794	Addition of arabinofuranose to the arabinan branches, α(1→5) Synthesis of the terminal arabinan region	Alderwick et al., 2005; Escuyer et al., 2001
EmbB	Rv3795	Addition of arabinofuranose to the arabinan branches, α(1→5) Synthesis of the terminal arabinan region	Alderwick et al., 2005; Escuyer et al., 2001

AftC	Rv2673	Formation of arabinose branches within arabinan domains, α(1→3)	Birch et al., 2008
AftD	Rv0236c	Formation of arabinose branches within arabinan domains, α(1→3)	Škovierová et al., 2009
PrsA	Rv1017c	Transfer of pyrophosphate onto C1 of ribose-5-phosphate to form phospho-α-D-ribosyl-pyrophosphate	Alderwick et al., 2011
UbiA	Rv3806	Formation of DPA from C_{50}-P and pRpp	Alderwick et al., 2005
Rv3807c	Rv3807c	Dephosphorylation of decaprenyl-1-monophosphate- 5-phosphoribose to decaprenyl-1-phosphoribose	Jiang et al., 2011
DprE1	Rv3790	Epimerisation of decaprenyl-1-phosphoribose to decaprenylphosphoryl-D-arabinose	Mikusova et al., 2005
DprE2	Rv3791	Epimerisation of decaprenyl-1-phosphoribose to decaprenylphosphoryl-D-arabinose	Mikusova et al., 2005
AftB	Rv3805c	Transfer of terminal β(1→2) arabinofuranose residues	Alderwick et al., 2006
PpgS	Rv3631	Synthesis of polyprenol-phospho-N-acetylgalactosamine	Škovierová et al., 2010
Lcp1	Rv3267	Attachment of arabinogalactan to the peptidoglycan	Harrison et al., 2016

After AftC catalyses the branching of the terminal arabinose domains through α(1→3) linkage, the terminal arabinofuranose residues are attached by the action of AftB through a through α(1→2) linkage which caps the domain preventing further elaboration (Alderwick et al., 2005; Birch et al., 2010, 2008). The two capping Ara*f* residues are able to have mycolic acids esterified onto them at the C5 position (Lea-Smith et al., 2007). The final step in AG maturation is the attachment onto the PG, this step is carried out by Lcp1 (Harrison et al., 2016).

The attached AG is then mycolated by the action of Antigen 85 (Ag85), there are three different isoforms of Ag85: A, B, and C (Backus et al., 2014). While the main function of each of these enzymes is the same, the transfer of mycolic acids to sugars on the external surface of the cell, the preferred substrate for each of these enzymes has not been determined (Backus et al., 2014). There is some evidence to suggest that Ag85A and Ag85B are more likely to mycolate the terminal arabinose than Ag85C due to differences in the flexibility of the enzymes (Backus et al., 2014).

1.3.5: Lipomannan, and lipoarabinomannan:

LM and LAM (Figures 1.17, 1.18) are unique lipoglycans found only in the Corynebacteriales, in virulent species, such as *Mtb*, they are involved in immunomodulation (Pitarque et al., 2008). Both LM and LAM have been shown to be present in the cytoplasmic membrane and the outer mycomembrane, however the ratio of lipoglycans on present in the cytoplasmic membrane to those present in the outer membrane is as yet unknown (Pitarque et al., 2008). The binding of mannosylated LAM (manLAM) acts as a key method of preventing the maturation of the phagolysosome, along with other interactions with the host immune system (Hmama et al., 2015).

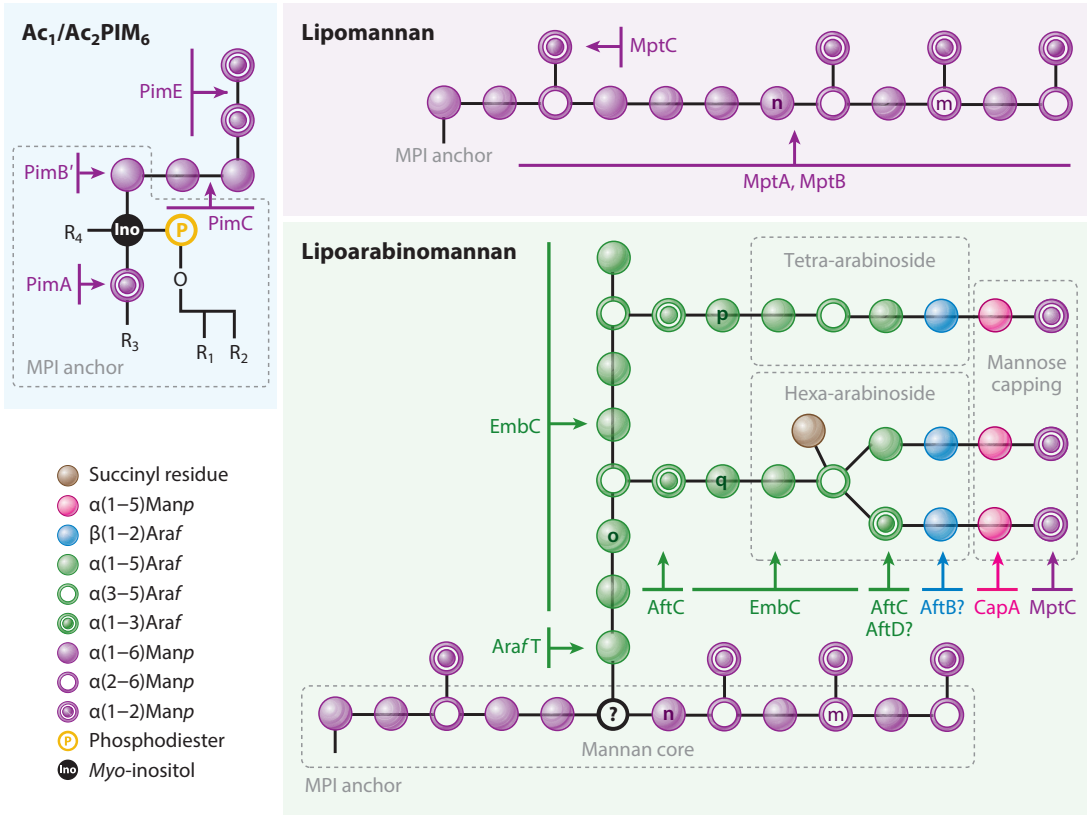

Figure 1.17: Structure and biosynthesis of mycobacterial LM and LAM. Showing the overlap between the synthesis of the arabinan domains of AG and LAM, with various enzymes involved in AG synthesis also involved in LM and LAM synthesis. Figure reproduced with permission from Jankute et al 2015.

In mycobacterial species both LM and LAM are formed through elongation of the PIM species, which as previously described are synthesised from PI (Figure 1.18). Both LM and LAM are found in both the inner and outer membrane of mycobacteria (Ortalo-Magne et al., 1996).

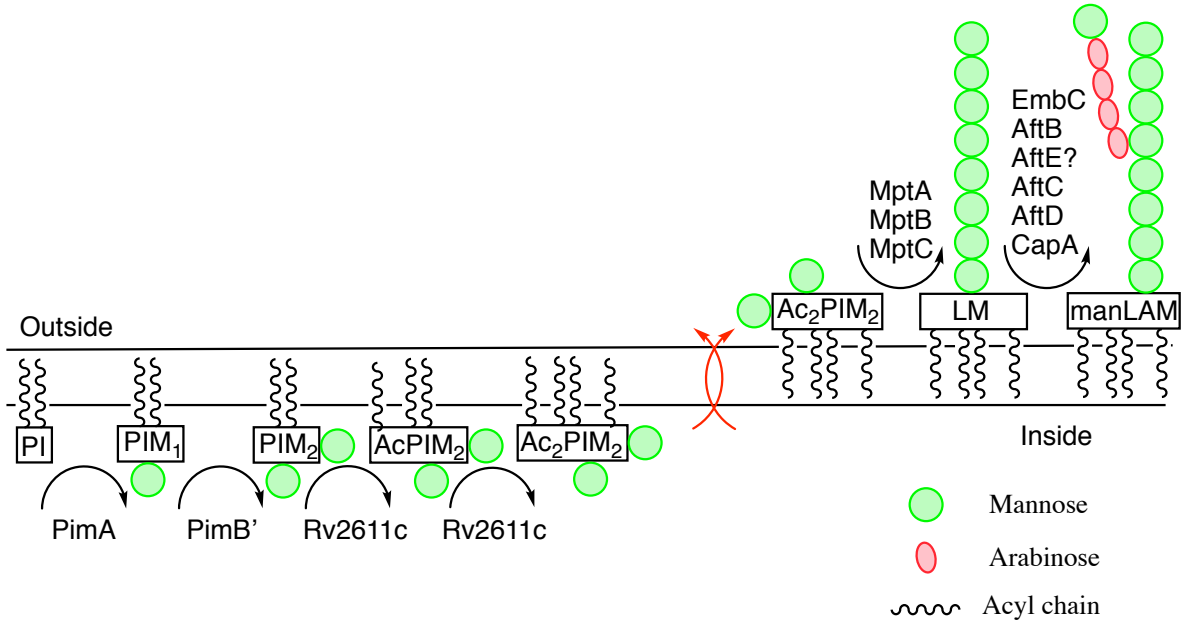

Figure 1.18: Biosynthetic pathway of LM and LAM from PI in *Mtb*. Showing genes responsible for the process(es). Processes without proteins known, or predicted, to provide the function highlighted in red.

LM and LAM are attached through non-covalent interactions between the PIM lipid anchor and either the phospholipid bilayer that makes up the plasma membrane, or the covalently bound fatty acids and mycolic acids attached to the AG that form the outer membrane (Ortalo-Magne et al., 1996; Pitarque et al., 2008). While many of the biosynthetic enzymes for LM and LAM are involved only in the synthesis of LM and LAM, there is significant overlap with AG in the biosynthesis of the arabinan domains, with many of the biosynthetic enzymes used in formation of both of these domains, as shown in Tables 1.2 and 1.3.

The synthesis of LM and LAM in mycobacteria starts from PIM species, after they have been translocated to the external face of the plasma membrane (Figure 1.18). With the protein

responsible for the transport of PIM species across the cytoplasmic membrane remaining unknown (Abrahams and Besra, 2016). Once on the external face of the inner membrane, LM and LAM biosynthesis most likely starts from Ac_1/Ac_2-PIM_4 (Figure 1.18). This starting substrate is thought be channelled by a putative lipoprotein, LpqW, into either the higher PIMs or into LM and LAM biosynthesis (Crellin et al., 2008). The mannosyltransferases responsible for the extension of the mannan core, by way of α(1→6) glycosidic linkages, are MptA and MptB (Mishra et al., 2007, 2008a) The mannan core is decorated with α(1→2) linkages with monomannan side chains (Kaur et al., 2008; Mishra et al., 2012).

The mature mycobacterial LM can then be further decorated with arabinose to form LAM, resulting in the addition of between 50 and 80 Ara*f* residues, using DPA as the source of arabinose. The enzyme responsible for the priming of the LM chain is as yet unknown, however once the chain is primed it is elongated with the α(1→5) glycosidic bonds formed by the action of EmbC (Shi et al., 2006). The arabinan branches of LAM are made up of 12- 15 Ara*f* residues, and the process of the addition of the arabinose is the same as the arabinose decoration of the arabinan domains on the AG (Alderwick et al., 2011; Shi et al., 2006).

Mycobacterial LAM can then be further decorated with the addition of terminal mannopyranose (Man*p*) to form ManLAM. The initial Man*p* addition is catalysed by CapA, which introduces a α(1→5) linkage (Kaur et al., 2008). From the branch point the chain is then elongated with α(1→2) linkages catalysed by MptC (Kaur et al., 2008). The mannose residues can then be further elaborated with the addition of an α(1→4) linked 5-deoxy-5-methyl-thio-xylofuranose (MTX) residue, with the enzyme responsible for the addition of the MTX residue is still unknown (Ludwiczak et al., 2002; Turnbull et al., 2004).

As mature lipoglycans have been detected in the cytoplasmic membrane as well as being exposed on the cell surface, and the amphipathic nature of lipoglycans, there is likely a transport mechanism responsible for shuttling LM and LAM to the cell surface. This is because the hydrophobic lipid anchor is unlikely to be removed from the cytoplasmic membrane solely by diffusion, similarly the hydrophilic mannan and arabinan domains are unlikely to pass through the hydrophobic outer membrane without the aid of a transport protein. The presence of the transport system has been predicted in mycobacteria, but as yet remains unidentified (Pitarque et al., 2008).

Table 1.3: Biosynthetic genes involved in the synthesis of lipomannan and lipoarabinomannan in *Mtb*. Showing the gene name where given, the *Mtb* H37Rv accession number, the function of the gene, and the first available reference describing the gene function.

Gene name	*Mtb* H37RV accession number	Gene function	Reference
Ino1	Rv0046c	Conversion of glucose-6-phosphate to inositol-1-phosphate	Bachhawat, 1999
PgsA1	Rv2612c	PI synthesis from inositol and CDP-diacylglycerol	Jackson et al., 2000
PimA	Rv2610c	Mannosylation of PI from UDP-mannopyranose α (1→2)	Korduláková et al., 2002
PimB'	Rv2188c	Mannosylation of PIM1 from UDP-mannopyranose α(1→6)	Lea-Smith et al., 2008
Rv2611c	Rv2611c	Acylation of PIM_1 or PIM_2 to Ac_1PIM_1, or Ac_2PIM_1 or Ac_1PIM_2, or Ac_2PIM_2	Korduláková et al., 2003

PimC	Unknown	α (1→6) mannosylation of PIM_2 to PIM_4, with mannopyranose	Kremer et al., 2002
PimE	Rv1159	α (1→2) mannosylation of PIM_4 to PIM_6, with mannopyranose	Morita et al., 2006
MptA	Rv2174	Generation of the mannan core from DPM through α (1→6) linkages	Mishra et al., 2007
MptB	Rv1459c	Generation of the mannan core from DPM through α (1→6) linkages	Mishra et al., 2008
EmbC	Rv3793	Extension of the arabinose domains after addition of primary arabinofuranose from DPA through α(1→5) linkages	Alderwick et al., 2011
AftC	Rv2673	Branching of arabinan domain by addition of α(1→3) arabinofuranose from DPA	Birch et al., 2008
AftD	Rv0236c	Hypothesised to branch arabinan domain by addition of α(1→3) arabinofuranose from DPA	Škovierová et al., 2009
AftB	Rv3805c	Transfer of terminal β(1→2) arabinofuranose residues from DPA	Jankute et al., 2017
CapA	Rv1635c	Capping of terminal arabinose of LAM with α (1→5) mannopyranose from DPM	Dinadayala et al., 2006

MptC	Rv2181	Terminal addition of α(1→2) mannopyranose from DPM either on terminal domain or mannan core	(Mishra et al., 2011)
Ppm1	Rv2051c	Synthesis of polyprenyl-phosphate mannose from polyprenyl-phosphate and GDP-mannose	Gurcha et al., 2002
PrsA	Rv1017c	Transfer of pyrophosphate onto C1 of ribose-5-phosphate to form phospho-α-D-ribosyl-pyrophosphate	Alderwick et al., 2011
UbiA	Rv3806	Formation of decaprenyl-1-monophosphate- 5-phosphoribose	Alderwick et al., 2005
Rv3807c	Rv3807c	Dephosphorylation of decaprenyl-1-monophosphate- 5-phosphoribose to decaprenyl-1-phosphoribose	Jiang et al., 2011
DprE1	Rv3790	Epimerisarion of decaprenyl-1-phosphoribose to decaprenylphosphoryl-D-arabinose	Mikusova et al., 2005
DprE2	Rv3791	Epimerisarion of decaprenyl-1-phosphoribose to decaprenylphosphoryl-D-arabinose	(Mikusova et al., 2005)
LpqW	Rv1166	Channelling of intermediates into synthesis of PIM_6 or LM and LAM	(Crellin et al., 2008)

1.3.6: Mycolic acids:

Mycobacteria are known to produce a unique type of lipid, the mycolic acid, which are found on the outer layers of the cell wall. Mycolic acids are either covalently bound to the arabinogalactan, or non-covalently in the outer membrane, as free mycolates, or attached to various sugar containing moieties such as trehalose to form trehalose monomycolate (TMM) or trehalose dimycolate (TDM) (Bhatt et al., 2008, 2007; Butler and Ahearn, 1986; Gande et al., 2004).

Mycolic acids are only found in species belonging to: *Mycobacteria*, *Corynebacteria*, *Nocardia*, and *Rhodococcus* (Brennan, 2003; Brennan and Nikaido, 1995; Butler and Ahearn, 1986). While mycolic acids are found in these species they vary significantly between genus'. Mycobacterial mycolic acids are the largest and most complex, while also showing significant variability in size between species, with mycobacterial mycolic acids containing 60- 90 carbons (Butler and Ahearn, 1986). Corynebacteria produce the smallest of mycolic acids, containing between 22- 36 carbon atoms, while nocardial and rhodococcal mycolic acids contain 36- 66 carbons (Alshamaony et al., 1976; Butler and Ahearn, 1986; Minnikin et al., 1977).

In mycobacteria mycolic acids are essential for viability, as they are involved in maintaining the hydrophobic nature of the external cell surface, especially in virulent strains where this impermeable barrier is essential in the prevention of the uptake of various antibiotics (Lanéelle et al., 2001; Liu et al., 1996). Mycobacterial mycolic acids are formed of a meromycolate fatty acid chain (C_{42-62}), condensed with an additional saturated fatty acid chain (C_{24-26}), to produce a unique α-alkyl-β-hydroxy fatty acid (Figure 1.19) (Brennan and Nikaido, 1995; Butler and Ahearn, 1986).

In order to produce these unique lipids, mycobacteria possess two different fatty acid synthases (FAS). FAS I is a multifunctional polypeptide, encoded by Rv2524c (Bhatt et al., 2007), responsible for the generation of fatty acids with a variety of lengths depending on if the requirements for phospholipid biosynthesis or mycolic acid biosynthesis (Takayama et al., 2005). The longer chain fatty acids (C_{20} and C_{26}), can either become the saturated α-branch, or be elongated by FAS II to become the meromycolate chain (Bhatt et al., 2007; Takayama et al., 2005). The synthesis of fatty acids by both FAS I and FAS II are well understood, with a sequential series of reactions leading to the addition of two carbons after each cycle (Figure 1.19).

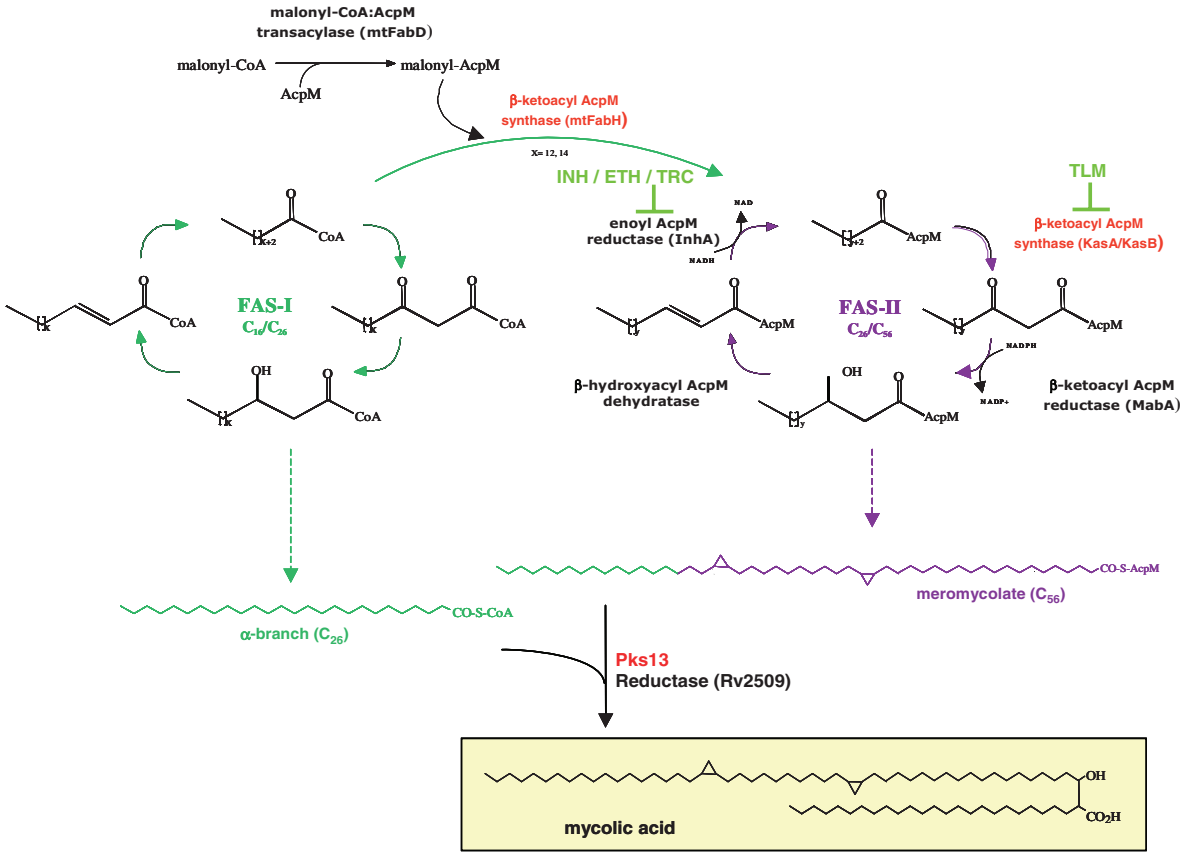

Figure 1.19: Biosynthetic pathway of mycolic acids in mycobacterial species. Showing synthesis of de-novo fatty acids into the α branch by the action of FAS-I, and the extension of FAS-I products to generate the meromycolate by FAS-II. Figure reproduced, with permission, from: Bhatt et al 2007

The further elongation of the short chain fatty acid depends on the availability of malonyl-CoA, and the acyl-carrier protein: AcpM (Kremer et al., 2001b). The acyl chain is transferred to the AcpM, and channelled into the FAS II, where it is extended in cycles. Each cycle catalyses the addition of two carbons onto the acyl chain until the meromycolate chain reaches the mature length (C_{42-62}). The meromycolate chain is then modified by the addition of methoxy groups, methyl groups, keto groups, and cis-/trans-cyclopropanation to form the mature meromycolate (Figure 1.20) (Barkan et al., 2010; Bhatt et al., 2007; Dubnau et al., 2000; Glickman, 2003; Glickman et al., 2000). The meromycolate and the short chain fatty acid are then linked through the action of Pks13 to produce a α-alkyl-β-keto-mycolic acid (Gande et al., 2004; Portevin et al., 2004). The mature mycolate undergoes a final reduction step, catalysed by Rv2509 in *Mtb* (Figure 1.19) (Bhatt et al., 2008).

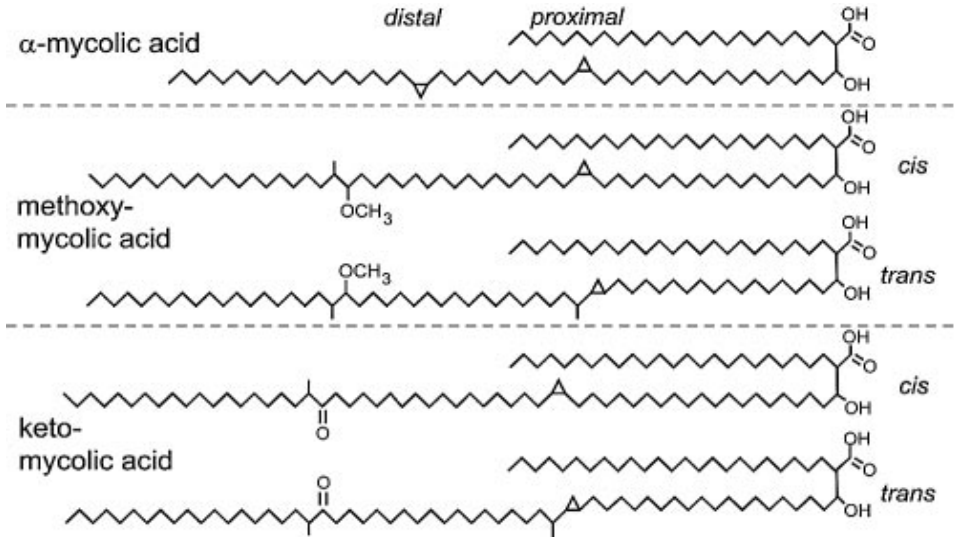

Figure 1.20: Structures of mycobacterial mycolic acids. Figure reproduced with permission from Takayama et al, 2005.

In *Mtb* mycolic acids are classified as either; α-, methoxy-, or keto- mycolic acids, depending on the modifications on the meromycolate chain (Figure 1.20). The methylation patterns of mycolates in mycobacterial species vary, with mycolic acids extracted from *Mtb*, only having

methyl groups on carbons that originally were the 2 position of the acetate during synthesis, while in *Mycobacterium smegmatis* the opposite is seen, with methyl groups only on carbons that were in the 1 position of the acetate (Schroeder and Barry, 2001).

The mechanism of the translocation of the synthesised mycolic acids from the site of cytoplasmic synthesis to the external site of attachment to the cell wall and insertion in the outer membrane has been determined to be conducted by Mmpl3, with TMM being the transported substrate (Su et al., 2019). This hypothesis is supported by discovery that Antigen 85 is able to transfer mycolates from TMM to the arabinogalactan and onto TMM to form TDM, suggesting that TMM acts as a primary source of mycolic acids (Abrahams and Besra, 2016; Backus et al., 2014; Takayama et al., 2005).

1.3.7: The mycobacterial capsule

The mycobacterial capsule is the outermost layer of the mycobacterial cell envelope, and is comprised of polysaccharides, secreted proteins, and lipids (Dinadayala et al., 2008; Koliwer-Brandl et al., 2016; Raynaud et al., 1998). The mycobacterial capsule is not covalently bound to the surface of the cell, and is able to be shed into the growth medium (Lemassu et al., 1996).

The primary component of the capsule are the α-glucans, a branched homopolysaccharide of α-D-glucose, where the monosaccharides are connected by α(1→4) glycosidic linkages, and the branch points are connected by α(1→6) glycosidic linkages. α-glucan is a large polysaccharide, with a mass of approximately 100 kDa (Dinadayala et al., 2008). The remaining polysaccharide component of the capsule is comprised of mannan and arabinomannan, which are structurally similar to LM and LAM respectively, and as such have

been hypothesised to be the cleaved from surface exposed LM and LAM (Kalscheuer et al., 2019).

The remaining capsular material is composed of species specific proteins and lipids (Kalscheuer et al., 2019; Ortalo-Magne et al., 1995; Raynaud et al., 1998). With the *Mtb* capsule having been shown to contain LpqH, PstS1and components of the Ag85 complex (Ortalo-Magne et al., 1995), with the other studies focussing on the enzymatic activity of the capsule showing the association of proteins such as: BlaC, Adh, and SodA (Raynaud et al., 1998). As with the protein composition, the lipid composition of the capsule varies depending on the mycobacterial species, with the most abundant lipid species in the capsule being PIMs, and diacylated trehaloses such as TDM (Ortalo-Magné et al., 1996).

1.4.1: Membrane associated proteins and transmembrane proteins:

Membrane proteins account for between 15- 30 % of bacterial genes and have been determined to make up approximately 50 % of the bacterial cytoplasmic membrane, performing a range of functions many of which are essential for viability (Rawlings, 2016; Strahl and Errington, 2017). However, the biological characterisation of these proteins has fallen behind that of soluble proteins due to the increased difficulty of purification while maintaining functionality (Rawlings, 2016; Strahl and Errington, 2017; Teo et al., 2019; Wang et al., 2017).

Membrane proteins can be separated into two categories: membrane associated proteins, and integral membrane proteins. Membrane associated proteins can associate with the membrane either through a covalently bound lipid anchor at the C-terminus of the protein, or through amino acid residues preferentially interacting with either the hydrophobic interior of the

phospholipid bilayer, or with interactions between both the hydrophobic core and the hydrophilic head groups of the bilayer. Membrane associated proteins that interact with the hydrophobic core do not span the membrane. Membrane associated proteins that are not bound to the membrane using a lipid anchor are often found to have a helical domain which provides the interactions with the membrane. These helices are usually hydrophobic on one face and hydrophilic on the other providing a substantial interaction with the membrane (Strahl and Errington, 2017).

Transmembrane proteins can span membranes, either through a single α-helix or multiple α-helices, or as a β-barrel. α-helical structures in membrane proteins are typically found in the cytoplasmic membrane, with proteins having different numbers of transmembrane α-helices depending on the protein function (Braibant et al., 2000; Tommassen, 2010). A single spanning region typically are predicted to act as an anchor to the cytoplasmic membrane, such as is predicted in the case of Lcp1 (Harrison et al., 2016). While multiple spanning α-helices are required for transporters to function, as multiple transmembrane helices are necessary in order to form a pore for the transported molecule to pass through. Though it is common for transporters in the inner membrane to form dimers in order to form a fully functional pore (Braibant et al., 2000; Beis, 2015, Locher, 2016).

Proteins that span the bacterial outer membrane tend to be found in a β-barrel architecture, where the membrane spanning region is composed of β-sheets. This structure is more stable and therefore better able to withstand exposure to the surrounding environment (Kuhn et al., 2017; Tommassen, 2010). The β-barrel structure is also less hydrophobic compared to α-helices which reduces the likelihood of aggregation during synthesis, as the primary structure of the protein is less hydrophobic than is required for an α-helix. This alternative structure also

ensures they reach the appropriate destination, as the majority of membrane proteins are translocated across the inner membrane by the same pathway (Kuhn et al., 2017; Tommassen, 2010).

The amount of structural information on transmembrane proteins is significantly smaller than that of soluble proteins, due to the environment they are located in making them more difficult to purify (Shimizu et al., 2018). Transmembrane proteins have also been seen to favour specific phospholipid environments, adding an additional layer of difficulty for study, as detergent based purification methods tend to remove all associated lipids (Postis et al., 2015; Rothnie, 2016; Seeger, 2018). While it is possible to reconstitute purified proteins back into a membrane bilayer environment with native lipids requires additional steps and does not ensuring that the protein is in the correct environment for any assay on activity to be guaranteed to representative of the *in vivo* activity (Prabudiansyah et al., 2015; Teo et al., 2019).

1.4.2: Insertion of proteins into the membrane:

Both inner and outer membrane proteins can be inserted or transported respectively by the Sec translocon. The majority of inner membrane proteins are translated and translocated simultaneously. This prevents aggregation of the transported protein by reducing the exposure of the hydrophobic membrane spanning regions to the aqueous cytosol (Kuhn et al., 2017).

Translocation of proteins by the Sec pathway is conserved throughout all domains of life (Denks et al., 2014). The core transmembrane region of the Sec pathway being formed by SecYEG complex formed of SecY, SecE and SecG (Andersson and von Heijne, 1993; Frauenfeld et al., 2011). SecY spans the inner membrane ten times to form the pore through

which proteins are transported. This pore has two exits where hydrophobic and hydrophilic regions can exit the transmembrane region through either the lateral gate or the pore ring respectively. The lateral gate is formed by four of the transmembrane helices in SecY, and is essential for the function of the protein (Frauenfeld et al., 2011; Plath et al., 1998). The channel of the SecYEG pore is hydrophobic and so the translocation of hydrophilic sections of protein through the pore requires the use of an ATPase, SecA, to overcome the energetic barrier. One exception to this is the case of small hydrophilic regions, where the translocation is coupled to the energetically favourable insertion of a transmembrane region (Andersson and von Heijne, 1993; Deitermann et al., 2005; Wang et al., 2017).

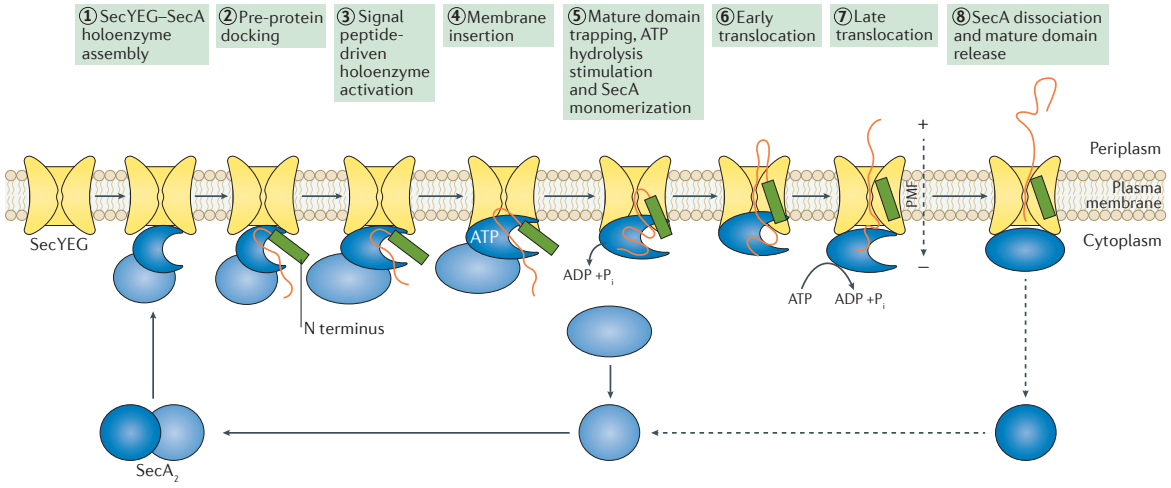

Figure 1.21: Sec mediated transloaction of proteins. Showing the steps by which the SecYEG complex interacts with SecA, and the substrate protein in order to translocate the substrate protein across the plasma membrane into the periplasm. Figure reproduced with permission from Tsirigotaki et al., 2017.

SecA additionally functions as a mediator between the ribosome and the SecYEG complex, resulting in simultaneous translation and translocation of inner membrane proteins. This is done by interactions between SecA and the nascent polypeptide exit tunnel of the 70S ribosome, as well as the nascent polypeptide itself (Huber et al., 2011; Singh et al., 2014; Tsirigotaki et al., 2017). This function of SecA is likely to ensure that proteins to be inserted

into the inner membrane are exposed to the hydrophilic cytosol as little as possible during translation to prevent mis-folding (Wang et al., 2017).

While the Sec membrane insertion and translocation mechanism is an important mechanism for the insertion of proteins into the membrane, it is not always required. Various proteins have been found to be inserted without the use of the Sec machinery, with some proteins using YidC rather than the Sec translocon to insert into the membrane (Kiefer and Kuhn, 2018). YidC is also used for the insertion of proteins into the membrane, functioning either independently of the Sec pathway or through interaction with the SecYEG complex (Kiefer and Kuhn, 2018; von Heijne, 1994). The size of the periplasmic domain to be inserted into the membrane plays a large role in the determination of the translocation system, with alterations to the size of periplasmic domains changing the proteins required for translocation from YidC to the SecYEG complex (Kiefer and Kuhn, 2018; van der Laan et al., 2004, 2001).

1.5.1: ABC-transporters:

ATP binding cassette (ABC) transporters are an important superfamily of membrane proteins found in all domains of life (ter Beek et al., 2014). ABC-transporters are one of the protein families that transport molecules across membranes, functioning when energy is required for translocation. Energy can be required either due to a concentration gradient resisting the movement, or due to energetically unfavourable interactions with the membrane (Seeger, 2018; Yamaguchi and Mano, 2019). The molecules transported by these proteins range from the import of nutrients and micronutrients, to the export of cell wall precursors and signalling molecules (Bi et al., 2018; Locher, 2016). The energetic cost of ABC-transporters has been estimated to vary between 10- 60 % of the total hydrolysis of ATP by cells depending on the

conditions (Rees et al., 2009). Braibant et al. 2000 found that there are at least 37 complete and incomplete ABC-transporters in the *Mtb* genome.

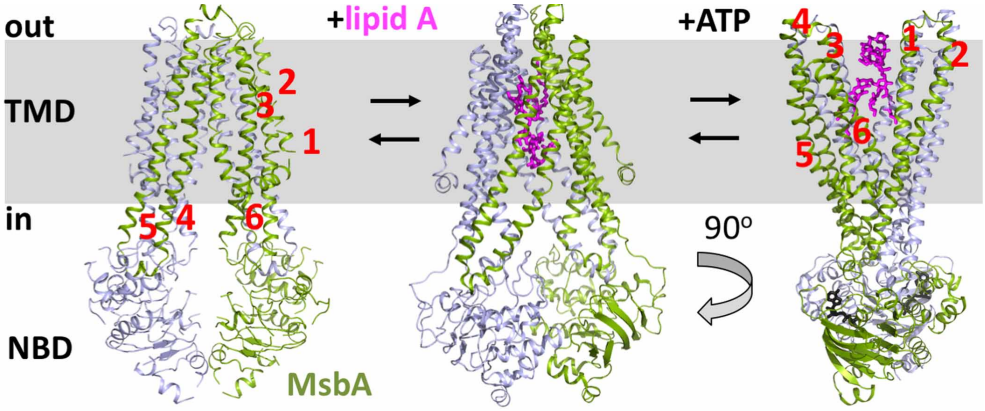

Figure 1.22: Structure of the ABC transporter MsbA. Showing the transmemberane domain (TMD, helicies labelled 1-6) and the nucleotide binding domain (NBD). Left to right showing the open conformation of MsbA (left) to allow for the binding of lipid A (centre), and the conformational change to allow release of lipid A upon addition of ATP (right). Figure reproduced with permission Ford and Beis, 2019.

ABC-transporters are capable of both importing and exporting molecules coupled the conversion of ATP to ADP and inorganic phosphate (Ford and Beis, 2019; Locher, 2016). They contain at least four domains; two membrane spanning domains (MSDs) typically comprised of four to eight transmembrane helices each, and two nucleotide binding domains (NBDs) (Braibant et al., 2000). These domains can be transcribed either independently as individual domains required to form a tetramer to function, or as a multi-domain polypeptides, which can contain all four domains or form either a homo- or hetero- dimer to function (Braibant et al., 2000; Locher, 2016). The pairs of MSDs and NBDs that make up an ABC-transporter tend to be either similar or identical (Higgins and Linton, 2004).

The superfamily of ABC-transporters has been classified into twelve different sub-families, of which *Mtb* is predicted to express members of nine different sub-families (Figure 1.24) (Braibant et al., 2000; Rees et al., 2009).

In addition to the core components of ABC-transporters that function as importers have an additional protein, called a substrate binding protein (SBP). SBPs are periplasmic proteins which in Gram positive bacteria are either attached to the membrane by an anchoring lipid tail, or bound to the transporter. SBPs bind to the substrate of transporter and present it to the binding site of the ABC-transporter for import (Berntsson et al., 2010).

All 15 putative SBPs in *Mtb* have a predicted lipid attachment site. The presence of a lipid attachment site is expected, as while mycobacteria are known to possess an pseudo outer membrane, they are most closely related to Gram positive bacteria (Braibant et al., 2000; Gao and Gupta, 2012). This results in the presence of a Gram positive SBP motif as opposed to the SBP being freely mobile in the periplasm organisation commonly seen in Gram negative bacilli (Berntsson et al., 2010).

1.5.2: Nucleotide binding domains of ABC-transporters:

The NBDs of ABC-transporters are themselves formed from two sub-domains: a catalytic core, and an α-helical domain (Beis, 2015). The catalytic core is the more conserved of the two subdomains, and contains the motifs required for ATP binding and hydrolysis. Such as the Walker A motif (also called the P-loop), the Walker B motif, as well as the Q-loop, A-loop and the H-motif (Figure 1.23) (Ambudkar et al., 2006; Beis, 2015; Rees et al., 2009). While the α-helical domain contains the ABC-signature motif, a peptide sequence of LSSGQ, which is

required for binding the nucleotide, though single point mutations in the consensus sequence can be tolerated (Braibant et al., 2000; Locher, 2016). The orientation of the α-helical domain is determined by the nucleotide binding state of the complex (Karpowich et al., 2001).

The A-loop is a generally conserved region upstream of the Walker A motif which has been shown to interact with the adenosine of ATP through an aromatic residue, most commonly tyrosine (Ambudkar et al., 2006). While the A-loop is involved in the binding of ATP, it is not found in all ABC-transporters (Ambudkar et al., 2006). Residues in both the Walker A and

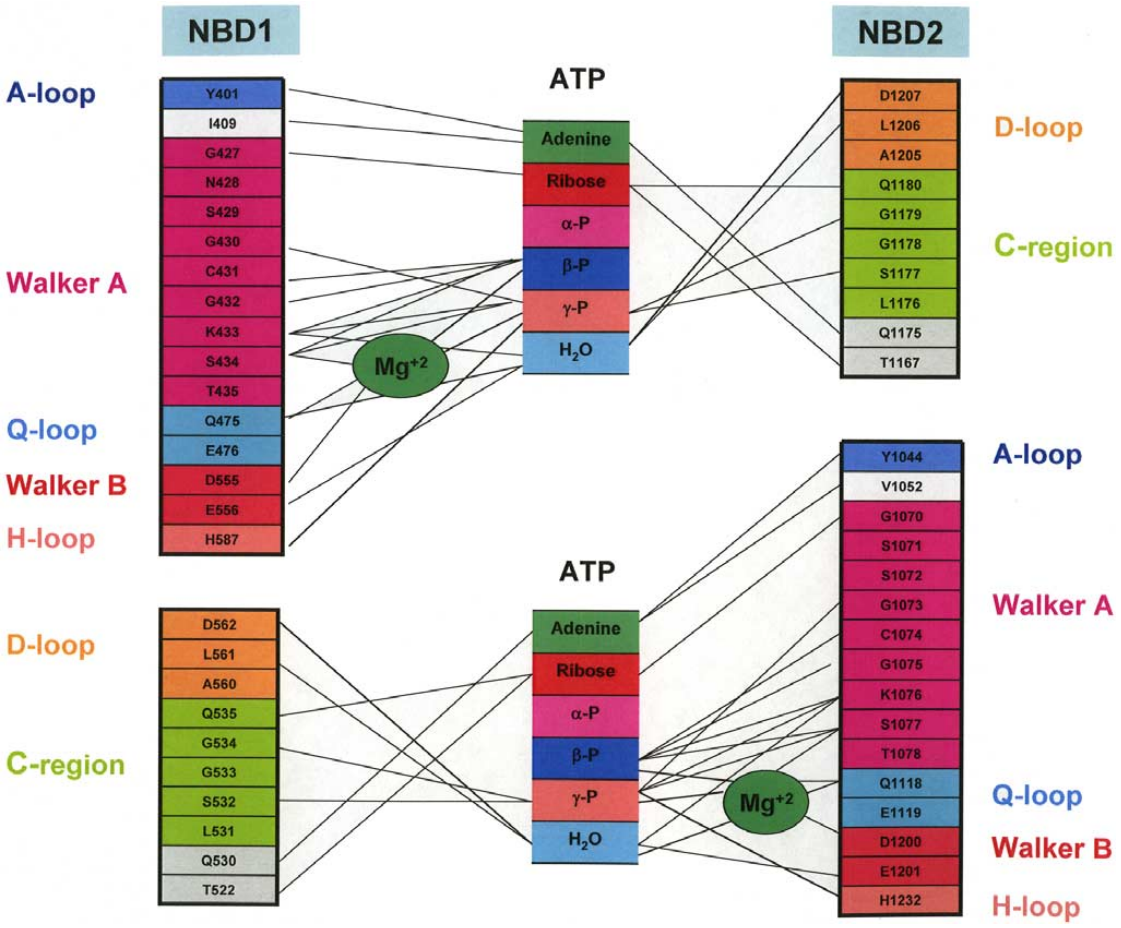

Figure 1.23: Interactions between the nucleotide binding domain of a human ABC-transporter and ATP. Showing the residues of the conserved ABC-transporter motifs and where they interact with ATP in human Pgp. Figure reproduced with permission from Ambudkar et al 2006.

Walker B motifs interacting with a chelated Mg^{2+} which is essential for the binding of ATP through interactions with the α and β phosphates (Figure 1.23) (Ambudkar et al., 2006; Beis, 2015). The Walker A motif is a conserved sequence of nucleotide binding domains, with a consensus sequence of: (A/G)XXXXGK(S/T), where "X" notes any amino acid and residues in parenthesis denoting multiple amino acids capable of forming the motif (Braibant et al., 2000). The Walker B motif is formed of DEØØØØD, where "Ø" notes a hydrophobic amino acid (Rees et al., 2009).

The Q-loop is a flexible region of the nucleotide binding domain which is responsible for the majority of the interactions with the membrane spanning domains, it is approximately nine residues long, beginning with a conserved glutamine, followed by either seven or eight amino acids. This region is flexible, and the interactions it makes with the active site by the conserved glutamine is thought to be involved in regulating the changes in the conformational state of the protein to cause either transport or release of the substrate (Beis, 2015; Jones and George, 2002).

The H-motif is formed of a short loop of hydrophobic amino acids followed by a histidine, downstream of the Walker B motif, this interacts with the gamma-phosphate of the ATP and has been shown to be essential for several ABC-transporters to function (Figure 1.20) (Ambudkar et al., 2006; Walter et al., 1992).

While the motifs found in the NBDs of ABC-transporters are generally conserved, and the consensus sequences are usually maintained there are some discrepancies in the literature as to the required sequences, and to the degree of conservation required for functionality of the ABC transporter (Braibant et al., 2000; Rees et al., 2009).

In order for the full ATP binding site to be formed, the two NBDs must dimerise, with dimer formation exclusively occurring in a head-to-tail structure. This is due to the requirement of motifs in both proteins to form a functional active site for each ATP binding site. The binding of ATP causes a conformational change that brings the two domains closer together which allows for the nucleophilic attack of an activated water molecule onto the γ-phosphate of ATP. The conserved glutamic acid of the Walker B motif is responsible for activating the water (Beis, 2015). The production of ADP and inorganic phosphate from this reaction disrupts the interface between the nucleotide binding domain, and allows for the release of the products (Hohl et al., 2014).

1.5.3: Membrane spanning domains of ABC-transporters:

MSDs are less well conserved than nucleotide binding domains, with some motifs that are only seen in a subset of the sub-families. Typically a MSD will contain four to eight transmembrane helices, and are encoded the same operon as the nucleotide binding domain that they associate with if they are expressed as separate proteins (Braibant et al., 2000).

The coupling of the energy released by ATP hydrolysis to the transport of the substrate is mediated through a structurally conserved, but sequentially variable α-helix located in the cytoplasmic loops between transmembrane domains (Beis, 2015). The overall structure of transmembrane domains shows significant variability, with structures being separated into three categories; importer type I, importer type II, and exporter (Rees et al., 2009). However due to the relative scarcity of structures of membrane proteins, and therefore by extension MSDs it is difficult to draw a consensus on structural similarities of these domains. The

determination of a structural consensus is likely to be further complicated by the differences in the substrates being transported ranging from relatively small molecules, such as lipids, to large polysaccharides which is likely to have a substantial effect on the quaternary structure of the complex (Beis, 2015).

1.5.4: Mycobacterial ABC-transporters:

15 of the predicted *Mtb* ABC-transporters are formed of clusters of genes comprising only one of the four domains required for a functional transporter. However, none of these is a cluster of four separate genes suggesting that the MSDs, and NBDs dimerise. The remaining transporters all contain at least one fused domain (protein contains either two fused MSDs, or one MSD and one NBD), to form a total of 25 complete predicted ABC-transporters (Figure 1.21), of which 15 have an associated SBP. Leading to the prediction of 15 ABC-transporters functioning as importers, with the remaining 10 being extruders (Braibant et al., 2000).

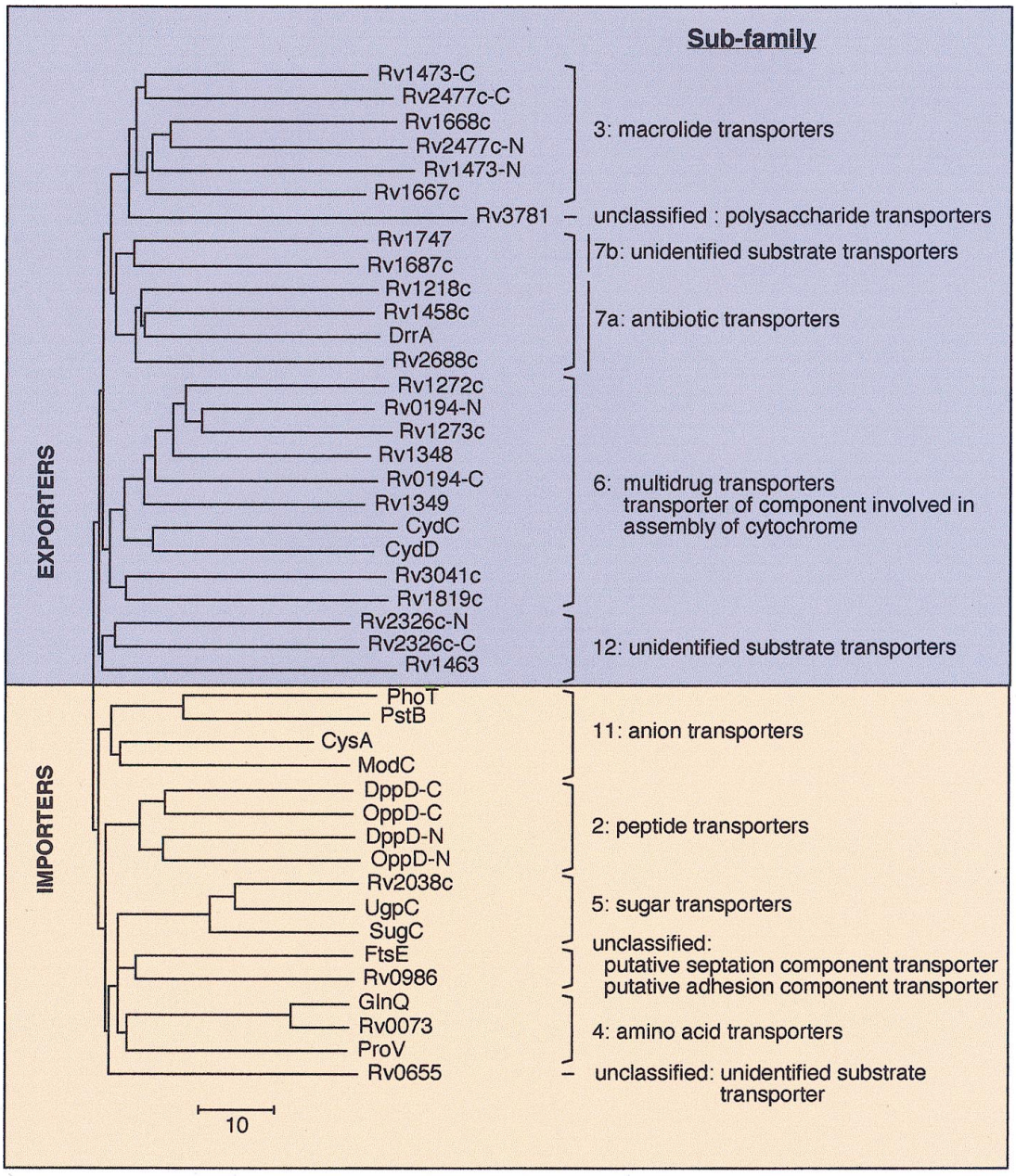

Figure 1.24: Classification of the ABC-transporters in Mtb. Showing the predicted importers and exporters along with the predicted ABC-transporter subfamily. Figure reproduced, with permission from Braibant et al 2000.

Of the complete transporters predicted within the *Mtb* genome, two have not been categorized into a sub-family, Rv0655, and Rv3781 (Braibant et al., 2000). Comparison between the *Mtb* genome and the genomes of *Escherichia coli*, and *Bacillus subtilis*, show that *E. coli* is predicted to express 57 ABC-transporters, of which only 13 are presumed to be extruders, while *B. subtilis* encodes for a predicted 78 ABC-transporters, of which 40 are predicted to be

extruders showing that *Mtb* encodes for a relatively small number of ABC-transporters as opposed to other bacteria, which is fitting considering the reduced range of environments that *Mtb* faces *in vivo* as it is an obligate pathogen (Linton and Higgins, 1998; Quentin et al., 1999).

1.6: Aims and Objectives:

To determine and characterize the currently unidentified protein or proteins responsible for the transport of PIMs across the plasma membrane in Mycobacteria.

To determine the effect of the gene deletions causing Ethambutol sensitivity in *C. glutamicum* and point mutations restoring Ethambutol resistance on the composition of the cell envelope.

To recombinantly express, and purify, the proteins predicted to be responsible for the transport of galactan in *M. smegmatis*, and to determine the binding affinities of galactan analogues to the purified putative galactan transporter proteins.

Chapter 2:

Characterization of a PIM transporter system in *C. glutamicum*

2.1: Introduction:

C. glutamicum is used as a model organism for *Mtb*, due to the highly similar cell wall structure, while having an increased tolerance to cell wall mutations that would be lethal in *Mtb* (Alderwick et al., 2005). This reduces the need for the generation of conditional knockouts for the investigation into the function of genes essential in mycobacterial species. This has allowed for insights into the function of various genes conserved in clinically significant mycobacterial species, with investigations into the biosynthetic pathways of AG, PIM, LM and LAM (Alderwick et al., 2006; Batt et al., 2010; Jankute et al., 2017; Mishra et al., 2012).

The corynebacterial cell wall shares much of the cell wall core that is found in *Mtb*, including various cell wall polysaccharides such as the lipid anchored LM and LAM, which are synthesised from PIMs, a major component of the mycobacterial membrane (Jankute et al., 2015). The core structure of these lipopolysaccharides is conserved between *Mtb* and *C. glutamicum*, with the exception of an additional lipid anchor for Cg-LM and Cg-LAM found in *C. glutamicum,* formed of a di-acylglycerol attached to a glucuronic acid (Gl-A) (Tatituri et al., 2007). A second major difference between Cg-LAM and mycobacterial LAM is the truncated arabinan domains in Cg-LAM (Tatituri et al., 2007).

Mycobacterial LM and LAM is anchored through either Ac_2PIM or Ac_1PIM (Crellin et al., 2008). The mannan core of the polysaccharide is built by the addition of Man*p* through α(1→6) glycosidic linkages on the mannose extending from the C6 of the inositol ring. The addition of these mannose residues is catalysed by the action of PimB', PimC, MptA and MptB, to build the mannan core decorated with single Man*p* residue branches to form LM (Mishra et al., 2007, 2008a).

The LM core can then be further built upon by the action of an unknown arabinosyl transferase (AraT) which primes the addition of further arabinofuranose residues to create LAM (Abrahams and Besra, 2016). Once the mannan core has been primed with single arabinofuranose to form the base of the branch, the branches are built by the action of EmbC, AftC, AftB, and potentially AftD to build the base arabinan domains using DPA as the source of arabinose (Alderwick et al., 2011; Jankute et al., 2017; Škovierová et al., 2009). These arabinan domains can then be further capped with mannose residues by the action of CapA and MptC to form ManLAM (Dinadayala et al., 2006; Mishra et al., 2011).

While the core structure of LM an LAM is conserved within mycobacterial species the structural differences found between mycobacterial species results in significant changes to the immune response (Birch et al., 2010; Stoop et al., 2013). The importance of these molecules in the immune response and virulence during infection has resulted in research into both the immunological and biosynthetic aspects of these molecules (Ishikawa et al., 2017; Nigou et al., 2004).

In mycobacteria LM and LAM have been found to be exposed on the cell surface. These lipoglycans have been indicated in the activation of signalling pathways that lead to apoptosis of macrophages, and the induction of interleukin 12 (IL-12) from infected cells (Dao et al., 2004). LM and LAM have been shown to interact with various signalling proteins expressed by macrophages including: toll-like receptor 1 and 2 (TLR-1 and -2), as well as C-type lectin receptors such as SIGNR3 (Elass et al., 2005; Ishikawa et al., 2017; Tanne et al., 2009). These interactions are altered by the different forms of LM and LAM produced by *Mtb*. Purified

ManLAM from *Mtb* does not cause the same phenotypic response as purified LAM, despite still inducing the expression of IL-12 transcript (Dao et al., 2004).

LAM is also involved in the prevention of the activation of macrophages, by inhibiting the activation of mitogen-activate protein kinase (MAPK). MAPK acts as an activator for signalling cascades, and is activated by the protein phosphatase SHP-1, preventing the transfer of signals, resulting in an altered immune response favouring the bacteria (Knutson et al., 1998; Pieters, 2008).

C. glutamicum possesses a singular Emb gene (as opposed to the three Emb proteins found in mycobacterial species), Cg-Emb provides the same functions as EmbA and EmbB in mycobacteria, acting as an porcessive AraT responsible for extension of the arabinan domains of AG (Alderwick et al., 2005; Jankute et al., 2018). However, Cg-Emb does not elongate the arabinose domains in LAM which is catalysed by the action of EmbC. The fact that Cg-Emb does not catalyse the extension of arabinan domains of Cg-LAM results in LAM with single arabinose residues as opposed to the extended arabinan domains in mycobacteria.

While the synthesis of PIMs LM and LAM (from synthesis of inositol for the core lipid that forms the PIMs, and elaboration of PI to the various PIM mannosylation and acylation states) has been largely identified (Table 1.3), the process by which PIMs are transported from the inner leaflet of the cytoplasmic membrane to the outer leaflet has yet to be identified (Abrahams and Besra, 2016; Jackson et al., 2000). Translocation of the PIMs to the outer leaflet of the cytoplasmic membrane is essential for both the biosynthesis of mature LM and LAM, and the maintenance of the plasma membrane. This is due to the PIM species forming a significant proportion of the lipid mass of mycobacteria, as well as their function as the anchor for LM

and LAM (Bansal-Mutalik and Nikaido, 2014; Lea-Smith et al., 2008). As such, determining the process by which PIMs are transported to the outer leaflet of the mycobacterial plasma membrane is important for our understanding of how the mycobacterial membrane is synthesised, as well as how the cell surface is synthesised.

Due to the amphipathic nature of the PIM species it is unlikely that the process for transfer to the outer leaflet of the cytoplasmic membrane does not require the input of energy by the action of a dedicated transporter. This energy requirement has been shown in the transport of other lipid molecules exported to the external face of the cytoplasmic membrane, supporting the need for a transporter for translocation of PIMs to the external leaflet of the membrane (Xie et al., 2015). One example of a lipid transporter in *E. coli* is MsbA (Figure 1.21), an extensively characterized ABC-transporter, responsible for the export of lipid A to the outer leaflet of the cytoplasmic membrane (H. Singh et al., 2016). Due to the structural similarity of lipid A and PIMs (Figure 2.1) it is likely that the transport proteins for the translocation to the periplasmic face of the cytoplasmic membrane for these lipids share some similarity. As the Corynebacteriales suborder does not produce lipid A, a transporter homologous to MsbA may transport molecules similar to Lipid A.

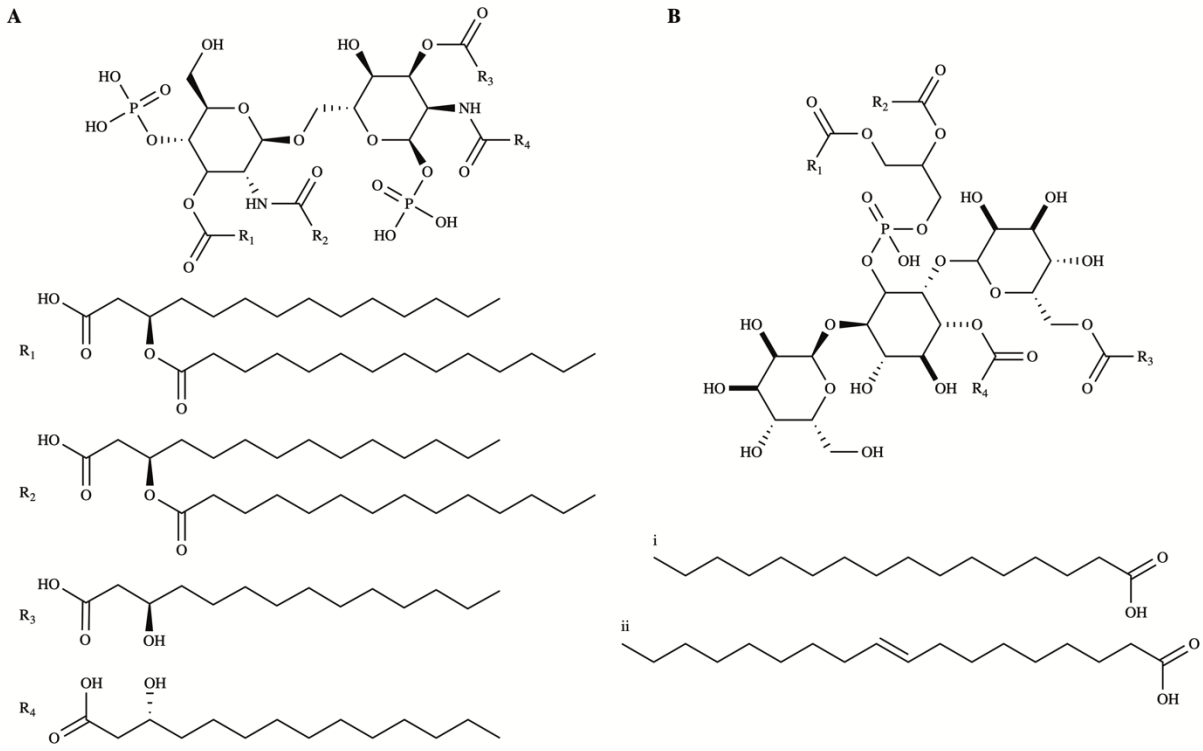

Figure 2.1: Lipid structure comparison of *E. coli* lipid A, and Ac_2PIM_2. A) Lipid A, with R_1-R_4 corresponding to the acyl chains attached in their respective positions, B) Ac_2PIM_2, i and ii being the two acyl chains predominantly found in PIM species, ($C_{16:0}$ and $C_{18:1}$ respectively), with the exact positions of each chain unconfirmed. Lipid A is the transport substrate of MsbA, is a multiply acylated sugar containing phospholipid, similar to Ac_2PIM_2.

Here we aim to identify and characterise the genes responsible for translocating PIMs from the inner to the outer leaflet of the cytoplasmic membrane in *Corynebacteriacea.* We used MsbA (the well characterised Gram-negative lipid A flippase), as an archetypal lipid transporter to mine the genomes of CMN bacteria in order to detect and identify putative PIM transport genes. The function of these putative PIM transporters was determined by a comprehensive phenotyping of knock out mutants generated in *C. glutamicum*.

2.2: Results:

2.2.1: Bioinformatic analysis of Mycobacterial MsbA homologs:

MsbA has been shown to be the transporter of lipid A across the inner membrane in *E. coli* (Xie et al., 2015). Due to the similarity of the structures of Lipid A and PIM species (Figure 2.1), we predicted that the *Mtb* ABC-transporter responsible for the export of PIMs to the periplasmic leaflet of the cytoplasmic membrane would show homology to MsbA.

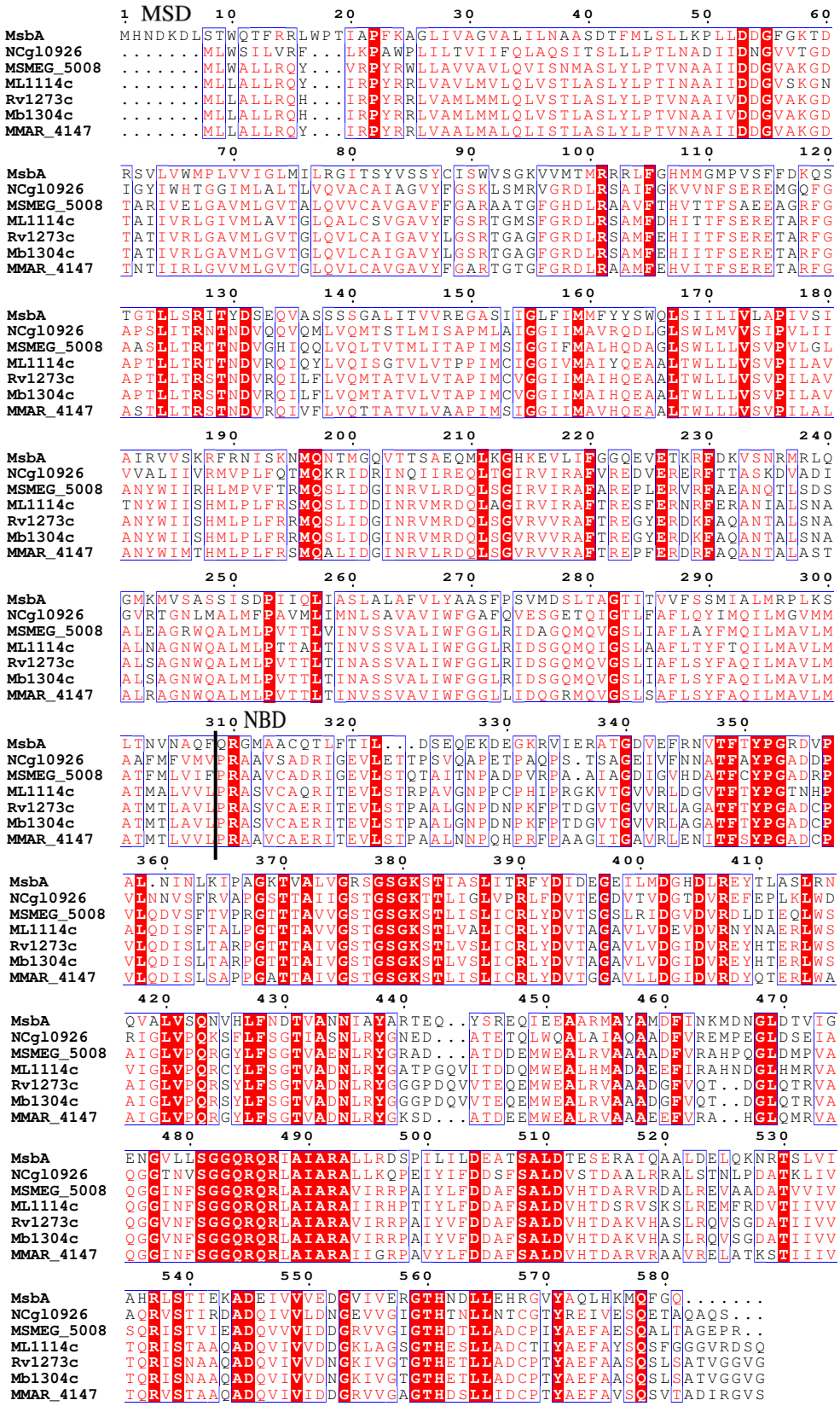

Figure 2.2: Multiple sequence alignment of *E. coli* K12 MsbA and Mycobacterial and *C. glutamicum* orthologs of Rv1273c. Predicted end of MSD and beginning of NBD marked by black line, at residue 308. Similar sections highlighted by blue boxes, residues conserved in all proteins in white on red, residues in a position with conserved charge in red, gaps in the alignment indicated with "**.**". Method 6.1.1.

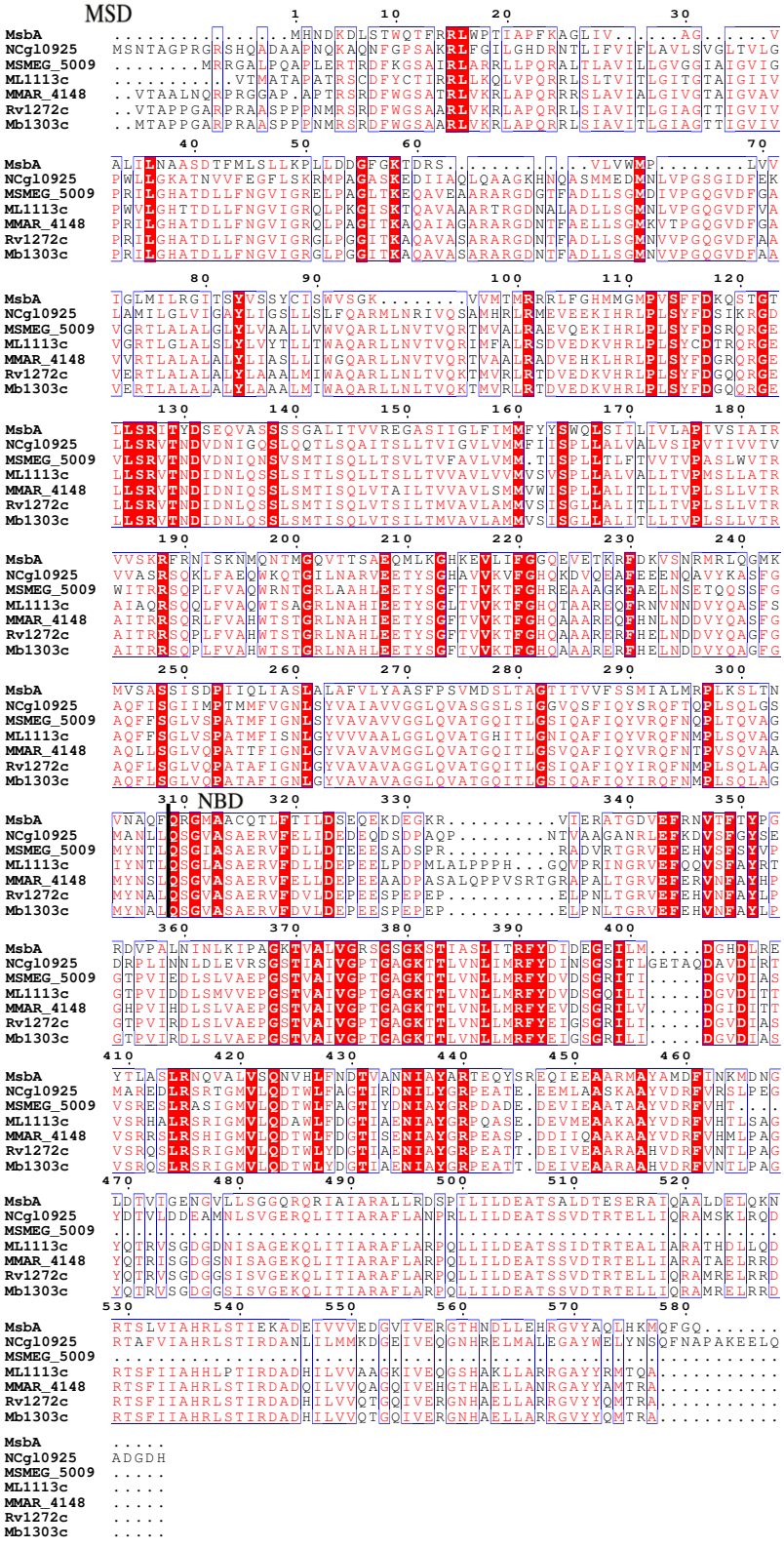

Figure 2.3: Multiple sequence alignment of E. coli K12 MsbA and Mycobacterial and C. glutamicum orthologs of Rv1272c. Predicted end of MSD and beginning of NBD marked by black line, at residue 308. Similar sections highlighted by blue boxes, residues conserved in all proteins in white on red, residues in a position with conserved charge in red, gaps in the alignment noted as "**.**". Method 6.1.1

Table 2.1: Heatmap of sequence identity of Mycobacterial and Corynebacterial protein sequences against MsbA and predicted Mtb MsbA homologs. Showing homology through all tested mycobacterial species and into C. glutamicum. Rv corresponds to gene expressed in *Mtb*, Mb corresponds to gene expressed in *M. bovis*, MMAR_ corresponds to gene expressed in *M. marinum*, MSMEG_ corresponds to gene expressed in *M. smegmatis*, and NCgl corresponds to gene expressed in *C. glutamicum*. Identity, residues conserved at each position compared to the reference sequence. Positive, residues with conserved physiological properties. Cells formatted on percent values, 0% = Red, 50% = Orange, 100% = Green.

	MsbA		Rv1272c		Rv1273c	
	Identity (%)	Positives (%)	Identity (%)	Positives (%)	Identity (%)	Positives (%)
Rv1272c	36	56	100	100	34	52
Mb1303c	36	56	99	100	34	52
ML1113c	30	52	75	85	35	53
MMAR_4148	33	53	82	88	35	51
MSMEG_5009	31	54	74	85	34	52
NCgl0925	31	53	54	71	30	50
Rv1273c	28	49	34	53	100	100
Mb1304c	28	49	34	53	100	100
ML1114c	27	49	32	53	78	87
MMAR_4147	27	51	34	53	81	90
MSMEG_5008	26	50	33	54	69	83
NCgl0926	28	51	34	55	50	70

Using BLAST analysis of the primary protein structure of *E. coli* K12 MsbA against the *Mtb* non-redundant protein database (Method 6.1), resulted in the selection of two proteins for further study (Rv1272c and Rv1273c), as they have high sequence identity to MsbA and the likelihood that they comprise a single complete heterodimeric ABC-transporter, due to the genomic location (Braibant et al., 2000). Both selected genes were tested to determine the degree of conservation across slow and fast-growing mycobacterial species' as well as both infectious and non-infectious species as well as *C. glutamicum* (Figures 2.2, 2.3). The genetic synteny across a selection of various mycobacterial species provides additional evidence to support a common function, as the surrounding genes are also generally conserved, particularly notable in *M. leprae* which is regarded as a minimal mycobacterial genome (Figures 2.2, 2.3, 2.5) (Cole et al., 2001). Sequence identity of the identified ABC-transporters tabulated, compared to MsbA, or *Mtb* identified homologs is shown in Table 2.1.

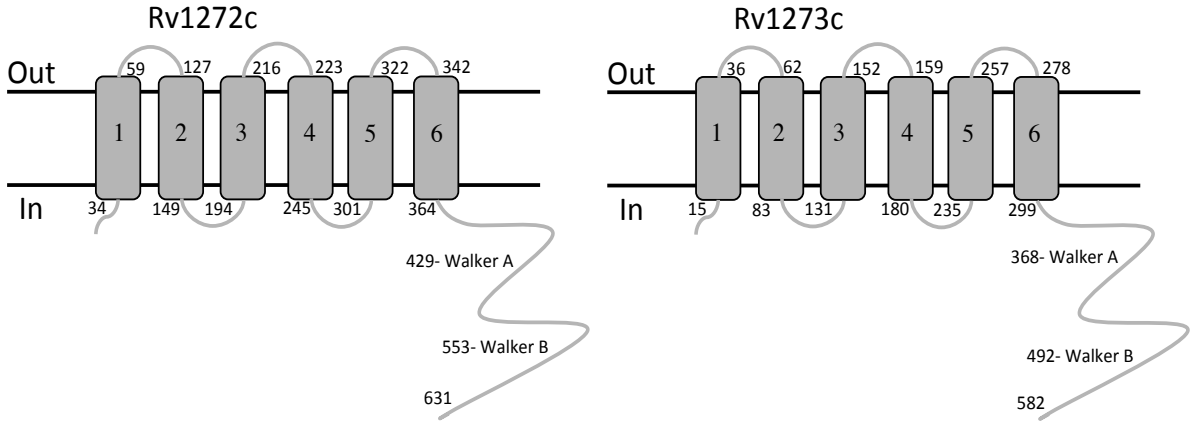

Figure 2.4: Predicted membrane topology model of Rv1272c and Rv1273c. Residue numbers for first amino acid inserted into the membrane and first amino acid external to the membrane noted. First residues of the Walker A and B motifs annotated. Transmambrane predictions generated from TMHMM and Expasy TMPred, Appendix 1.

Sequences of predicted MsbA homologs were searched for conserved ABC-transporter motifs (Figure 2.6), and membrane topology of mycobacterial genes predicted using the Hidden

Markov model using both Transmembrane helix Hidden Markov Model (TMHMM), and EXpasy TMPred (Appendix 1) which predict the location of transmembrane helices from the primary protein structure. Leading to the prediction of six transmembrane helices, consistent with the four to eight transmembrane helices for a membrane spanning domain, required for the formation of a pore through the membrane upon formation of a dimer (Figure 2.4). The conservation of the ABC-transporter motifs, taken with the predicted conserved membrane

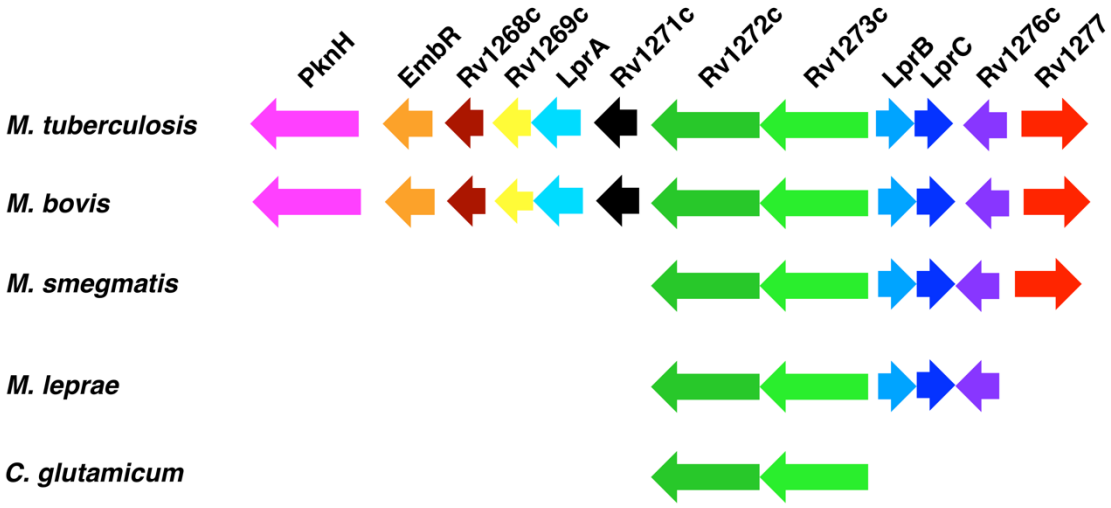

Figure 2.5*:* Genetic synteny of mycobacterial genes predicted to be identified as putative PIM transporters. Conservation of the genes surrounding predicted PIM transporters through various mycobacterial species, including *M. leprae*, a mycobacterial genome regarded as the minimal mycobacterial genome (Cole et al., 2001), as well as conservation the neighbouring genes LprB and LprC suggest a conservation of this region of the genome, and potentially a conserved function.

topological structure lead to prediction that Rv1272c and Rv1273c form a functional transporter responsible for the translocation of PIMs across the cytoplasmic membrane.

The identification of Rv1272c and Rv1273c as potential lipid transporters, contradicts the prediction of Braibant et al. in 2000, where Rv1272c and Rv1273c are predicted to function as

a multidrug efflux pump. However, in the past 20 years since the publication of these predictions there has been no corroborating evidence for this prediction. Due to the limited functional dataset available to Braibant et al. 2000 at the time of prediction, it is likely that the most similar characterised transporter at the time was an antibiotic efflux pump.

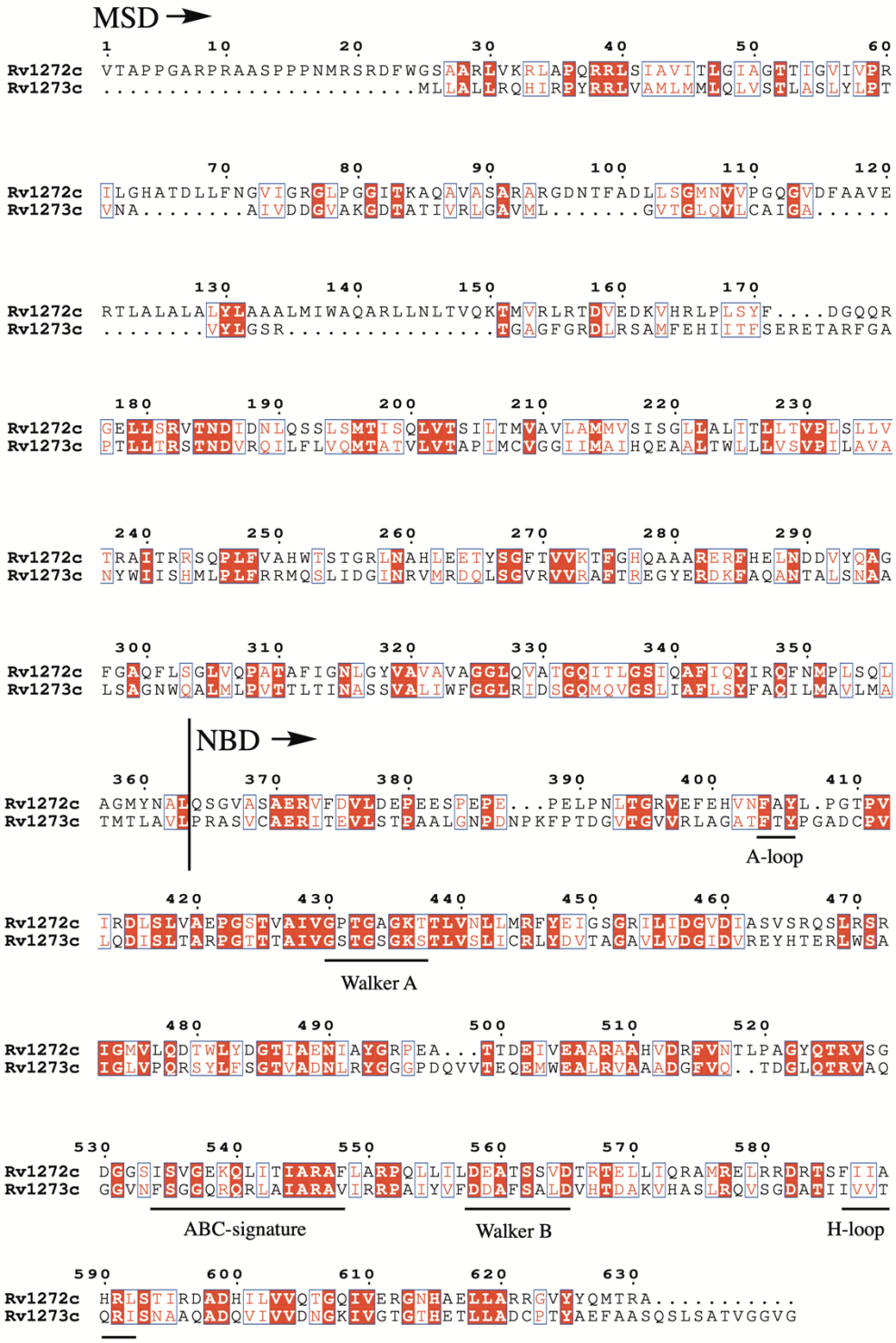

Figure 2.6: Primary protein structure of predicted *Mtb* H37Rv MsbA homologs, Rv1272c and Rv1273c. Aligned sequences annotated with conserved consensus sequences present in nucleotide binding domains of ABC-transporters Rv1272c, and Rv1273c. A-loop, Walker A, ABC signature, Walker B, H-loop motif sequences underlined. Showing that essential conserved regions are present in both Rv1272c and Rv1273c, alongside six transmembrane helices contained within the membrane spanning domain (MSD).

2.2.2: Generation of *M. smegmatis*Δ*MSMEG_5008- 5009* double deletion mutant:

Attempts to generate a *M. smegmatisΔMSMEG_5008- 5009* double deletion mutant were unsuccessful (Method 6. 3.1), with no mutants able to be generated with both *MSMEG_5008* and *MSMEG_5009* deleted. The inability to generate this double deletion mutant suggests that these genes are either essential individually or become essential upon deletion of the other.

2.2.3: Generation of *C. glutamicum*Δ*NCgl0925- 0926* double deletion mutant in *C. glutamicum*:

Generation of a *C. glutamicum*Δ*NCgl0925- 0926* double deletion mutant from the parental *C. glutamicum* ATCC13032 strain was conducted by J. Marienhagen's group in Julich (Method 6.3.2). We hypothesised that the generation of a double deletion mutant of the *C. glutamicum* orthologs (NCgl0925 and NCgl0926) would not be lethal, due to the increased tolerance of cell wall mutations.

The *C. glutamicum*Δ*NCgl0925- 0926* deletion mutant was generated using pk19*mobsacB*-Δ*NCgl0925- 0926* plasmid (Figure 2.7 A), with homologous recombination used to replace selected genes with non-coding DNA. The deletion of NCgl0925 and NCgl0926 confirmed using PCR (Figure 2.7 B). Analysis of the PCR product in the shows a reduction in the size of the product in the *C. glutamicum*Δ*NCgl0925- 0926* double deletion mutant, from ~4 kb to ~1 kb, which corresponds to the deletion of NCgl0925 and NCgl0926.

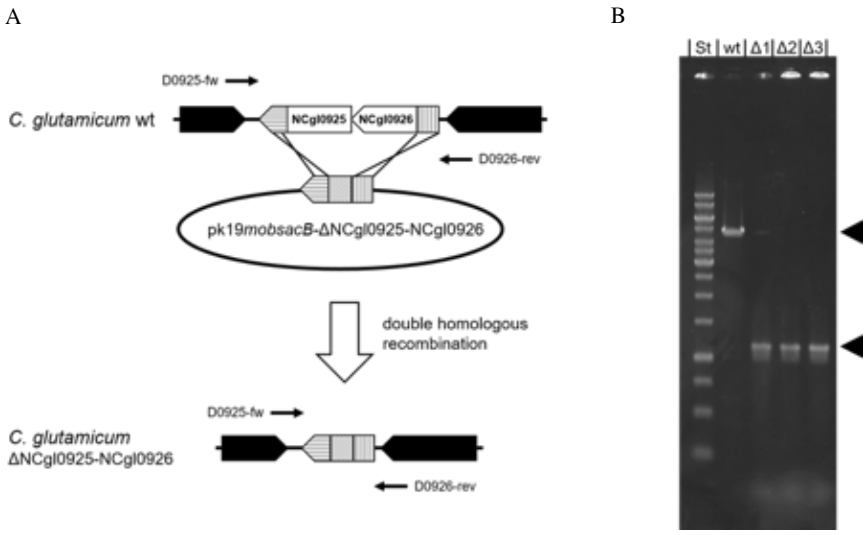

Figure 2.7: Generation of *C. glutamicumΔNCgl0925- 0926* double deletion mutant. A) Schematic of generation of *C. glutamicumΔNCgl0925- 0926* double deletion mutant, B) Agarose gel electrophoresis of PCR of NCgl0925-0926 confirming the of deletion of NCgl0925-0926. Comparison of the PCR product between the WT *C. glutamicum* and the *C. glutamicumΔNCgl0925- 0926* double deletion mutant shows a shift in the size of the PCR product, consistent with the deletion of NCgl0925 and NCgl0926. Figure made by J. Marienhagen's group

2.2.4: Growth rate analysis in WT *C. glutamicum* and *C. glutamicumΔNCgl0925- 0926* double deletion mutant:

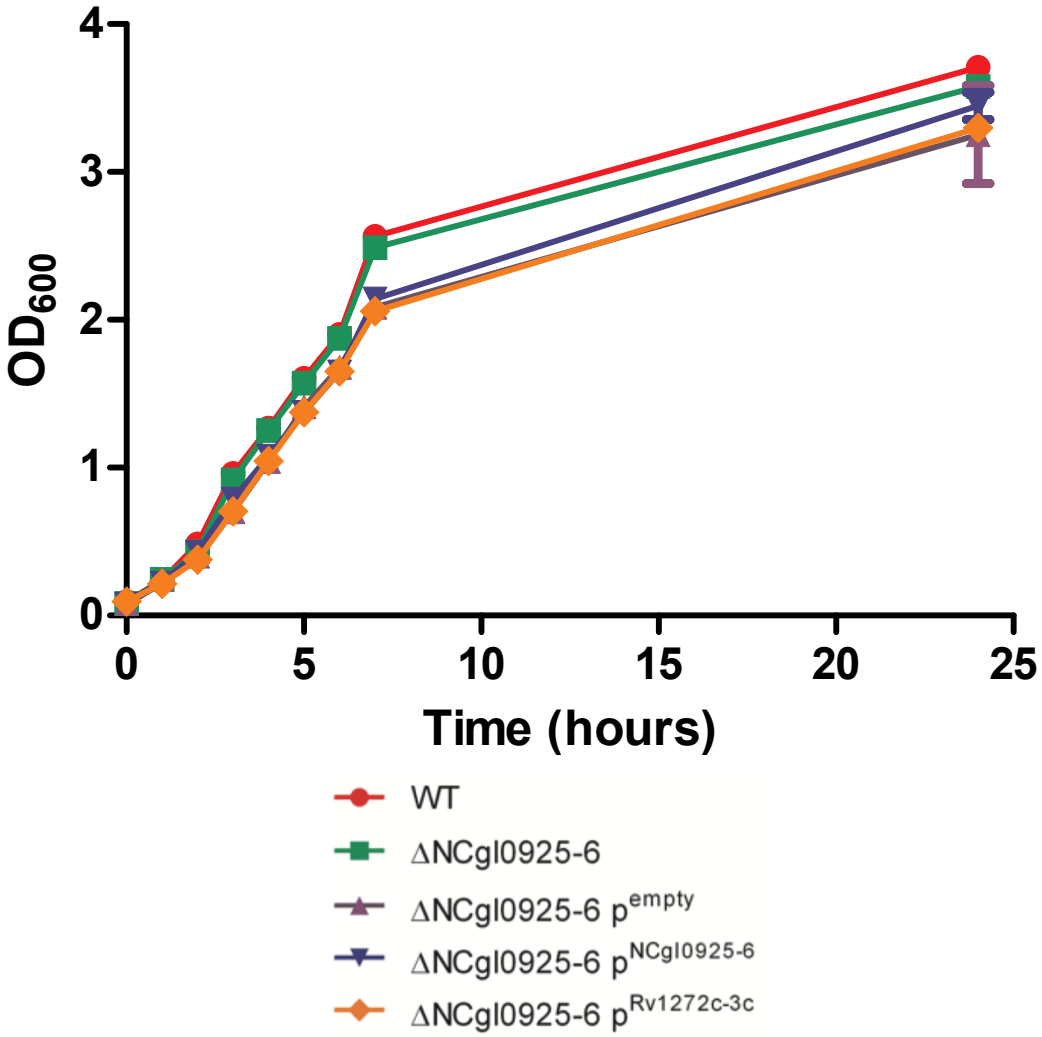

Figure 2.8: Growth rate analysis of *C. glutamicum* strains in rich media as measured by OD_{600}. Expression of complements induced with 1mM IPTG, n=3. Use of Bonferroni corrected ANOVA to analyse the OD_{600} readings throughout the experiment show no significant change ($q > 0.05$) between the deletion mutant and the WT *C. glutamicum* strain. Bonferroni corrected ANOVA of strains expressing the pEKEx3 plasmid does result in a reduced growth rate during throughout the experiment ($q < 0.05$), however there is no significant difference between the level of growth attained at 24 hours post inoculation, between any of the strains containing the pEKEx3 plasmid (p^{empty}, $p^{NCgl0925-6}$, and $p^{Rv1272c-3c}$) and the WT *C. glutamicum* or *C. glutamicumΔNCgl0925- 0926* double deletion mutant strain, nor is there a significant difference between the strains restoring the native genes, or the homologous *Mtb* genes and the strain containing only the unmodified vector ($q > 0.05$). Error bars: Standard deviation.

Initial testing of the deletion mutants to determine the effect of gene loss on growth rate phenotype was carried out (Figure 2.8, Method 6.10), as the deletion or disruption of genes involved in certain pathways often results in a growth defect (Alderwick et al., 2005). In order to induce the expression of the complementing genes on the pEKEx3 plasmid the growth media was supplemented with 0.5 mM IPTG.

Analysis of the OD_{600} values, using Bonferroni corrected ANOVA, throughout all timepoints showed that the WT *C. glutamicum* and the *C. glutamicum*Δ*NCgl0925-0926* double mutant strain showed no significant change in the growth at any time point ($q > 0.05$), while *C. glutamicum*Δ*NCgl0925-0926* double mutant strains expressing pEKEx3 plasmids with or without gene inserts showed a statistically significant reduction in growth when compared to either the WT *C. glutamicum* or *C. glutamicum*Δ*NCgl0925-0926* double mutant strain at all time points from 4 hours post-inoculation, except for 24 hours post-inoculation, when using an Bonferroni-corrected ANOVA ($q > 0.05$) at each timepoint.

There is no significant difference between any of the three strains containing the empty vector, or either of the plasmids recombinantly expressing either the deleted NCgl0925 and NCgl0926, or the *Mtb* homologs, Rv1272c and Rv1273c. This implies that the reduction in the growth rate is likely due to the fitness cost of either maintaining a plasmid or caused by the addition of antibiotic into the media to maintain the plasmid. This shows that in culture these genes are non-essential in culture medium, and do not affect the ability of the bacteria to grow.

2.2.5: Cell surface permeability characterization of WT *C. glutamicum* and *C. glutamicumΔNCgl0925- 0926* double deletion mutant:

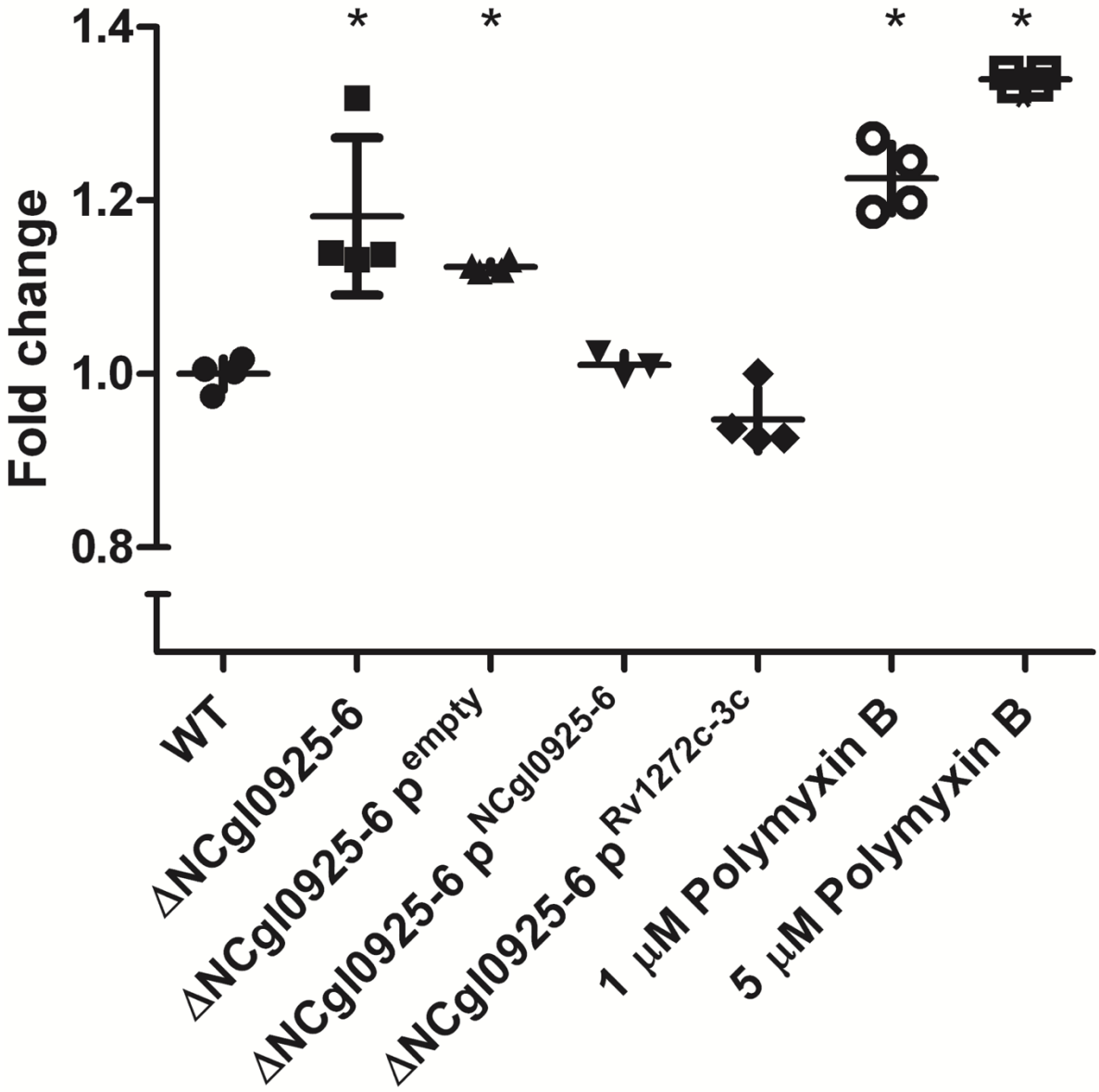

Figure 2.9: Cell surface permeability of *C. glutamicum* strains to DPH. Data normalised to show fold change from WT *C. glutamicum* strain. Bonferroni corrected ANOVA of data showed significant increase in permeability from the WT *C. glutamicum* in both the *C. glutamicumΔNCgl0925- 0926* double deletion mutant, and *C. glutamicumΔNCgl0925- 0926* pEKEx3 strain (p^{empty}), while the *C. glutamicumΔNCgl0925- 0926* pEKEx3-NCgl0925- 0926 ($p^{NCgl0925-6}$), *C. glutamicumΔNCgl0925- 6* pEKEx3-Rv1272c- 1273c ($p^{Rv1272c-3c}$) showed no significant change. Polymyxin B used as a positive control to increase permeability. Differences between strains that were statistically significant to the WT *C. glutamicum* ($q < 0.01$) marked by "*".Error bars: Standard deviation, n= 4.

Cell surface permeability is affected by the lipid composition of the cell envelope, our prediction of the function of NCgl0925 and NCgl0926 as being involved in the transport of PIMs to the outer leaflet of the cytoplasmic membrane, lead to the prediction of a change in cell permeability in the deletion mutants.

Using Bonferroni-corrected ANOVA to assess the change in permeability of the cell surface to 1, 6- diphenyl- hexa- 1, 3, 5- triene (DPH, Method 6.11), resulted in a statistically significant increase in permeability of the both the *C. glutamicum*ΔNCgl0925- 0926, and the *C. glutamicum*ΔNCgl0925-0926 pEKEx3 strains when compared to the WT ($q > 0.01$) (Figure 2.9). The complementation of either the deleted NCgl0925 and NCgl0926, or Rv1272c and Rv1273c, restored the basal level (including at a reduced stringency of $q > 0.05$). The strains recombinantly expressing either NCgl0925 and NCgl0926 or Rv1272c and Rv1273c, both showed a significant difference to the ΔNCgl0925-0926 double mutant strain.

The loss of NCgl0925 and NCgl0926 results in a significant increase in the permeability of the surface of the cell, in line with the hypothesis that these genes are involved in the maintenance of the cell surface, possibly through the transport of lipids across the cytoplasmic membrane. Complementation of the *C. glutamicumΔNCgl0925- NCgl0926* strain with either: *NCgl0925* and *NCgl0926* or *Rv1272c* and *Rv1273c* restored the wild type permeability phenotype, showing that the cause of the permeability change is due to the loss of NCgl0925 and NCgl0926 rather than the result of an off target effect, as well as supporting the prediction of a shared function in both *C. glutamicum* and *Mtb*.

2.2.6: Antibiotic susceptibility screening of WT *C. glutamicum* and *C. glutamicum*Δ*NCgl0925- 0926* double deletion mutant:

As Rv1272c and Rv1273c are predicted to function as an antibiotic efflux pump, we tested the efficacy of various antibiotics against WT *C. glutamicum*, and the *C. glutamicum*Δ*NCgl0925-0926* double deletion mutant (Method 6.19) to characterise the effect of loss of NCgl0925 and NCgl0926 on the bacterial survival in the presence of various antibiotics (Braibant et al., 2000; Wang et al., 2010).

Of the antibiotics selected affecting both intra- and extra- cellular functions to determine if the change in the permeability of the cell is responsible for any changes in the tolerance of *C. glutamicum* strains to antibiotics.

Table 2.2: Antibiotic susceptibility screening of *C. glutamicum* strains to antibiotics. Showing the MIC_{99} values of various antibiotics against WT *C. glutamicum*, *C. glutamicumΔNCgl0925- 0926*, *C. glutamicumΔNCgl0925- 0926* pEKEx3, *C. glutamicumΔNCgl0925- 0926 pEKEx3- NCgl0925- 0926*, *C. glutamicumΔNCgl0925- 0926* pEKEx3- Rv1272c-1273c.

	Chloramphenicol (μM)	Amoxicillin (μM)	Ampicillin (μM)	Rifampicin (μM)	Ethambutol (μM)	Polymyxin B (μM)
WT *C. glutamicum*	7.813	0.977	0.977	>0.488	<500	3.906
C. glutamicum△NCGL0925-0926	7.813	0.977	0.977	>0.488	<500	3.906
C. glutamicum△NCGL0925-0926 pEKEx3	7.813	0.977	0.977	>0.488	<500	3.906
C. glutamicum△NCGL0925-0926 pEKEx3-NCgl0925-0926	7.813	0.977	0.977	>0.488	<500	3.906
C. glutamicum△NCGL0925-0926 pEKEx3-Rv1272c-1273c	7.813	0.977	0.977	>0.488	<500	3.906

Determination of the MIC_{99} for WT *C. glutamicum*, *C. glutamicum*Δ*NCgl0925- 0926*, *C. glutamicum*Δ*NCgl0925- 0926* pEKEx3, *C. glutamicum*Δ*NCgl0925- 0926* pEKEx3- *NCgl0925- 0926*, and *C. glutamicum*Δ*NCgl0925- 0926* pEKEx3- *rv1272c-1273c*, showed no detectable changes in MIC_{99} (Table 2.3). The lack of changes in tolerance to antibiotics

between the WT *C. glutamicum*, and the *C. glutamicum*Δ*NCgl0925- 0926* double deletion mutant suggests that the function of these genes is not, as predicted by Braibant et al 2000, an antibiotic efflux pump. This, while not supporting the hypothesis that Rv1272c and Rv1273c function as the PIM transporter, does suggest that the annotation of these genes was incorrect.

2.2.7: Characterization of the free lipid phenotype of WT *C. glutamicum* and *C. glutamicum*Δ*NCgl0925- 0926* double deletion mutant:

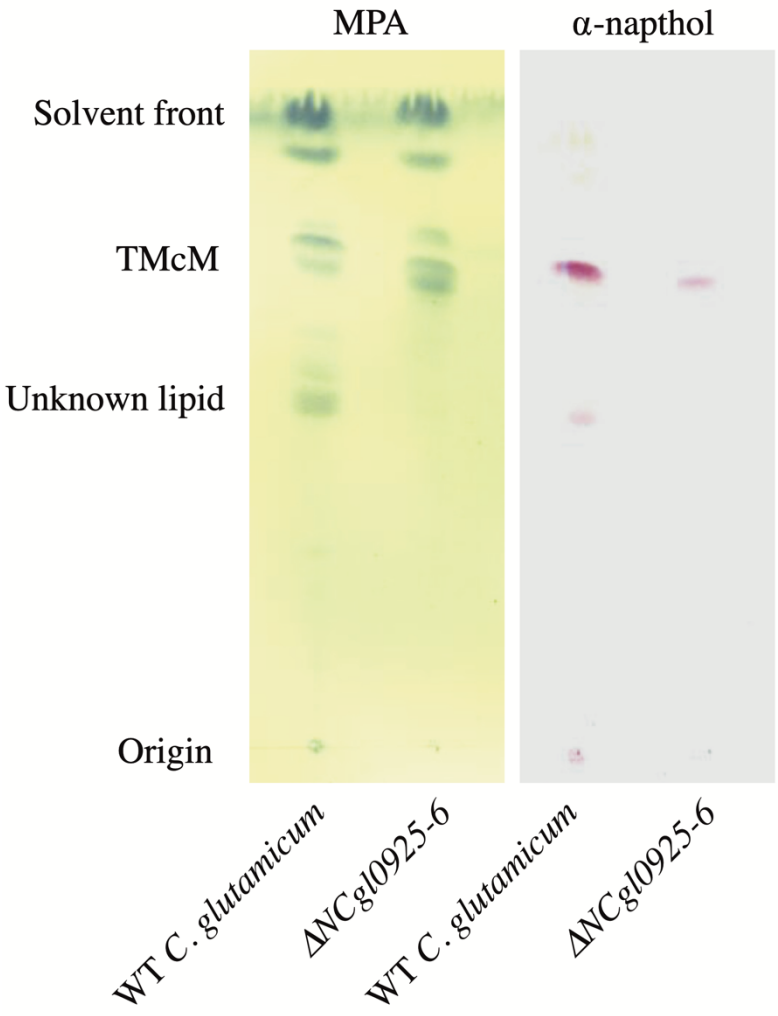

Figure 2.10: TLC apolar outside lipid extraction from *C. glutamicum* strains. Showing the loss of a sugar containing lipid in the C. glutamicumΔNCgl0925- 0926 double deletion mutant, when compared to WT *C. glutamicum*. Solvent system- 65: 25: 0.5: 3.6 chloroform: methanol: 12 M ammonium hydroxide: water. TMcM- trehalose monocorynemycolate.

The increase in the cell surface permeability implied that the deletion of NCgl0925 and NCgl0926 results in a change in the lipid composition of the *C. glutamicum* cell surface. Therefore, characterisation of the overall lipid composition of the *C. glutamicum*Δ*NCgl0925-0926* double deletion mutant using the standard polar-apolar lipid extraction procedure was used to analyse the lipid composition (Singh et al., 2016).

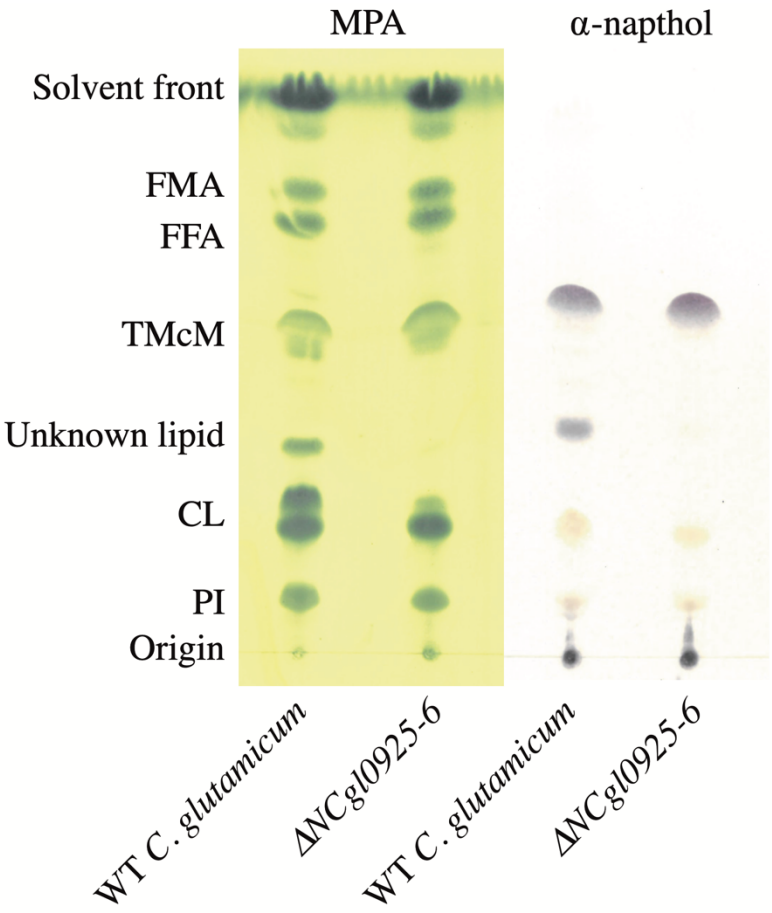

Figure 2.11: TLC analysis of apolar inside lipid extraction fraction from *C. glutamicum* strains. Showing loss of unknown sugar containing lipid in the *C. glutamicum*ΔNCgl0925- 0926 double deletion mutant when compared to the WT *C. glutamicum* strain. MPA staining for lipids, α-napthol staining for sugars. Solvent system- 30: 8: 1 chloroform: methanol: water. FMA- free mycolic acid, TMcM-trehalose monocorynemycolate, CL- cardiolipin, PI- phosphatidylinositol.

TLC analysis of the apolar outside lipid fractions (Method 6.12.1) extracted from WT *C. glutamium* and the *C. glutamicum*ΔNCgl0925-0926 double deletion mutant strain shows the depletion of a free lipid, staining positive for both fatty acids (TLC stained with MPA), and sugars (TLC stained with α-napthol, labelled unknown lipid in Figure 2.10).

Similarly, TLC analysis of the apolar inside lipid fractions (Method 6.12.1) extracted from both the WT *C. glutamium* and the *C. glutamicum*ΔNCgl0925- 0926 double deletion mutant showed the same phenotype, with the loss of a lipid staining positive for both fatty acids and sugars (Figure 2.11).

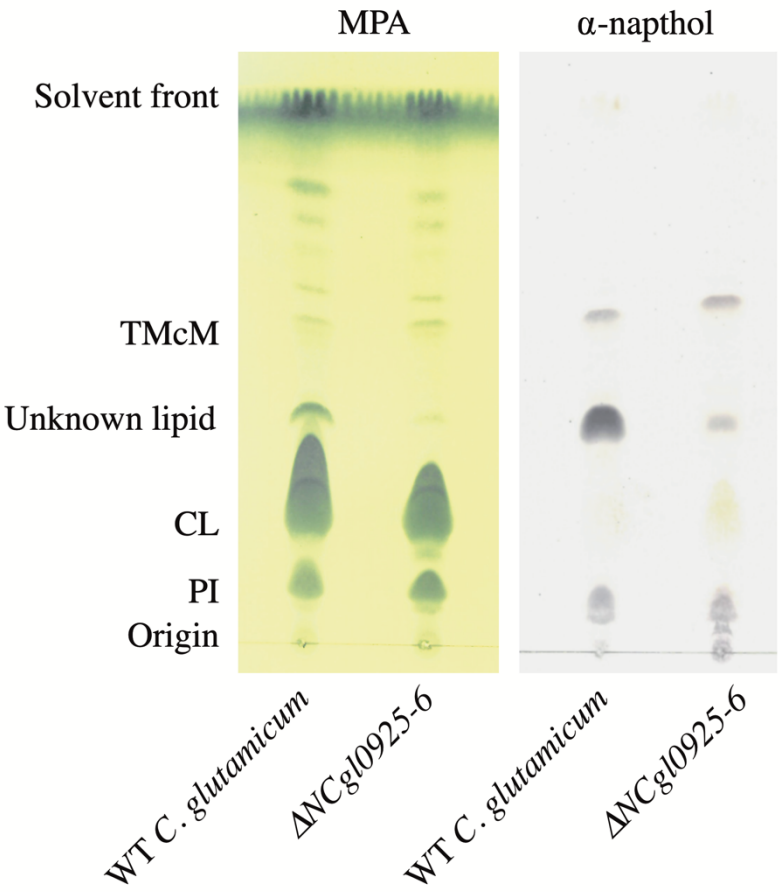

Figure 2.12: TLC analysis of polar lipid extraction fraction from *C. glutamicum* strains. Showing slight depletion of an unknown sugar containing lipid. MPA staining for lipids, *α*-napthol staining for sugars. Solvent system- 30: 8: 1 chloroform: methanol: water. TMcM-trehalose monocorynemycolate, CL- cardiolipin, PI-phosphatidylinositol.

TLC analysis of the remaining extractable lipids (Method 6.12.1) from *C. glutamicum* strains resulted in the determination of a similar phenotype to the apolar inside and apolar outside fractions, with a depletion, but crucially not loss, of the same sugar containing lipid in the *C. glutamicum*ΔNCgl0925-0926 double deletion mutant, that was absent in the previously extracted fractions (Figure 2.12).

Initial characterisation of the lipid characterisation of the WT *C. glutamicum* and the *C. glutamicumΔNCgl0925-0926* mutant identified a loss of a sugar containing lipid. The most notable reductions were in the lipid fractions composed of mostly outer membrane lipids (Figures 2.10, 2.11), consistent with a PIM species. However, the nature of the extraction method does not lend itself to the determination of the precise location of the depleted lipid.

2.2.8: Characterization of the cell wall bound lipid phenotype of WT *C. glutamicum*, and *C. glutamicumΔNCgl0925- 0926*:

To determine if the loss of an extractable free lipid from the bacteria also resulted in an alteration of the cell wall bound lipids, lipids were extracted from *C. glutamicum* cells which had previously been treated to remove all non-covalently bound lipids and analysed by TLC.

Cell wall bound lipid extractions (Method 6.12.4) show no significant changes in the cell wall bound lipids (Figure 2.13), suggesting that the depleted lipid does not serve as a source of fatty acids, or corynemycolic acids for attachment to the cell wall. We did not expect to see changes in the lipid composition of the cell wall core, as there is no published evidence suggesting that the PIM species act as a source of fatty acids for attachment to the cell wall.

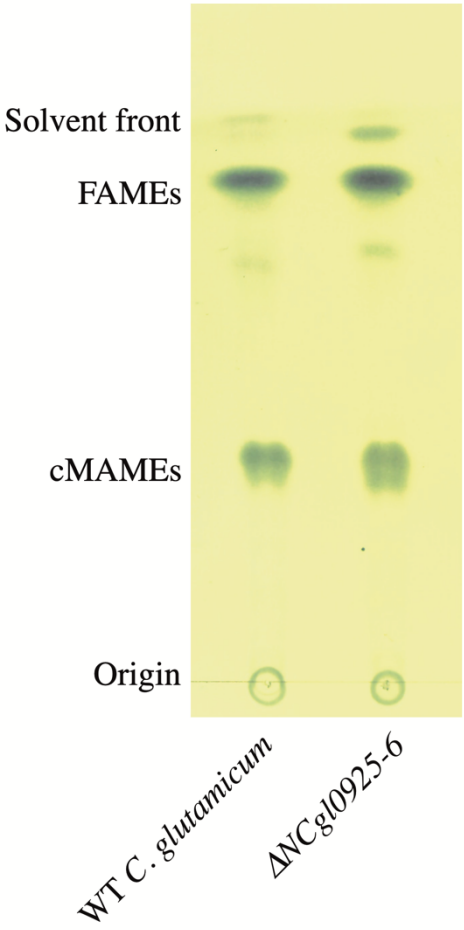

Figure 2.13: TLC analysis of *C. glutamicum* cell wall bound lipid extraction. No significant change in the cell wall bound lipids, detectable between the WT *C. glutamicum and C. glutamicum*ΔNCgl0925- 0926 double deletion mutant. Solvent system: 95: 5 Petroleum ether 60-80: acetone, lipids visualised with MPA.

2.2.9: Characterization of the outer and inner membrane lipid phenotype of WT *C. glutamicum*, and *C. glutamicum*ΔNCgl0925- 0926:

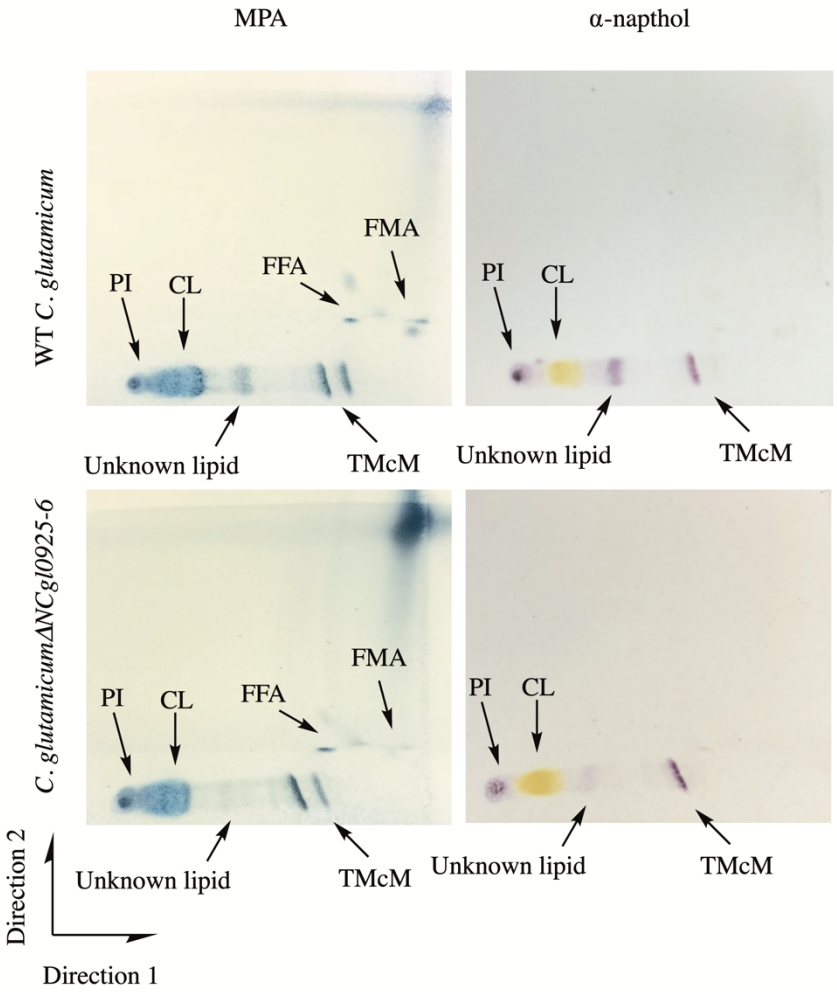

Figure 2.14: TLC analysis of outer membrane lipid extraction of *C. glutamicum* strains. Showing depletion in the level of unknown, sugar containing lipid present in the outer membrane in the WT *C. glutamicum* but substantially reduced in the *C. glutamicumΔNCgl0925- 0926* double deletion mutant. MPA staining for lipids, *α*-napthol staining for sugars. Solvent system: direction 1- 30: 8: 1 chloroform: methanol: water, direction 2- 70: 30: 1 hexane: diethyl ether: acetic acid. FMA- free mycolic acid, FFA- free fatty acid, TMcM- trehalose monocorynemycolate, CL- cardiolipin, PI- phosphatidylinositol.

Upon observation of a lipid depletion phenotype in the polar-apolar lipid extraction of the *C. glutamicum*Δ*NCgl0925- 0926* double deletion strain, determination of the location of the lipid was essential for the full characterisation of the effect of the loss of *NCgl0925* and *NCgl0926*

on the composition of the outer membrane. If NCgl0925 and NCgl0926 form the transporter for the PIMs (which are found in both the outer and inner membrane), a selective extraction of the *C. glutamicum* outer membrane is essential to fully characterise the effect of the gene loss.

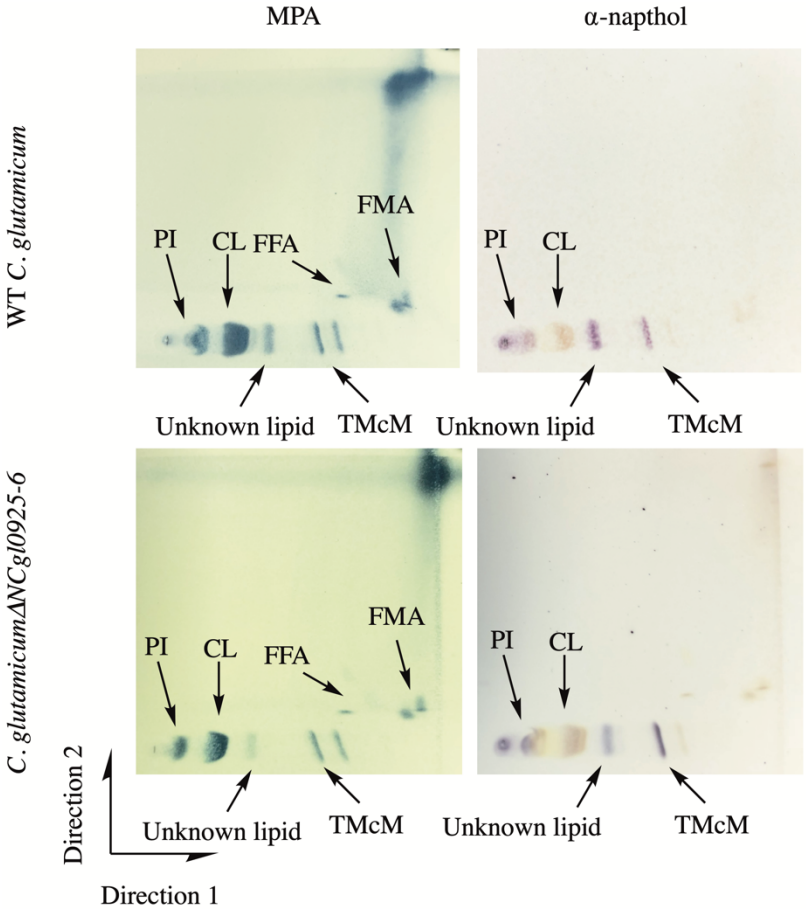

Figure 2.15: TLC analysis of inner membrane lipid extraction from *C. glutamicum* strains. No significant changes to the lipid composition were detectable between the inner membrane extraction of the WT and the *C. glutamicumΔNCgl0925- 0926* double deletion mutant. MPA staining for lipids, α-napthol staining for sugars. Solvent system: direction 1- 30: 8: 1 chloroform: methanol: water, direction 2- 70: 30: 1 hexane: diethyl ether: acetic acid. FMA- free mycolic acid, FFA- free fatty acid, TMcM- trehalose monocorynemycolate, CL- cardiolipin, PI- phosphatidylinositol.

Analysis of the separated outer and inner membrane fractions (Method 6.12.2) by TLC showed loss of the same unknown sugar containing lipid in the outer membrane fraction (Figure2.14), while maintaining equivalent levels in the inner membrane fraction (Figure 2.15).

This depletion of the unknown lipid in the outer membrane suggests that the loss of the lipid is in the outer, mycomembrane, where the loss of a transporter for a lipid found in both the inner and outer membrane is likely to be determined leads to further support of the hypothesis that NCgl0925 and NCgl0926 are responsible for the export of a sugar containing phospholipid in *C. glutamicum*.

Some contamination of the outer membrane fraction was observed, through the detection of a carotenoid species in the outer membrane fraction, a lipid known to be only present in the inner membrane (Bansal-Mutalik and Nikaido, 2011). As there is detectable contamination of the outer membrane fraction with inner membrane lipids, the detection of some unknown lipid is likely to be caused by contamination of the inner membrane lipids in the outer membrane fraction.

2.2.10: Surface lipid phenotype characterization of WT *C. glutamicum*, and *C. glutamicum*Δ*NCgl0925- 0926*:

To determine the location of the depleted lipid, reverse micellar extraction of cell surface lipids was used to selectively remove the surface lipids without disturbing the inner membrane. Reverse micelles are functionally distinct from micelles as the solvent system used for solubilising the detergent is an apolar one, such as heptane, rather than a polar solvent such as water, resulting in the hydrophobic regions of the molecule are exposed, rather than the polar

region. Sodium docusate (AOT) has been studied as a method for the selective extraction of the outer membrane lipids (Bansal-Mutalik and Nikaido, 2014, 2011). This extraction method selectively extracts lipids either through insertion into micelles (Figure 2.16B) or solubility in heptane.

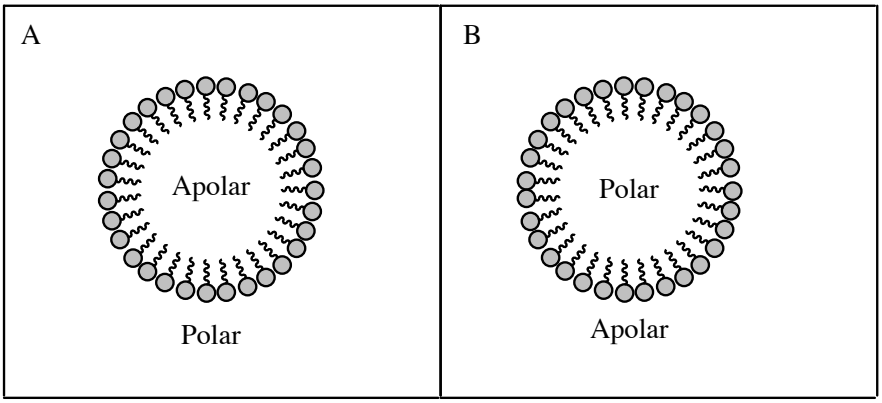

Figure 2.16: Polar characteristics of standard and reverse micelles. A) Standard sodium docusate micelles, where the apolar regions of an amphipathic molecule are sequestered from the polar solvent. B) Reverse sodium docusate micelles, where the polar regions of an amphipathic molecule are sequestered from the apolar solvent.

Initial characterisation of the functionality of the lipid extraction method was used to separate the lipids extractable by solvent and those extractable by the action of the reverse micelles (Figure 2.17).

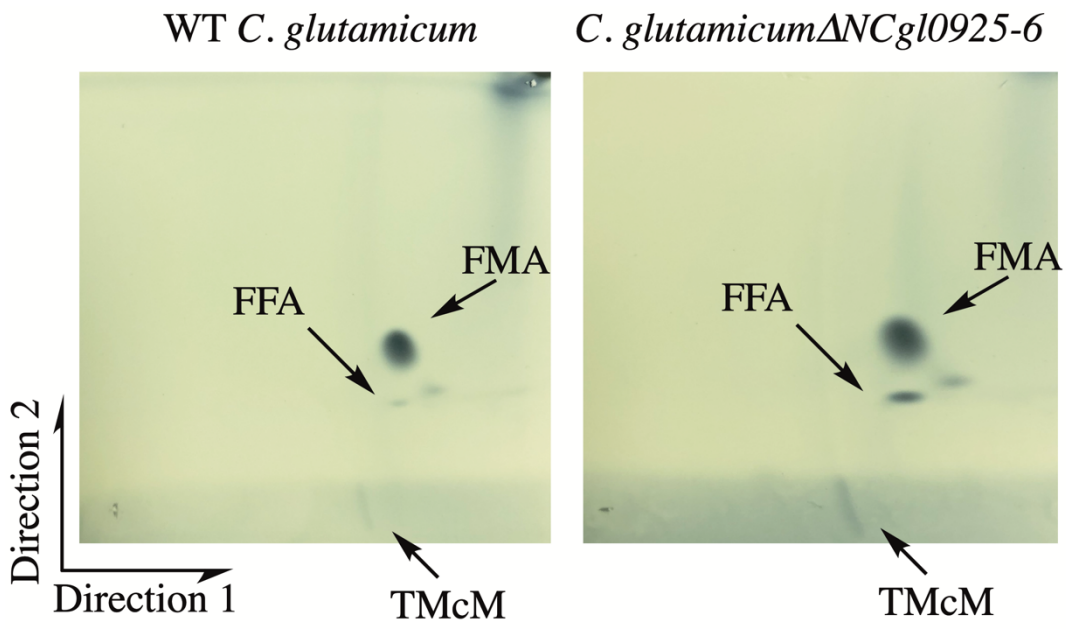

Figure 2.17: TLC analysis of lipids extractable from *C. glutamicum* with heptane. TLCs showing partial extraction of the outer membrane by use of extraction method not containing AOT. A) lipids extracted from the WT *C. glutamicum*, B) lipids extracted from the *C. glutamicumΔNCgl0925- 0926* double deletion mutant. Solvent system: direction 1- 30: 8: 1 chloroform: methanol: water, direction 2- 70: 30: 1 hexane: diethyl ether: acetic acid. FMA- free mycolic acid, FFA- free fatty acid, TMcM- trehalose monocorynemycolate.

Extraction of the surface lipids (Method 6.12.3) shows a depletion in the same sugar containing lipid identified in both the polar- apolar lipid extraction, and the inner membrane- outer membrane lipid extraction, confirming that the lipid lost is present on the surface of then cell. To confirm the restoration of functionality of the complementation vectors reverse micellar extraction was repeated on the complemented *C. glutamicum*ΔNCgl0925- 0926 double deletion mutant strains (Figure 2.18).

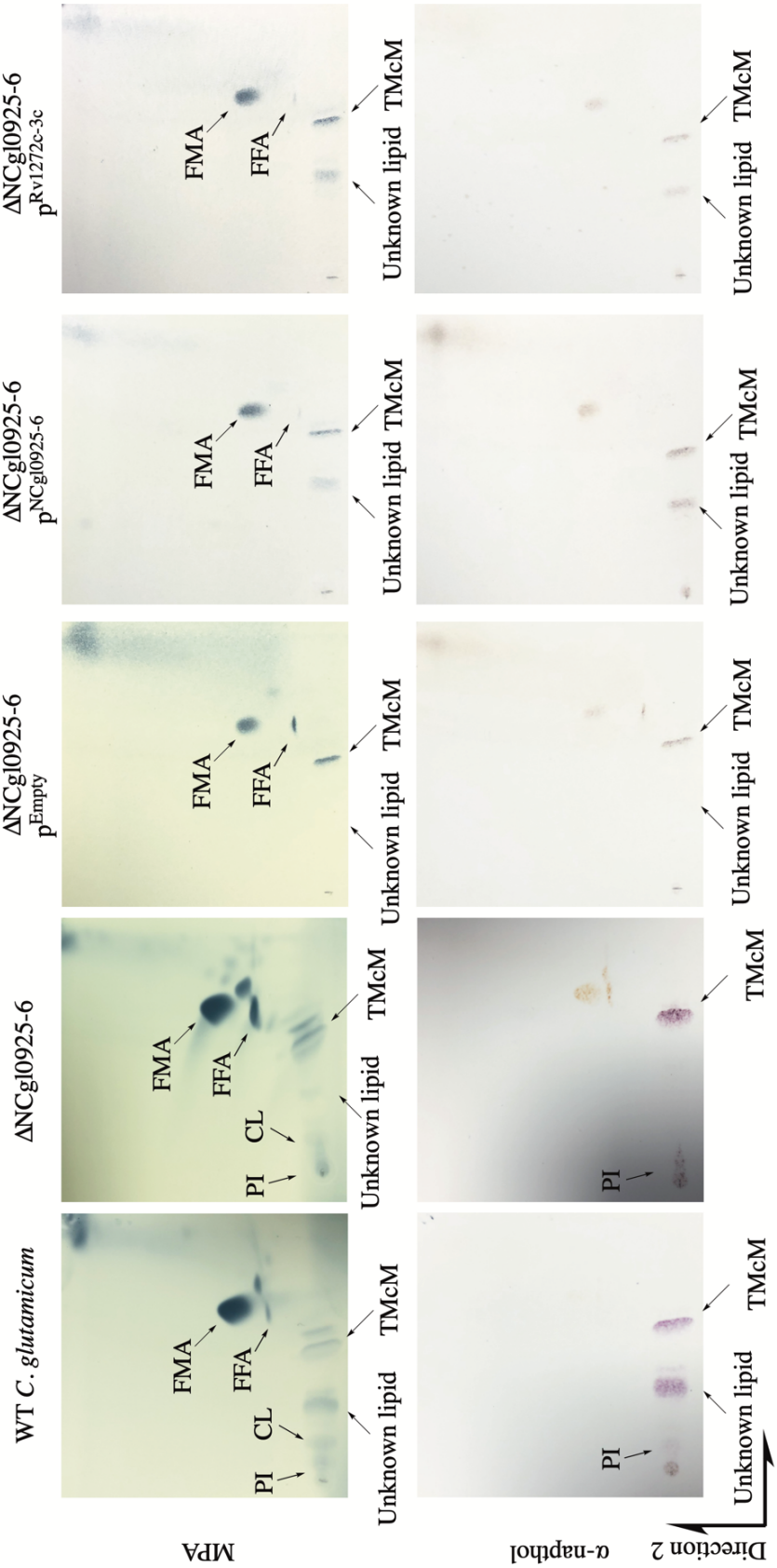

Figure 3.18: Surface lipid extraction of *C. glutamicum* strains. Showing the loss of a surface exposed lipid (labelled unknown lipid), in the ΔNCgl0925-6 mutant, which stains positive for both lipid (MPA) and sugar (α-napthol). The lipid is restored when complemented with either NCgl0925 and NCgl0926 or Rv1272c and Rv1273c. Solvent system: direction 1- 1 chloroform: methanol: water, direction 2- 70: 30: 1 hexane: diethyl ether: acetic acid. FMA- free mycolic acid, FFA- free fatty acid, TMcM- trehalose monocorynemycolate.

Analysis surface lipid composition of the strains recombinantly expressing either the corynebacterial genes deleted, or the *Mtb* orthologs resulting in restoration of WT lipid composition (Figure 2.18). This confirms that the restoration of NCgl0925 and NCgl0926, or complementation with Rv1272c and Rv1273c, results in a reversion to the WT lipid phenotype. Further supporting the hypothesis that the function of NCgl0925 and NCgl0926 is conserved into mycobacterial species.

The significant difference between the reverse micellar lipid extraction and the outer membrane lipid extract is that there is a carotinoid species that runs similarly to CL, in the outer membrane extraction method, which is not detectable in the reverse micellar extraction, which shows that the extraction method is less disruptive to the cell than the water saturated butanol extraction of the outer membrane extraction protocol.

2.2.11: Purification of lipid depleted from surface lipid extractions in *C. glutamicum*Δ*NCgl0925- 0926* from WT *C. glutamicum*:

While the extraction of surface lipids has shown that deletion of NCgl0925 and Ncgl0926 results in the depletion of an unknown lipid on the *C. glutamicum* cell surface, determining the identity of the lipid is essential for assigning function to these proteins. In order to determine the identity of the lipid depleted on the cell surface of the *C. glutamicum*Δ*NCgl0925-0926* mutant, purified lipid extracted from WT *C. glutamicum* was used. Purification of the depleted lipid by preparative TLC yielded an excess of contaminating AOT, due to the similar retention factors (Rf, the distance molecules move on a TLC plate when run in a solvent system system) values in previously defined systems, and relative abundance of the lipid to be purified from other extraction methods making analysis post extraction unreliable. The similar migration

patterns of the unknown lipid and AOT suggested that the lipid is, as predicted, a PIM as they have been seen to have similar migration patterns in the solvent system used (Figure 2.19, AOT) (Bansal-Mutalik and Nikaido, 2011).

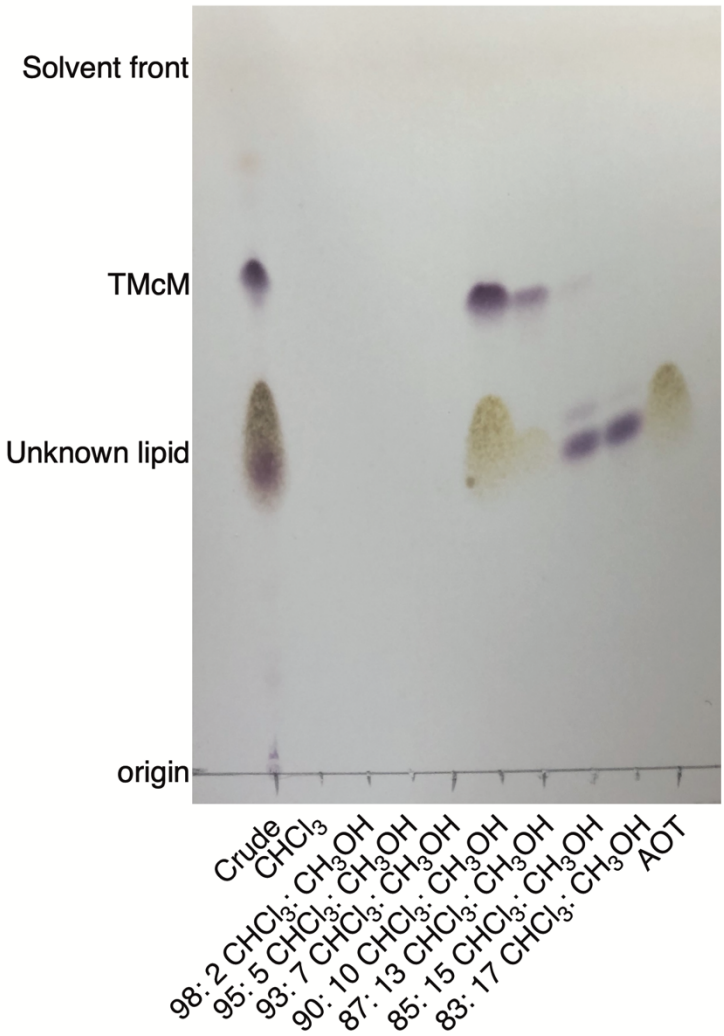

Figure 2.19: TLC analysis of lipid purification by silica column. Showing gradual elution of lipids from the silica column, and the removal of the co-migrating contaminating AOT. Solvent system- 30:8:1 chloroform: methanol: water, visualized using α-napthol. TMcM- trehalose corynemycolate.

Therefore, use of a silica column (Method 6.13), washed with a stepwise chloroform: methanol gradient for gradual removal of lipid contaminants from large scale reverse micellar extraction was used for lipid purification from reverse micellar extracted lipids. Yielding 3 mg of pure lipid with no detectable contaminating AOT by TLC stained with α-napthol (Figure 2.19).

2.2.12: Analysis of surface lipid extracts and purified lipid from extractions from WT *C. glutamicum*, and *C. glutamicum*Δ*NCgl0925- 0926*:

Crude and purified lipid samples were analysed by direct infusion electrospray mass spectrometry (Method 6.15), in both positive and negative flight modes to determine changes in the lipid composition of the crude extracts and the identity of the purified lipid, with minimal fragmentation. Data obtained from the crude and purified lipid samples compared within a single experimental setup between samples compared in Figure 2.20.

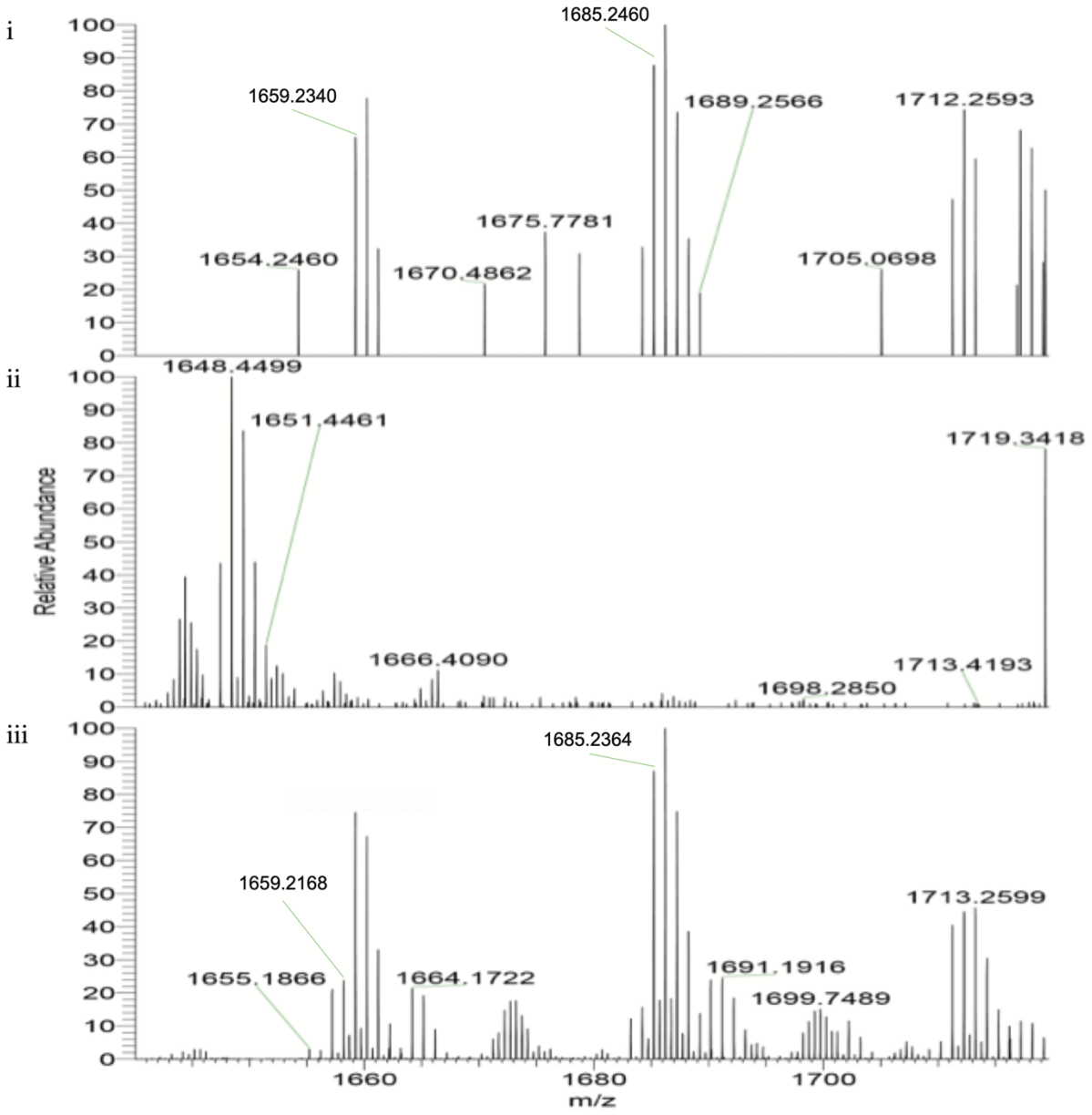

Figure 2.20: Direct infusion electrospray mass spectrometry of lipid samples. Lipid samples diluted in 2: 1 7.5 mM ammonium acetate: chloroform, in positive mode. i) WT *C. glutamicum* reverse micellar extracted lipid sample, ii) reverse micellar lipid extraction from *C. glutamicumΔNCgl0925- 0926* double deletion mutant, iii) purified depleted lipid extracted from WT *C. glutamicum*.

Comparison of the crude reverse micellar extractions from reverse micellar lipid extractions from WT *C. glutamicum*, *C. glutamicum*Δ*NCgl0925- 0926* double deletion mutant, and purified lipid seen to be depleted in the *C. glutamicum*Δ*NCgl0925- 0926* double deletion

mutant strain (Figure 2.20). Figure 2.20ii shows the *C. glutamicum*ΔNCgl0925- 0926 double deletion mutant having a loss of peaks at m/z: 1659.2340 and 1685.2640. Masses obtained from mass spectrometry were compared to structural models of various PIM species, such as PIM_1 PIM_2, Ac_1PIM_2 and Ac_2PIM_2 (Figure 2.21), and found to correspond to sodium adducts of Ac_2PIM_2 species with the difference in mass corresponding to changes in the fatty acid

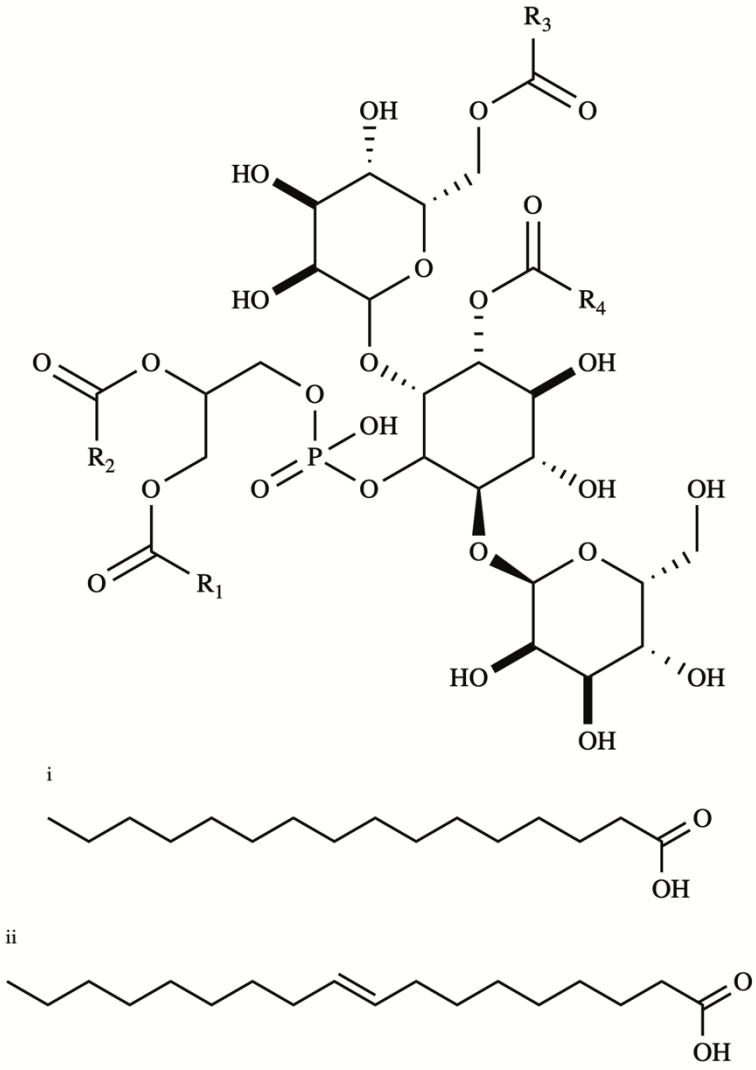

Figure 2.21: Structural model of *C. glutamicum* Ac_2PIM_2. Ac_2PIM_2 structure used to determine the identity of the lipid purified from WT *C. glutamicim*, and reverse micellar lipid extraction fractions from WT *C. glutamcicum* and *C. glutamicumΔNCgl0925- 0926* double deletion mutant. $R_{1\text{-}4}$ denote attachment of fatty acyl chains, where in the case of PIM_2 and Ac_1PIM_2 R_3 and R_4 are H. Fatty acid chains present in the identified lipid modelled in un-esterified form i) C16:0, ii) C18:1

composition of the lipid, either C16:0 or C18:1 (Figure 2.21i and 2.21ii respectively). Data collected from the purified lipid showed peaks at m/z: 1659.2168 and 1685.2364, supporting the hypothesis that the change in the spectra is due to the loss of Ac_2PIM_2 from the mutant.

2.2.13: SDS-PAGE analysis of lipoglycan extractions from WT *C. glutamicum*, and *C. glutamicum*Δ*NCgl0925- 0926*:

As both Cg-LM and Cg-LAM can be generated from a PIM anchor and the identification of the depleted lipid to be Ac_2PIM_2, the cell lipoglycan composition was analysed, with the expectation that there would be a change in the composition due to the loss of one of the anchors. Howeverm due to the presence of an alternative Gl-A anchored unit, the change was not expected to be as significant as it would be in mycobacterial species.

Extraction and analysis of the lipoglycan fraction (Methods 6.16.1, 6.17.1, 6.17.2) of the *C. glutamicum* lipoglycans in both the WT *C. glutamicum* and *C. glutamicum*Δ*NCgl0925- 0926* double deletion mutant strain show that there is a slight change in the overall size of the lipoglycans, with both the Cg-LAM being slightly smaller than the in the WT *C. glutamicum* strain. However, complementation with either the *C. glutamicum* or the *Mtb* genes does not fully restore the WT *C. glutamicum* phenotype (Figure 2.22).

The alteration of the lipoglycan profile is expected as the loss of *NCgl0925* and *NCgl0926* leads to the depletion of PIMs on the external face of the cell, and PIM species act as an anchoring lipid for Cg-LM and Cg-LAM the alteration of the ratio of anchors will likely affect the synthesis of lipoglycans on the external face of the cytoplasmic membrane.

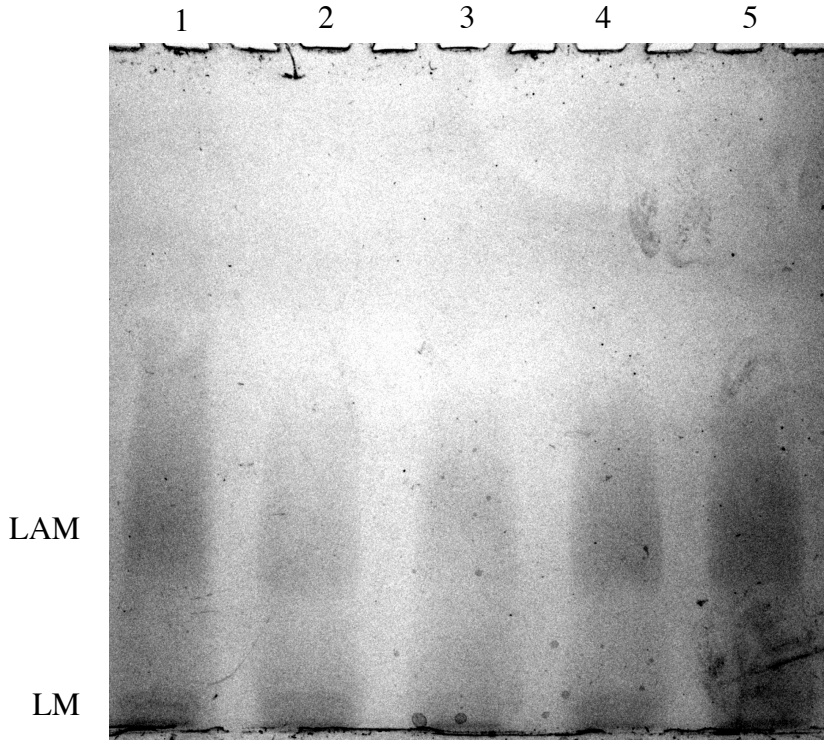

Figure 2.22: SDS-PAGE analysis of lipoglycan extractions from *C. glutamicum*, visualised using silver staining. 1) WT *C. glutamicum*, 2) *C. glutamicum*ΔNCgl0925-NCgl0926, 3) *C. glutamicum*ΔNCgl0925- 0926 pEKEx3, 4) *C. glutamicum*ΔNCgl0925- 0926 pEKEx3- NCgl0925- 0926, 5) *C. glutamicum*ΔNCgl0925- 0926 pEKEx3-Rv1272c-1273c. Showing a slight decrease in the upper end of the size of LAM, with minimal impact on the LM. This reduced change is likely due to the presence of the an alternate lipoglycan anchor.

2.2.14: Monosaccharide composition analysis of lipoglycan extractions from WT *C. glutamicum*, and *C. glutamicum*Δ*NCgl0925- 0926*:

As the profiles of the lipoglycan extractions showed potential differences, the overall sugar composition was predicted to be altered. To determine the sugar composition of the lipoglycans, extracted lipoglycan mixture was hydrolysed, and derivatized to form aditol acetates in order to improve the separation when using gas chromatography (GC Methods 6.18.1, 6.18.2, Appendix 3). Derivatized monosaccharides were analysed using GC to quantify the ratio of arabinose to mannose and inositol in the overall extraction.

Table 2.3: Arabinose: Mannose: inositol ratios of aditol acetate derivatised lipoglycan extractions from *C. glutamicum* strains.

	Ara:Man:Ino
WT *C. glutamicum*	1:33.4:1.3
C. glutamicum△NCGL0925-0926	1:6.2:0.6
C. glutamicum△NCGL0925-0926 pEKEx3	1:11.7:0.6
C. glutamicum△NCGL0925-0926 pEKEx3-NCgl0925-0926	1:11.2:0.6
C. glutamicum△NCGL0925-0926 pEKEx3-Rv1272c-1273c	1:14.2:0.5

Composition determination of aditol acetate derivatised Cg-LM and Cg-LAM (Appendix 3) resulted in two peaks corresponding to arabinose (retention time ~ 9.1- 9.5 min), mannose (retention time ~ 12.4-12.6 min), and inositol (retention time ~ 14.6- 15 min). The analysis of the resulting spectra (Table 2.3), lead to the determination that the arabinose: mannose: inositol ratio changes from 1:33.4: 1.0 in the WT *C. glutamicum* strain, to 1:6.2: 0.6 in the *C. glutamicum*Δ*NCgl0925-0926* mutant. Analysis of the lipoglycan composition of the *C. glutamicum*Δ*NCgl0925-0926* pEKEx3 strain gave a ratio of 1: 11.7: 0.6 arabinose: mannose: inositol, while the *C. glutamicum*Δ*NCgl0925-0926* pEKEx3-*NCgl0925-0926,* and *C.*

*glutamicum*Δ*NCgl0925-0926* pEKEx3-*Rv1272c-1273c* strains gave mannose: arabinose ratios of: 1:11.2: 0.6, and 1:14.2: 0.5 respectively.

While the change in the ratio of arabinose to mannose and inositol is expected to be different to the WT *C. glutamicum* in both the *C. glutamicum*Δ*NCgl0925- 0926* double deletion mutant and the *C. glutamicum*Δ*NCgl0925- 0926* pEKEx3 strain, the recombinant expression of both the corynebacterial and *Mtb* genes do not restore the WT *C. glutamicum* ratio, instead maintaining the ratio found in the *C. glutamicum*Δ*NCgl0925- 0926* pEKEx3 strain. This indicates that while the recombinant expression leads to a restoration of the WT strain lipid and lipoglycan size profile, there is an impact on the sugar composition of the lipoglycans which remains as yet unexplained.

Additionally, the maintained presence of inositol in the extracted Cg-LM and Cg-LAM in the *C. glutamicum*Δ*NCgl0925- 0926* double deletion mutant, and the *C. glutamicum*Δ*NCgl0925-0926* pEKEx3 strain does not necessitate the presence of inositol anchored Cg-LM and Cg-LAM. This is due to the disruptive nature of the extraction procedure, which does not extract only the surface layers of the, resulting in contaminating PIM species in the extraction. These PIM species can come from either the outer membrane, or the cytoplasmic membrane, and therefore it is probable that the presence of inositol in the extractions, is due to these contaminating cytoplasmic membrane lipids.

2.3: Discussion:

PIMs, LM, and LAM are vital for the integrity of the cell wall. With the PIM species forming a significant portion of the membranes, and LM and LAM involved in the evasion of the immune response, as such understanding of how these molecules are synthesised is important in understanding how mycobacteria interact with their environment. While much of the biosynthetic processes have previously been determined, the transport mechanism has, until now, remained unknown (Abrahams and Besra, 2016; Alderwick et al., 2007).

Our data supports our initial hypothesis that the *Mtb* homologs of MsbA, Rv1272c and Rv1273c, are involved in the transport of PIMs across the inner membrane of *Mtb*. As a clear loss of a lipid on the *C. glutamicum*Δ*NCgl0925- 0926* cell surface was detected and the depleted lipid characterised as Ac_2PIM_2. The complementation of the *C. glutamicum*Δ*NCgl0925- 0926* strain with either NCgl0925 and NCgl0926 or Rv1272c and Rv1273c resulted in a restoration of the WT *C. glutamicum* phenotype in all conditions, with the exception of the arabinose: mannose: inositol ratio in the Cg-LM and Cg-LAM, implies that the function of these genes is conserved across all mycobacteria (Alderwick et al., 2005). The generation of a conditional knockout in a mycobacterial species such as *M. bovis* BCG would allow for the confirmation of this hypothesis.

The presence of Ac_2PIM_2 in the inner membrane lipid extraction fraction supports our hypothesis that the cause of the loss of the surface lipid is due to an export defect, rather than a biosynthetic defect. As Ac_2PIM_2 is present in the inner membrane, we predict that it is present as part of the inner leaflet, with attempts to yield an outer leaflet extraction of the inner membrane unsuccessful. The development of a selective lipid extraction method for extracting

the outer leaflet of an exposed cytoplasmic membrane would allow for further testing of this hypothesis.

Further, the data presented supports that both Rv1272c and Rv1273c are functional transporters within the ABC-transporter superfamily, as while they are predicted to contain the correct elements and consensus sequences, no available literature has confirmed their function (Braibant et al., 2000; Martin and Daniel, 2018).

The determination of the function of NCgl0925 and NCgl0926 fills a gap in the knowledge of the biosynthesis of both the mycobacterial and corynebacterial cell surface and the synthesis of LM and LAM in both mycobacteria, and corynebacteria. This allows for an updated schematic of the biosynthetic pathways of LM and LAM (Figure 2.23), with the addition of NCgl0925 and NCgl0926 as the ABC-transporter responsible for the translocation of Ac_2PIM_2 in *C. glutamicum*.

The maintained presence of Cg-LM and Cg-LAM in the *C. glutamicum*Δ*NCgl0925- 0926* double deletion mutant, is likely formed from the alternative Gl-A anchor. This raises the question of the presence of an additional, as yet uncharacterised, ABC-transporter in *C. glutamicum* responsible for the translocation of Gl-A (Mishra et al., 2008b). With further bioinformatic analysis of the *C. glutamicum* genome required to determine putative transporters, and

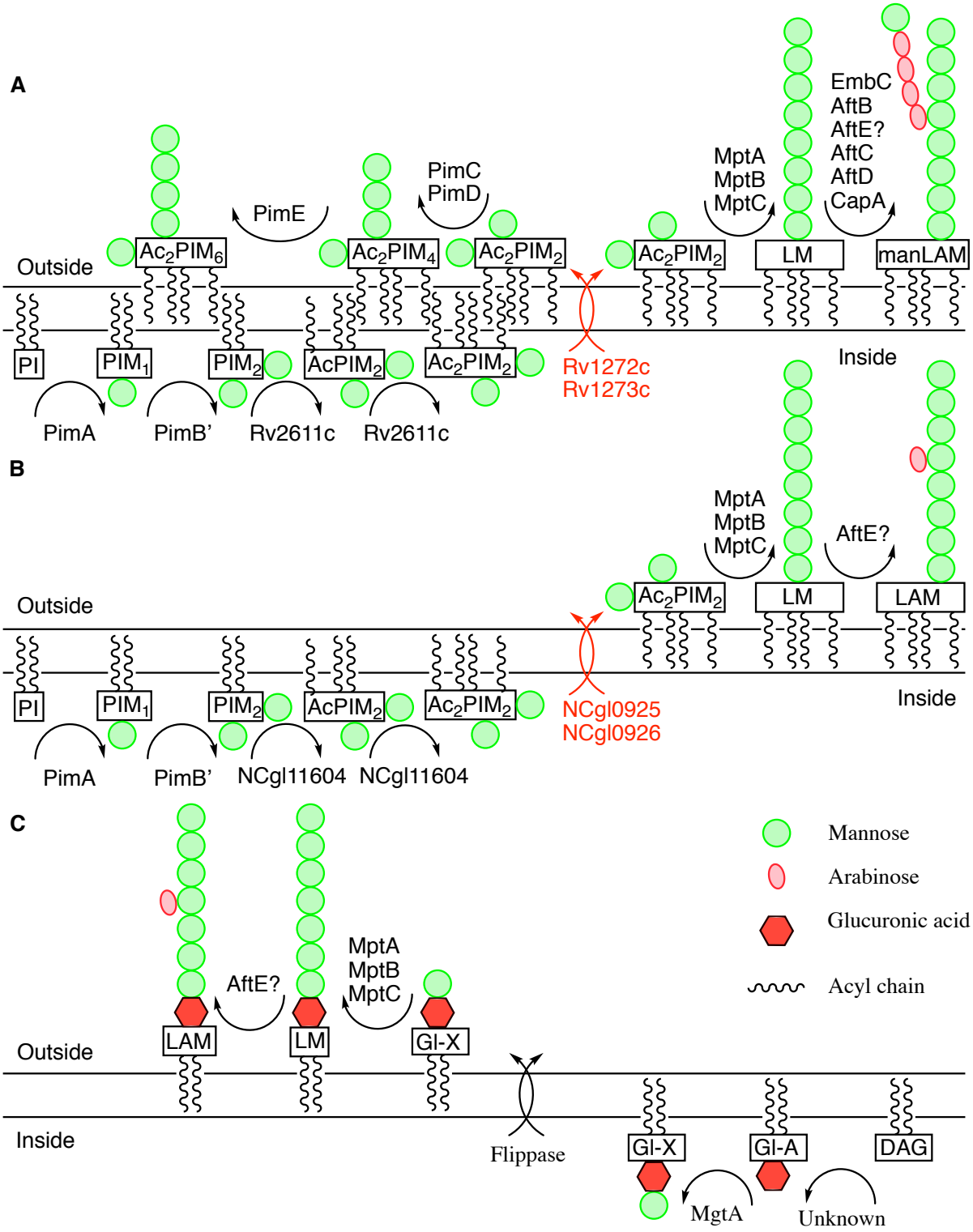

Figure 2.23: Updated biosynthetic pathways for the synthesis of PIMs, LM, and LAM. Updated processes highlighted in red. A) PIM, LM, and LAM synthetic pathway in *Mtb*. B) PIM anchored Cg-LM and Cg-LAM synthetic pathway in *C. glutamicum*. C) GL-A anchored pathway for the Cg-LM and Cg-LAM synthesis in *C. glutamicum*.

characterisation of the identified genes to determine the *C. glutamicum* genes responsible for the translocation of this alternative lipoglycan anchoring lipid.

The inability to generate a double deletion mutant in *M. smegmatis* indicates that the deletion of both MSMEG_5008 and MSMEG_5009 is lethal (Cox et al., 2016), therefore at least one of these genes must be present for cell viability. The generation of a conditional deletion mutant with complementation with MSMEG_5008 and MSMEG_5009 expression under separate control would either confirm or disprove this hypothesis. Additionally, due to the use of a double deletion mutant in *C. glutamicum* to determine this phenotype further research into the level of redundancy of these genes would be required, with characterisation of the effect of complementation of a double deletion mutant with individual genes, and investigation of the phenotype of single deletions of both NCgl0925 and NCgl0925.

Investigation into the *in vivo* conformation of these proteins is necessary, as predictions into the formation of a heterodimer remain predictions (Braibant et al., 2000). This requires *in vivo* or *in vitro* confirmation, either by bacterial two-hybrid, or far Western blotting (Lim et al., 2019; Martin and Daniel, 2018). If positive these results would suggest either the formation of a single heterodimeric transporter, or an equilibrium between the formation of hetero- and homo- dimeric isoforms. A negative result would suggest the formation of two distinct homodimeric transporters, likely with differing affinities to PIM species.

In addition to the characterisation of the conformation of these proteins, determination of where they localise within the cell of the bacteria and how this changes during the replication cycle of the bacteria would provide insight into the maintenance of the cytoplasmic membrane (Heinkel et al., 2019). As it is possible that the transporter could disperse across the entirety of

the bacteria, or remain localised to a particular region if they reside within a functional membrane microdomain (Wagner et al., 2017). Determination of localisation within the cell would enable a more nuanced understanding of synthesis of the external membrane as proteins required for the transport of PIMs to the outer membrane would likely interact with the transport mechanism to the external face of the membrane, as the transporters would be likely to have an increased PIM presence and therefore would increase the efficiency of transport to the outer membrane.

Investigation of the physical structure of these proteins would provide insight into the mechanism by which the PIMs are transported across the membrane, and would allow for structure-based drug design targeting this protein (Méndez et al., 2019; Skalic et al., 2019). Which due to the inability to generate a double deletion mutant in *M. smegmatis* is likely essential could lead to the development of a novel therapeutic agent for the treatment of TB (Cox et al., 2016).

Chapter 3:

Investigation of SNPs involved in corynebacterial EMB resistance on the corynebacterial cell envelope

3.1: Introduction:

The *Mtb* genome includes three arabinofuranosyl transferases (AraTs) (EmbA, EmbB and EmbC) within a single operon located in the genome at Rv3793-Rv3795, embCAB. Individually, these AraT genes are non-essential, however when either *embA* or *embB* are disrupted the other is predicted to become essential due to a redundancy in their function (Alderwick et al., 2005). Both EmbA and EmbB are involved in the synthesis of the arabinian domains in AG, which is serves to connect the outer myco-membrane to peptidoglycan via the galactan core. Conversely, EmbC is involved only in the synthesis of the arabinian domains of LAM (Escuyer et al., 2001; Zhang et al., 2003).

The EmbCAB proteins have been the subject of research due to the high frequency of mutations found in *Mtb* strains resistant to EMB, which led to the naming of these proteins (Abrahams and Besra, 2016; Belanger et al., 1996; Takayama and Kilburn, 1989; Tsukamura, 1965).

While mycobacteria are able to tolerate the deletion of either EmbA or EmbB with minor changes to the terminal domain of the AG, the deletion of both EmbA and EmbB together is lethal, which has made characterising the function of these proteins challenging. In order to better characterise the effect of the loss of both these genes, the *Mtb* model organism *C. glutamicum* has been used (Alderwick et al., 2005; Batt et al., 2010). The *C. glutamicum* genome inclused a single Emb protein, Cg-Emb, which functions as a model for the mycobacterial EmbA and EmbB. The major reason for the use of *C. glutamicum* for the study of AG biosynthesis is due to the ability of *C. glutamicum* to tolerate the deletion of Cg-Emb in media supplemented with sorbitol (which acts as an osmoprotectant), preventing the bacteria

from lysing due to the inability to maintain a structurally sound cell wall (Alderwick et al., 2005; Jankute et al., 2018).

The deletion of *Cg-emb* results in an almost complete loss of arabinose from the AG, with only the priming arabinose residues remaining. The deletion of *Cg-emb* also results in the total loss of the cell wall bound corynemycolic acid methyl esters (cMAMEs), due to the inability to extend the primed branching points of the arabinan domains, and the resulting loss in the attachment site of the cMAMEs, which anchor the mycobacterial outer membrane (Figure 1.10, Figure 1.16) (Alderwick et al., 2005).

The function of the Emb proteins is conserved between the *Mtb* and *C. glutamicum*, with all Emb proteins acting as arabinosyl transferases, formed of two domains, a domain comprised of transmembrane helices, and a binding domain exposed on the periplasm (Figure 3.1). The function of *Mtb* EmbA and EmbB, is the extension of the arabinose branches after the initial priming of the branch point by the attachment of the single Ara*f* catalysed by AftA. The Emb proteins then extend the branch through the synthesis of $\alpha(1\rightarrow5)$ glycosidic linkages, with DPA acting as the source of arabinose (Alderwick et al., 2005).

Comparison of the predicted tertiary structures of mycobacterial and corynebacterial Emb proteins shows significant similarities between the *Mtb* EmbA and EmbB, and Cg-Emb (Seidel et al., 2007b). Prediction of the numbers of transmembrane helices of *Mtb* EmbA and EmbB results in the prediction of an N-terminal domain composed of 11- 13 transmembrane helices (Escuyer et al., 2001), while the N-terminal domain of Cg-Emb in *C. glutamicum* is predicted to contain 15 transmembrane helices (Seidel et al., 2007b).

The C-terminal domains of all the Emb proteins is a type C lectin, and is strongly conserved within the Corynebacteriales, a diverse group of proteins bound to the membrane which catalyse the transfer of lipid bound sugars onto their substrate rather than nucleotide bound sugars which are only found in the cytoplasm of the bacteria (Alderwick et al., 2011).

The front line drug EMB was discovered in 1961, however the mechanism of action was not determined until significantly later, upon the generation of EMB resistant mutants, and phenotypic analysis of the effects on EMB on whole cells (Belanger et al., 1996; Takayama and Kilburn, 1989; Zumla et al., 2013). However, while the target of EMB has been determined through generation of spontaneous resistant mutations, there has not yet been conclusive mechanistic evidence on how EMB inhibits the Emb protein targets. EMB is specific in inhibiting the Emb proteins, and does not have an impact on other arabinosyl transferases such meaning that it is unlikely to inhibit the active site of Emb as this would likely also result in inhibition of other mycobacterial AraTs. As the active site is likely to share significant similarity as they all rely on the same DPA pool as a source of arabinose and therefore are likely to have similar recognition methods (Alderwick et al., 2006; Birch et al., 2008; Seidel et al., 2007a).

Mtb EmbB has been studied as the site of many point mutations associated with EMB resistance. The mutation of the methionine at position 306, to a hydrophobic residue such as valine, isoleucine, or leucine is associated with both EMB and multidrug resistance (D. Shi et al., 2011; Srivastava et al., 2009). However other mutations in EmbB, in locations such as: codon 406 and 497 (glycine and glutamine respectively in WT EmbB) are frequently seen in EMB resistant strains where no mutation is seen at EmbB306 (D. Shi et al., 2011).

A *C. glutamicum* strain with significantly reduced tolerance to EMB was generated through the deletion of *steA* and *ripA* (Lim et al., 2019). RipA is an endopeptidase which is involved in degrading and recycling peptidoglycan and has been shown to localise to the poles and septa of mycobacterial cells (Chao et al., 2013). As such, a *ripA* deletion mutant affects cell division and leads to increased antibiotic susceptibility due to disrupted daughter cell separation (Hett et al., 2008, 2007). SteA is less well characterized, but has been shown to function as a component of the cytokinetic ring (Lim et al., 2019).

As the *C. glutamicum*Δ*steA*Δ*ripA* strain was generated *C. glutamicum* a strain that shows a loss of three prophage regions when compared to the reference strain (*C. glutamicum* ATCC13032), with unknown functionality. Phenotypic analysis of the strain in comparison to ATCC13032 shows no fitness cost for the bacteria, with an improved tolerance to DNA damage inducing the SOS-response (Baumgart et al., 2013).

Here we aim to characterise the effect of the combined of *steA* and *ripA* double deletion on the cell envelope of *C. glutamicum* that causes susceptibility to EMB, and to characterise any additional effects caused by spontaneously generated point mutations restoring resistance to EMB on the cell envelope.

3.2: Results:

3.2.1: Generation, and mutation mapping of EMB resistant strains of *C. glutamicum*Δ*steA*Δ*ripA*:

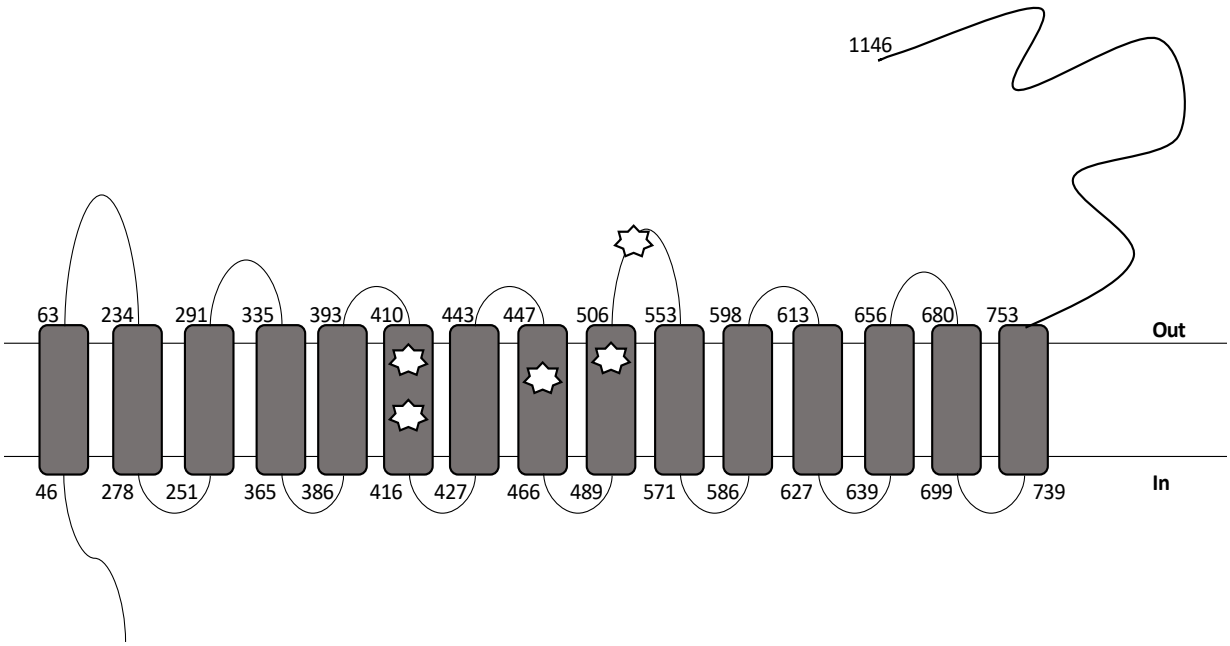

Figure 3.1: Membrane topology and point mutation locations of *C. glutamicum* Emb. Transmembrane helix predicted first and last residue marked. Stars marking position of mutations in the Emb protein resulting in increased tolerance to EMB.

*C. glutamicum*Δ*steA*Δ*ripA* and *C. glutamicum*Δ*steA*Δ*ripA* Cg-Emb point mutations generated by T. Bernhardt's group (Methods 6.3.3, 6.4.1, and 6.4.2). Strains generated from the *C. glutamicum*Δ*steA*Δ*ripA* mutant by the exposure to EMB to produce resistant mutants resulted in various point mutations within the Cg-*emb* gene, producing six strains with restored resistance to EMB, all of which are within the transmembrane domain of the Cg-Emb protein. Genome sequencing of the resistant strains showed no mutations other than the documented *Cg-emb* mutations. The six different point mutations provided for testing are: Cg-Emb^{G411S}, Cg-Emb^{P414T}, Cg-Emb^{A453V}, Cg-Emb^{A453E}, Cg-Emb^{P505L}, and Cg-Emb^{S528A} (Figure 3.1).

3.2.2: Growth rate analysis of WT *C. glutamicum*, *C. glutamicumΔsteAΔripA*, and *C. glutamicumΔsteAΔripA* Cg-Emb point mutant strains:

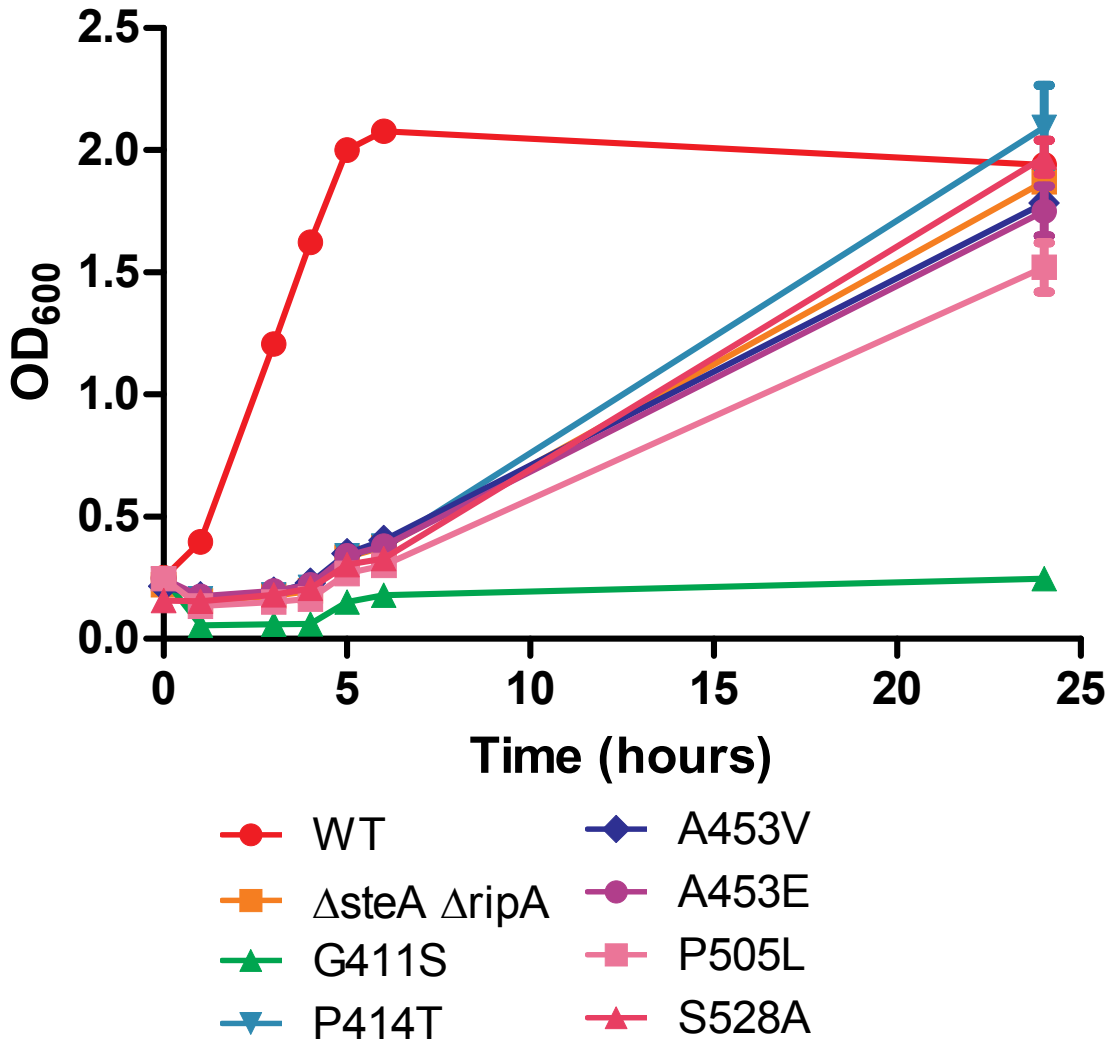

***Figure 3.2*: Growth curves of *C. glutamicum* strains in rich media, measured by OD_{600}.** Biological replicates, n=3. The *C. glutamicumΔsteAΔripA* strain which forms the basis of the Cg-Emb point mutants, shows a slow growth phenotype when compared to the WT *C. glutamicum* up until 24 hours post-inoculation. Of the point mutations in C-gEmb, the Cg-Emb^{P414T}, Cg-Emb^{A453E} mutant strains show no significant difference to the *C. glutamicumΔsteAΔripA* strain at any point. The Cg-Emb^{G411S} mutant strain shows a significant different in growth rate at all time points. The Cg-Emb^{A453V}, Cg-Emb^{P505L}, and Cg-Emb^{S528A} mutant strains show significant differences growth in at least one timepoint when compared to the *C. glutjamicumΔsteAΔripA* strain. All differences calculated using Bonferroni corrected ANOVA, $q > 0.01$. Error bars: Std. deviation, n=3.

To determine the overall fitness cost the deletion of *steA* and *ripA*, required to generate the EMB hypersensitive strain of *C. glutamicum*, and the effect of the point mutations in Cg-Emb which restore resistance to EMB, growth rate analysis was conducted (Method 6.10), with assistance from S. Benedict (Figure 3.2).

Analysis of the growth rate of the WT *C. glutamicum*, *C. glutamicum*Δ*steA*Δ*ripA* strain, and *C. glutamicum*Δ*steA*Δ*ripA* strains with point mutations in Cg-Emb, showed that the loss of steA and ripA results in a significant increase in the lag phase of growth in all strains, with all strains sharing a slowed growth phenotype when compared to the WT *C. glutamicum* until 24 hours post inoculation, where only the *C. glutamicum*Δ*steA*Δ*ripA* Cg-Emb^{G411S} strain has a significant difference in growth to the WT strain ($q > 0.01$) (Figure 3.2).

Comparison of the OD_{600} readings of the *C. glutamicum*Δ*steA*Δ*ripA* strain and the Cg-Emb point mutant strains shows that similar to the comparison of the Cg-Emb^{G411S} strain to the WT *C. glutamicum* strain, there is a significant difference between the OD_{600} at all timepoints, with Cg-Emb^{G411S} showing a significantly slowed growth. The Cg-Emb^{P505L} strain shows significant differences to the *C. glutamicum*Δ*steA*Δ*ripA* strain at 4-, 5-, and 6- hours post-inoculation, with all other differences not significant to $q > 0.01$. Measurement of the Cg-Emb^{A453V} strain at four hours post-inoculation lead to a significant difference when compared to the *C. glutamicum*Δ*steA*Δ*ripA* strain.

This data shows that the deletion of *steA* and *ripA* results in a significant increase in the lag phase of the bacteria, with further some mutations in the Cg-Emb protein leading to a further growth perturbation, while others result in no overall change to the growth phenotype compared to the *C. glutamicum*Δ*steA*Δ*ripA* strain.

3.2.3: Growth rate analysis in media supplemented with sorbitol of WT *C. glutamicum*, *C. glutamicumΔsteAΔripA*, and *C. glutamicumΔsteAΔripA* Cg-Emb point mutant strains:

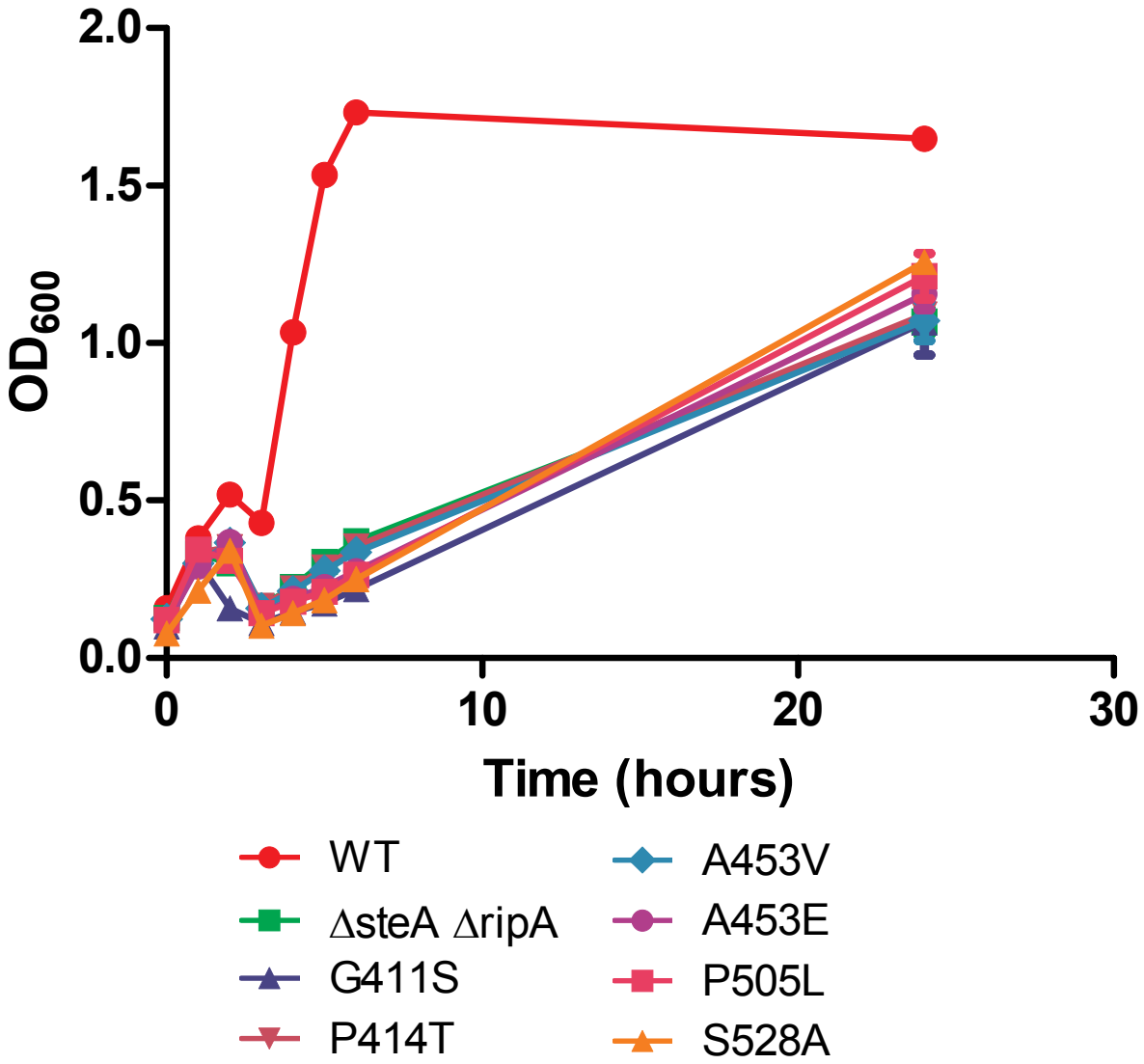

Figure 3.3: Growth curve of *C. glutamicum* strains in rich media supplemented with 0.5 M sorbitol, measured using OD_{600}. Biological replicates, n=3. Similar to growth in un-supplemented media, the *C. glutamicumΔsteAΔripA* strain shows significantly reduced growth at all time points when compared to the WT strain. Both the Emb^{P414T} and Emb^{A453V} straisn show no difference to the *ΔsteAΔripA* strain at any time point. The Emb^{G411S} strain shows a significant difference in all time points until 24 hours post-inoculation. The Emb^{P505L} strain shows a significant difference to the *ΔsteAΔripA* strain at 4-, 5-, and 6- hours post-inoculation, but no significant difference at 24 hours post-inoculation. The Emb^{S528A} strain shows a significant difference to the *ΔsteAΔripA* strain at all point until 24 hours post-inoculation. All differences calculated using Bonferroni corrected ANOVA, $q > 0.01$. Error bars: Std. deviation, n=3.

To determine if the change in the growth rate of the *C. glutamicum*Δ*steA*Δ*ripA* strain relative to the WT *C. glutamicum* strain, and the change in the growth rate of the Cg-Emb^{G411S} strain relative the *C. glutamicum*Δ*steA*Δ*ripA*, is due to a reduction in the structural integrity of the cell wall core, growth rate analysis of the *C. glutamicum* strains was conducted in media supplemented with 0.5 M sorbitol (Method 6.10), with assistance from S. Benedict (Figure 3.3). Sorbitol acts as an osmoprotectant, and has been used to rescue mutants unable to maintain the cell wall in standard media, of particular relevance is the use of sorbitol for growth of the *C. glutamiucm*Δ*emb* strain (Alderwick et al., 2005).

The addition of sorbitol to the media did not result in the restoration of the WT *C. glutamicum* growth rate in the *C. glutamicum*Δ*steA*Δ*ripA* strain, and did result in there being a significant difference in the cell density 24 hours post-inoculation ($q > 0.01$), where in media not containing sorbitol there was no significant difference. Both the Cg-Emb^{P414T} and the Cg-Emb^{A453V} strains showed no significant difference at any timepoint ($q > 0.01$). The Cg-Emb^{A453E} and the Cg-Emb^{P505L} strains show a significant difference at 4-, 5- and 6- hours post-inoculation ($q > 0.01$). Cg-Emb^{S528A} showed a significant difference at all time points expect for 24 hours post-inoculation ($q > 0.01$).

The cause of the drop in OD_{600} at 3 hours post-inoculation is unknown, I hypothesise that this is likely due to an error in the readings at 1- and 2-hours post-inoculation, as the readings from 3-hours are consistent beyond this point.

Analysis of the data generated showed a significant difference between the Cg-Emb^{G411S} strain and the *C. glutamicum*Δ*steA*Δ*ripA* strain at all time points except for 24 hours post-inoculation ($q > 0.01$), while there is still a statistical difference between many of the timepoints, the

difference between the strains growth rates is substantially reduced, with comparison of the timepoints from media containing and not containing sorbitol showing significant differences at all points. This shows that the supplementation of the growth media with sorbitol, while not fully restoring the *C. glutamicum*Δ*steA*Δ*ripA* strain growth phenotype, does significantly improve the ability of the Cg-Emb^{G411S} strain to grow.

As the use of osmoprotectants in bacterial growth media is used to allow for the growth of strains less able to synthesise and maintain a fully functional cell wall. The effect it has on the Cg-Emb^{G411S} mutant strain implies that, while this mutation does not cause the cell wall to become completely non-functional, as the strain is able to grow in un-supplemented media, the change in the Cg-Emb protein likely leads to a reduction in the functionality of Cg-Emb, potentially leading to a hybrid phenotype between the *C. glutamicum*Δ*steA*Δ*ripA* strain and the *C. glutamicum*Δ*Emb* strain characterised by Alderwick et al. 2005.

3.2.4: Cell surface permeability analysis of WT *C. glutamicum*, *C. glutamicumΔsteAΔripA*, and *C. glutamicumΔsteAΔripA* Cg-Emb point mutant strains:

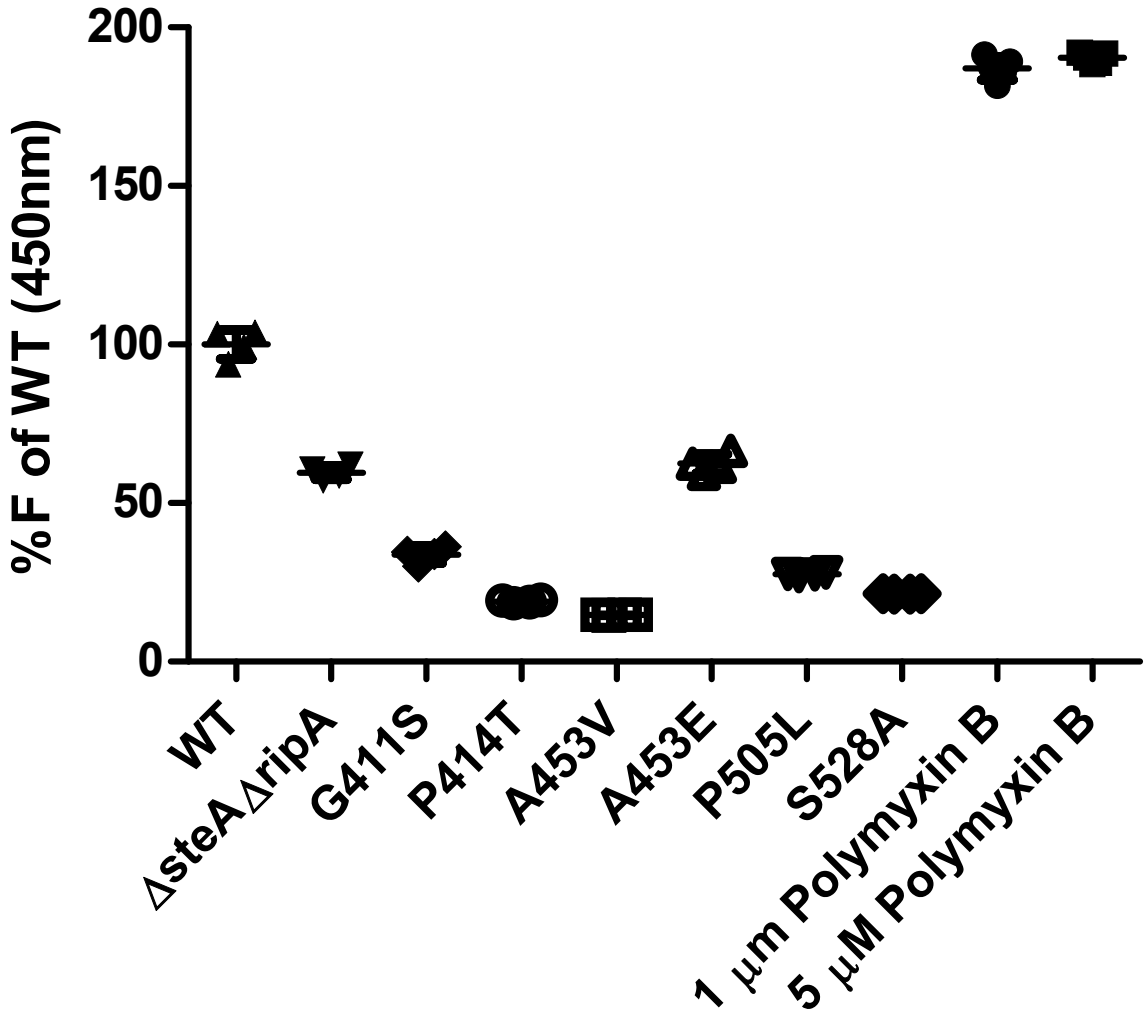

Figure 3.4: Cell surface permeability of *C. glutmicum* strains. Mutations listed are point mutations in Cg-Emb generated from the *C. glutamicumΔsteAΔripA* strain, with only location of the point mutation in Cg-Emb given. The *C glutamicumΔsteAΔripA* mutant shows a significant reduction in permeability, with all mutants except the Cg-Emb^{A453E} mutant resulting in a further reduction in permeability. Polymyxin B used as a positive control to increase permeability. All differences calculated using Bonferroni corrected ANOVA, $q > 0.01$, significantly different values indicated in Table 3.1. Error bars: Std. deviation, n=4

Table 3.1: Bonferroni corrected ANOVA analysis of cell surface permeability testing. Significance level tested to $q > 0.01$. Green indicates significant difference between strains, red indicates no significant difference between strains.

	S528A	P505L	A453E	A453V	P414T	G411S	ΔsteA ΔripA	WT
WT								
ΔsteA ΔripA								
G411S								
P414T								
A453V								
A453E								
P505L								
S528A								

Due to the changes in the growth phenotype of the *C. glutamicum*Δ*steA*Δ*ripA* strain the and Emb point mutant strains, analysis of the permeability of the *C. glutamicum* cell surface was undertaken (Method 6.11) to investigate if there is a change in the permeability of the cells (Figure 3.4, Table 3.1).

Figure 3.4, shows that the *C. glutamicum*Δ*steA*Δ*ripA* strains shows a statistically significant reduction in the permeability of the cell to DPH compared to the WT *C. glutamicum* strain. Furthermore, all mutant strains, with the exception of the Cg-Emb^{A453E} strain show an additional statistically significant reduction in surface permeability (Table 3.1). This shows that there is a significant impact on the permeability of the cell surface to DPH, both in the *C. glutamicm*Δ*steA*Δ*ripA* strain and the Cg-Emb point mutant strains, as well as showing that the degree to which the mutations affect the cell surface is not uniform, potentially due to different effects on the activity of Cg-Emb.

3.2.5: Assessing Antibiotic susceptibility of WT *C. glutamicum, C. glutamicum*Δ*steA*Δ*ripA,* and *C. glutamicum*Δ*steA*Δ*ripA* Cg-Emb point mutant strains:

The reduction in the permeability of the cell is likely to have an impact on the ability of antibiotics to reach their target. Therefore, the effects of the Cg-Emb mutations on the sensitivity to other antibiotics was measured (Table 3.2, Method 6.19). Using antibiotics that target either intra- or extra- cellular enzymes. Amoxicillin is a beta-lactam inhibiting transpeptidation, while chloramphenicol, kanamycin, and streptomycin all inhibit protein synthesis. Rifampicin inhibits transcription, and vancomycin binds to the pentapeptide stem of peptidoglycan to prevent polymerisation (Abrahams and Besra, 2016; Alifano et al., 2015; Bartlett, 1982; Reynolds, 1989; Rolinson, 1994; Zumla et al., 2013). Experiments conducted by S. Benedict.

We found that the *C. glutamicum*Δ*steA*Δ*ripA* strain had MIC_{99} changes when compared to WT *C. glutamicum*, with the point mutations in Cg-Emb resulting in further changes from the *C. glutamicum*Δ*steA*Δ*ripA* strain across a range of antibiotics. Multiple strains expressing Cg-Emb point mutations showed increased resistance to both antibiotics with intracellular and extracellular targets (Table 3.2). However, due to the increased tolerance to stress causing DNA damage, it is possible that some of the changes seen are due to the differences between the ATCC13032 and MB001 strains (Baumgart et al., 2013).

The *C. glutamicum*Δ*steA*Δ*ripA* strain, showed an increase in the MIC_{99} against Kanamycin, Amoxicillin, Chloramphenicol, and Streptomycin, ranging from a 4 to 16-fold increase. However, the change in the resistance was not universal, nor specific to a single target location, with both Rifampicin and Vancomycin both showing no change in MIC_{99}.

Table 3.2: Fold change in MIC of *C. glutamicum* strains. MIC_{99} fold changes measured against either WT *C. glutamicum*, or *C. glutamicumΔsteAΔripA* strain.

Conditional formatting: Green=0 fold change, Yellow= 50 fold change, Red= 200 fold change.

	WT		ΔsteA ΔripA		G411S		P414T		A453V		A453E		P505L		S528A	
	WT	ΔsteA ΔripA	WT	ΔsteA ΔripA	WT	ΔsteA ΔripA	WT	ΔsteA ΔripA	WT	ΔsteA ΔripA	WT	ΔsteA ΔripA	WT	ΔsteA ΔripA	WT	ΔsteA ΔripA
KAN	1.00	0.06	15.99	1.00	63.97	4.00	46.75	2.92	15.99	1.00	1.00	0.06	31.99	2.00	15.99	1.00
RIF	1.00	1.00	1.00	1.00	1.00	1.00	1.00	1.00	1.00	1.00	1.00	1.00	1.00	1.00	1.00	1.00
VANC	1.00	1.00	1.00	1.00	1.00	1.00	184.40	184.40	1.00	1.00	2.00	2.00	1.00	1.00	1.00	1.00
AMOX	1.00	0.25	4.00	1.00	128.01	32.00	128.01	32.00	2.00	0.50	128.01	32.00	128.01	32.00	128.01	32.00
CHLOR	1.00	0.25	4.00	1.00	16.00	4.00	15.42	3.86	8.00	2.00	16.00	4.00	8.00	2.00	4.00	1.00
STREP	1.00	0.13	8.00	1.00	15.99	2.00	66.41	8.30	8.00	1.00	31.99	4.00	15.99	2.00	15.99	2.00

The various point mutations in the Cg-Emb protein resulted in further changes in the antibiotic sensitivity from the *C. glutamicumΔsteAΔripA* strain. All mutations tested resulted in resistance to Amoxicillin to over 500 µM, except for the Cg-Emb^{A453V} mutant where the strain shows a 2-fold reduction in MIC. However, this decrease compared to the *C. glutamicumΔsteAΔripA* strain MIC_{99} still maintains a 2-fold increase when compared to the WT *C. glutamicum* strain.

Only two of the point mutations in Cg-Emb had an effect on the MIC_{99} of vancomycin, Emb^{P414T} and Emb^{A453A}, resulting in a 184-fold increase, and a 2-fold increase in MIC_{99} respectively. All mutants, except for the Emb^{S528A}, showed an altered MIC_{99} to chloramphenicol. The Cg-Emb^{A453V}, and Cg-Emb^{P505L} strains showing a 2-fold increase, and Cg-Emb^{P414T}, Cg-Emb^{A453E}, and Cg-Emb^{G411S} strains showing a 4-fold increase in MIC_{99}. Streptomycin showed a similar effect, with all strains apart from Cg-Emb^{A453V} showing a change in the MIC_{99}. The Cg-Emb^{P505L}, Cg-Emb^{S528A}, and Cg-Emb^{G411S} strains show a 2-fold increase in MIC, while the Cg-Emb^{A453E} strain shows a 4-fold increase and Cg-Emb^{P414T} strain shows an 8-fold increase.

No strain showed a detectable increased resistance to Rifampicin. The Cg-Emb^{A453V} and Cg-Emb^{S528A} strains showed no change in Kanamycin MIC_{99} compared to the *C. glutamicumΔsteAΔripA* strain, the Cg-Emb^{P505L} strain showed a 2-fold increase in MIC_{99}, the Cg-Emb^{P414T} strain showed a 3-fold increase in MIC_{99}, and the Cg-Emb^{G411S} strain showed a 4-fold increase in MIC_{99}. While Cg-Emb^{A453E} reverted back to WT *C. glutamicum* with a 16-fold decrease in MIC_{99}.

3.2.6: Characterization of the free lipid phenotype of WT *C. glutamicum*, *C. glutamicum*Δ*steA*Δ*ripA*, and *C. glutamicum*Δ*steA*Δ*ripA* Cg-Emb point mutant strains:

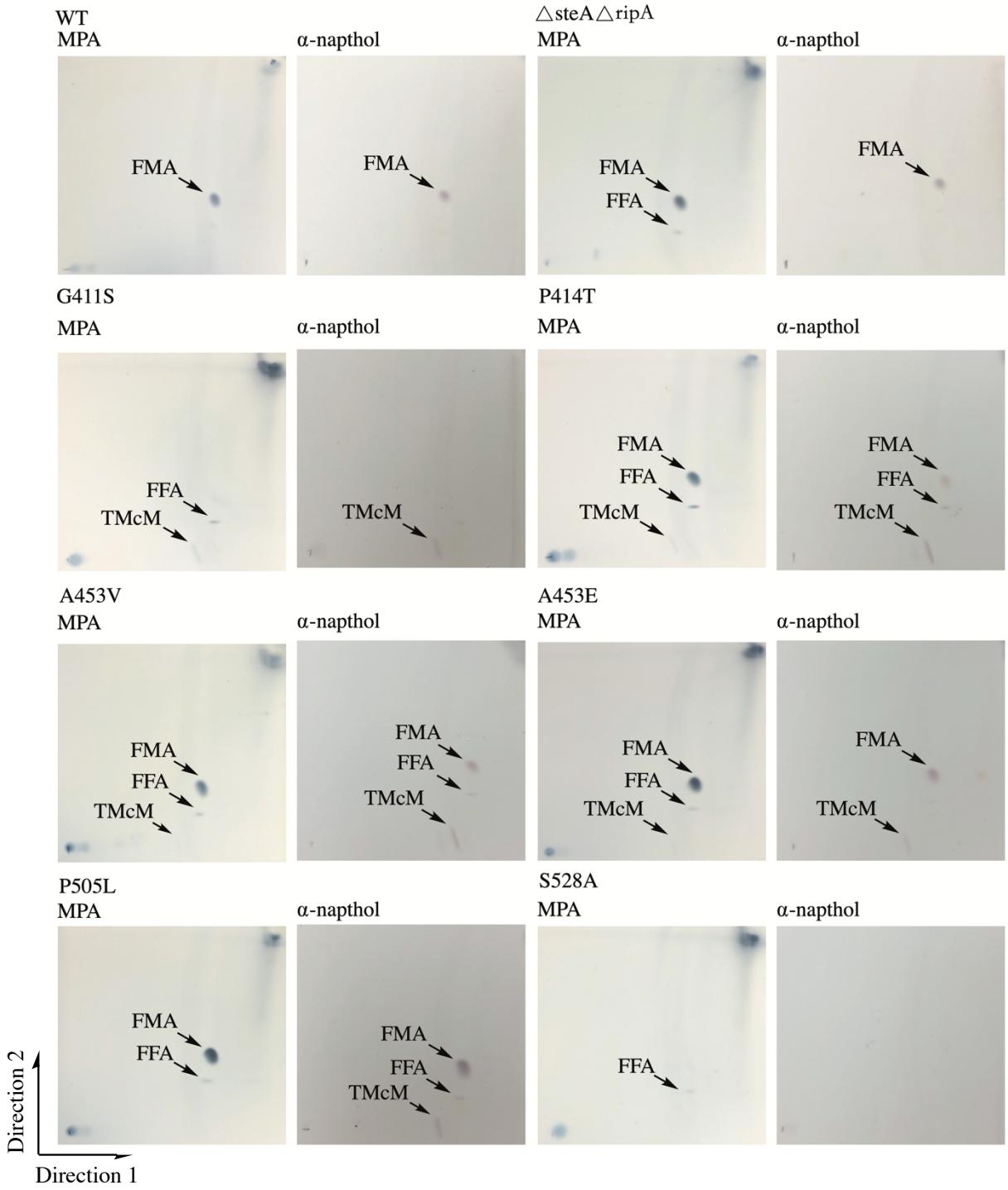

Figure 3.5: TLC analysis of apolar outside lipid extraction from *C. glutamicum* strains. Solvent system: direction 1- 30: 8: 1 chloroform: methanol: water, direction 2- 70: 30: 1 hexane: diethyl-ether: acetic acid. FMA: free mycolic acid, FFA: free fatty acid, TMcM: trehalose corynemycolate.

All strains tested showed significant changes in the permeability of the cell surface (Figure 3.4), as well as antibiotic resistance (Table 3.2). Due to these changes we hypothesised that the free lipid composition of the strains was likely to be altered, and potentially contributed towards these changes. As the lipid composition of the outer membrane forms the key barrier in mycobacterial antibiotic resistance (Abrahams and Besra, 2016).

Characterisation of the lipid composition of the *C. glutamicum*Δ*steA*Δ*ripA* strain and the Cg-*emb* point mutants generated from it (Method 6.12.1), resulted in the identification of subtle changes in the lipid composition, with the *C. glutamicum*Δ*steA*Δ*ripA* strain, and all subsequently generated mutants, showing a slight increase in the relative amount of free fatty acids, present in the apolar outside, compared to the WT *C. glutamicum* strain (Figure 3.5, Table 3.3).

Characterisation of the lipid composition of this fraction in the Cg-Emb mutant strains resulted in further changes to the lipid composition, with the Cg-Emb^{G411S} strain (Figure 3.5, Table 3.3) showing a reduction in the free mycolic acids compared to both the WT *C. glutamicum* and *C. glutamicum*Δ*steA*Δ*ripA* strains, while showing an increase in production of TMcM. The Cg-Emb^{P414T}, Cg-Emb^{A453V}, Cg-Emb^{A453E}, and Cg-Emb^{P505L} strains (Figure 3.5) showed a similar increase in TMcM, however there was no change in the production of free mycolic acids, relative to the *C. glutamicum*Δ*steA*Δ*ripA* strain. While the Cg-Emb^{S528A} strain (Figure 3.5) also showed a similar reduction in the free mycolic acid production to the Cg-Emb^{G411S} strain.

Characterisation of the remaining extractable apolar lipids, results in the reduction of free mycolic acids, in the *C. glutamicum*Δ*steA*Δ*ripA* strain, compared to the WT *C. glutamicum*

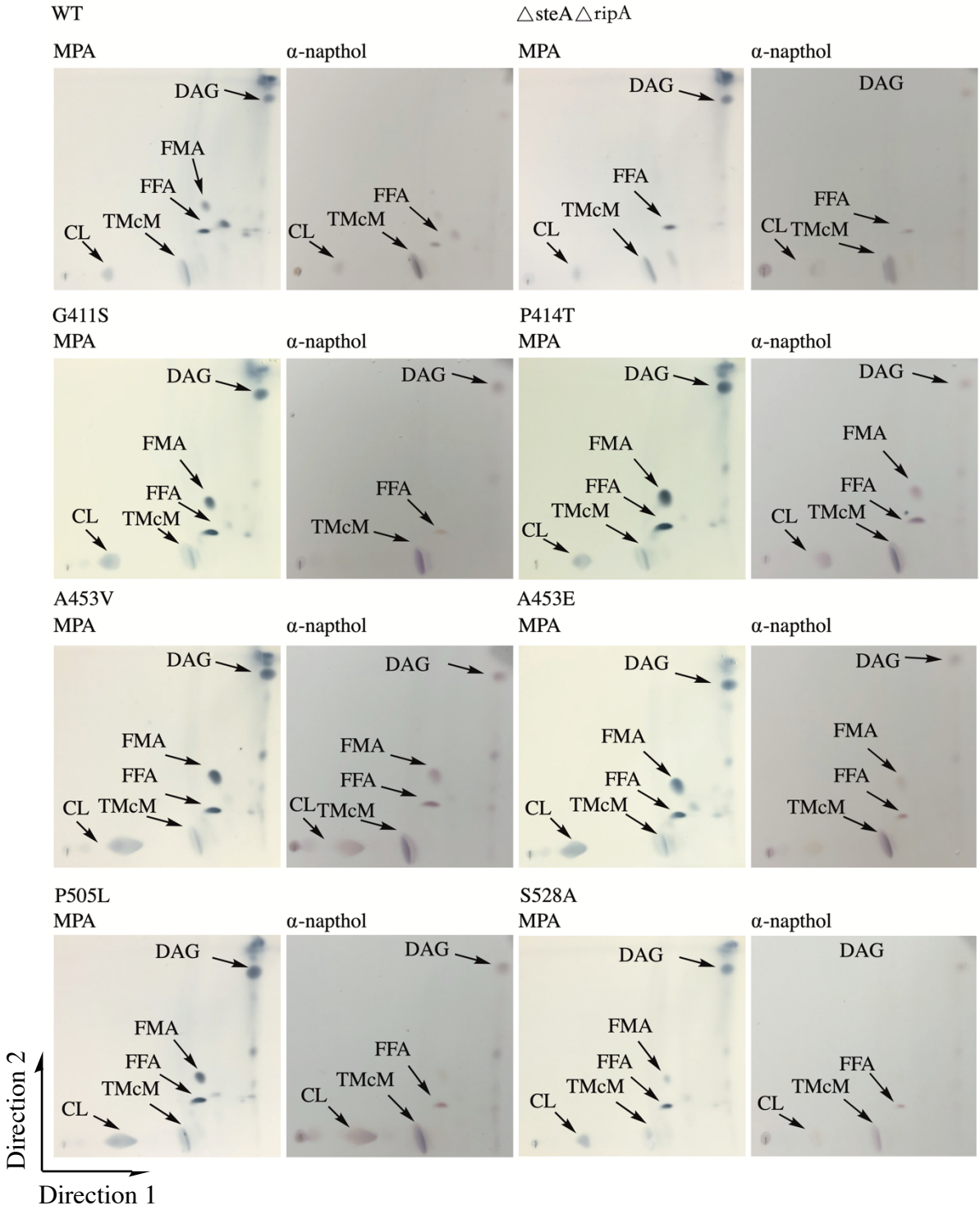

Figure 3.6: TLC analysis of apolar inside lipid extraction fraction from *C. glutamicum* strains. Solvent system: direction 1- 30: 8: 1 chloroform: methanol: water, direction 2- . DAG: diacyl glycerol, FMA: free mycolic acid, FFA: free fatty acid, TMcM: trehalose corynemycolate, CL: cardiolipin.

strain, with no significant changes in the levels of diacyl-glycerol (DAG), TMcM, free fatty acids, or CL.

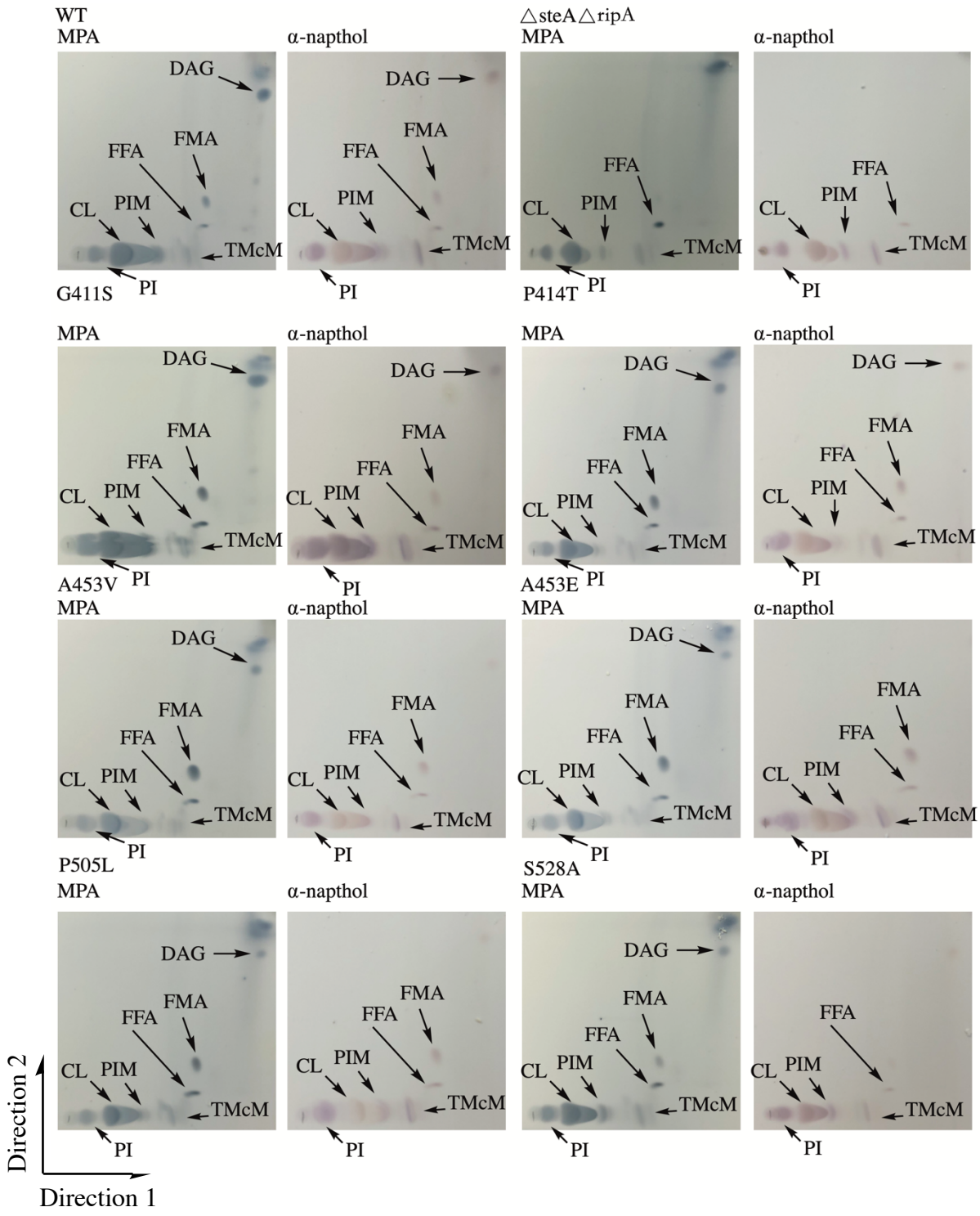

Figure 3.7: TLC analysis of polar lipid extraction fraction from *C. glutamicum* strains. Solvent system: direction 1- 30: 8: 1 chloroform: methanol: water, direction 2- 70: 30: 1 hexane: diethyl ether: acetic acid. DAG: diacylglycerol, FMA: free mycolic acid, FFA: free fatty acid, TMcM: trehalose corynemycolate, PIM: phosphotidyl-*myo*-inositol mannoside, CL: cardiolipin, PI: phosphotidyl inositol.

All of the Cg-Emb mutant strains showed fewer changes to the lipid composition in the Apolar

inside fraction than the Apolar outside when compared to the WT *C. glutamicum* strain (Figure 3.6, Table 3.3). All Emb mutant strains showed an increase in free mycolic acids relative to the *C. glutamicumΔsteAΔripA* strain. However, there is no change relative to the WT *C. glutamicum* strain, with the remaining profile being unchanged, with the exception of CL. With the Cg-Emb^{A453V}, Cg-Emb^{A453E}, and Cg-Emb^{P505L} strains all showing an increase in the level of CL.

Table 3.3: Changes in lipid composition *of C. glutamicum* strains. Changes are shown relative to either WT *C. glutamicum*, or *C. glutamicumΔsteAΔripA*. "+" Increase in lipid in respect to reference strain, "-" decrease in lipid in respect to reference strain, "ND" no difference in lipid

	Apolar outside							
	C. glutamicum strain							
Lipid	Reference strain	△steA△ripA	G411S	P414T	A453V	A453E	P505L	S528A
FMA	WT	ND	-	ND	ND	ND	ND	-
	△steA△ripA	ND	-	ND	ND	ND	ND	-
FFA	WT	+	+	+	+	+	+	+
	△steA△ripA	ND	ND	ND	ND	ND	ND	ND
TMcM	WT	ND	+	+	+	+	ND	ND
	△steA△ripA	ND	+	+	+	+	ND	ND
	Apolar inside							
	C. glutamicum strain							
Lipid	Reference strain	△steA△ripA	G411S	P414T	A453V	A453E	P505L	S528A
FMA	WT	-	ND	ND	ND	ND	ND	ND
	△steA△ripA	ND	+	+	+	+	+	+
FFA	WT	ND	ND	ND	ND	ND	ND	ND
	△steA△ripA	ND	ND	ND	ND	ND	ND	ND
TMcM	WT	ND	ND	ND	ND	ND	ND	ND
	△steA△ripA	ND	ND	ND	ND	ND	ND	ND
DAG	WT	ND	ND	ND	ND	ND	ND	ND
	△steA△ripA	ND	ND	ND	ND	ND	ND	ND
CL	WT	ND	ND	ND	+	+	+	ND
	△steA△ripA	ND	ND	ND	+	+	+	ND
	Polar							
	C. glutamicum strain							
Lipid	Reference strain	△steA△ripA	G411S	P414T	A453V	A453E	P505L	S528A
FMA	WT	-	ND	ND	ND	ND	ND	ND
	△steA△ripA	ND	+	+	+	+	+	+
FFA	WT	ND	ND	ND	ND	ND	ND	ND
	△steA△ripA	ND	ND	ND	ND	ND	ND	ND
TMcM	WT	ND	ND	ND	ND	ND	ND	ND
	△steA△ripA	ND	ND	ND	ND	ND	ND	ND
DAG	WT	-	ND	ND	ND	ND	ND	ND
	△steA△ripA	ND	+	+	+	+	+	+
CL	WT	-	+	+	+	+	ND	ND
	△steA△ripA	ND	+	+	+	+	+	+
PIM	WT	ND	ND	ND	ND	ND	ND	ND
	△steA△ripA	ND	ND	ND	ND	ND	ND	ND
PI	WT	ND	+	ND	ND	ND	ND	ND
	△steA△ripA	ND	+	ND	ND	ND	ND	ND

Analysis of the remaining polar lipid fraction (Figure 3.7, Table 3.3), showed a reduction in remaining free mycolic acids, DAG, and CL in the *C. glutamicum*Δ*steA*Δ*ripA* strain. The Emb mutant strains show a restoration of these lipids, with the Cg-Emb^{G411S}, Cg-Emb^{P414T}, Cg-Emb^{A453V}, and Cg-Emb^{A453E} strains resulting in an increase in CL relative to WT *C. glutamicum*. The Cg-Emb^{G411S} strain also shows an increase in PI relative to WT *C. glutamicum*.

3.2.7: Characterization of the cell wall bound lipid phenotype of WT *C. glutamicum, C. glutamicum*Δ*steA*Δ*ripA,* and *C. glutamicum*Δ*steA*Δ*ripA* Cg-Emb point mutant strains:

As there were alterations to the free lipid composition, the cell wall bound lipids were also analysed by hydrolysis from the cell wall core and conversion to fatty acid methyl esters (FAMEs), or corynemycolic acid methyl esters (cMAMEs), to determine if there was an effect on the attachment of lipids to the arabinogalactan in these strains (Method 6.12.4), if the mutations result in a significant decrease in the arabinosyltransferase activity of the Cg-Emb protein the effect this would have the AG would likely lead to an altered AG structure, and potentially from there result in a change to the attachment of lipids to the cell wall core.

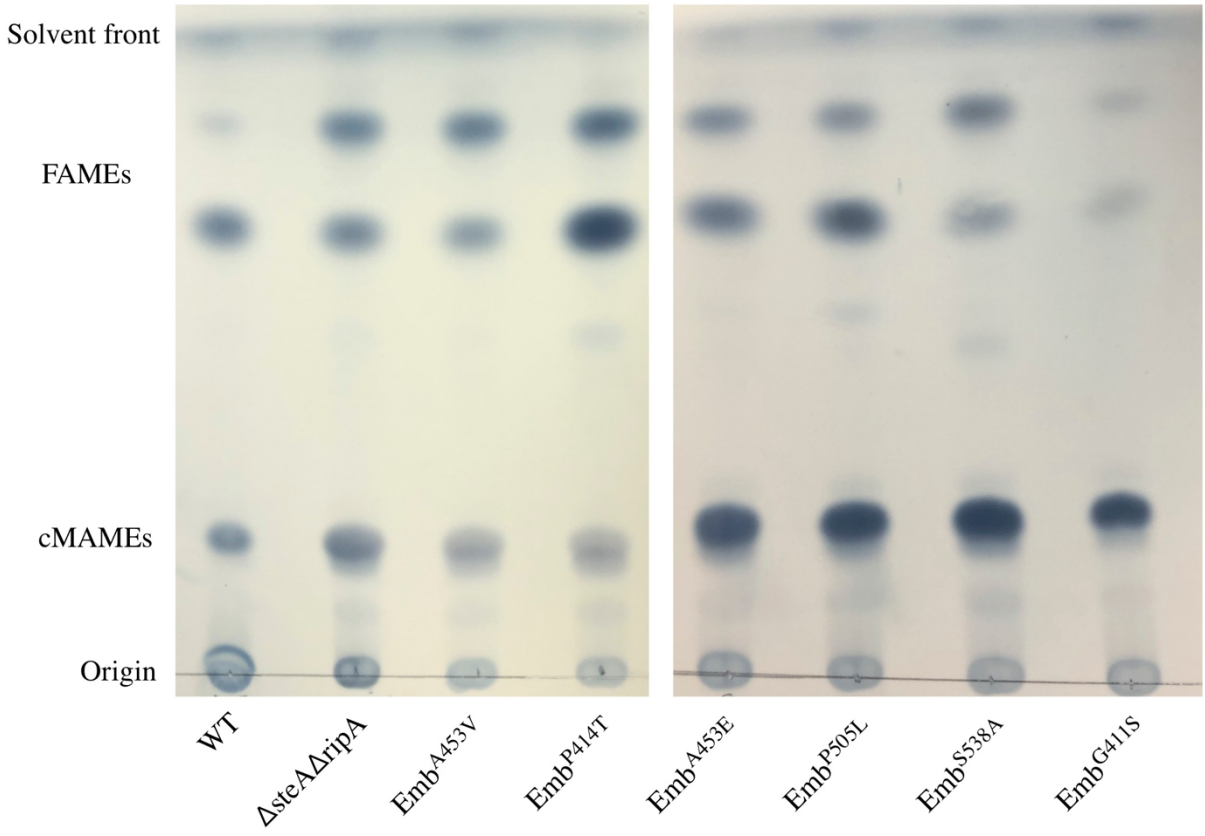

Figure 3.8: TLC analysis of cell wall bound lipid extraction from *C. glutamicum* strains. Effect of loss of *steA* and *ripA* results in a slight reduction in the higher Rf FAMEs in the cell wall bound lipid profile. Mutations in Cg-*emb* result in no change in the overall cell wall bound lipid profile, except for Cg-Emb^{G411S} results in a decrease in the cell wall bound fatty acids, while other mutations lead to no overall change to the lipid composition of the cell wall core. Solvent system- 95: 5 Petroleum ether 60-80: acetone, visualised with MPA.

Figure 3.8, shows that in the *C. glutamicum*Δ*steA*Δ*ripA* strain there is an increase in the level of corynemycolation of the cell wall core, compared to the WT *C. glutamicum* strain, with not significant changes in the attachment rate of the fatty acids. However, in the Cg-Emb^{G411S} strain there is an almost complete loss of fatty acid attachment and a reversion to the WT *C. glutamicum* strain level of corynemycolation, suggested that there is an impairment of the activity of either antigen 85 transferring the corynemycolates onto the cell wall core, or in the synthesis of the attachment site for corynemycolation, or fatty acid esterification. This altered phenotype in the cell wall core additionally potentially explains the relative increase in the

levels of TMcM in the free lipid extraction, as TMcM acts as the substrate for the transfer of corynemycolates, due to the nature of the mutations present in the bacteria it is likely that the change is due to an alteration in the activity of the Cg-Emb protein.

The alteration of the level of fatty acid esterification to the cell wall core in the Cg-Emb^{G411S} strain provides further support for the change in the structure of the AG as it has been seen that the AG can have either fatty acids, or mycolic acids attached to terminal domain of the AG, although a significant amount of the cell wall attached lipids in *C. glutamicum* are attributed to the attachment of cardiolipin to the peptidoglycan (Bansal-Mutalik and Nikaido, 2011).

3.2.8: SDS-PAGE lipoglycan characterization from WT *C. glutamicum, C. glutamicum*Δ*steA*Δ*ripA,* and *C. glutamicum*Δ*steA*Δ*ripA* Cg-Emb point mutant strains:

Further to the effect on the lipid composition, we predicted that there would be changes in the lipoglycan composition. This is due to the mutations in the Cg-Emb protein, which potentially changes the levels of DPA through changes in the activity of Cg-Emb. With the changes in AraT impacting on the arabinan domain of lipoarabinomannan.

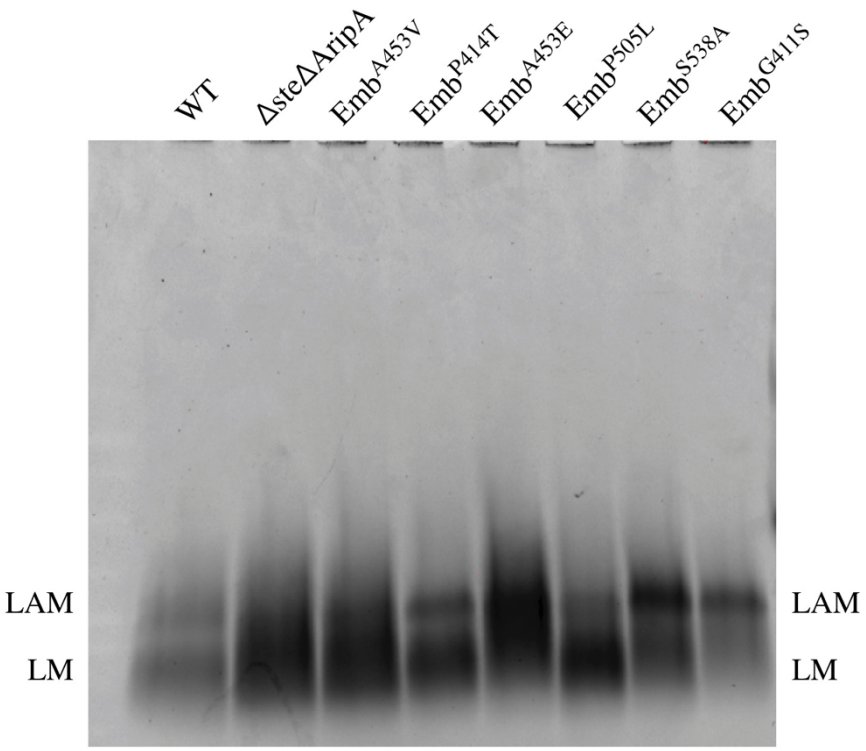

Figure 3.9: SDS-PAGE analysis of lipoglycan extraction from *C. glutamicum* strains visualised using Pro-Q Emerald 300. Loss of *steA* and *ripA* results in the Cg-LM and Cg-LAM bands merging, implying a change in the composition of the lipoglycans. Mutations in the Cg-Emb protein result in either further changes from the *C. glutamicumΔsteAΔripA* strain, or a restoration towards the WT *C. glutamicum* phenotype. Cg-Emb^{G411S} and Cg-Emb^{S538A} show a reduction in the relative amount of Cg-LM compared to Cg-LAM. Cg-Emb^{A453V} and Cg-Emb^{A453E} show an unchanged phenotype to the *C. glutamicumΔsteAΔripA* strain. The Cg-Emb^{P414T} and Cg-Emb^{P505L} strains show a relative return to the WT *C. glutamicum* strain.

Analysis of the lipoglycan extraction (Methods 6.16, 6,17.1, 6.17.3), shown in Figure 3.9 shows some changes to the relative levels of Cg-LM and Cg-LAM when the WT *C. glutamicum*, *C. glutamicum*Δ*steA*Δ*ripA* and mutant strains are compared. The *C. glutamicm*Δ*steA*Δ*ripA* strain shows a subtle change in the Cg-LM and Cg-LAM size profile, with the distribution altering to a point where the bands are not separated as they are in the WT *C. glutamicum*.

The effect of the mutations on the lipoglycan profile vary depending on the strain. The Cg-Emb^{A453V} and Cg-Emb^{A453E} strains both show no significant noticeable effect on the lipoglycan profile. The Cg-Emb^{P414T}, Cg-Emb^{P505L}, and Cg-Emb^{S528A}, mutations show a restoration of the separation between these bands, however the relative levels of the Cg-LM and Cg-LAM vary. Most notable in the Cg-Emb^{S528A} strain, where the relative abundance on Cg-LM is significantly reduced compared to the Cg-LAM. Finally, the Emb^{G411S} mutation results in a similar phenotype to the Cg-Emb^{S528A} strain, however the level of Cg-LM is reduced further.

3.2.9: Aditol acetate derivatized monosaccharide composition analysis of extracted lipoglycans from WT *C. glutamicum, C. glutamicum*Δ*steA*Δ*ripA,* and *C. glutamicum*Δ*steA*Δ*ripA* Cg-Emb point mutant strains:

In order to further understand the effect on the changes in the lipoglycan profile the composition of the whole extract was determined by generation of hydrolysed aditol acetate derivatives and analysis by gas chromatography to determine the sugar composition of the lipoglycans (Methods 6.18.1, 6.18.2, Appendix 3).

Table 3.4: Mannose: arabinose ratio of aditol acetate derivatized lipoglycan extractions from *C. glutamicum* strains.

	WT	△SteA△RipA	Emb^{A453V}	Emb^{P414T}	Emb^{A453E}	Emb^{P505L}	Emb^{S528A}	Emb^{G411S}
Man: Ara	33.4:1	7.9:1	2.0:1	24.0:1	14.6:1	3.5:1	3.7:1	1.0:1

Composition determination of derivatised of the lipoglycans resulted in two peaks corresponding to arabinose, retention time ~ 9.1- 9.5 min, and mannose, retention time ~ 12.4-12.6 min. The analysis of the resulting spectra (Table 3.3, Appendix 3), lead to the determination that the mannose: arabinose ratio changes from 33.4: 1 in the WT *C. glutamicum*

strain, to 7.9: 1 in the *C. glutamicum*Δ*steA*Δ*ripA* strain, showing that the change in these genes, increased the arabinose content of the Cg-LM and Cg-LAM profile.

The point mutations in the Cg-Emb gene all altered the relative abundance of arabinose in lipoglycan profile. The Cg-Emb^{G411S} strain resulted in the largest increase in the relative arabinose composition, with a ratio of: 1:1, implying that the mutation is reducing the activity of Cg-Emb, and in order to allow for the use of the decaprenyl phosphate anchor for other purposes a higher ratio of LM is being arabinosylated.

Contrary to the Cg-Emb^{G411S} strain, the both the Cg-Emb^{P414T}, and Cg-Emb^{A453E} strains reverted closer to the WT *C. glutamicum*, with a mannose: arabinose ratio of 24: 1, and 14.6:1 respectively. While these changes do not fully restore the WT ratio, there is a reversion towards the WT *C. glutamicum* from the *C. glutamicum*Δ*steA*Δ*ripA* strain. The remaining Cg-Emb mutants all resulted in a similar, if reduced, phenotype to the Cg-Emb^{G411S} mutant strain, with Cg-Emb^{P505L}, Cg-Emb^{A453V}, and Cg-Emb^{S528A}, resulting in mannose: arabinose ratios of: 3.5: 1, 2: 1, and 3.6: 1 respectively. Suggesting that they have a similar impact on the activity of Emb, though of reduced severity the Emb^{G411S} mutant.

3.2.10: Cell free Cg-Emb glycosyl transferase activity of WT *C. glutamicum, C. glutamicum*Δ*steA*Δ*ripA,* and *C. glutamicum*Δ*steA*Δ*ripA* Cg-Emb point mutant strains:

In order to determine the effect of the mutations on the rate of Emb activity cell free arabinosyltranferase activity was tested (Methods 6.20.1, 6.20.2). This allowed for the testing of both the *in vitro* activity of both the WT and mutant Cg-Emb proteins, as well as the sensitivity of the respective proteins to EMB, using a C_8-*Araf-Araf* (YHF-1) acceptor as a

standard, purifiable anchor, and ^{14}C labelled pRpp for detection of incorporation by AraT activity (Figure 3.10).

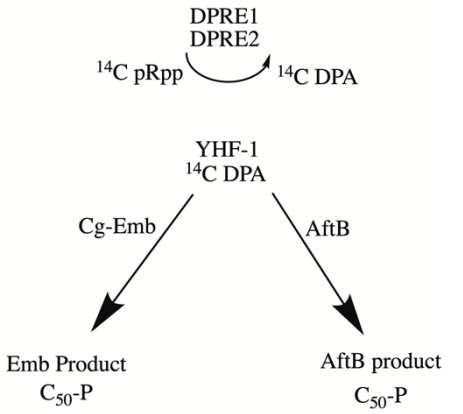

Figure 3.10: Cell free Emb glycosyl transferase activity assay schematic. ^{14}C labelled pRpp is converted into DPA by DPRE1 and DPRE2, the ^{14}C labelled DPA is then transferred onto the acceptor by either Emb or AftB. The resulting products are purified from the ^{14}C donor and separated by TLC.

As expected the WT *C. glutamicum* and *C. glutamicum*Δ*steA*Δ*ripA* strain, show sensitivity to of EMB (Figure 3.11), as the *C. glutamicum*Δ*steA*Δ*ripA* strain produces the WT Cg-Emb and such the WT *C. glutamicum* and *C. glutamicum*Δ*steA*Δ*ripA* strain phenotypes should be identical, therefore upon supply of an excess of substrate in the form of pRpp, the synthesis should occur at a similar rate. The addition of EMB to the reaction mixture resulted in an almost complete reduction in the activity of Cg-Emb in both strains.

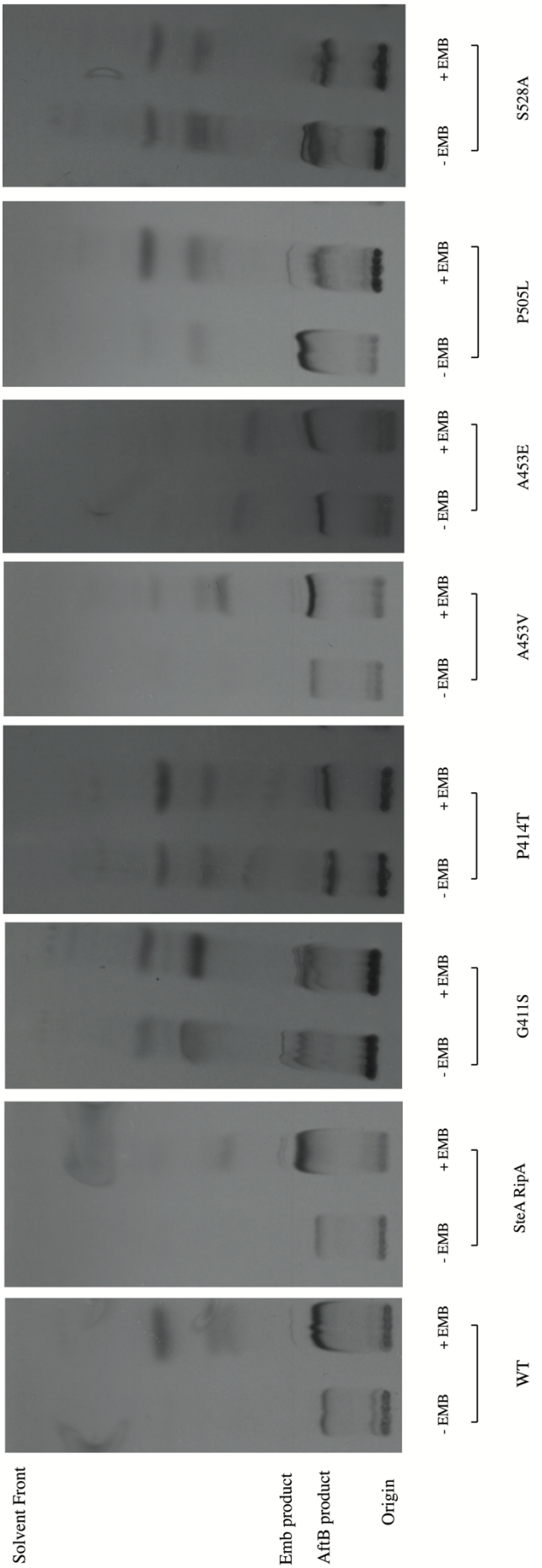

Figure 3.11: Cell free Emb functionality assay of membranes purified from *C. glutamicum* strains. *In vitro* analysis of Cg-Emb activity analysed by separation of products formed from ^{14}C labelled pRpp, analysing the effect of EMB on the activity of Cg-Emb. The presence of EMB in the reaction mixture results in the loss of bands in the WT *C. glutamicum* and *C. glutamicumΔsteAΔripA* strain when compared to the respective reaction where no EMB is present, with not phenotypic difference between the WT *C. glutamicum* and the *C. glutamicumΔsteAΔripA* strains in either condition. Cg-Emb^{A453V} shows WT *C. glutamicum* phenotype when treated with EMB, while all others show either a minor reduction in the activity of EMB in the case of Cg-Emb^{P505L}, or no detectable change in the activity of Cg-Emb in the presence of EMB in the case of the other mutant strains. Solvent system: 70: 25: 0.5 2.5 chloroform: methanol: ammonium hydroxide: water.

The *C. glutamicum* strains with point mutations in the Cg-Emb protein, with the exception of the Cg-Emb^{A453V} mutant strain, showed an altered response in the absence of EMB to the reaction mixture when compared to either the WT *C. glutamicum* strain or the *C. glutamicum*Δ*steA*Δ*ripA* strain. Where the absence of EMB in the reaction mixture of the WT *C. glutamicum* and *C. glutamicum*Δ*steA*Δ*ripA* strains, resulted in the loss of multiple bands of higher Rf, when compared to the reaction containing EMB, the mutant strains showed no significant change in overall product formation. The only Cg-Emb mutant strain to not show this response was the Cg-Emb^{A453V} mutant which showed the same phenotype as the WT strain upon addition of EMB.

While the majority of the mutant showed no alteration in the reaction profile in the absence of EMB, the Cg-Emb^{P505L} strain showed a reduction in the higher Rf bands upon addition of EMB, however not the complete loss of these bands seen in the WT *C. glutamicum* and *C. glutamicum*Δ*steA*Δ*ripA* strains.

In addition to the lack of any change in the reaction profile based on the presence or lack of EMB in the reaction mixture, of the Cg-Emb^{G411S} and Cg-Emb^{S528A} strains, the overall profile in the absence of EMB was altered slightly compared to the strains expressing the WT Cg-Emb. With the band produced by the action of AftB, and the initial band lost in the presence of EMB in the WT *C. glutamicum* strain, appearing as multiple overlapping bands with similar Rfs, where in both the WT *C. glutamicum*, and the various mutant strains this band appeared as a single product band.

3.3: Discussion:

Here we show that point mutations in the Cg-Emb protein in *C. glutamicum* results in significant changes in the cell surface, and antibiotic resistance profile of *C. glutamicum*. While this provides advantages in some situations, there is a reduction in the growth rate associated with the tested mutations in Cg-Emb when not under antibiotic stress compared to WT *C. glutamicum*, as well as a significant decrease in the permeability of the cell surface to DPH (Freihofer et al., 2016; Wang et al., 2019). These phenomena are likely to be linked as a change in the permeability of the cell is likely to affect the ability of some antibiotics to be able to reach the target required for efficacy (Lanéelle et al., 2001). However, due to the hydrophobic nature of the method for testing permeability, further testing into the permeability of the cell surface to hydrophilic compounds would also be required, as the decrease in permeability of the cell surface does not result in a universal increase in the ability of the bacteria to withstand antibiotics.

Antibiotic sensitivity screening of the Cg-Emb point mutations in the *C. glutamicum*Δ*steA*Δ*ripA* strain significantly alters the sensitivity of *C. glutamicum* to antibiotics, further confirmation of the effect of these mutations by the generation of complements of the *C. glutamicum*Δemb strain recombinantly expressing Cg-Emb containing the studied point mutations to confirm that these mutations affect the WT *C. glutamicum* strain in the same way as they do the *C. glutamicum*Δ*steA*Δ*ripA* strain. This would confirm that these changes in sensitivity are not due confounding factors caused by changes in the physiology of the cell resulting from the deletion of multiple genes.

Further study into the effect of the mutations on the composition of the cell wall core in the Cg-Emb point mutation strains is required to understand how the surface of the cell is affected by these mutations. One method of this would be to purify the mAGP (Moynihan et al., 2019), the composition could then be determined by use of gas chromatography of aditol acetate derivatized material (Methods 6.18.1 and 6.18.2). With investigation of the composition of the AG attached to the cell wall required to determine the effect on the AG in addition to the effect on the LM and LAM (Alderwick et al., 2005). The effect is likely to be minimal in the mutants, as only the Cg-Emb^{G411S} strain showed a clear alteration in the cell wall bound lipids to provide a potential explanation as to the change in the permeability of the cell.

The changes in the lipoglycan composition is likely due to the changes in the availability of the polyprenyl anchor which is required for both DPA and for DPM, with DPA acting as the source of arabinose for Cg-Emb alterations to the activity of Cg-Emb will have an impact on the pool of lipid anchored sugars available and as such will have a knock-on effect on the LM and LAM (Kolly et al., 2014). In addition to the changes in the ratio of Cg-LM to Cg-LAM which result in changes to the ratio of mannose to arabinose in the Cg-LM and Cg-LAM extraction from both the *C. glutamicum*Δ*steA*Δ*ripA* in comparison to the WT *C. glutamicum* strain and the relative change compared to the composition of the Cg-Emb point mutant strains suggests that, while Cg-Emb is not involved in the synthesis of these lipoglycans, the change in the activity of the enzyme results in large scale changes to the composition of the entire cell, with further work to characterise these changes required to fully understand the effect of mutations in Cg-Emb on the cell as a whole (Alderwick et al., 2006, 2005).

Due to the location of the mutations in the Cg-Emb proteins will all of the mutations in this study occurring in the transmembrane domain of Cg-Emb, further study of both the full-length

Cg-Emb and *Mtb*-Emb protein is required *in vitro* (Alderwick et al., 2011; Goude et al., 2009). Due to the difficulty in the expression and purification of membrane proteins the majority of the research in to the function of Cg-Emb, both in *C. glutamicum* and *Mtb* has been focussed on the soluble C-terminal domain removed from the transmembrane domain (Alderwick et al., 2011; Shi et al., 2006). This is likely to have impeded understanding of the mechanism by which EMB acts, as the conservation of a large membrane spanning domain of all Emb proteins implies that the domain is vital for the function of the protein beyond ensuring that it remains close to the membrane where the substrates are bound, with it being identified as the recognition domain (Anandan and Vrielink, 2016; Goude et al., 2009; Jeffery, 2016).

Further analysis on the effect the deletion of either *steA* or *ripA* on the cell surface of *C. glutamicum*, would provide insight into the mechanism by which the deletion of these genes results in increased sensitivity to EMB. Further characterising the functions of SteA and SteB through the purification of recombinantly expressed protein determination of their *in vitro* functionality, would also provide insight into why the deletion of proteins is linked to an increased sensitivity to EMB. RipA acts as an endopeptidase, degrading the peptidoglycan, and has been shown to localise to the septa of dividing cells, and as such deletions in this gene are likely to affect the integrity, and potentially the composition of, the peptidoglycan (Böth et al., 2011; Chao et al., 2013; Lim et al., 2019; Nikitushkin et al., 2015).

Chapter 4:

Biochemical investigation of a mycobacterial galactan transport system

4.1: Introduction:

AG provides a scaffold for multiple components of the mycobacterial cell envelope and its structure and biosynthesis has been extensively studied (Abrahams and Besra, 2016; Alderwick et al., 2008, 2005; Birch et al., 2008). The transport mechanism responsible for the translocation of galactan from the inner leaflet of the cytoplasmic membrane to the external leaflet, has yet to be precisely determined, although the transporter responsible has been predicted (Abrahams and Besra, 2016; Dianišková et al., 2011).

AG synthesis occurs in two stages: the cytoplasmic synthesis of galactan attached to decaprenyl pyrophosphate, and the periplasmic decoration of the galactan with arabinan domains. Galactan is built on a linker unit formed of a GlcNAc (1→3) L-rhamnose (Rha) attached to a decaprenyl pyrophosphate. The formation of this linker unit is catalysed by the action of WecA and WbbL (Jin et al., 2010; McNeil et al., 1990; Mills et al., 2004). With WecA responsible for the addition of the GlcNAc-1-phosphate onto the decaprenyl phosphate from a UDP-GlcNAc carrier. The addition of Rha to form the linking unit is catalysed by Wbbl, from a TDP-Rha carrier.

The galactan core is then built upon the linker unit (C_{50}-P-GlcNAc-Rha) with the addition of the first two galactofuranose residues catalysed by the action of GlfT1, using UDP-Gal*f* as a substrate (Alderwick et al., 2008; Mikusova et al., 2006). The nascent galactan chain is then elongated by the addition of GlfT2, introducing alternating α(1→5) α(1→6) glycosidic bonds, with the mature galactan comprising ~30 Gal*f* residues (Kremer et al., 2001a; Rose et al., 2006). While the enzymes responsible for the synthesis of the galactan are known (Table 1.2, Figure 4.1), the mechanism by which the process is terminated, and the process by which the galactan

is flipped across the cytoplasmic membrane remains unclear (Abrahams and Besra, 2016; Daffe et al., 1990).

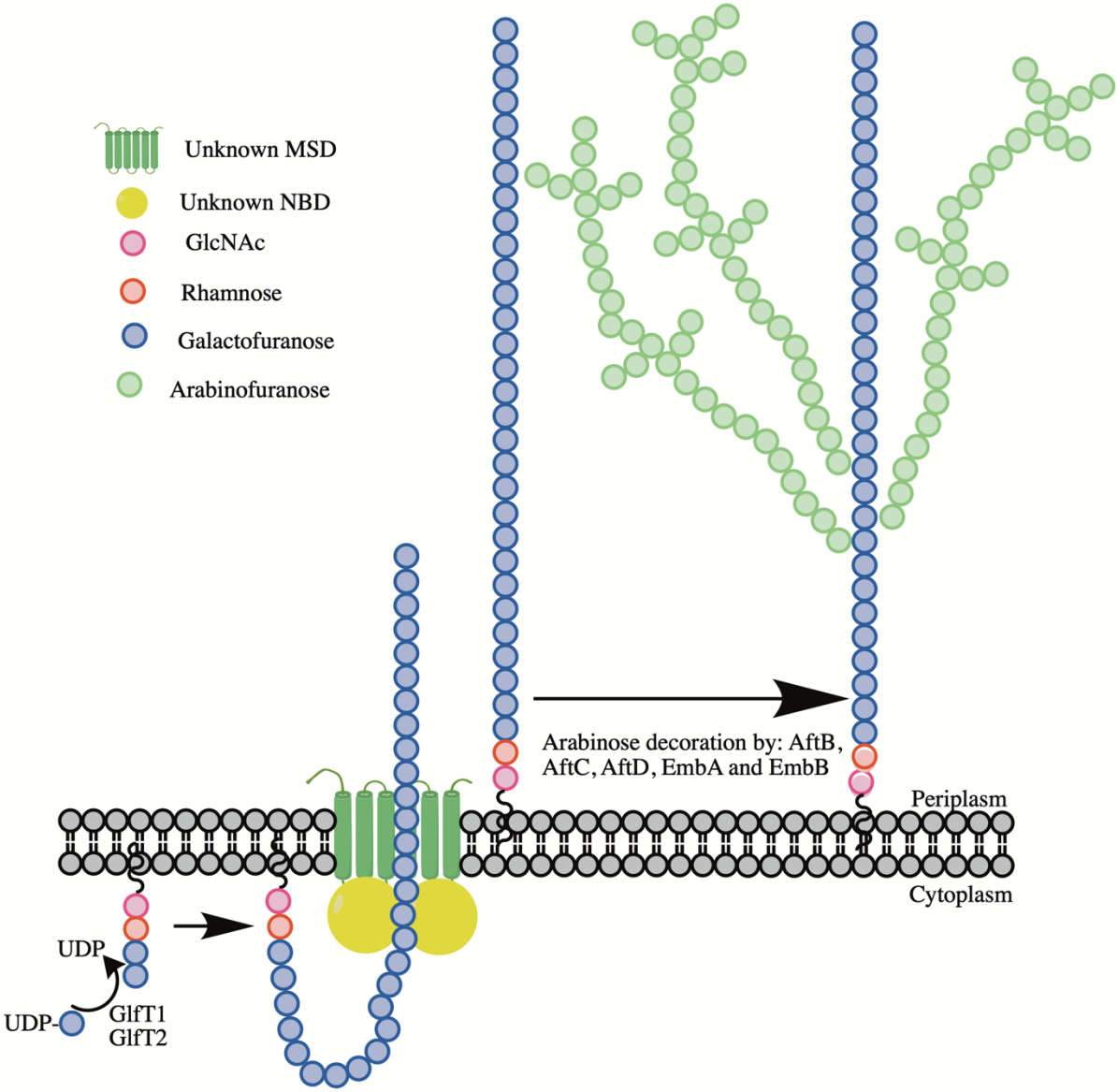

Figure 4.1: Synthesis, and translocation of arabinogalactan in mycobacterial species. Showing the process by which galactan is synthesised in the cytoplasm of mycobacterial cells, and how the translocated galactan is decorated with arabinan domains after translocation.

Upon flipping of the mature galactan to the external leaflet of the cytoplasmic membrane, the galactan is decorated with three Ara*f* chains (Figure 4.1). The three branch points are located at residues: 8, 10, and 12 of the galactan chain. The addition of the initial, priming, arabinose

is catalysed by the action of AftA. AftA catalyses the transfer of arabinfuranose onto the galactan chain through the formation of an α(1→5) glycosidic bonds, using DPA as a source of arabinose (Alderwick et al., 2005). Once the branches are primed they are extended by the action of EmbA and EmbB, which extend the arabinan domain through a series of α(1→5) glycosidic bonds, using DPA as a source of arabinose (Escuyer et al., 2001). Branching points are introduced into the arabinan domain by the action of AftC, and AftD, through the formation of α(1→3) glycosidic bonds, using DPA as a source of arabinose (Birch et al., 2008; Škovierová et al., 2009).

The terminal region of the arabinan domain is a branched hexarabinofuranose motif, and is produced by AftB, AftC, AftD, EmbA, and EmbB. With the terminal β(1→2) linked ara*f* residues added by the action of AftB, using DPA as the source of arabinose (Alderwick et al., 2006, 2005; Birch et al., 2008; Escuyer et al., 2001; Jankute et al., 2017; Škovierová et al., 2009, 2009). The mature arabinogalactan is cleaved from the decaprenyl phosphate, and attached to the muramic acid of the PG, by Lcp1 (Harrison et al., 2016). The terminal arabinose residues act as the attachment site for mycolic acids, catalysed by Antigen 85, with the 5' carbon of the terminal arabinose residues being esterified to the mycolic acids (Backus et al., 2014).

While there has been a comprehensive study predicting the ABC-transporters in *Mtb*, identifying at least 26 complete and 11 incomplete ABC-transporters. Of these transporters predicted to function as a polysaccharide transporter is Rv3781, and Rv3783, which have been predicted to form a tetrameric ABC-transporter (Braibant et al., 2000). Rv3781 is predicted to function as the nucleotide binding domain responsible for the hydrolysis of ATP providing the energy required for the substrate transport, and Rv3783 is predicted to form the transmembrane

pore across the cytoplasmic membrane (Beis, 2015; Braibant et al., 2000; Dianišková et al., 2011).

The location of these genes in the *Mtb* genome among various genes involved in the biosynthesis of arabinogalactan (Table 1.2). The importance of these predicted ABC transporters have been confirmed, as the Rv3781 ortholog in *M. smegmatis*, MSMEG_6366 has been shown to essential for bacterial survival. However, the predicted membrane spanning domain for galactan transport, MSMEG_6369, was found to be non-essential (Dianišková et al., 2011).

Here we aim to over-express, purify and characterise recombinant proteins from the mycobacterial galactan transporter system. Making use of chemically synthesised galactan oligomers, we investigated the precise biochemical interactions between the NBD component of the *M. smegmatis* orthologs of Rv3781/Rv3783 ABC transporter system and respective AG biosynthetic intermediates.

4.2: Results:

4.2.1: Bioinformatic analysis of Rv3781, Rv3783, and *M. smegmatis* orthologs:

While the conservation of the mycobacterial proteins predicted to be involved in galactan export have been shown (Dianišková et al., 2011), a basic bioinformatic analysis (Method 6.1.2) of Rv3781 and Rv3783 alongside predicted *M. smegmatis* and *M. leprae* orthologs was conducted to ensure the accuracy of previous predictions. *M. smegmatis* was selected due to the previously available information on the deletion of the predicted orthologs, while *M. leprae* was selected due to the level of genomic depletion of the bacteria, which ensures that if the gene is conserved between *Mtb* and *M. leprae* the gene is likely to be required for survival (Cole et al., 2001; Dianišková et al., 2011).

Table 4.1*:* BLASTp analysed primary structure of Rv3781 and Rv3783 against *M. smegmatis* and *M. leprae* orthologs. Showing high levels of conservation in both the NBDs, and in the MSDs.

	Identity (%)	Positives (%)
Rv3781 vs MSMEG_6366	90	94
Rv3781 vs Ml0114c	91	96
Rv3783 vs MSMEG_6369	80	88
Rv3783 vs Ml0112C	84	90

Sequence analysis of the *Mtb* proteins (Rv3781 and Rv3783) against the *M. smegmatis* orthologs (MSMEG_6366 and MSMEG_6369) showed significant levels of homology to both the NBD and the MSD (Table 4.1). There is 90 % and 91 % amino acid sequence identity between Rv3781 against the *M. smegmatis* and *M. leprae* orthologs respectively, this high level of sequence conservation supports the prediction that the functions of these genes are conserved between the three species.

The MSDs are more sequentially diverse, with *M smegmatis* and *M. leprae* orthologs having identity of 80 % and 84 % to Rv3783. However, as increased structural variability across all MSDs is observed, due one of their primary functions being the formation of a pore rather than providing enzymatic function, this increase in the sequence divergence can be accounted for.

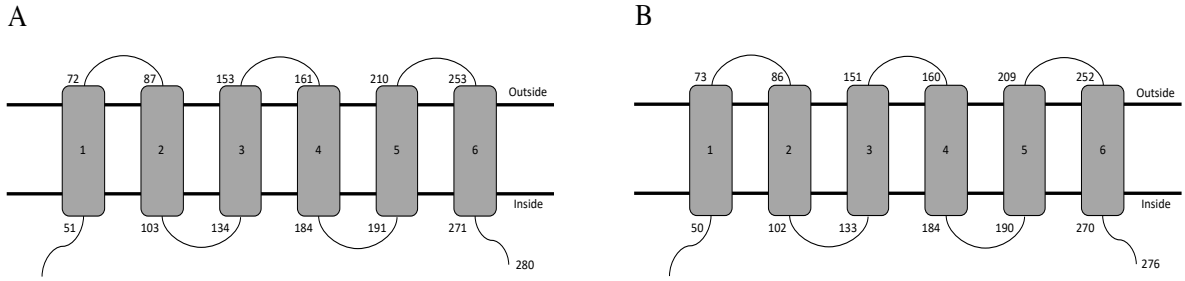

Figure 4.2: Transmembrane prediction of mycobacterial MSDs. A) Rv3783, B) MSMEG_6369. Predictions generated using TMHMM, and TMPred, amino acids predicted to be the first and final residue of the transmembrane helix given, final residue noted. Both the *Mtb* and the *M. smegmatis* ortholog show six transmembrane helices, with similar start and end points, as expected by the sequence comparison. Transmembrane predictions listed in Appendix 2.

Analysis of the number and location of transmembrane helices in both the predicted membrane spanning domain and the predicted nucleotide binding domain predict that the membrane spanning domains all form six transmembrane helices (Figure 4.1, Appendix 1). Membrane spanning domains contain 4- 8 transmembrane helices and require the formation of a dimer in order to be able to function (Braibant et al., 2000, Higgins and Linton, 2004). Prediction of the membrane topology of Rv3783 and MSMEG_6369 predicts that the sequence similarity of these proteins' is predicted to transfer into almost identical membrane topology.

As expected, the nucleotide binding domains are not predicted to contain any transmembrane helices. Further analysis of the sequence of these proteins was used to confirm the presence of the conserved NBD motifs that are essential for functionality; Walker A, Walker B, ABC-signature (Figure 4.3).

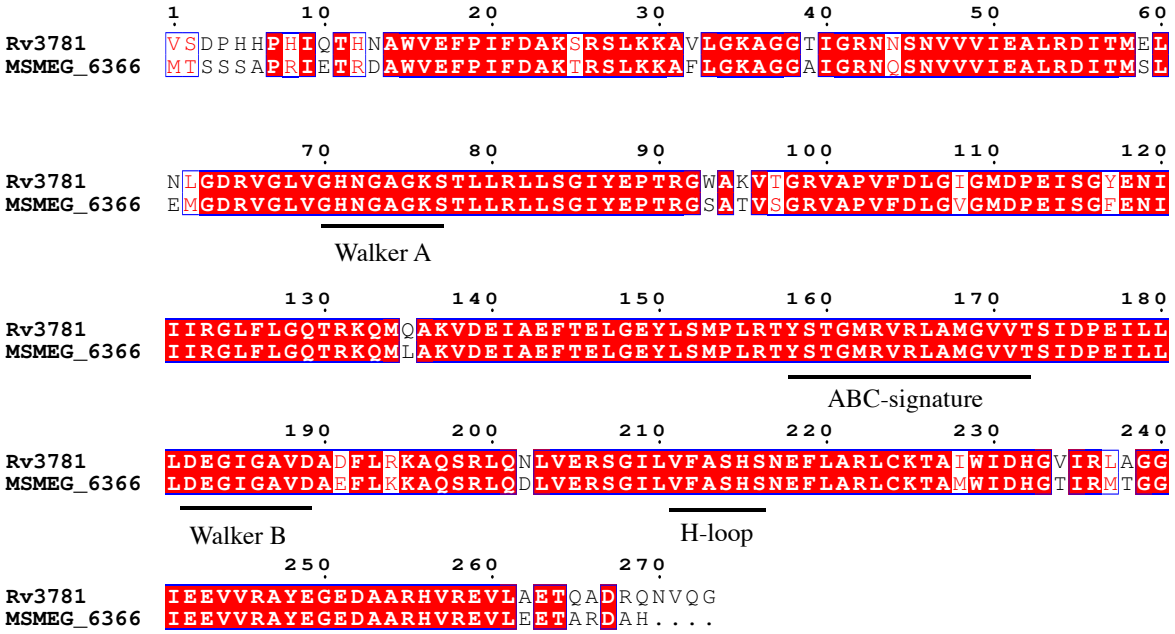

Figure 4.3: Sequence alignment of Rv3781, and MSMEG_6366. Predicted nucleotide binding domains analysed for conserved motifs found throughout ABC-transporters. Walker A, ABC-signature, Walker B, and H-loop motifs annotated. Notably absent is the A-loop, upstream of the Walker A motif, however this motif is not conserved in all NBDs of ABC-transporters, but is seen in the majority.

Both Rv3781 and MSMEG_6366 contain Walker A, Walker B, H-loop, and ABC signature motifs (Figure 4.3). Additionally, both Rv3781, and MSMEG_6366, do not contain the A-loop, composed of an aromatic amino acid residue, most commonly a phenylalanine, 23- 27 residues upstream of the Walker A motif. The A-loop forms an interaction with the adenosine ring of ATP (Ambudkar et al., 2006). However, while this residue is seen in many ABC-transporters, it is not conserved in all ABC-transporters. Therefore, the lack of this residue in both proteins

is unlikely to indicate that they are non-functional, although there may be an impact on the binding affinity of ATP, and therefore the maximal rate of ATP turnover.

Due to the presence of individually transcribed domains, and the predicted number of transmembrane helices in the MSD, the fully functional ABC-transporter is predicted to form a tetramer comprised of two copies of both the NBD and the MSD.

4.2.2: Expression and purification of maltose binding protein (MBP) tagged MSMEG_6366:

Purification of MSMEG_6366 from *E. coli* BL21 (DE3) expressing pMAL-c2x-MSMEG_6366, and purified using an amylose resin MBP-trap column (Methods 6.21.1, 6.21.3). Resulting in the purification of a protein corresponding to the molecular weight of MSMEG_6366, tagged with MBP (72 kDa), with minimal contaminating proteins (Figure 4.4).

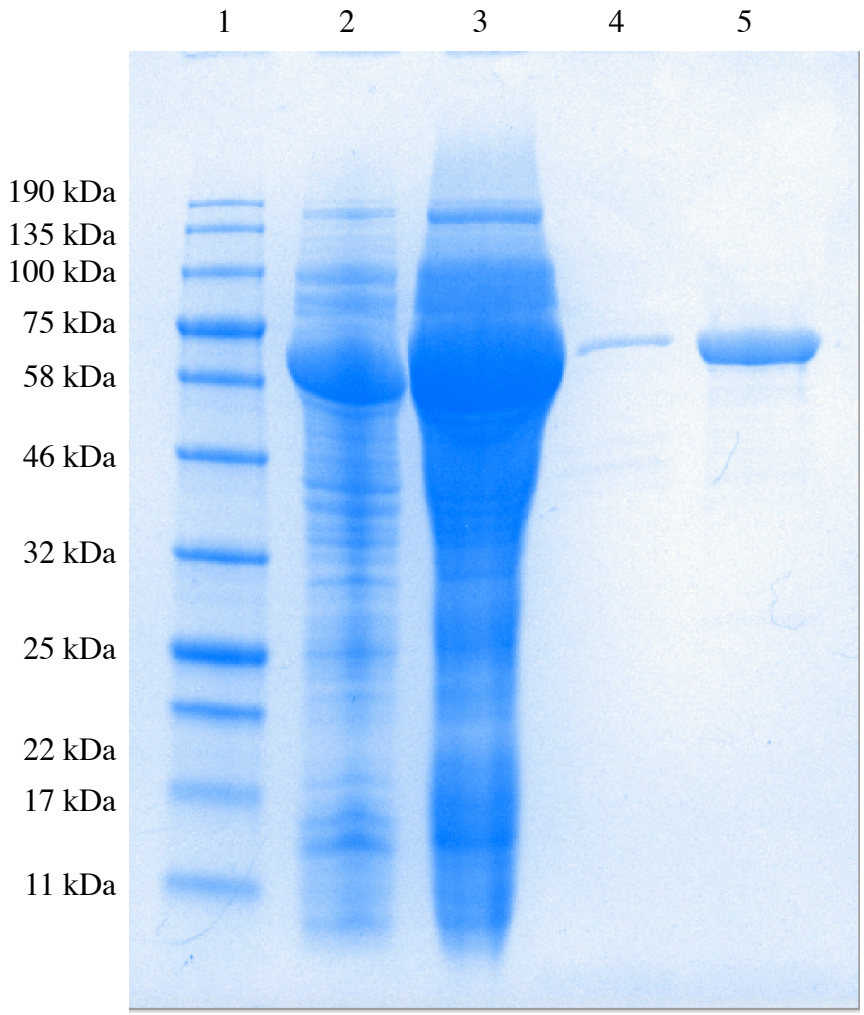

Figure 4.4: SDS-PAGE analysis of purification of MBP-tagged MSMEG_6366. 1) Protein standard ladder, 2) clarified *E. coli* cell lysate, 3) cell lysate flowthrough, 4) protein column wash, 5) protein elution. Showing purification of MBP-tagged MSMEG_6366 from *E. coli*.

The effect of the presence of low-level contaminating proteins on assays is likely to be negligible as the abundance of MSMEG_6366 outweighs any contaminating proteins.

4.2.3: Intrinsic tryptophan fluorescence ligand binding assay of MSMEG_6366 to chemically synthesised galactan analogues:

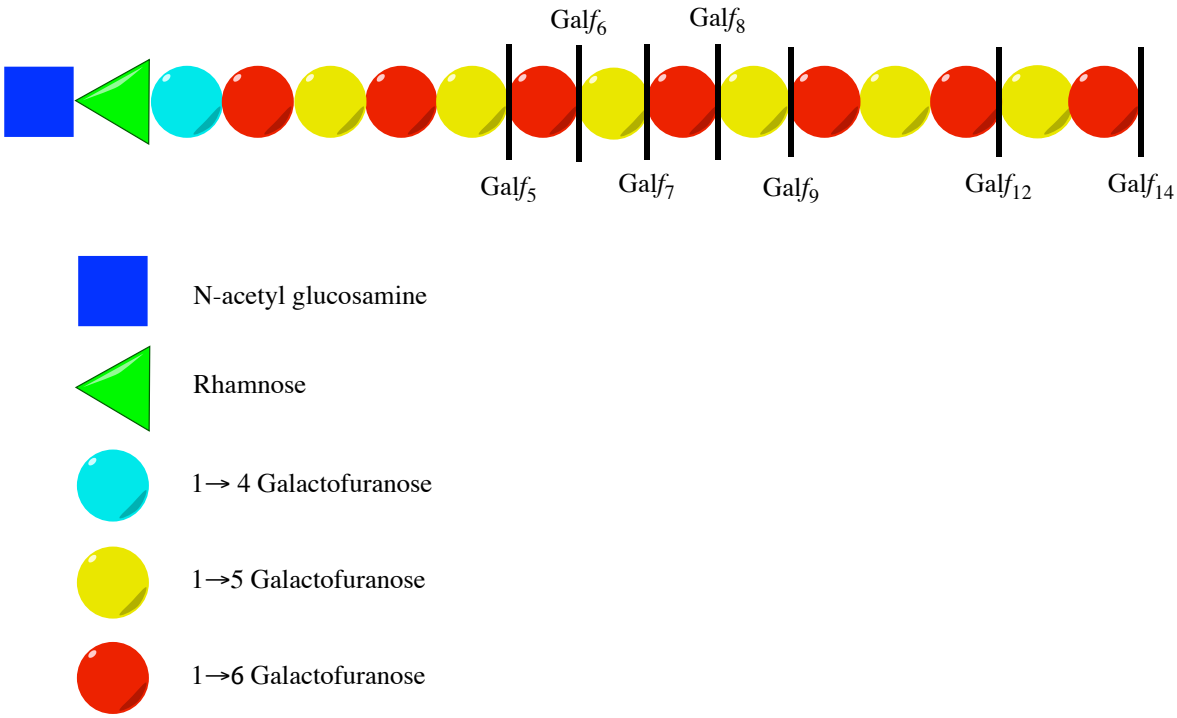

Figure 4.5: Schematic representation of galactan analogues. Showing the linker unit attached to the variable length galactofuranose chain (chain length of ligands used noted as Galf_n). formed of an N-acetyl glucosamine rhamnose linking unit extended by 1→ 4 glycosidic linkage to the galactofuranose chain, followed by alternating 1→ 6, 1→ 5 glycosidic linkages.

To determine if MSMEG_6366 is able to interact with the galactan molecule either during or before the initiation of translocation across the membrane, purified MSMEG_6366 intrinsic tryptophan fluorescence (ITF, Methods 6.21.4, 6.21.5) measuring fluorescence change at 350 nm was used to measure ligand binding. The change in fluorescence, beyond the effect of dilution, of the protein when galactan analogues (Figure 4.5) were titrated was used to calculate the binding affinity.

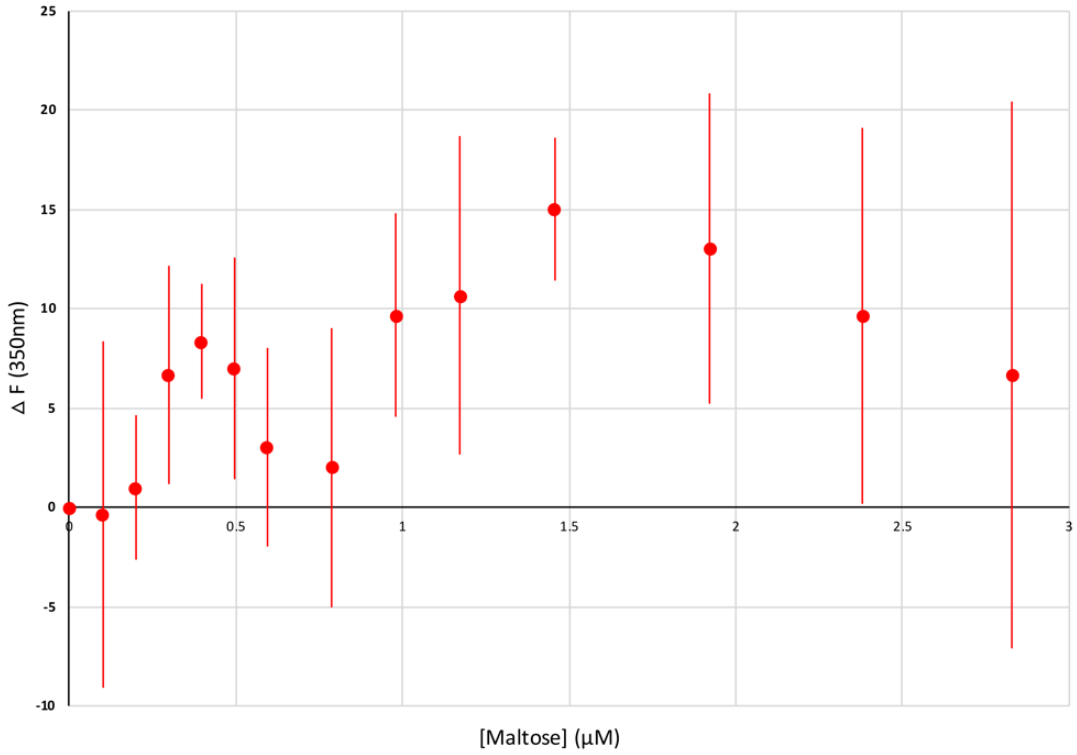

Figure 4.6: Binding curve of maltose to MSMEG_6366. Analysis of binding gave no binding coefficients, showing there is no effect on intrinsic tryptophan fluorescence upon titration of maltose. N=3

To determine that interactions were specific to galactan analogues, and that changes in fluorescence were not the result of non-specific interactions to MSMEG_6366 ITF was conducted using maltose as a control ligand (Figure 4.6). which showed no detectable interactions with MSMEG_6366.

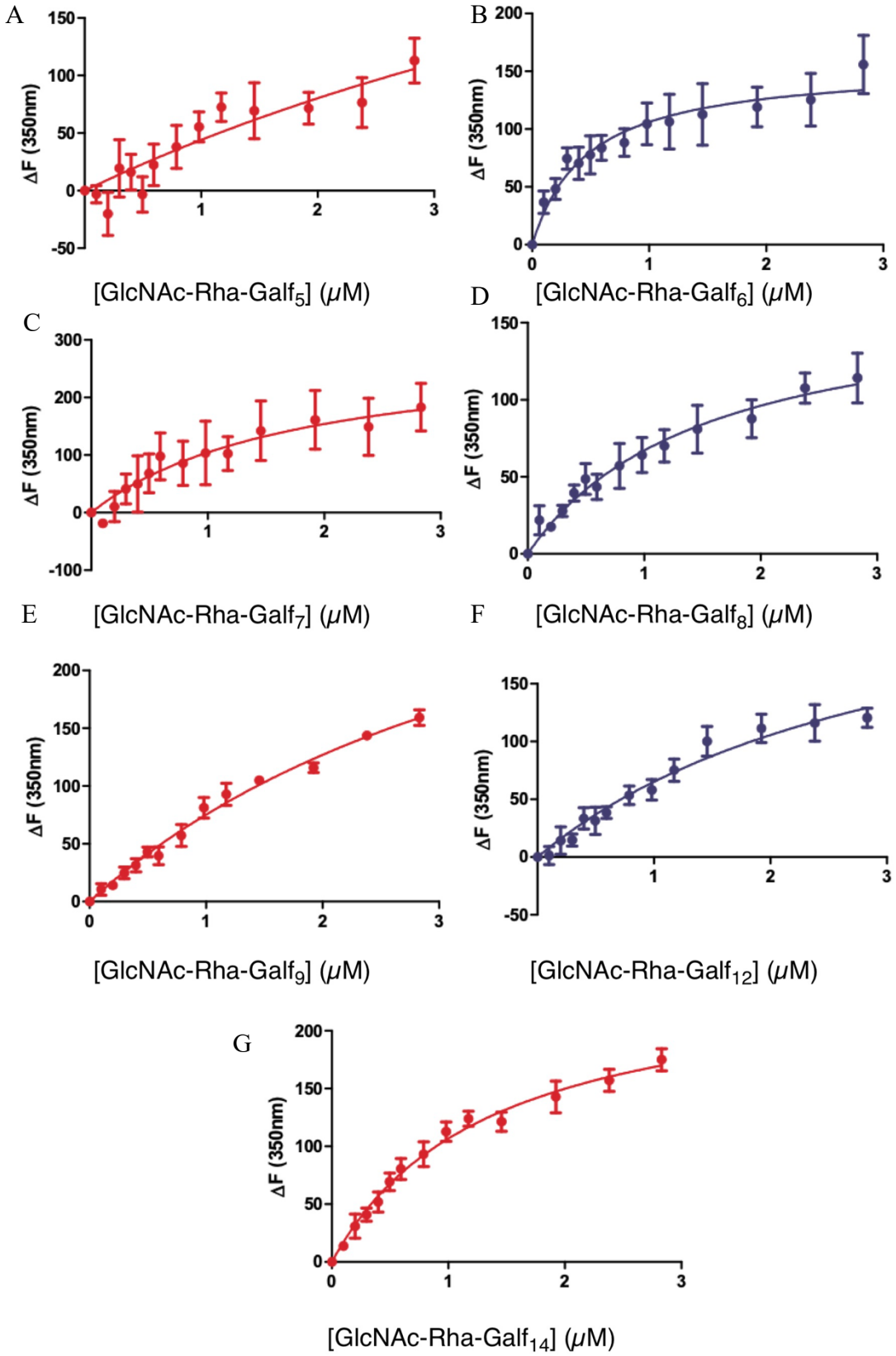

Figure 4.7: Binding curves of galactan analogues to MSMEG_6366. A) GlcNAc-Rha-Gal*f*$_5$, B) GlcNAc-Rha-Gal*f*$_6$, C) GlcNAc-Rha-Gal*f*$_7$, D) GlcNAc-Rha-Gal*f*$_8$, E) GlcNAc-Rha-Gal*f*$_9$, F) GlcNAc-Rha-Gal*f*$_{12}$, G) GlcNAc-Rha-Gal*f*$_{14}$. Showing MSMEG_6366 is able to bind to the galatan analogues, with variable binding affinity depending on the length of the Gal*f* chain length. N=3

Initial characterisation of ligand affinity was conducted using a galactan analogue composed of GlcNAc-Rha-Gal*f*$_6$, with the determination of a relatively high affinity interaction with MSMEG_6366, K_d: 0.47 μM (Figure 4.6, Table 4.2). This suggests that MSMEG_6366 is able to interact in some way to either the linker unit or the galactan chain, as such the use of different length polygalactofuranose analogues were tested to attempt to determine the effect of extending the chain on the affinity of the protein to the ligand.

Table 4.1: Binding constants of synthesised galactan analogues to MSMEG_6366. Showing dissociation constant (K_d), and maximal change in fluorescence upon saturation of all binding sites (B_{max}) and standard error

	K_d (μM)	Std. Error	B_{max} (ΔF_{450})	Std. Error
GlcNAc-Rha-Gal*f* $_5$	9.15	13.91	447.7	560.2
GlcNAc-Rha-Gal*f* $_6$	0.47	0.14	155.8	15.0
GlcNAc-Rha-Gal*f* $_7$	1.8	1.21	292.5	107.3
GlcNAc-Rha-Gal*f* $_8$	1.52	0.42	169.4	24.1
GlcNAc-Rha-Gal*f* $_9$	4.41	0.91	406.9	59.3
GlcNAc-Rha-Gal*f* $_{12}$	3.28	1.10	278.8	61.3
GlcNAc-Rha-Gal*f* $_{14}$	1.35	0.20	251.2	18.1

Analysis of the ligand binding affinities of MSMEG_6366 (Method 6.21.4, Figure 4.5, Table 4.2) to various artificially generated galactan analogues further suggest that MSMEG_6366 interacts with galactan analogues, and therefore with the galactan *in vivo*, with different affinities depending on the length of the poly-galactofuranose chain. However, due to the limitations of the experiment not all binding curves achieved saturation, and therefore there is significant error in the K_d and B_{max} values for these ligands.

The galactan analogue with the highest affinity for MSMEG_6366 was comprised of six galactofuranose residues attached to the linking unit. Analysis of the effect of the length of the galactofurnaose chain of the ligand on the binding affinity to MSMEG_6366 shows that there is no correlation between the length of the analogue and the binding affinity (Figure 4.6). This

suggests that the effect of increasing the length of the polygalactofuranose chain is not the sole factor for the change in the binding affinity. If the chain length was the sole factor this would be likely to lead a decrease in the binding affinity upon the sequential extension of galacofuranose chain, as the flexibility of the analogue would increase and so there would be increased forces acting to break the interactions between MSMEG_6366 and the ligand, assuming the same number of interaction points between the ligand and MSMEG_6366.

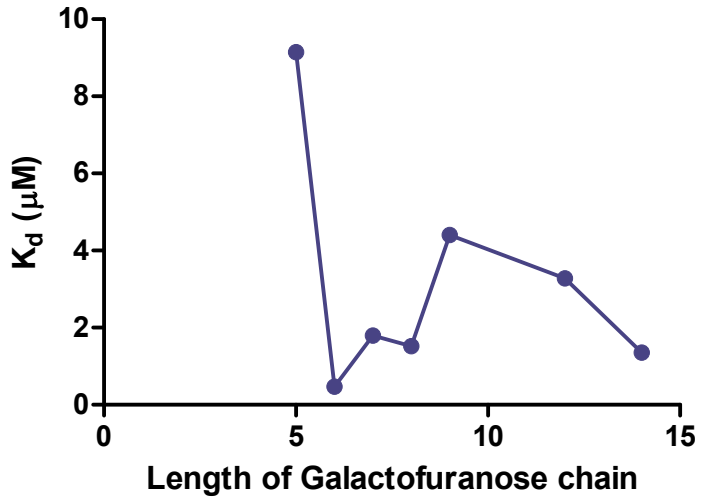

Figure 4.8: Galactofuranose chain length plotted against binding affinity to MSMEG_6366. Data does not show the predicted inverted bell curve of an optimum chain length with decreased affinity for chain lengths longer or shorter than the optimal binding length.

4.2.4: Predicted physiochemical properties of galactan analogues against binding affinity to MSMEG_6366:

As the chain length of the galactan analogue does not appear to be the sole contributing factor in the changes in binding affinity, predictions of the chemical properties were generated to attempt to understand the cause for the changes in the affinity between the various galactan analogues and MSMEG_6366. The physiochemical properties of the various analogues were calculated using the Chemicalize chemoinformatics tool (https://chemicalize.com/#/calculation, Method 2.22), resulting in the generation of predictions including: isoelectric point, Van der Waals surface area, hydrogen bond donor count, and hydrogen bond acceptor count (Table 4.3).

As the binding affinity of the galactan analogues to MSMEG_6366 does not show the predicted bell curve where galactan analogues with shorter gal*f* chains show lower affinity, with affinity increasing until reaching the optimum chain length before decreasing once extended beyond the optimum, the chemical properties of the ligands (Table 4.3), were plotted against K_d in order to determine if any of the predicted properties of these molecules would explain the unexpected binding affinity data (Figure 4.7).

Table 4.2: Predicted physiochemical properties of synthesised galactan analogues. Chemical predictions generated from SMILES structures, using Chemicalize prediction model.

	Kd (μM)	Hydrogen bond donor count	Hydrogen bond acceptor count	Topological polar surface area (Å^2)	Polarizability (Å^3)	Molar refractivity (cm^3/mol)	Isoelectric point	Van der Waals volume (Å^3)	Van der Waals surface area (Å^2)	Solvent accessible surface area (Å^2)	Minimum projection area (Å^2)	Maximum projection area (Å^2)	Minimum projection radius (Å)	Maximum projection radius (Å)	Hydrogen bond donors/ hydrogen bond acceptors
GlcNAc-Rha-Galf$_5$	9.150	22	35	573.92	101.57	240.18	4.88	995.41	1548.60	1292.38	148.30	231.67	9.1	10.64	0.6286
GlcNAc-Rha-Galf$_6$	0.467	25	40	653.07	115.38	272.59	4.91	1127.88	1755.50	1453.76	167.64	274.34	10.46	13.87	0.625
GlcNAc-Rha-Galf$_7$	1.798	28	45	732.22	129.19	305.01	4.93	1262.51	1962.55	1632.53	173.83	295.83	10.42	16.47	0.622
GlcNAc-Rha-Galf$_8$	1.524	31	50	811.37	143.01	337.42	4.94	1397.05	2168.11	1788.96	176.88	329.26	10.43	19.08	0.62
GlcNAc-Rha-Galf$_9$	4.407	34	55	890.52	156.82	369.83	4.95	1531.77	2375.92	1968.21	178.75	358.15	10.43	20.33	0.618
GlcNAc-Rha-Galf$_{12}$	3.277	43	70	1127.97	198.27	467.07	4.97	1935.62	2996.04	2466.24	232.27	419.44	10.48	22.32	0.614
GlcNAc-Rha-Galf$_{14}$	1.352	49	80	1286.27	225.90	531.9	4.98	2204.85	3412.96	2809.87	271.78	459.60	12.19	23.79	0.613

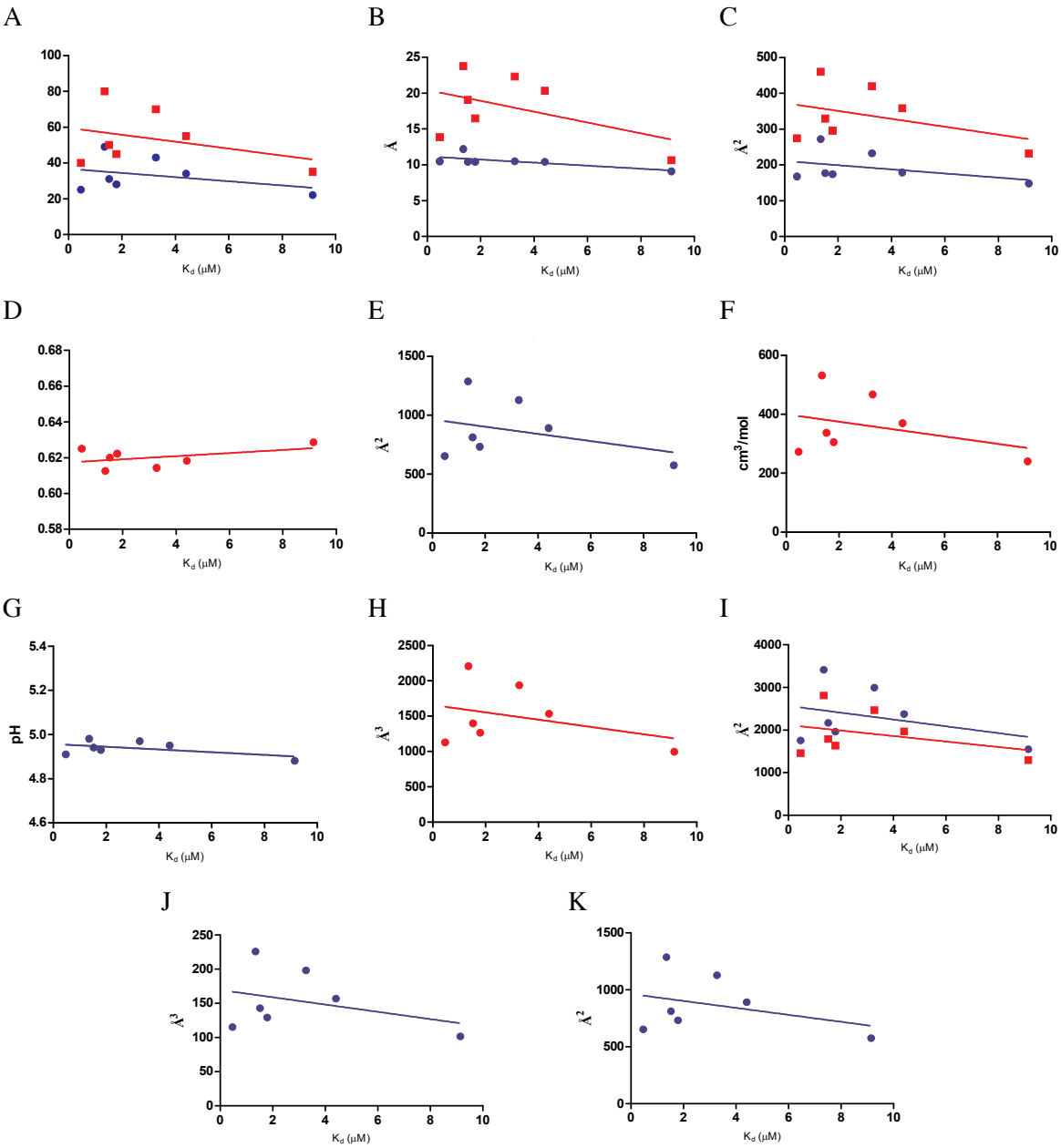

Figure 4.9: Predicted physiochemical properties of galactan analogues plotted against K_d to MSMEG_6366.

A) number of hydrogen bond donors in blue, number of hydrogen bond acceptors in red, B) minimum projection radius in blue, maximum projection radius in red, C) minimum projection area in blue, maximum projection area in red, D) number of hydrogen bond donors: number of hydrogen bond acceptors, E) topological polar surface area, F) molecular refractivity, G) isoelectric point, H) Van der Waals volume, I) Van der Waals surface area in blue, solvent accessible surface area in red, J) polarizability, K) topological polar surface area. Showing limited relationship between K_d and the predicted physiochemcical properties of the galactan analogues to MSMEG_6366.

Comparison of the predicted properties of the ligands against the K_d to MSMEG_6366 resulted in no factors giving an R^2 value above 0.5 using linear regression, therefore none of the predicted values correlate to 50 % of the variance in the experimental data (Table 4.4). That the best model for predicting the binding affinity of the ligand is the minimum projection radius, suggests that prediction of the properties is not enough to accurately determine cause of the change in the binding affinity, or that it is a factor of more than one property. The cause of this increase in correlation is that the minimum projection radius shows a small range, with only the range of the predicted isoelectric point being smaller (Table 4.4), and therefore the correlation is skewed.

Table 4.3: Linear regression analysis of predicted physiochemcial properties of galactan analogues against the determined dissociation constant. Calculated R^2 giving a range of 0- 1, 0 corresponding to no correlation, and 1 corresponding to perfect correlation showing no single predicted property of the ligands analysed correlates with the binding affinity to MSMEG_6366.

	Linear least squares fit
Hydrogen bond donor count	0.1232
Hydrogen bond acceptor count	0.1232
Topological polar surface area ($Å^2$)	0.1232
Polarizability ($Å^3$)	0.1232
Molar refractivity (cm^3/mol)	0.1232
Isoelectric point	0.2761
Van der Waals volume ($Å^3$)	0.1222
Van der Waals surface area ($Å^2$)	0.1232
Solvent accessible surface area ($Å^2$)	0.1209
Topological polar surface area ($Å^2$)	0.1232
Minimum projection area ($Å^2$)	0.1555
Maximum projection area ($Å^2$)	0.1635
Minimum projection radius ($Å$)	0.4943
Maximum projection radius ($Å$)	0.2269
Hydrogen bond donor/ hydrogen bond acceptor ratio	0.2016

4.2.5: Structural characterisation of MSMEG_6366:

Attempts to characterise the structure of purified MSMEG_6366 (Method 6.23) both with and without ligand present, at various protein concentrations, did not result in the generation of protein crystals of a resolution high enough to allow for structural determination.

Attempts at optimisation of the buffer conditions for the protein to form high-resolution crystals lead to no detectable increase in organisation of the structure. Attempts to remove the MBP-tag in order to remove the flexible linking region between MSMEG_6366 and the MBP-tag did not yield significant protein cleavage.

4.2.6: Expression and purification of MBP-tagged MSMEG_6369:

Standard in *E. coli* strains used for the expression of recombinant protein, such as *E. coli* BL21 DE3 and *E. coli* C41 DE3 (Safarpour et al., 2017; Schlegel et al., 2015), did not yield any detectable levels of expression upon induction of expression of MSMEG_6369, using Western blot at a molecular weight of 74 kDa. However, low level expression of MBP-MSMEG_6369 was detected in *E. coli* Shuffle T7 by Western blot (Method 6.21.2), with further investigation showing in low level soluble expression of MBP-MSMEG_6369 (Figure 4.8).

Due to the low-level expression and the reduced biomass in the strain able to express detectable levels of MBP-MSMEG_6369 present in the clarified lysate of *E. coli* no purified MSMEG_6369 was obtained. Due to the presence of membrane fragments in the clarified lysate, we predicted that MSMEG_6369 has inserted into the *E. coli* cytoplasmic membrane.

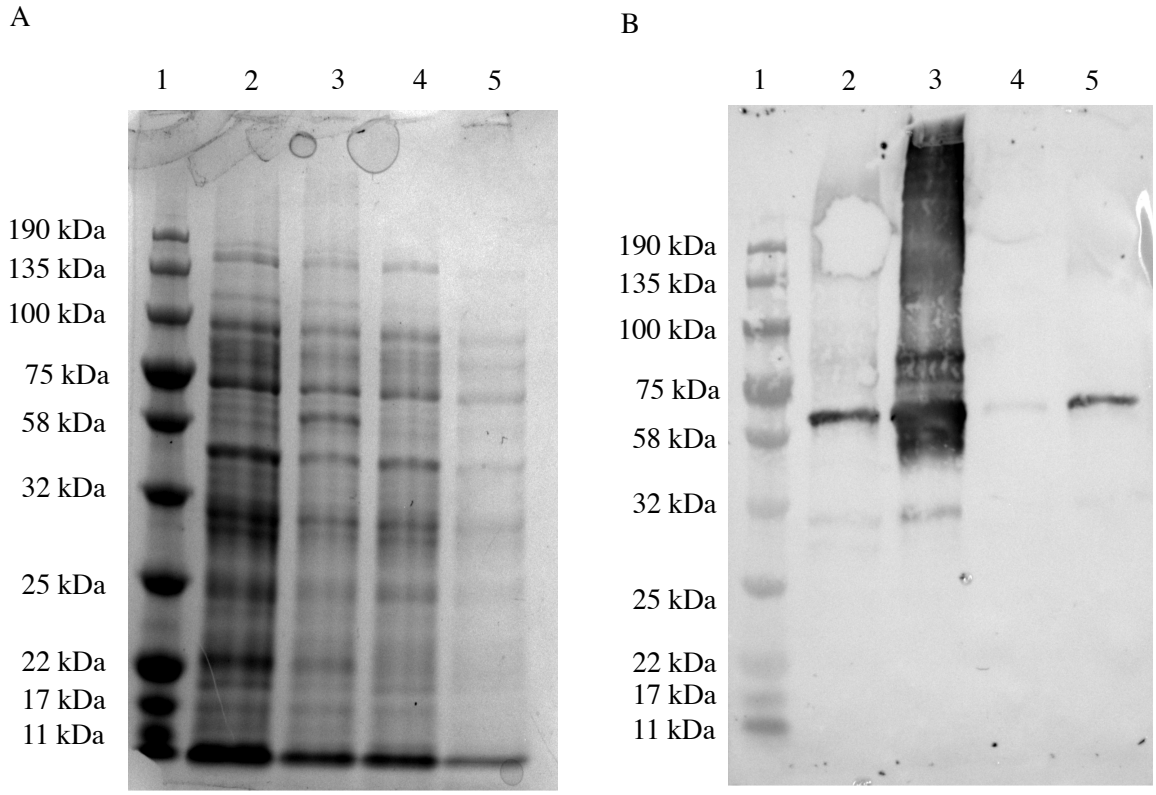

Figure 4.10: Western blot of inducible expression of MSMEG_6369 in *E. coli* K12 Shuffle T7. A) SDS-PAGE separation of proteins, B) anti-MBP Western blot of proteins. 1) Protein standard ladder, 2) cell lysate of uninducted cells, 3) cell lysate of cells induced with 1 mM IPTG, 4) clarified cell lysate of uninduced cells, 5) clarified cell lysate of cells induced with 1 mM IPTG. Showing expression of MBP-tagged MSMEG_6369 present in the clarified lysate of *E. coli* both with and without IPTG, showing some un-induced expression, with increased expression upon induction.

4.3: Discussion:

The determination of the binding of galactan analogues to MSMEG_6366 when not in a full complex lends further support for the identification of Rv3781 and Rv3783 and their *M. smegmatis* orthologs as the transporters for galactan across the inner membrane (Abrahams and Besra, 2016; Dianišková et al., 2011). Providing evidence for interactions between the transporter and the substrate, that there was no detectable interaction between MSMEG_6366 and maltose when used as a control supporting that the interactions are not an artefact. Additional experiments are required to fully characterise the binding of MSMEG_6366 to these ligands as much of the binding data presented is incomplete and would require additional binding experiments to confirm and improve the binding data presented as well as the use of additional controls including using polysaccharides that are not analogous to galactan as controls.

The change in the affinity of the analogues caused by the addition of further galactofuranose residues is to be expected, as changes in the length of the ligand are likely to alter the interactions between the protein and the solvent. There are likely to be few high energy interactions, in order to allow efficient transport across the membrane binding would likely be relatively weak (Cuthbertson et al., 2007).

Further study of the binding affinities of galactan analogues to MSMEG_6366 is required to determine the full range of binding affinities, as well as to confirm the binding affinities of ligands that did not achieve saturation. One method that potentially would overcome the issues encountered with ITF that did not allow for saturation to be achieved would be the use of isothermal calorimetry. Additionally extending the galactofuranose chain beyond 14 residues

would provide insights into the interactions between MSMEG_6366 and mature galactan (Benabdelhak et al., 2003). As the trend of binding constants against length of the galctofuranose chain does not follow a clear pattern, determining the effect on the binding for GlcNAc-Rha-Galf_n, where n is one to the maximal length for mature galactan would potentially provide information on the periodicity of the galactan structure as well as aid in understanding the interactions between the ligands and MSMEG_6366.

Galactan has been predicted to form a helical structure (Alderwick et al., 2005). However, due to the difficulty of structurally characterising polysaccharide structures, caused by the many potential hydrogen binding patterns of polysaccharide chains, and the inherent flexibility of polysaccharide chains, there is still no experimentally confirmed structure. As such defining the full pattern of binding affinities of the different lengths of galactan, in both the *M. smegmatis* and *Mtb* proteins might provide insight into this structure (Duus et al., 2000). Use of the ligands used in this study would potentially reduce the complexity of the process required to elucidate the physical structure of galactan as mature galactan contains 30 gal*f* residues. The use of shorter analogues would decrease the difficulty of experiments such as ^{1}H-^{1}H nuclear overhauser effect spectroscopy (NOESY). NOESY is used to determine the signals that arise from protons that are close in space to each other. This would allow for some determination of which residues are spatially close together and therefore could give some insight into the structure of the molecule, as it would potentially highlight which sugar residues are close to each other in solution (Cescutti et al., 2016; Duus et al., 2000; Leeflang et al., 2000).

While it is possible to predict the properties of polysaccharides such as galactan, it is difficult to determine how accurate these predictions are, as polysaccharides are generally flexible, and therefore difficult to generate crystal structures of. This is difficulty is compounded by the

incorporation of water into the structure (Duus et al., 2000). In addition to the use ^{1}H-^{1}H NOESY it would be possible to gain insights into secondary structure by labelling mycobacterial cells with ^{13}C galactose, and purification of the labelled galactan from the cell wall by running NOESY experiments using the NMR detectable ^{13}C, which would potentially highlight residues in the galactan chain that are close enough to each other in space to be detectable by NMR (Zhang et al., 2019).

While the work presented lends some evidence to the prediction that Rv3781 and Rv3783 are involved in the transport of galactan, further work is required to fully characterise these proteins. With structural characterisation of these proteins both as a complex and interacting either with the artificial galactan analogues utilised in this study, or with galactan purified from the mycobacterial cell wall would allow for improved ability to determine the residues involved in the interactions between galactan and Rv3781. This would then allow for expression and purification of proteins with single amino acid point mutations to confirm these predictions (Cox et al., 2016).

As the efforts in this project focussed primarily on the generation of un-cleaved fusion proteins and attempts to remove the tag were unsuccessful, further work would likely require the use of alternate constructs of both MSMEG_6366 and MSMEG_6369. These constructs should express these proteins with a less flexible, and less bulky, tag to reduce the structural variability of the protein in solution and therefore potentially improve the ability of the protein to crystalize (Smyth et al., 2003).

Further to structural work to characterise these proteins, work to determine the rate of transport of galactan across the membrane would allow for a greater understanding of how the

mycobacterial cell wall is built, and give further insight into the energy requirements of cell wall synthesis on the cell, which to a point is understood due to the size and complexity of the unique cell wall structures, however the energy cost of transport of many of the cell wall elements has not been characterised (Dong et al., 2017; Touchette and Seeliger, 2017).

While no purified MSMEG_6369 could be generated during this project, inducible expression of MSMEG_6369 was achieved. Further work to optimise the expression conditions and increase the yield of MSMEG_6369 from what was achieved during this project (Figure 4.10), would hopefully allow for purification of MSMEG_6369. Additionally the use of other methods of extracting proteins from the membrane may improve the efficiently of protein purification (Anandan and Vrielink, 2016; Pandey et al., 2016; Rothnie, 2016).

Further work to build on this stable protein expression could lead to the generation of an ABC-transport system, when combined with purification of MSMEG_6366, this would allow for the generation of an ATP-turnover assay to calculate the rate of ATP hydrolysis by coupling of maintenance of ATP levels by the action of pyruvate kinase conversion of ADP and phosphoenyol pyruvate, to pyruvate and ATP. Pyruvate can then be converted to lactate by the action of lactate dehydrogenase, which causes NADH to be converted into NAD^+. The conversion of NADH to NAD^+, changes the fluorescence spectrum of the solution, therefore allowing the both the detection of ATP turnover, while also maintaining the level of ATP in the reaction solution (Rule et al., 2016).

Chapter 5:

General discussion

The mycobacterial cytoplasmic membrane is a vital component of the mycobacterial cell, with both the inner and outer leaflet acting as the site for the synthesis of various cell wall structures. The inner leaflet of the cytoplasmic membrane is the site of synthesis for essential cell wall compounds, such as the galactan domain of AG, and the lipoglycans (Alexander et al., 2004; Birch et al., 2008; Escuyer et al., 2001).

In the last decade numerous publications have revealed the mechanisms of biosynthesis of the mycobacterial cell envelope (Harrison et al., 2016; Mishra et al., 2011; Škovierová et al., 2010). Most of the discrete enzymes involved in cell envelope anabolism have been characterised by either direct biochemical investigation or reverse genetic approaches (Alderwick et al., 2008, 2005; Cai et al., 2014; Mishra et al., 2012). Many of these enzymes have also been identified as having potential to be targeted by small molecule inhibitors.

The nature of scientific investigation dictates that the most experimentally tractable systems are usually studied first, due to the relative ease of working with cytosol soluble proteins. This has resulted in a significant increase in our understanding of mycobacterial cell envelope biosynthetic processes. In contrast, the mechanisms and processes by which cell envelope intermediates pass through the cytoplasmic membrane (the primary barrier of the cell) have been neglected, largely due to the difficulty in studying complex cell membrane processes (Shimizu et al., 2018).

This “final frontier” of mycobacterial physiology deserves significant attention due to its importance in the pathway to the establishment of a mature and fully functional cell envelope. While there has been much research focussing on the development of anti-mycobacterial compounds, the determination of the precise mechanism of action has not always been able to

be determined before clinical use (Goude et al., 2009; Safi et al., 2008; Srivastava et al., 2009; Tsukamura, 1965). The prime example of this is the use of EMB for the treatment of TB. The understanding of how EMB inhibits the essential arabinosyltransferase proteins (EmbCAB) remains a point of debate (Alderwick et al., 2007; Belanger et al., 1996; Goude et al., 2009; Khoo et al., 1996; Pawar et al., 2019; Takayama and Kilburn, 1989). With initial determination of the mechanism of action being determined from the generation of resistant mutations in clinical isolates leading to the identification of the EmbCAB proteins as the targets (Radmacher, 2005; Safi et al., 2008; Srivastava et al., 2009).

LM and LAM are key immunomodulatory glycoconjugates distributed throughout the mycobacterial cell envelope (Pitarque et al., 2008). During the synthesis of LM and LAM, the pathways progresses though an undefined translocation system (Figure 1.17). Analogous biosynthetic pathways appear in other bacterial organisms with the formation of Lipid A in Gram negative species being a prime example (H. Singh et al., 2016; Xie et al., 2015). In Chapter 2, we sought to identify the protein(s) responsible for moving PIMs across the cytoplasmic membrane. This lead to use of the known *E. coli* lipid A transporter, MsbA to identify Rv1272c and Rv1273c as putative homologs in *Mtb* through bioinformatic analysis (Figures 2.2, 2.3, Table 2.1) (H. Singh et al., 2016). The generation and characterisation of a double deletion mutant strain in the model organism *C. glutamicum*, and complementation with the Rv1272c and Rv1273c led to the identification of NCgl0925 and NCgl0926 as the components of a conserved predicted heterodimeric ABC-transporter in the Corynebacteriales suborder, as the complex responsible for the translocation of PIMs (Figures 2.10-12, 2.14, 2.18, 2.20) (Gupta et al., 2019; Wang et al., 2010). With future work required to understand the mechanism of translocation of PIMs, potentially leading to the generation of an inhibitor capable of disrupting this process, either through the development of novel small molecule inhibitors, or through

drug repurposing (Cha et al., 2018; Patel et al., 2019; Pushpakom et al., 2019; Singh et al., 2019).

AG provides the base upon which the mycomembrane is attached (Alderwick et al., 2015). EMB has been hypothesised to target the Emb proteins responsible for the extension of the arabinan domains of AG and LAM. However the precise mechanism of these interactions between Emb and EMB remain unknown (Srivastava et al., 2009). Chapter 3 presents data showing the effect of mutations in the Cg-Emb protein leading to restoration of EMB resistance in an EMB hypersensitive strain of *C. glutamicum*. Cell envelope analysis of strains expressing Cg-Emb with specific point mutations compared to strains expressing the WT Cg-Emb reveals the knock-on effect mutations in Cg-Emb have on the composition of the cell envelope (Figures 3.4-3.8). As the transmembrane helix domains contained all the SNPs conferring resistance highlighting the requirement for the determination of a structure of the EmbCAB proteins in mycobacteria, both in the presence of EMB and without EMB to confirm the hypothesis that the Emb proteins are the target for EMB as well to improve the understanding of how these proteins function (Srivastava et al., 2009).

The AG biosynthetic pathway, requires the translocation of galactan across the cytoplasmic membrane for the addition the arabinan domains. The proteins responsible for the export of this glycoconjugate precursor have been predicted for almost a decade, however the experimental evidence for this prediction has remained inconclusive (Dianišková et al., 2011). In Chapter 4, we sought to determine if the predicted *M. smegmatis* galactan transporter interacts with a synthetic galactan analogue. This led to the recombinant expression and purification of the soluble NDB (MSMEG_6366) and the determination of the binding constants of ligands corresponding to immature galactan chains. This determination of the

interaction between MSMEG_6366 and the immature galactan supports the predicted function of Rv3781 and Rv3783 as forming the ABC-transporter responsible for the export of galactan. Though further investigation into the key residues required for these interactions, as well as completion of the determination of the binding constants of curves that did not achieve saturation, and how the MSMEG_6366/MSMEG_6369 complex converts the hydrolysis of ATP to the translocation of galactan is required to understand how this process is controlled *in vivo* to prevent the translocation of immature galactan. The development of this assay system would allow for the targeted development of small molecule inhibitors, as well as the screening of clinically available, FDA approved drugs for to act as either scaffolds for alteration, or potentially as candidates for drug repurposing (Cha et al., 2018; Patel et al., 2019; Pushpakom et al., 2019; Singh et al., 2019).

Chapter 6:

Materials and methods.

6.1.1: Bioinformatic analysis of MsbA against mycobacterial and corynebacterial proteins:

BLASTp analysis of *E. coli* K12 MsbA primary protein structure against non-redundant protein database of *Mtb* H37Rv. Mycobacterial protein sequences for comparative analysis selected from Mycobrowser (https://mycobrowser.epfl.ch/ Kapopoulou et al., 2011). BLASTp analysis of primary protein structure identified from the initial BLASTp analysis (Rv1272c and Rv1273c) against additional mycobacterial species (*M. bovis, M. leprae, M. smegmatis, M. marinum*) was used to confirm conservation of orthologous genes.

Sequence alignment of selected proteins of interest conducted using Clustal Omega (https://www.ebi.ac.uk/Tools/msa/clustalo/ Sievers et al., 2011). Sequence alignment of protein sequences generated using ESPript 3.0 (http://espript.ibcp.fr/ESPript/ESPript/ Gouet et al., 1999).

Topological predictions of proteins predicted to include the number and location of transmembrane helices generated using TMHMM 2.0 (http://www.cbs.dtu.dk/services/TMHMM/), and ExPASy TMPred (https://embnet.vital-it.ch/software/TMPRED_form.html).

6.1.2: Bioinformatic analysis of predicted mycobacterial galactan transporters:

BLASTp analysis of the primary protein structure of the previously hypothesised *M. smegmatis* galactan transporter (MSMEG_6366, and MSMEG_6369) against non-redundant protein

database of *Mtb* H37Rv, and *M. leprae* (taxid: 1769). Mycobacterial protein sequences for analysis selected from Mycobrowser (https://mycobrowser.epfl.ch/ Kapopoulou et al., 2011).

Sequence alignment of selected proteins of interest conducted using Clustal Omega (https://www.ebi.ac.uk/Tools/msa/clustalo/ Sievers et al., 2011). Sequence alignment of protein sequences generated using ESPript 3.0 (http://espript.ibcp.fr/ESPript/ESPript/ Gouet et al., 1999).

Topological predictions of proteins predicted to include the number and location of transmembrane helices generated using TMHMM 2.0 (http://www.cbs.dtu.dk/services/TMHMM/), and ExPASy TMPred (https://embnet.vital-it.ch/software/TMPRED_form.html).

6.2: Culture conditions of *E. coli*, *C. glutamicum*, and *M. smegmatis*:

M. smegmatis and *E. coli* grown on lysogeny broth (LB) agar (Difco), at 37 °C for colony generation, incubated for three days or one day respectively, unless stated otherwise. *M. smegmatis* and *E. coli* grown in LB (Difco), at 37 °C, 180 rpm, for liquid culture, unless otherwise stated. *M. smegmatis* liquid culture supplemented with 0.05 % TWEEN-80 to prevent clumping. *C. glutamicum* grown on Brain heart infusion (BHI) agar (Difco), at 30 °C, incubated for one day for single colony generation, unless otherwise stated. *C. glutamicum* liquid culture grown in BHI broth (Difco), at 30 °C, 180 rpm, unless stated otherwise.

6.3.1: Generation of double knockout of MSMEG_5008 and MSMEG_5009 in *M. smegmatis*:

DNA sequence amplified by PCR using purified *M. smegmatis* genomic DNA Q5 DNA polymerase, with high GC enhancer (NEB) annealing gradient 65-79 °C, 45 sec extension time, following manufacturers guidelines using the following primers:

5'- TTTTTTTTCCATAAATTGGCGGCCCGTACTGCAGGACGTGTCGTTC -3',

5'- TTTTTTTTCCATTTCTTGGCGACAACAGATCCGCGAACGTCCCGTC -3',

5'- TTTTTTTTCCATAGATTGGCGTCTCGCGATCGCGCGTGCGGTGATC -3', and

5'- TTTTTTTTCCATCTTTTGGGAGCGACGCGTGATCCACCGCGTCACC -3'.

Modified p0004s plasmid, containing inserted DNA flanking a *hyg- sacB* insertion element by use of Van91I digestion of amplified sequences, inserted into the conditionally replicating phasmid phAE159 into its PacI site to yield ph∆*MSMEG*_5008-5009 (Bardarov et al., 2002). Two step homologous recombination using ph∆*MSMEG*_5008-5009, leading to the replacement of the genomic sequence between the amplified sequences with a *hyg-sacB* insertion element replacing the deleted genes and conferring Hygromycin resistance (Bhatt et al., 2008)

6.3.2: Generation of *C. glutamicum*∆*NCgl0925- 0926* strain:

Conducted by: J. Marienhagen's group

pk19*mobsacB*-∆*NCgl0925- 0926* generated using:

5'- CGTTAAGCTTAGCCGTTCTACGGTTTCCGTTCC -3'

5’- CCCATCCACTAAACTTAAACAATATCGACCACAGCATGAATGTATTC -3’

5’- TGTTTAAGTTTAGTGGATGGGGCGAAAGAAGAATTACAGGCTGACG -3’ and

5’- GCTTGGATCCTCATGCGCGAAGCCCACCTCAC -3’

DNA sequence amplified using purified chromosomal DNA extracted from *C. glutamicum* ATCC13032, using Q5 DNA polymerase, with high GC enhancer (NEB) annealing gradient 65-79 °C, 45 sec extension time. Correct insertion of respective genes inserted confirmed by DNA sequencing (Eurofins). Two step homologous recombination using pk19*mobsacB*-Δ*NCgl0925- 0926* replacing the deleted genes, without conferring antibiotic resistance Schäfer et al., 1994.

6.3.3: Generation of *C. glutamicum*Δ*steA*Δ*ripA* MB001:

Conducted by T. Bernhardt’s group

Generation of *C. glutamicum*Δ*steA*Δ*ripA* as described in Lim et al., 2019.

6.4.1: Generation of EMB resistant *C. glutamicum*Δ*steA*Δ*ripA* MB001:

Conducted by T. Bernhardt’s group

25 million CFU of *C. glutamicum*Δ*steA*Δ*ripA* plated on agar plates containing 0.1 μg/ml EMB to generate resistant mutants. Mutant generation rate determined at 1 $x10^{-7}$.

6.4.2: Mutation mapping of EMB resistant *C. glutamicum*Δ*steA*Δ*ripA* MB001:

Conducted by T. Bernhardt's group

Genomic DNA of *C. glutamicum*Δ*steA*Δ*ripA* strains resistant to EMB purified and sequenced as described in Baym et al., 2015. Single nucleotide polymorphisms identified by comparison of the resistant strains and the parental *C. glutamicum*Δ*steA*Δ*ripA* strain.

6.5: Genomic DNA purification of *M. smegmatis*:

25 ml of *M. smegmatis* culture grown to OD_{600}: 0.4- 0.6, centrifuged at 4,000 rpm, RT, 30 mins. Supernatant removed and pellet re-suspended in 450 µl GTE buffer (25 mM Tris, pH 8, 10 mM EDTA, 50 mM glucose, 0.1 mg/ml RNAse). 50 µl lysozyme (10 mg/ml) added, suspension incubated at 37 °C, overnight. 100 µl 10 % Sodium dodecyl sulphate (SDS), and 20 µl Proteinase K (15 mg/ml) added and incubated at 55 °C, 3 hours. 10 µl RNAse A (10 mg/ml) added, and incubated 37 °C, 30 mins. 200 µl 5 M NaCl, 1 ml chloroform: isoamylalcohol (24:1) added, and centrifuged 13,000 rpm, 10 mins. Aqueous layer removed and added to 0.7 volumes ice cold isopropanol and gently mixed. Suspension centrifuged at 13,000 rpm, 4 °C, 30 mins, supernatant removed, pellet washed with 700 µl ice cold 70 % ethanol. Suspension centrifuged at 13,000 rpm, 4 °C, 30 mins, supernatant removed, pellet dried at RT. Pellet re-suspended in 20 ul dH_2O, incubated at RT, 15 mins, DNA concentration determined by A_{260}/A_{230} ratio using NanoDrop 2000 (ThermoScientific).

6.6.1: Generation of competent *E. coli*:

Single colony of *E. coli* strain to be made competent selected and used to inoculate 5 ml of sterile media, culture then incubated at 37 °C, 180 rpm overnight. 1 ml of culture used to inoculate 100 ml of sterile media, and grown at 37 °C, 180 rpm until the culture reaches OD_{600}: 0.4- 0.8. Culture then centrifuged at 4,000 rpm for 20 mins at 4 °C, supernatant removed. Pellet re-suspended in 10 ml ice cold sterile 100 mM $CaCl_2$. Suspension centrifuged at 4,000 rpm for 20 mins at 4 °C, supernatant removed. Pellet re-suspended in 2.5 ml ice cold sterile 100 mM $CaCl_2$, 15 % glycerol and aliquoted into 100 µl fractions. Fractions then flash frozen in liquid nitrogen ($_{lq}N_2$) and stored at -80 °C.

6.6.2: Transformation of plasmid into competent *E. coli*:

Competent *E. coli* thawed on ice and mixed with 50 ng of plasmid, and incubated on ice for 10 mins. Cells then heat shocked at 42 °C for 30 seconds, and incubated on ice for 10 mins. 250 µl of sterile media added and cells incubated at 37 °C for 1 hour before being transferred onto agar plates with the appropriate antibiotic for selection of the plasmid (Kanamycin 50 µg/ml, Hygromycin B 150 µg/ml, Ampicillin 100 µg/ml). Plates then incubated at 37 °C overnight.

6.6.3: Purification of plasmid from *E. coli*:

Single colony of *E. coli* expressing plasmid to be purified used to inoculate 5 ml of sterile media and incubated at 37 °C, 180 rpm, overnight. Culture centrifuged at 4,000 rpm for 10 mins, and supernatant removed. Plasmid extracted using QIAprep spin miniprep protocol (Qiagen).

6.7.1: Generation of competent *C. glutamicum*:

500 ml culture of *C. glutamicum* grown to OD_{600}: 1.75. Culture chilled on ice, and centrifuged at 4,000 rpm, 4 °C, 30 min. Supernatant removed, cell pellet washed in 20 ml sterile TG-buffer (1 mM Tris-Cl, pH 7.5, 10 % glycerol), cell suspension centrifuged at 4,000 rpm, 4 °C, 30 min. Supernatant removed, cell pellet washed in 20 ml sterile TG-buffer. Cell suspension centrifuged at 4,000 rpm, 4 °C, 30 min. Supernatant removed, cell pellet washed in 20 ml sterile 10 % glycerol, cell suspension centrifuged at 4,000 rpm, 4 °C, 30 min. Supernatant removed, cell pellet resuspended in 1 ml sterile 10 % glycerol, Cell suspension separated into 100 µl aliquots, aliquots flash frozen in $_{lq}N_2$, and stored at -80 °C until needed.

6.7.2: Transformation of *C. glutamicum*:

1 µg plasmid DNA, mixed with 100 µl competent *C. glutamicum* on ice, in 1 mm electroporation cuvette. Mixture layered with 800 µl ice cold 10 % glycerol. Sample electroporated at: 25 µF, 200 Ω, 2500 V. Sample transferred to 4 ml sterile BHI pre-equilibrated to 46 ˚C, and incubated at 46 ˚C for 6 min. Sample incubated at 30 ˚C, 1- 3 hours. Samples centrifuged 3, 500 rpm, 10 min, 4 ˚C. Supernatant removed, cell pellet resuspended in remaining liquid, and transferred to BHI + 0.5 M sorbitol agar plates, 25 µg/ml spectinomycin. Agar plates incubated 30 ˚C 2 days, and checked for colonies denoting successful transformants.

6.8.1: Generation of pEKEx3-*NCgl0925- NCgl0926* plasmid:

Conducted by: J. Marienhagen's group

Primers used:

5'- GTCGACTCTAGAGGATCCCCAAGGAGATATAGATATGCTGTG-3' and

5'- TGAATTCGAGCTCGGTACCCTTATTAGTGATCTCCG-3'

Gene sequence amplified using purified chromosomal DNA extracted from *C. glutamicum* ATCC13032 using Q5 DNA polymerase, with high GC enhancer (NEB) annealing gradient 65-79 °C, 190 sec extension time. Correct insertion of respective genes inserted confirmed by DNA sequencing (Eurofins).

6.8.2: Generation of pEKEx3-*Rv1272c- Rv1273c* plasmid:

Conducted by: J. Marienhagen's group

Primers used:

5'GTCGACTCTAGAGGATCCCCAAGGAGATATAGATATGCTCCTGGCCCTGCTGC

G-3' and

5'- TG AATTCGAGCTCGGTACCCTTATTAGGCCCGCGTCATCTGGTAATAG-3'

Gene sequence amplified using purified chromosomal DNA extracted from *M. tuberculosis* H37Rv using Q5 DNA polymerase, with high GC enhancer (NEB) annealing gradient 65-79

°C, 190 sec extension time. Correct insertion of respective genes inserted confirmed by DNA sequencing (Eurofins).

6.9.1: Generation of the pMAL-c2x-MSMEG_6366 plasmid:

MSMEG_6366 gene sequence amplified by PCR using purified *M. smegmatis* genomic DNA with Q5 DNA polymerase, with high GC enhancer (NEB) annealing gradient 65-79 °C, 45 sec extension time, following manufacturers guidelines, using primers:
5'-TTTTTTGAATTCGTGACATCCTCTTCTGCACCGCGCAT-3' and
5'-TTTTTTAAGCTTTCAGTGTGCGTCAGCCGCGGTTTCCT-3'

PCR product generated from purified chromosomal DNA extracted from *M. smegmatis* MC^2 155 using Q5 DNA polymerase, with high GC enhancer (NEB) annealing gradient 65-79 °C. PCR product and pMAL-c2x digested using EcoRI and HindIII, ligated together using T4 DNA-ligase (NEB) following manufacturer guidelines. Ligation mix transformed into *E. coli*, successful ligation products confirmed by DNA sequencing (Eurofins).

6.9.2: Generation of the pMAL-c2x-MSMEG_6369 plasmid:

MSMEG_6369 gene sequence amplified by PCR using purified *M. smegmatis* genomic DNA with Q5 DNA polymerase, with high GC enhancer (NEB) annealing gradient 65-79 °C, 45 sec/kb extension time, following manufacturers guidelines, using primers:
5'- TTTTTTGAATTCATGACTTTCACCGACGCGGCGGCGCAGT-3' and
5'- TTTTTTAAGCTTTCAGACCCAGTAGGGCACGCGGCCGCGGT-3'

PCR product generated from purified chromosomal DNA extracted from *M. smegmatis* MC^2 155. PCR product and pMAL-c2x digested using EcoRI and HindIII, ligated together using T4 DNA-ligase (NEB) following manufacturer guidelines. Ligation mix transformed into *E. coli*; successful ligation products confirmed by DNA sequencing (Eurofins).

6.10: Growth rate analysis in *C. glutamicum*:

C. glutamicum strains to be analysed streaked onto BHI agar to generate single colonies. 5 ml of media inoculated with single colony, grown to OD_{600}: 1- 2. Culture diluted into 5 ml fresh BHI, or BHI + 0.5 M sorbitol, for OD_{600}: 0.05, timepoints measured using OD_{600}.

6.11: Cell surface permeability analysis of *C. glutamicum* strains:

C. glutamicum cultures grown to OD_{600}: 1- 2. Cells harvested, 4,000 rpm, 5 mins, RT, supernatant removed. Cell pellet resuspended and fixed in 2 ml 0.25 % formaldehyde in PBS, incubated 1 hour, RT. Fixed cells harvested 4,000 rpm 5 mins, RT, supernatant removed, pellet washed twice in PBS. Fixed cells resuspended in PBS to OD_{600}: 1 in either: 0.25 μM 1, 6-diphenyl- hexa- 1, 3, 5- triene (DPH) in PBS, or PBS, transferred to 96-well black walled, black bottom, flat bottom, microtitre plate, incubated at 37 °C, 1 hour. Fluorescence of cells determined at Excitation 350 nm, Emission 450 nm.

Intrinsic fluorescence of cells and of DPH in PBS averaged and subtracted from the fluorescence of cells in DPH. Resulting data collected normalised with wild type strain average set to 100 %, with fold change of all strains and controls calculated against this value. Statistical significance of permeability changes determined using Bonferroni corrected ANOVA.

6.12.1: Extraction of *C. glutamicum* polar-apolar lipids:

50 ml culture grown to OD_{600}: 1- 2, culture centrifuged 4,000 rpm, 30 mins, supernatant removed. Pellet resuspended in 10 ml sterile phosphate buffered saline (PBS), centrifuged 3,000 rpm, 30 mins, supernatant removed. Pellet dried at 50 °C, under nitrogen. Cell pellet resuspended in 4 ml petroleum ether 60-80 (PE60), incubated at RT under agitation 1 hour. Suspension centrifuged 3,000 rpm, 10 mins, RT. Supernatant, containing external free lipids transferred to clean tube, pellet resuspended in 4 ml PE60, incubated at RT under agitation 1 hour. Suspension centrifuged 3,000 rpm, 10 mins. Supernatant removed and pooled with previous extraction, dried at 50 °C, under N_2 for apolar outside lipids.

Cell pellet dried and resuspended in 2 ml 10: 1 methanol: 0.3 % NaCl, and 2 ml PE60 added. Cell suspension incubated RT, under agitation, 15 mins. Suspension centrifuged at 4,000 rpm, 5 mins, upper phase, containing the internal non-polar lipids, transferred to clean tube. 2 ml PE60, incubated at RT for 15 mins under agitation. Centrifuged at 3,000 rpm, 5 mins, upper phase pooled with the previously extracted apolar inside lipids. Sample, and cell pellet dried at 50 °C, under nitrogen.

Pellet resuspended in 2.3 ml 9: 10: 3 chloroform: methanol: 0.3 % NaCl, incubated at RT, under agitation, 1 hour. Suspension centrifuged 3,000 rpm, 15 mins. Supernatant, transferred to a clean tube. Pellet resuspended twice in 750 µl 5: 10: 4 chloroform: methanol: 0.3 % NaCl, incubated at RT, under agitation, 30 mins. Suspension centrifuged 3,000 rpm, 15 mins. Supernatant pooled with previous extractions. 2.6 ml 1: 1 $CHCl_3$: 0.3 % NaCl added to the pooled extracts, incubated at RT, 5 mins under agitation. Lower phase, containing polar lipids, removed to a fresh tube, dried at 50 °C, under nitrogen.

6.12.2: Extraction of *C. glutamicum* inner membrane - outer membrane lipids:

50 ml culture grown to OD_{600}: 1- 2, culture centrifuged 4,000 rpm, 30 mins, supernatant removed, cell pellet dried under N_2 at 50 °C in a glass tube with PTFE cap. Cell pellet resuspended in 2 ml dH_2O saturated butan-1-ol (approximately 2-3 ml dH_2O for every 10 ml butan-1-ol), incubated under agitation at RT, 1 hour. Suspension centrifuged, 5 mins, 3,000 rpm, RT. Supernatant removed and dried under N_2 at 50 °C, repeated twice to removed outer membrane lipids. Dried extraction washed with 2: 1 $CHCl_3$: CH_3OH, to selectively solubilise lipids removing contaminating proteins due to differing solubility.

Pellet dried and resuspended in 2 ml 2: 1 $CHCl_3$: CH_3OH, under agitation at RT for 1 hour. Suspension centrifuged 3000 rpm, 5 mins, RT, supernatant removed and dried under N_2 at 50 °C repeated twice to extract inner membrane lipids. Dried extraction washed with 2: 1 $CHCl_3$: CH_3OH, to selectively solubilise lipids removing contaminating proteins.

6.12.3: Reverse micellar extraction of surface lipids from *C. glutamicum*:

50 ml culture grown to OD_{600}: 1- 2, culture centrifuged 4,000 rpm, 30 mins, supernatant removed, cell pellet dried under N_2 at 50 °C in a glass tube with PTFE cap. Dried cell pellet resuspended in 2 ml 10 mM sodium docusate (AOT) in heptane, and incubated under agitation 2 hours, RT. Cell suspension centrifuged 3,000 rpm, 5 mins, RT, supernatant removed and transferred to clean tube, dried under N_2 at 50 °C. Process repeated twice, with supernatant pooled, to maximise extraction of surface lipids. Extracted lipids resuspended in 500 µl 2: 1 $CHCl_3$: CH_3OH and washed with dH_2O in order to remove contaminating docusate.

6.12.4: Extraction of *C. glutamicum* cell wall bound lipids:

Dried delipidated cell pellet resuspended in 2 ml 5 % tetrabutylammonium hydroxide (TBAH), incubated 95 °C, overnight. 2 ml H_2O, 4 ml dichloromethane, and 50 µl iodomethane added and incubated at RT, 30 mins, under agitation. Sample centrifuged, 3,000 rpm, 10 mins, lower phase transferred to fresh tube. 4 ml H_2O added to removed lower phase, and incubated under agitation 30 mins, RT. Sample centrifuged 3,000 rpm, 10 mins, upper phase discarded and process repeated. Upper phase discarded, lower phase dried at 50 °C, under N_2. Sample resuspended in 4 ml diethyl ether, sonicated in sonicating water bath, 5 mins, RT, Suspension centrifuged 3,000 rpm, 10 mins, RT. Supernatant transferred to clean tube, and dried at 50 °C, under N_2 for the fatty acid methylesters (FAMEs) and corynemycolic acid methyl esters (cMAMEs).

6.13: Silica column lipid purification

Silica column equilibrated with 3 column volumes 100 % $CHCl_3$. Crude reverse micellar lipid extract gently transferred into column. Column sequentially washed with 100 ml of: 100 % $CHCl_3$, 98: 2 $CHCl_3$: CH_3OH, 95: 5 $CHCl_3$: CH_3OH, 93: 7 $CHCl_3$: CH_3OH, 90: 10 $CHCl_3$: CH_3OH, 88: 12 $CHCl_3$: CH_3OH, 85: 15 $CHCl_3$: CH_3OH, 83: 17 $CHCl_3$: CH_3OH, and 80: 20 $CHCl_3$: CH_3OH, collected in 12 ml fractions. Eluted fractions analysed by TLC to determine lipid composition, elution fractions containing equivalent lipids pooled, dried under N_2, 50 °C and mass of purified lipid determined.

6.14.1: Lipid analysis by thin layer chromatography (TLC):

Lipid analysis conducted on F_{242} silica TLC plates, using various solvent systems.

Lipids extracted from previously described methods of lipid extraction analysed by 2 directional (2D) TLC, using various systems:

TLC systems for free and Non-polar lipids	
System	Direction 1 solvent system (Times run)
A	PE60: Ethyl acetate 98: 2 (3)
B	PE60: Acetone 92: 8 (3)
C	Chloroform: Methanol 96:4 (1)
D	Chloroform: methanol: water 100: 14: 0.8 (1)

TLC systems for free and Non-polar lipids	
System	Direction 2 solvent system (Times run)
A	PE60: acetone 98: 2 (1)
B	Toluene: acetone 95: 5 (1)
C	Toluene: acetone 80: 20 (1)
D	Chloroform: methanol: acetone: water 50: 60: 2.5: 3 (1)

TLC systems for polar lipids	
System	Direction 1 solvent system (Times run)
D	Chloroform: methanol: water 100: 14: 0.8 (1)
E	Chloroform: methanol: water 60: 30: 6 (1)

TLC systems for polar lipids	
System	Direction 2 solvent system (Times run)
D	Chloroform: methanol: acetone: water 50: 60: 2.5: 3 (1)
E	Chloroform: acetic acid: methanol: water 40: 25: 3: 6 (1)

Two directional TLCs used for all fractions:

Direction	Solvent system (Times run)
1	Chloroform: methanol: water 30: 8: 1 (1)
2	Hexane: diethyl ether: Acetic acid 70: 30: 1 (1)

One directional TLC systems used to analyse lipids:

Lipid analysed	Solvent system (Times run)
Fatty acid methyl esters (FAMEs) and Mycolic acid methyl esters (MAMES)	PE60: acetone 95: 5 (1)
All extracted fractions	Chloroform: methanol: H_2O 30: 8: 1 (1)
All extracted fractions	Chloroform: methanol: ammonium hydroxide (25%): H_2O 65: 25: 0.5: 3.6 (1)
All extracted fractions	Chloroform: methanol: ammonium hydroxide: ammonium acetate (1 M): H_2O 180: 140: 9: 9: 23 (1)

6.14.2: Preparative TLC:

Lipid extraction fraction containing lipid to be extracted run on TLC as described in Method 6.14.1. TLC imaged using: 0.5% (w/v) DPH in 95:5 $CHCl_3$: CH_3CH_2OH, lipids visualised by UV light excitation: 350 nm, emission: 400-550 nm (visible spectrum). Detectable bands marked, and TLC run using solvent system: 100 % PE60 to remove DPH. Silica containing desired lipid removed from TLC plate, washed 3 times with 5 ml 2:1 $CHCl_3$: CH_3OH, solvent removed and dried between washes. The resulting extracted lipid weighed and the lipid identity confirmed by TLC (Method 6.14.1) against crude lipid fraction.

6.15: Direct infusion mass spectrometry of *C. glutamicum* lipids:

Lipid samples resuspended to 1 mg/ml in $CHCl_3$: CH_3OH (v/v), diluted 1: 10 in 7.5 mM ammonium acetate: $CHCl_3$ (2: 1 v/v). Lipid samples analysed using direct infusion electrospray mass spectrometry (Orbitrap Elite, Advisor: Nanomate), 1.5 kV. Analysis of collected spectra conducted in Xcalibur.

6.16: Lipoglycan extraction from *C. glutamicum*

Cell pellet from 1 L culture dried at 50 °C, under nitrogen. 4 ml 50 % ethanol added to dried cell pellet, and incubated at 80 ºC, 2 hours. suspension cooled to RT and centrifuged 4,000 rpm, 20 mins, RT. Supernatant removed and dried at 50 °C, under N_2. 3 ml sterile PBS, added and sonicated using sonicating water bath, 10 mins, RT. Sample made up to 50 % phenol, incubated 80 ºC, 2 hours. Samples cooled to RT, centrifuged 4,000 rpm, 10 mins, aqueous phase removed and dialysed in dH_2O, using 3.5 kDa membrane. Samples dried under N_2, 50 °C and weighed, resuspended in sterile dH_2O at 100 mg/ml.

6.17.1: SDS-PAGE:

SDS-loading buffer (0.375 M Tris, pH 6.8, 12 % SDS, 60 % glycerol, 0.6 M DTT, 0.06 % bromophenol blue) diluted 6-fold with samples to be analysed, incubated at 90 °C, 10 min. 5-20 µl of sample loaded into 10- 12 % polyacrylamide gel (BioRAD), using SDS-running buffer (2.5 mM Tris, pH 8.3, 19.2 mM glycine, 0.01 % SDS), samples separated at: 200 V, 50 mAmp, 35 min.

Protein samples to be visualised directly incubated in InstantBlue (Expedeon), RT, > 20 mins, with gentle agitation. Lipoglycan samples stained using either silver straining, or Pro-Q Emerald 300 protocols, samples for western blot analysis stained using western blot protocol.

6.17.2: Silver staining of lipoglycans

250 μg of purified lipoglycan extraction (Method 6.16) separated by SDS-PAGE (Method 6.17.1), staining protocol conducted in glass dish as described in the table below.

Step	Solution composition	Duration (mins)
1	50 % Methanol, 12 % Trichloroacetic acid, 2 % CuCl2	> 20
2	10 % Ethanol, 5 % Acetic acid	10
3	0.7 % Periodic acid, 40 % Ethanol, 5 % Acetic acid	10
4	10 % Ethanol	10
5	Deionised water	20
6	0.1 % Silver nitrate	10
7	10 % Di-potassium carbonate	5
8	2 % Di-potassium carbonate	Overnight

6.17.3: Pro-Q Emerald 300 glycoprotein stain

Lipoglycans separated by SDS-PAGE (Method 6. 17.1) stained using 250 μg of purified lipoglycans (Method 6.16). Gel containing lipoglycan samples stained using Pro-Q Emerald 300 glycoprotein staining protocol (Invitrogen).

Gel containing run samples fixed in 50 % CH_3OH, 5 % acetic acid, 45 min, RT, with gentle agitation. Gel washed in 3 % acetic acid, 20 min, RT, gentle agitation, repeated once. Samples oxidised using 3 % acetic acid, 2.7 mM periodic acid, 30 min, RT gentle agitation. Gel washed with 3 % acetic acid, 20 min, RT, gentle agitation, repeated twice. Samples stained with 50-fold dilute Pro-Q Emerald 300 stock solution in staining buffer (Invitrogen), 2 hours, RT, gentle agitation. Gel washed in 3 % acetic acid, 20 min, RT, gentle agitation, repeated once.

6.17.4: Western blot:

Samples separated by SDS-PAGE transferred onto nitrocellulose membrane following iBlot standard protocol (https://assets.thermofisher.com/TFS-Assets/LSG/manuals/iblot2_device_qrc.pdf). Nitrocellulose membrane blocked in 5 % bovine serum albumin (BSA), 0.5 % TWEEN-80, in Tris-buffered saline (TBS, 50 mM Tris, 150 mM NaCl), 16 hours, RT, with gentle agitation. Membrane washed with 0.5 % Tween-80 in TBS (TBS-T), 10 min, RT, with gentle agitation, repeated twice. Membrane washed with primary antibody solution (1: 25,000 anti-MBP antibody: TBS-T + 2.5 % bovine serum albumin (BSA)), incubated 2 hours, RT, with gentle agitation. Membrane washed, TBS-T, 10 mins, RT, with gentle agitation, repeated twice. Membrane washed with secondary antibody (1: 2,000 secondary antibody: TBS-T + 2.5 % BSA), incubated 1 hour, RT, with gentle agitation. Membrane washed, TBS-T, 10 min, RT, with gentle agitation, repeated twice. Membrane visualised using 5-Bromo-4-chloro-3-indolyl-phosphate (BCIP, Thermofisher), incubated RT, with gentle agitation, until developed.

6.18.1: Aditol acetates derivatization of extracted *C. glutamicum* polysaccharides:

10 mg of purified extracted lipoglycan suspended in 250 µl trifluoroacetic acid, incubated 120 °C, 2 hours, to hydrolyse lipoglycans into component monosaccharides. Monosaccharide solution cooled and dried under N_2, 50 °C. Monosaccharides resuspended in 50 µl 1:1 10 mg/ml NaB_2H_4 in ethanol: 1 M NH_4OH, and incubated 3 hours, RT. Samples dried under N_2, 50 °C, resuspended in 3 drops acetic acid, dried under N_2, 50 °C. Resuspended in 3 drops CH_3OH, dried under N_2, 50 °C. Samples resuspended in 100 µl acetic anhydride, incubated 100 °C, 1 hour. Sample cooled, 100 µl toluene added, dried under N_2, 50 °C. Samples partitioned 2 ml $CHCl_3$, 2 ml H_2O, organic phase transferred to fresh tube, dried under N_2, 50 °C.

6.18.2: Gas Chromatography of aditol acetate derivatised polysaccharides:

Samples analysed using Shimadzu GC-2010 with DB-225 column (Agilent Technologies) ID: 0.25 mm, length: 30 m, df: 0.15 µm. the oven was programmed to maintain isothermal temperature of 220 °C with a run time of 20 mins. Peaks detected by change in µV. Sugar composition of samples determined by comparison of retention time of peaks to known standards. Ratio of sugars calculated from area under curve of peaks corresponding peaks of interest.

6.19: Antibiotic susceptibility of *C. glutamicum* strains:

C. glutamicum strains to be tested grown from single colonies in 5 ml sterile media to mid-log, OD_{600}: 1- 2. Culture diluted to OD_{600}: 0.05, in fresh BHI media. 100 µl of cell culture transferred into 96-well microtitre plate containing 5 µl compounds to be tested in 40 %

Dimethyl sulfoxide (DMSO), incubated 30 °C, 24 hours. 30 µl 0.02 % resazurin, 12.5 µl 20 % TWEEN-80 added to each well, incubated 30 °C, 2 hours. Fluorescence measured at Excitation: 544 nm, Emission: 590 nm, 37 °C. Percent survival determined using:

$$\% \, Survival = \left(\frac{(X - Y)}{(Y - Z)}\right) \times \, 100$$

Where X= sample fluorescence, Y= mean of negative controls, and Z= mean of positive controls

6.20.1: Membrane purification of *C. glutamicum* strains:

Cell pellet from 1 L culture of *C. glutamicum* thawed on ice and suspended in 30 ml lysis buffer, culture lysed using French press (1,000 psi, 4 °C, 3 cycles), lysate centrifuged 18,000 rpm, 4 °C, 45 mins, supernatant removed and centrifuged 100,000 xG, 4 °C, 1 hour. Supernatant stored 4 °C, pellet re-suspended in 10 ml lysis buffer at 4 °C.

6.20.2: Cell free Emb activity assay:

2 µl of 20 mM C_8-*Araf-Araf* (YHF-1) acceptor dried under N_2, 2 µl of 2 mM adenosine triphosphate (ATP) and nicotinamide adenine dinucleotide phosphate hydrogen (NADPH) added and dried under N_2. 80 µg of purified corynebacterial membrane (Method 6.20.1) in PBS added, 5 µl ^{14}C pRpp in 500 mM sodium acetate corresponding to 50,000 cpm added, volume made up to 100 µl, incubated 37 °C overnight. Reaction quenched with 533 µl $CHCl_3$: CH_3OH (1:1 v/v), centrifuged 13,000 rpm, 5 mins, RT. Supernatant transferred to clean tube, dried under N_2, 50 °C.

Samples resuspended 50 % ethanol, contaminants removed using liquid chromatography-strong anion exchange (LC-SAX) column equilibrated in 50 % ethanol, samples recovered with 2 ml 50% ethanol, dried under N_2, 50 °C. Samples resuspended in water: butanol biphasic solution, centrifuged 3,000 rpm, 5 mins, RT. Upper phase containing product removed, dried under N_2, 50 °C. Samples resuspended in 40 µl $CHCl_3$: CH_3OH (2: 1 v/v), sample cpm determined using 5 % sample volume. 100 % of remaining samples analysed by TLC using $CHCl_3$: CH_3OH: NH_4OH: H_2O (70: 25: 0.5: 2.5 v/v/v/v). TLC imaged using X-Ray film (Kodak), incubated 1 week, RT. Film imaged.

6.21.1: Expression of recombinant MSMEG_6366:

The pMAL-c2x-MSMEG_6366 plasmid was introduced to *E. coli* (BL21 DE3) by heat shock transformation. Colonies containing the vector selected for using 100 µg/ml ampicillin. Single colony used to inoculate 5 ml sterile LB, incubated overnight, 37 °C, 180 rpm. 1 L sterile LB, containing 100 µg/ml ampicillin, inoculated with 1 ml culture, incubated 37 °C, 180 rpm, until OD_{600}: 0.5- 0.8. Recombinant expression of MSMEG_6366 induced by addition of 1 mM isopropyl-beta-D-1-thiogalactoside (IPTG, Bioline), and incubated 16 hours, at 16 ˚C, 180 rpm. Cells harvested at 4,000 rpm, 4 °C, 20 min. Cell pellet was washed with PBS, and stored at -20 °C.

6.21.2: Expression of MBP-tagged MSMEG_6369 in *E. coli*:

E. coli Shuffle T7 C3026H cells transformed with pMAL-c4x-MSMEG_6369, streaked out on agar, containing 100 µg/ml Amp, incubated at 37 °C overnight, for generation of single colonies. Single colony used to inoculate 5 ml sterile media, incubated at 37 °C, 180 rpm,

overnight. 1 ml bacterial culture used to inoculate 1 L sterile media, containing 100 mg/ml Amp, incubated to reach OD_{600}: 0.4- 0.8. Culture induced with 1 mM IPTG, incubated 16 °C overnight. Culture harvested 4,000 rpm, 20 mins, bacterial pellet washed with sterile PBS, harvested 4,000 rpm, 20 min. 100 ul of *E. coli* cell pellet resuspended in 1.9 ml lysis buffer (50 mM Tris pH 7.5, 300 mM NaCl), with 0.5 g 0.1 mm diameter glass beads (Thistle Scientific), cells lysed using bead beater (MP Bio) 3 cycles, 6 m/s, 30 seconds on, 1 minute off on ice. Aliquot of cell lysate sample tested removed, stored on ice for analysis by SDS-PAGE. Cell lysate centrifuged, 14,500 rpm, 4 °C, 30 min. Cell lysate and clarified cell lysate analysed separated by SDS-PAGE, analysed for expression of MBP-tagged protein by western blot.

6.21.3: Purification of recombinant MBP-tagged MSMEG_6366:

E. coli BL21 (DE3) cell pellets from 1 L cultures expressing MBP-tagged MSMEG_6366 thawed and resuspended in 35 ml lysis buffer (50 mM Tris pH 7.5, 300 mM NaCl). Cells were sonicated using a probe sonicator, 13 Amplitude microns, 30 seconds ON, 30 seconds OFF, 10 cycles, on ice. Cell lysate centrifuged 18,000 rpm, 60 mins, 4 °C. Supernatant removed and passed through 0.22 μM filter. Clarified lysate washed over 1 ml MBP-trap column pre-washed in lysis buffer. Flow through collected, column washed with 50 column volumes lysis buffer. Protein eluted with 10 column volumes lysis buffer containing 10 mM maltose. Sample purity determined by SDS-PAGE electrophoresis. Sample concentration determined by addition of 100 μl Bradford reagent (Bio-Rad), to 2 μl protein sample, A_{595} absorbance measured. Protein concentration determined by comparison to a BSA standard curve.

6.21.4: Ligand binding assay of MSMEG_6366 using Intrinsic tryptophan fluorescence:

Purified protein diluted to 0.5 μM, on ice, protein equilibrated to 22 °C. Fluorescence measured Ex: 280 nm, Em: 350 nm, 22 °C. 0.5 mM ligand, diluted in isotonic buffer, titrated into protein. Sample mixed, 1 min, to allow binding equilibrium and thermal equilibration. Measurement repeated n=3.

6.21.5: Analysis of ligand binding data:

Raw data adjusted to compensate for dilution of protein by ligand using:

$$X = \frac{F \times (500 + volume\ ligand\ added)}{initial\ volume}$$

Where F= sample fluorescence.

Volume corrected data normalised against initial fluorescence at 450 nm of sample, K_d and B_{max} calculated using Michealis-Menten non-linear regression analysis in Graphpad Prism 5.

6.22: Prediction of chemical properties of galactan analogues:

Chemical structures of galactan analogues produced using ChemDraw Professional 17.1 (PerkinElmer). Chemical structures used to generate SMILES structures of galactan analogues. Smiles structures used to predict chemical properties, using Chemicalize (chemicalize.com, ChemAxon).

6.23: Protein crystallization of MBP-tagged MSMEG_6366:

Sitting drop vapour diffusion method of protein purification using the commercially available protein crystallography screens: JCSG+, MIDAS, and Morpheus. Reservoir volume of 40 µl used, 0.3 µl of MSMEG_6366 at variable concentrations (20 mg/ml, 15 mg/ml, and 10 mg/ml) in 50 mM Tris pH 7.5, 300 mM NaCl, with 0.3 µl of reservoir solution, and incubated at 18 °C. Drops screened for crystal formation, conditions showing crystal growth optimised by varying precipitant concentration and pH depending on the condition, typically varying precipitant concentration with 12 conditions tested, with the original condition being the centre of the range each condition being 1- 2 % different from the neighbouring conditions, and varying pH with 8 conditions tested alongside precipitant conditions, with pH conditions being 0.1 pH units different from neighbouring conditions.

6.24: Sprays and reagents:

Phosphomolybdic acid (MPA) staining solution: 5 % MPA (w/v), in ethanol. α-napthol staining solution: 2.4 % α-napthol (w/v), 10 % sulfuric acid (v/v), 87.6 % ethanol (v/v).
Reagents supplied by Sigma-Aldrich unless stated otherwise.

Chapter 7:

References.

Abrahams, K.A., Besra, G.S., 2016. Mycobacterial cell wall biosynthesis: a multifaceted antibiotic target. Parasitology 1–18. https://doi.org/10.1017/S0031182016002377

Addo, K.K., Owusu-darko, K., Yeboah-manu, D., Caulley, P., Minamikawa, M., Bonsu, F., Leinhardt, C., Akpedonu, P., Ofori-adjei, D., 2010. Mycobacterial species causing pulmonary tuberculosis At the korle bu teaching hospital, Accra,. Ghana Med. J. 41. https://doi.org/10.4314/gmj.v41i2.55293

Alderwick, L.J., Birch, H.L., Mishra, A.K., Eggeling, L., Besra, G.S., 2007. Structure, function and biosynthesis of the *Mycobacterium tuberculosis* cell wall: arabinogalactan and lipoarabinomannan assembly with a view to discovering new drug targets. Biochem. Soc. Trans. 35, 1325–1328. https://doi.org/10.1042/BST0351325

Alderwick, L.J., Dover, L.G., Veerapen, N., Gurcha, S.S., Kremer, L., Roper, D.L., Pathak, A.K., Reynolds, R.C., Besra, G.S., 2008. Expression, purification and characterisation of soluble GlfT and the identification of a novel galactofuranosyltransferase Rv3782 involved in priming GlfT-mediated galactan polymerisation in Mycobacterium tuberculosis. Protein Expr. Purif. 58, 332–341. https://doi.org/10.1016/j.pep.2007.11.012

Alderwick, L.J., Harrison, J., Lloyd, G.S., Birch, H.L., 2015. The Mycobacterial Cell Wall—Peptidoglycan and Arabinogalactan. Cold Spring Harb. Perspect. Med. 5, a021113. https://doi.org/10.1101/cshperspect.a021113

Alderwick, Luke J., Lloyd, G.S., Ghadbane, H., May, J.W., Bhatt, A., Eggeling, L., Fütterer, K., Besra, G.S., 2011. The C-Terminal Domain of the Arabinosyltransferase Mycobacterium tuberculosis EmbC Is a Lectin-Like Carbohydrate Binding Module. PLoS Pathog. 7, e1001299. https://doi.org/10.1371/journal.ppat.1001299

Alderwick, L. J., Lloyd, G.S., Lloyd, A.J., Lovering, A.L., Eggeling, L., Besra, G.S., 2011. Biochemical characterization of the Mycobacterium tuberculosis phosphoribosyl-1-pyrophosphate synthetase. Glycobiology 21, 410–425. https://doi.org/10.1093/glycob/cwq173

Alderwick, L.J., Radmacher, E., Seidel, M., Gande, R., Hitchen, P.G., Morris, H.R., Dell, A., Sahm, H., Eggeling, L., Besra, G.S., 2005. Deletion of Cg-emb in Corynebacterianeae Leads to a Novel Truncated Cell Wall Arabinogalactan, whereas Inactivation of Cg-ubiA Results in an Arabinan-deficient Mutant with a Cell Wall Galactan Core. J. Biol. Chem. 280, 32362–32371. https://doi.org/10.1074/jbc.M506339200

Alderwick, L.J., Seidel, M., Sahm, H., Besra, G.S., Eggeling, L., 2006. Identification of a Novel Arabinofuranosyltransferase (AftA) Involved in Cell Wall Arabinan Biosynthesis in Mycobacterium tuberculosis. J. Biol. Chem. 281, 15653–15661. https://doi.org/10.1074/jbc.M600045200

Alexander, D.C., Jones, J.R.W., Tan, T., Chen, J.M., Liu, J., 2004. PimF, a Mannosyltransferase of Mycobacteria, Is Involved in the Biosynthesis of Phosphatidylinositol Mannosides and Lipoarabinomannan. J. Biol. Chem. 279, 18824–18833. https://doi.org/10.1074/jbc.M400791200

Alifano, P., Palumbo, C., Pasanisi, D., Talà, A., 2015. Rifampicin-resistance, rpoB polymorphism and RNA polymerase genetic engineering. J. Biotechnol. 202, 60–77. https://doi.org/10.1016/j.jbiotec.2014.11.024

Alshamaony, L., Goodfellow, M., Minnikin, D.E., 1976. Free Mycolic Acids as Criteria in the Classification of Nocardia and the “rhodochrous” Complex. J. Gen. Microbiol. 92, 188–199. https://doi.org/10.1099/00221287-92-1-188

Ambudkar, S.V., Kim, I.-W., Xia, D., Sauna, Z.E., 2006. The A-loop, a novel conserved aromatic acid subdomain upstream of the Walker A motif in ABC transporters, is critical for ATP binding. FEBS Lett. 580, 1049–1055. https://doi.org/10.1016/j.febslet.2005.12.051

Anandan, A., Vrielink, A., 2016. Detergents in Membrane Protein Purification and Crystallisation, in: Moraes, I. (Ed.), The Next Generation in Membrane Protein Structure Determination. Springer International Publishing, Cham, pp. 13–28. https://doi.org/10.1007/978-3-319-35072-1_2

Andersson, H., von Heijne, G., 1993. Sec dependent and sec independent assembly of E. coli inner membrane proteins: the topological rules depend on chain length. EMBO J. 12, 683–691. https://doi.org/10.1002/j.1460-2075.1993.tb05702.x

Bachhawat, N. et al, 1999. Identification of the INO1 Gene of Mycobacterium tuberculosis H37Rv Reveals a Novel Class of Inositol-1-phosphate Synthase Enzyme 6.

Backus, K.M., Dolan, M.A., Barry, C.S., Joe, M., McPhie, P., Boshoff, H.I.M., Lowary, T.L., Davis, B.G., Barry, C.E., 2014. The Three *Mycobacterium tuberculosis* Antigen 85 Isoforms Have Unique Substrates and Activities Determined by Non-active Site Regions. J. Biol. Chem. 289, 25041–25053. https://doi.org/10.1074/jbc.M114.581579

Bansal-Mutalik, R., Nikaido, H., 2014. Mycobacterial outer membrane is a lipid bilayer and the inner membrane is unusually rich in diacyl phosphatidylinositol dimannosides. Proc. Natl. Acad. Sci. 111, 4958–4963. https://doi.org/10.1073/pnas.1403078111

Bansal-Mutalik, R., Nikaido, H., 2011. Quantitative lipid composition of cell envelopes of Corynebacterium glutamicum elucidated through reverse micelle extraction. Proc. Natl. Acad. Sci. 108, 15360–15365. https://doi.org/10.1073/pnas.1112572108

Bardarov, Stoyan, Bardarov, Svetoslav, Pavelka, M.S., Sambandamurthy, V., Larsen, M., Tufariello, J., Chan, J., Hatfull, G., Jacobs, W.R., 2002. Specialized transduction: an

efficient method for generating marked and unmarked targeted gene disruptions in Mycobacterium tuberculosis, M. bovis BCG and M. smegmatis. Microbiology 148, 3007–3017. https://doi.org/10.1099/00221287-148-10-3007

Barkan, D., Rao, V., Sukenick, G.D., Glickman, M.S., 2010. Redundant Function of cmaA2 and mmaA2 in Mycobacterium tuberculosis cis Cyclopropanation of Oxygenated Mycolates. J. Bacteriol. 192, 3661–3668. https://doi.org/10.1128/JB.00312-10

Bartlett, J.G., 1982. Chloramphenicol. Med. Clin. North Am. 66, 91–102. https://doi.org/10.1016/S0025-7125(16)31444-4

Batt, S.M., Jabeen, T., Mishra, A.K., Veerapen, N., Krumbach, K., Eggeling, L., Besra, G.S., Fütterer, K., 2010. Acceptor Substrate Discrimination in Phosphatidyl- *myo* -inositol Mannoside Synthesis: STRUCTURAL AND MUTATIONAL ANALYSIS OF MANNOSYLTRANSFERASE CORYNEBACTERIUM GLUTAMICUM PimB'. J. Biol. Chem. 285, 37741–37752. https://doi.org/10.1074/jbc.M110.165407

Baumgart, M., Unthan, S., Rückert, C., Sivalingam, J., Grünberger, A., Kalinowski, J., Bott, M., Noack, S., Frunzke, J., 2013. Construction of a Prophage-Free Variant of Corynebacterium glutamicum ATCC 13032 for Use as a Platform Strain for Basic Research and Industrial Biotechnology. Appl. Environ. Microbiol. 79, 6006–6015. https://doi.org/10.1128/AEM.01634-13

Baym, M., Kryazhimskiy, S., Lieberman, T.D., Chung, H., Desai, M.M., Kishony, R., 2015. Inexpensive Multiplexed Library Preparation for Megabase-Sized Genomes. PLOS ONE 15.

Beis, K., 2015. Structural basis for the mechanism of ABC transporters. Biochem. Soc. Trans. 43, 889–893. https://doi.org/10.1042/BST20150047

Belanger, A.E., Besra, G.S., Ford, M.E., Mikusova, K., Belisle, J.T., Brennan, P.J., Inamine, J.M., 1996. The embAB genes of Mycobacterium avium encode an arabinosyl transferase involved in cell wall arabinan biosynthesis that is the target for the antimycobacterial drug ethambutol. Proc. Natl. Acad. Sci. 93, 11919–11924. https://doi.org/10.1073/pnas.93.21.11919

Belanova, M., Dianiskova, P., Brennan, P.J., Completo, G.C., Rose, N.L., Lowary, T.L., Mikusova, K., 2008. Galactosyl Transferases in Mycobacterial Cell Wall Synthesis. J. Bacteriol. 190, 1141–1145. https://doi.org/10.1128/JB.01326-07

Benabdelhak, H., Kiontke, S., Horn, C., Ernst, R., Blight, M.A., Holland, I.B., Schmitt, L., 2003. A Specific Interaction Between the NBD of the ABC-transporter HlyB and a C-Terminal Fragment of its Transport Substrate Haemolysin A. J. Mol. Biol. 327, 1169–1179. https://doi.org/10.1016/S0022-2836(03)00204-3

Berntsson, R.P.-A., Smits, S.H.J., Schmitt, L., Slotboom, D.-J., Poolman, B., 2010. A structural classification of substrate-binding proteins. FEBS Lett. 584, 2606–2617. https://doi.org/10.1016/j.febslet.2010.04.043

Besra, G.S., Khoo, K.-H., McNeil, M.R., Dell, A., Morris, H.R., Brennan, P.J., 1995. A new interpretation of the structure of the mycolyl-arabinogalactan complex of Mycobacterium tuberculosis as revealed through characterization of oligoglycosylalditol fragments by fast-atom bombardment mass spectrometry and 1H nuclear magnetic resonance spectroscopy. Biochemistry 34, 4257–4266.

Bhatt, A., Brown, A.K., Singh, A., Minnikin, D.E., Besra, G.S., 2008. Loss of a Mycobacterial Gene Encoding a Reductase Leads to an Altered Cell Wall Containing β-oxo- Mycolic Acid Analogs and Accumulation of Ketones. Chem. Biol. 15, 930–939. https://doi.org/10.1016/j.chembiol.2008.07.007

Bhatt, A., Molle, V., Besra, G.S., Jacobs, W.R., Kremer, L., 2007. The *Mycobacterium tuberculosis* FAS-II condensing enzymes: their role in mycolic acid biosynthesis, acid-fastness, pathogenesis and in future drug development. Mol. Microbiol. 64, 1442–1454. https://doi.org/10.1111/j.1365-2958.2007.05761.x

Bi, Y., Mann, E., Whitfield, C., Zimmer, J., 2018. Architecture of a channel-forming O-antigen polysaccharide ABC transporter. Nature 553, 361–365. https://doi.org/10.1038/nature25190

Birch, H.L., Alderwick, L.J., Appelmelk, B.J., Maaskant, J., Bhatt, A., Singh, A., Nigou, J., Eggeling, L., Geurtsen, J., Besra, G.S., 2010. A truncated lipoglycan from mycobacteria with altered immunological properties. Proc. Natl. Acad. Sci. 107, 2634–2639. https://doi.org/10.1073/pnas.0915082107

Birch, H.L., Alderwick, L.J., Bhatt, A., Rittmann, D., Krumbach, K., Singh, A., Bai, Y., Lowary, T.L., Eggeling, L., Besra, G.S., 2008. Biosynthesis of mycobacterial arabinogalactan: identification of a novel (13) arabinofuranosyltransferase. Mol. Microbiol. https://doi.org/10.1111/j.1365-2958.2008.06354.x

Böth, D., Schneider, G., Schnell, R., 2011. Peptidoglycan Remodeling in Mycobacterium tuberculosis: Comparison of Structures and Catalytic Activities of RipA and RipB. J. Mol. Biol. 413, 247–260. https://doi.org/10.1016/j.jmb.2011.08.014

Braibant, M., Gilot, P., Content, J., 2000. The ATP binding cassette (ABC) transport systems of Mycobacterium tuberculosis.

Brennan, P.J., 2003. Structure, function, and biogenesis of the cell wall of Mycobacterium tuberculosis. Tuberculosis 83, 91–97. https://doi.org/10.1016/S1472-9792(02)00089-6

Brennan, P.J., Nikaido, H., 1995. The envelope of mycobacteria. Annu Rev Biochem 29–63.

Briken, V., Porcelli, S.A., Besra, G.S., Kremer, L., 2004. Mycobacterial lipoarabinomannan and related lipoglycans: from biogenesis to modulation of the immune response: The mycobacterial lipoarabinomannan and related molecules. Mol. Microbiol. 53, 391–403. https://doi.org/10.1111/j.1365-2958.2004.04183.x

Butler, W.R., Ahearn, D.G., 1986. High-Performance Liquid Chromatography of Mycolic Acids as a Tool in the Identification of Corynebacterium, Nocardia, Rhodococcus, and Mycobacterium Species 23, 4.

Cai, L., Zhao, X., Jiang, T., Qiu, J., Owusu, L., Ma, Y., Wang, B., Xin, Y., 2014. Prokaryotic Expression, Identification and Bioinformatics Analysis of the Mycobacterium tuberculosis Rv3807c Gene Encoding the Putative Enzyme Committed to Decaprenylphosphoryl-d-arabinose Synthesis. Indian J. Microbiol. 54, 46–51. https://doi.org/10.1007/s12088-013-0418-8

Campbell, E.A., Korzheva, N., Mustaev, A., Murakami, K., Nair, S., Goldfarb, A., Darst, S.A., 2001. Structural Mechanism for Rifampicin Inhibition of Bacterial RNA Polymerase. Cell 104, 901–912. https://doi.org/10.1016/S0092-8674(01)00286-0

Cashmore, T.J., Klatt, S., Yamaryo-Botte, Y., Brammananth, R., Rainczuk, A.K., McConville, M.J., Crellin, P.K., Coppel, R.L., 2017. Identification of a Membrane Protein Required for Lipomannan Maturation and Lipoarabinomannan Synthesis in Corynebacterineae. J. Biol. Chem. jbc.M116.772202. https://doi.org/10.1074/jbc.M116.772202

Cescutti, P., De Benedetto, G., Rizzo, R., 2016. Structural determination of the polysaccharide isolated from biofilms produced by a clinical strain of Klebsiella pneumoniae. Carbohydr. Res. 430, 29–35. https://doi.org/10.1016/j.carres.2016.05.001

Cha, Y., Erez, T., Reynolds, I.J., Kumar, D., Ross, J., Koytiger, G., Kusko, R., Zeskind, B., Risso, S., Kagan, E., Papapetropoulos, S., Grossman, I., Laifenfeld, D., 2018. Drug repurposing

from the perspective of pharmaceutical companies: Drug repurposing in pharmaceutical companies. Br. J. Pharmacol. 175, 168–180. https://doi.org/10.1111/bph.13798

Chakraborty, S., Rhee, K.Y., 2015. Tuberculosis Drug Development: History and Evolution of the Mechanism-Based Paradigm. Cold Spring Harb. Perspect. Med. 5, a021147. https://doi.org/10.1101/cshperspect.a021147

Chao, M.C., Kieser, K.J., Minami, S., Mavrici, D., Aldridge, B.B., Fortune, S.M., Alber, T., Rubin, E.J., 2013. Protein Complexes and Proteolytic Activation of the Cell Wall Hydrolase RipA Regulate Septal Resolution in Mycobacteria. PLoS Pathog. 9, e1003197. https://doi.org/10.1371/journal.ppat.1003197

Chaurasiya, S.K., Srivastava, K.K., 2009. Downregulation of protein kinase C-alpha enhances intracellular survival of Mycobacteria: role of PknG. BMC Microbiol. 9, 271. https://doi.org/10.1186/1471-2180-9-271

Chen, Y.E., Fischbach, M.A., Belkaid, Y., 2018. Skin microbiota–host interactions. Nature 553, 427.

Chiaradia, L., Lefebvre, C., Parra, J., Marcoux, J., Burlet-Schiltz, O., Etienne, G., Tropis, M., Daffé, M., 2017. Dissecting the mycobacterial cell envelope and defining the composition of the native mycomembrane. Sci. Rep. 7. https://doi.org/10.1038/s41598-017-12718-4

Cole, S.T., Eiglmeier, K., Parkhill, J., James, K.D., Thomson, N.R., Wheeler, P.R., Honoré, N., Garnier, T., Churcher, C., Harris, D., Mungall, K., Basham, D., Brown, D., Chillingworth, T., Connor, R., Davies, R.M., Devlin, K., Duthoy, S., Feltwell, T., Fraser, A., Hamlin, N., Holroyd, S., Hornsby, T., Jagels, K., Lacroix, C., Maclean, J., Moule, S., Murphy, L., Oliver, K., Quail, M.A., Rajandream, M.-A., Rutherford, K.M., Rutter, S., Seeger, K.,

Simon, S., Simmonds, M., Skelton, J., Squares, R., Squares, S., Stevens, K., Taylor, K., Whitehead, S., Woodward, J.R., Barrell, B.G., 2001. Massive gene decay in the leprosy bacillus. Nature 409, 1007–1011. https://doi.org/10.1038/35059006

Cox, J.A.G., Abrahams, K.A., Alemparte, C., Ghidelli-Disse, S., Rullas, J., Angulo-Barturen, I., Singh, A., Gurcha, S.S., Nataraj, V., Bethell, S., Remuiñán, M.J., Encinas, L., Jervis, P.J., Cammack, N.C., Bhatt, A., Kruse, U., Bantscheff, M., Fütterer, K., Barros, D., Ballell, L., Drewes, G., Besra, G.S., 2016. THPP target assignment reveals EchA6 as an essential fatty acid shuttle in mycobacteria. Nat. Microbiol. 1, 15006. https://doi.org/10.1038/nmicrobiol.2015.6

Crellin, P.K., Kovacevic, S., Martin, K.L., Brammananth, R., Morita, Y.S., Billman-Jacobe, H., McConville, M.J., Coppel, R.L., 2008. Mutations in pimE Restore Lipoarabinomannan Synthesis and Growth in a Mycobacterium smegmatis lpqW Mutant. J. Bacteriol. 190, 3690–3699. https://doi.org/10.1128/JB.00200-08

Cuthbertson, L., Kimber, M.S., Whitfield, C., 2007. Substrate binding by a bacterial ABC transporter involved in polysaccharide export. Proc. Natl. Acad. Sci. 104, 19529–19534. https://doi.org/10.1073/pnas.0705709104

Daffe, M., Brennan, P.J., McNeil, M., 1990. Predominant structural features of the cell wall arabinogalactan of Mycobacterium tuberculosis as revealed through characterization of oligoglycosyl alditol fragments by gas chromatography/mass spectrometry and by 1H and 13C NMR analyses. J. Biol. Chem. 265, 6734–6743.

Dao, D.N., Kremer, L., Guerardel, Y., Molano, A., Jacobs, W.R., Porcelli, S.A., Briken, V., 2004. Mycobacterium tuberculosis Lipomannan Induces Apoptosis and Interleukin-12 Production in Macrophages. Infect. Immun. 72, 2067–2074. https://doi.org/10.1128/IAI.72.4.2067-2074.2004

De Siervo, A.J., 1969. Alterations in the phospholipid composition of Escherichia coli B during growth at different temperatures. J. Bacteriol. 100, 1342–1349.

Deitermann, S., Sprie, G.S., Koch, H.-G., 2005. A Dual Function for SecA in the Assembly of Single Spanning Membrane Proteins in *Escherichia coli*. J. Biol. Chem. 280, 39077–39085. https://doi.org/10.1074/jbc.M509647200

Denks, K., Vogt, A., Sachelaru, I., Petriman, N.-A., Kudva, R., Koch, H.-G., 2014. The Sec translocon mediated protein transport in prokaryotes and eukaryotes. Mol. Membr. Biol. 31, 58–84. https://doi.org/10.3109/09687688.2014.907455

Dianišková, P., Korduláková, J., Škovierová, H., Kaur, D., Jackson, M., Brennan, P., Mikušová, K., 2011. Investigation of ABC transporter from mycobacterial arabinogalactan biosynthetic cluster. Gen. Physiol. Biophys. 30, 239–250. https://doi.org/10.4149/gpb_2011_03_239

Dinadayala, P., Kaur, D., Berg, S., Amin, A.G., Vissa, V.D., Chatterjee, D., Brennan, P.J., Crick, D.C., 2006. Genetic Basis for the Synthesis of the Immunomodulatory Mannose Caps of Lipoarabinomannan in *Mycobacterium tuberculosis*. J. Biol. Chem. 281, 20027–20035. https://doi.org/10.1074/jbc.M603395200

Dinadayala, P., Sambou, T., Daffe, M., Lemassu, A., 2008. Comparative structural analyses of the -glucan and glycogen from Mycobacterium bovis. Glycobiology 18, 502–508. https://doi.org/10.1093/glycob/cwn031

Dong, H., Tang, X., Zhang, Z., Dong, C., 2017. Structural insight into lipopolysaccharide transport from the Gram-negative bacterial inner membrane to the outer membrane. Biochim. Biophys. Acta BBA - Mol. Cell Biol. Lipids 1862, 1461–1467. https://doi.org/10.1016/j.bbalip.2017.08.003

Dubnau, E., Chan, J., Raynaud, C., Mohan, V.P., Lanéelle, M.-A., Yu, K., Quémard, A., Smith, I., Daffé, M., 2000. Oxygenated mycolic acids are necessary for virulence of Mycobacterium tuberculosis in mice. Mol. Microbiol. 36, 630–637.

Duus, J.Ø., Gotfredsen, C.H., Bock, K., 2000. Carbohydrate Structural Determination by NMR Spectroscopy: Modern Methods and Limitations †. Chem. Rev. 100, 4589–4614. https://doi.org/10.1021/cr990302n

Egan, A.J.F., Cleverley, R.M., Peters, K., Lewis, R.J., Vollmer, W., 2017. Regulation of bacterial cell wall growth. FEBS J. 284, 851–867. https://doi.org/10.1111/febs.13959

Elass, E., Aubry, L., Masson, M., Denys, A., Guerardel, Y., Maes, E., Legrand, D., Mazurier, J., Kremer, L., 2005. Mycobacterial Lipomannan Induces Matrix Metalloproteinase-9 Expression in Human Macrophagic Cells through a Toll-Like Receptor 1 (TLR1)/TLR2- and CD14-Dependent Mechanism. Infect. Immun. 73, 7064–7068. https://doi.org/10.1128/IAI.73.10.7064-7068.2005

Escombe, A.R., Moore, D.A.J., Gilman, R.H., Pan, W., Navincopa, M., Ticona, E., Martínez, C., Caviedes, L., Sheen, P., Gonzalez, A., Noakes, C.J., Friedland, J.S., Evans, C.A., 2008. The Infectiousness of Tuberculosis Patients Coinfected with HIV. PLoS Med. 5, e188. https://doi.org/10.1371/journal.pmed.0050188

Escuyer, V.E., Lety, M.-A., Torrelles, J.B., Khoo, K.-H., Tang, J.-B., Rithner, C.D., Frehel, C., McNeil, M.R., Brennan, P.J., Chatterjee, D., 2001. The Role of the *embA* and *embB* Gene Products in the Biosynthesis of the Terminal Hexaarabinofuranosyl Motif of *Mycobacterium smegmatis* Arabinogalactan. J. Biol. Chem. 276, 48854–48862. https://doi.org/10.1074/jbc.M102272200

Ford, R.C., Beis, K., 2019. Learning the ABCs one at a time: structure and mechanism of ABC transporters. Biochem. Soc. Trans. 47, 23–36. https://doi.org/10.1042/BST20180147

Franco-Paredes, C., Marcos, L.A., Henao-Martínez, A.F., Rodríguez-Morales, A.J., Villamil-Gómez, W.E., Gotuzzo, E., Bonifaz, A., 2018. Cutaneous Mycobacterial Infections. Clin. Microbiol. Rev. 32. https://doi.org/10.1128/CMR.00069-18

Frauenfeld, J., Gumbart, J., Sluis, E.O. van der, Funes, S., Gartmann, M., Beatrix, B., Mielke, T., Berninghausen, O., Becker, T., Schulten, K., Beckmann, R., 2011. Cryo-EM structure of the ribosome–SecYE complex in the membrane environment. Nat. Struct. Mol. Biol. 18, 614–621. https://doi.org/10.1038/nsmb.2026

Freihofer, P., Akbergenov, R., Teo, Y., Juskeviciene, R., Andersson, D.I., Böttger, E.C., 2016. Nonmutational compensation of the fitness cost of antibiotic resistance in mycobacteria by overexpression of *tlyA* rRNA methylase. RNA 22, 1836–1843. https://doi.org/10.1261/rna.057257.116

Gande, R., Gibson, K.J.C., Brown, A.K., Krumbach, K., Dover, L.G., Sahm, H., Shioyama, S., Oikawa, T., Besra, G.S., Eggeling, L., 2004. Acyl-CoA Carboxylases (*accD2* and *accD3*), Together with a Unique Polyketide Synthase (*Cg-pks*), Are Key to Mycolic Acid Biosynthesis in *Corynebacterianeae* Such as *Corynebacterium glutamicum* and *Mycobacterium tuberculosis*. J. Biol. Chem. 279, 44847–44857. https://doi.org/10.1074/jbc.M408648200

Gao, B., Gupta, R.S., 2012. Phylogenetic Framework and Molecular Signatures for the Main Clades of the Phylum Actinobacteria. Microbiol. Mol. Biol. Rev. 76, 66–112. https://doi.org/10.1128/MMBR.05011-11

Gatfield, J., Pieters, J., 2000. Essential Role for Cholesterol in Entry of Mycobacteria into Macrophages. Science 288, 1647–1651. https://doi.org/10.1126/science.288.5471.1647

Gilleron, M., Quesniaux, V.F.J., Puzo, G., 2003. Acylation State of the Phosphatidylinositol Hexamannosides from *Mycobacterium bovis* Bacillus Calmette Guérin and *Mycobacterium tuberculosis* H37Rv and Its Implication in Toll-like Receptor Response. J. Biol. Chem. 278, 29880–29889. https://doi.org/10.1074/jbc.M303446200

Gilleron, M., Ronet, C., Mempel, M., Monsarrat, B., Gachelin, G., Puzo, G., 2001. Acylation State of the Phosphatidylinositol Mannosides from Mycobacterium bovis Bacillus Calmette Guerin and Ability to Induce Granuloma and Recruit Natural Killer T Cells. J. Biol. Chem. 276, 34896–34904. https://doi.org/10.1074/jbc.M103908200

Glickman, M.S., 2003. The *mmaA2* Gene of *Mycobacterium tuberculosis* Encodes the Distal Cyclopropane Synthase of the α-Mycolic Acid. J. Biol. Chem. 278, 7844–7849. https://doi.org/10.1074/jbc.M212458200

Glickman, M.S., Cox, J.S., Jacobs Jr, W.R., 2000. A novel mycolic acid cyclopropane synthetase is required for cording, persistence, and virulence of Mycobacterium tuberculosis. Mol. Cell 5, 717–727.

Goude, R., Amin, A.G., Chatterjee, D., Parish, T., 2009. The Arabinosyltransferase EmbC Is Inhibited by Ethambutol in Mycobacterium tuberculosis. Antimicrob. Agents Chemother. 53, 4138–4146. https://doi.org/10.1128/AAC.00162-09

Gouet, P., Courcelle, E., Stuart, D., Metoz, F., 1999. ESPript: analysis of multiple sequence alignments in PostScript. Bioinformatics 15, 305–308. https://doi.org/10.1093/bioinformatics/15.4.305

Guglielmetti, L., Mougari, F., Lopes, A., Raskine, L., Cambau, E., 2015. Human infections due to nontuberculous mycobacteria: the infectious diseases and clinical microbiology specialists' point of view. Future Microbiol. 10, 1467–1483. https://doi.org/10.2217/fmb.15.64

Gupta, S., Shukla, H., Kumar, A., Shukla, R., Kumari, R., Tripathi, T., Singh, R.K., Anupurba, S., 2019. *Mycobacterium tuberculosis* nucleoside diphosphate kinase shows interaction with putative ATP binding cassette (ABC) transporter, Rv1273c. J. Biomol. Struct. Dyn. 1–11. https://doi.org/10.1080/07391102.2019.1595150

Gurcha, S.S., Baulard, A.R., Kremer, L., Locht, C., Moody, D.B., Muhlecker, W., Costello, C.E., Crick, D.C., Brennan, P.J., Besra, G.S., 2002. Ppm1, a novel polyprenol monophosphomannose synthase from Mycobacterium tuberculosis. Biochem. J. 365, 441–450. https://doi.org/10.1042/bj20020107

Haley, C.A., 2019. Treatment of Latent Tuberculosis Infection 32.

Harrison, J., Lloyd, G., Joe, M., Lowary, T.L., Reynolds, E., Walters-Morgan, H., Bhatt, A., Lovering, A., Besra, G.S., Alderwick, L.J., 2016. Lcp1 Is a Phosphotransferase Responsible for Ligating Arabinogalactan to Peptidoglycan in *Mycobacterium tuberculosis*. mBio 7, e00972-16. https://doi.org/10.1128/mBio.00972-16

Hayashi, J.M., Luo, C.-Y., Mayfield, J.A., Hsu, T., Fukuda, T., Walfield, A.L., Giffen, S.R., Leszyk, J.D., Baer, C.E., Bennion, O.T., Madduri, A., Shaffer, S.A., Aldridge, B.B., Sassetti, C.M., Sandler, S.J., Kinoshita, T., Moody, D.B., Morita, Y.S., 2016. Spatially distinct and metabolically active membrane domain in mycobacteria. Proc. Natl. Acad. Sci. 113, 5400–5405. https://doi.org/10.1073/pnas.1525165113

Heinkel, F., Abraham, L., Ko, M., Chao, J., Bach, H., Hui, L.T., Li, H., Zhu, M., Ling, Y.M., Rogalski, J.C., Scurll, J., Bui, J.M., Mayor, T., Gold, M.R., Chou, K.C., Av-Gay, Y., McIntosh, L.P., Gsponer, J., 2019. Phase separation and clustering of an ABC transporter in *Mycobacterium tuberculosis*. Proc. Natl. Acad. Sci. 116, 16326–16331. https://doi.org/10.1073/pnas.1820683116

Hett, E.C., Chao, M.C., Deng, L.L., Rubin, E.J., 2008. A Mycobacterial Enzyme Essential for Cell Division Synergizes with Resuscitation-Promoting Factor. PLoS Pathog. 4, e1000001. https://doi.org/10.1371/journal.ppat.1000001

Hett, E.C., Chao, M.C., Steyn, A.J., Fortune, S.M., Deng, L.L., Rubin, E.J., 2007. A partner for the resuscitation-promoting factors of Mycobacterium tuberculosis. Mol. Microbiol. 66, 658–668. https://doi.org/10.1111/j.1365-2958.2007.05945.x

Higgins, C.F., Linton, K.J., 2004. The ATP switch model for ABC transporters. Nat. Struct. Mol. Biol. 11, 918–926. https://doi.org/10.1038/nsmb836

Hmama, Z., Peña-Díaz, S., Joseph, S., Av-Gay, Y., 2015. Immunoevasion and immunosuppression of the macrophage by *Mycobacterium tuberculosis*. Immunol. Rev. 264, 220–232. https://doi.org/10.1111/imr.12268

Hohl, M., Hurlimann, L.M., Bohm, S., Schoppe, J., Grutter, M.G., Bordignon, E., Seeger, M.A., 2014. Structural basis for allosteric cross-talk between the asymmetric nucleotide binding sites of a heterodimeric ABC exporter. Proc. Natl. Acad. Sci. 111, 11025–11030. https://doi.org/10.1073/pnas.1400485111

Houben, R.M.G.J., Dodd, P.J., 2016. The Global Burden of Latent Tuberculosis Infection: A Re-estimation Using Mathematical Modelling. PLOS Med. 13, e1002152. https://doi.org/10.1371/journal.pmed.1002152

Huang, H., Berg, S., Spencer, J.S., Vereecke, D., D'Haeze, W., Holsters, M., McNeil, M.R., 2008. Identification of amino acids and domains required for catalytic activity of DPPR synthase, a cell wall biosynthetic enzyme of Mycobacterium tuberculosis. Microbiology 154, 736–743. https://doi.org/10.1099/mic.0.2007/013532-0

Huang, H., Scherman, M.S., D'Haeze, W., Vereecke, D., Holsters, M., Crick, D.C., McNeil, M.R., 2005. Identification and Active Expression of the *Mycobacterium tuberculosis* Gene

Encoding 5-Phospho-α-D-ribose-1-diphosphate: Decaprenyl-phosphate 5-Phosphoribosyltransferase, the First Enzyme Committed to Decaprenylphosphoryl-D-arabinose Synthesis. J. Biol. Chem. 280, 24539–24543. https://doi.org/10.1074/jbc.M504068200

Huber, D., Rajagopalan, N., Preissler, S., Rocco, M.A., Merz, F., Kramer, G., Bukau, B., 2011. SecA Interacts with Ribosomes in Order to Facilitate Posttranslational Translocation in Bacteria. Mol. Cell 41, 343–353. https://doi.org/10.1016/j.molcel.2010.12.028

Ishikawa, E., Mori, D., Yamasaki, S., 2017. Recognition of Mycobacterial Lipids by Immune Receptors. Trends Immunol. 38, 66–76. https://doi.org/10.1016/j.it.2016.10.009

Jackson, M., Crick, D.C., Brennan, P.J., 2000. Phosphatidylinositol Is an Essential Phospholipid of Mycobacteria. J. Biol. Chem. 275, 30092–30099. https://doi.org/10.1074/jbc.M004658200

Jankute, M., Alderwick, L.J., Moorey, A.R., Joe, M., Gurcha, S.S., Eggeling, L., Lowary, T.L., Dell, A., Pang, P.-C., Yang, T., Haslam, S., Besra, G.S., 2018. The singular Corynebacterium glutamicum Emb arabinofuranosyltransferase polymerises the α(1→5) arabinan backbone in the early stages of cell wall arabinan biosynthesis. Cell Surf. https://doi.org/10.1016/j.tcsw.2018.06.003

Jankute, M., Alderwick, L.J., Noack, S., Veerapen, N., Nigou, J., Besra, G.S., 2017. Disruption of Mycobacterial AftB Results in Complete Loss of Terminal β(1 → 2) Arabinofuranose Residues of Lipoarabinomannan. ACS Chem. Biol. 12, 183–190. https://doi.org/10.1021/acschembio.6b00898

Jankute, M., Cox, J.A.G., Harrison, J., Besra, G.S., 2015. Assembly of the Mycobacterial Cell Wall. Annu. Rev. Microbiol. 69, 405–423. https://doi.org/10.1146/annurev-micro-091014-104121

Jeffery, C.J., 2016. Expression, Solubilization, and Purification of Bacterial Membrane Proteins: Purification of Bacterial Membrane Proteins, in: Coligan, J.E., Dunn, B.M., Speicher, D.W., Wingfield, P.T. (Eds.), Current Protocols in Protein Science. John Wiley & Sons, Inc., Hoboken, NJ, USA, pp. 29.15.1-29.15.15. https://doi.org/10.1002/0471140864.ps2915s83

Jiang, T., He, L., Zhan, Y., Zang, S., Ma, Y., Zhao, X., Zhang, C., Xin, Y., 2011. The effect of MSMEG_6402 gene disruption on the cell wall structure of Mycobacterium smegmatis. Microb. Pathog. 51, 156–160. https://doi.org/10.1016/j.micpath.2011.04.005

Jin, Y., Xin, Y., Zhang, W., Ma, Y., 2010. Mycobacterium tuberculosis Rv1302 and Mycobacterium smegmatis MSMEG___4947 have WecA function and MSMEG__4947 is required for the growth of M. smegmatis: Mycobacterial WecA. FEMS Microbiol. Lett. 310, 54–61. https://doi.org/10.1111/j.1574-6968.2010.02045.x

Jones, P.M., George, A.M., 2002. Mechanism of ABC transporters: A molecular dynamics simulation of a well characterized nucleotide-binding subunit. Proc. Natl. Acad. Sci. 99, 12639–12644. https://doi.org/10.1073/pnas.152439599

Kalscheuer, R., Palacios, A., Anso, I., Cifuente, J., Anguita, J., Jacobs, W.R., Guerin, M.E., Prados-Rosales, R., 2019. The Mycobacterium tuberculosis capsule: a cell structure with key implications in pathogenesis. Biochem. J. 476, 1995–2016. https://doi.org/10.1042/BCJ20190324

Kapopoulou, A., Lew, J.M., Cole, S.T., 2011. The MycoBrowser portal: A comprehensive and manually annotated resource for mycobacterial genomes. Tuberculosis 91, 8–13. https://doi.org/10.1016/j.tube.2010.09.006

Karakousis, P.C., Yoshimatsu, T., Lamichhane, G., Woolwine, S.C., Nuermberger, E.L., Grosset, J., Bishai, W.R., 2004. Dormancy Phenotype Displayed by Extracellular *Mycobacterium tuberculosis* within Artificial Granulomas in Mice. J. Exp. Med. 200, 647–657. https://doi.org/10.1084/jem.20040646

Karpowich, N., Martsinkevich, O., Millen, L., Yuan, Y.-R., Dai, P.L., MacVey, K., Thomas, P.J., Hunt, J.F., 2001. Crystal Structures of the MJ1267 ATP Binding Cassette Reveal an Induced-Fit Effect at the ATPase Active Site of an ABC Transporter. Structure 9, 571–586. https://doi.org/10.1016/S0969-2126(01)00617-7

Kaur, D., Obregón-Henao, A., Pham, H., Chatterjee, D., Brennan, P.J., Jackson, M., 2008. Lipoarabinomannan of Mycobacterium: mannose capping by a multifunctional terminal mannosyltransferase. Proc. Natl. Acad. Sci. 105, 17973–17977.

Kawai, F., Shoda, M., Harashima, R., Sadaie, Y., Hara, H., Matsumoto, K., 2004. Cardiolipin Domains in Bacillus subtilis Marburg Membranes. J. Bacteriol. 186, 1475–1483. https://doi.org/10.1128/JB.186.5.1475-1483.2004

Khoo, K.-H., Douglas, E., Azadi, P., Inamine, J.M., Besra, G.S., Mikušová, K., Brennan, P.J., Chatterjee, D., 1996. Truncated Structural Variants of Lipoarabinomannan in Ethambutol Drug-resistant Strains of Mycobacterium smegmatis INHIBITION OF ARABINAN BIOSYNTHESIS BY ETHAMBUTOL. J. Biol. Chem. 271, 28682–28690.

Kiefer, D., Kuhn, A., 2018. YidC-mediated membrane insertion. FEMS Microbiol. Lett. 365. https://doi.org/10.1093/femsle/fny106

Kim, S.J., Chang, J., Singh, M., 2015. Peptidoglycan architecture of Gram-positive bacteria by solid-state NMR. Biochim. Biophys. Acta BBA - Biomembr. 1848, 350–362. https://doi.org/10.1016/j.bbamem.2014.05.031

Knutson, K.L., Hmama, Z., Herrera-Velit, P., Rochford, R., Reiner, N.E., 1998. Lipoarabinomannan of *Mycobacterium tuberculosis* Promotes Protein Tyrosine Dephosphorylation and Inhibition of Mitogen-activated Protein Kinase in Human Mononuclear Phagocytes: ROLE OF THE Src HOMOLOGY 2 CONTAINING TYROSINE PHOSPHATASE 1. J. Biol. Chem. 273, 645–652. https://doi.org/10.1074/jbc.273.1.645

Koliwer-Brandl, H., Syson, K., van de Weerd, R., Chandra, G., Appelmelk, B., Alber, M., Ioerger, T.R., Jacobs, W.R., Geurtsen, J., Bornemann, S., Kalscheuer, R., 2016. Metabolic Network for the Biosynthesis of Intra- and Extracellular α-Glucans Required for Virulence of Mycobacterium tuberculosis. PLOS Pathog. 12, e1005768. https://doi.org/10.1371/journal.ppat.1005768

Kolly, G.S., Boldrin, F., Sala, C., Dhar, N., Hartkoorn, R.C., Ventura, M., Serafini, A., McKinney, J.D., Manganelli, R., Cole, S.T., 2014. Assessing the essentiality of the decaprenyl-phospho- D -arabinofuranose pathway in *M ycobacterium tuberculosis* using conditional mutants: Druggability of the *M. tuberculosis* DPA pathway. Mol. Microbiol. 92, 194–211. https://doi.org/10.1111/mmi.12546

Korduláková, J., Gilleron, M., Mikušová, K., Puzo, G., Brennan, P.J., Gicquel, B., Jackson, M., 2002. Definition of the First Mannosylation Step in Phosphatidylinositol Mannoside Synthesis: PimA IS ESSENTIAL FOR GROWTH OF MYCOBACTERIA. J. Biol. Chem. 277, 31335–31344. https://doi.org/10.1074/jbc.M204060200

Korduláková, J., Gilleron, M., Puzo, G., Brennan, P.J., Gicquel, B., Mikušová, K., Jackson, M., 2003. Identification of the Required Acyltransferase Step in the Biosynthesis of the Phosphatidylinositol Mannosides of *Mycobacterium* Species. J. Biol. Chem. 278, 36285–36295. https://doi.org/10.1074/jbc.M303639200

Kremer, L., Dover, L.G., Morehouse, C., Hitchin, P., Everett, M., Morris, H.R., Dell, A., Brennan, P.J., McNeil, M.R., Flaherty, C., Duncan, K., Besra, G.S., 2001a. Galactan Biosynthesis in *Mycobacterium tuberculosis*: IDENTIFICATION OF A BIFUNCTIONAL UDP-GALACTOFURANOSYLTRANSFERASE. J. Biol. Chem. 276, 26430–26440. https://doi.org/10.1074/jbc.M102022200

Kremer, L., Gurcha, S.S., Bifani, P., Hitchen, P.G., Baulard, A., Morris, H.R., Anne, D., Brennan, P.J., Besra, G.S., 2002. Characterization of a putative α-mannosyltransferase involved in phosphatidylinositol trimannoside biosynthesis in Mycobacterium tuberculosis. Biochem. J. 363, 437–447.

Kremer, L., Nampoothiri, K.M., Lesjean, S., Dover, L.G., Graham, S., Betts, J., Brennan, P.J., Minnikin, D.E., Locht, C., Besra, G.S., 2001b. Biochemical Characterization of Acyl Carrier Protein (AcpM) and Malonyl-CoA:AcpM Transacylase (mtFabD), Two Major Components of *Mycobacterium tuberculosis* Fatty Acid Synthase II. J. Biol. Chem. 276, 27967–27974. https://doi.org/10.1074/jbc.M103687200

Kuhn, A., Koch, H.-G., Dalbey, R.E., 2017. Targeting and Insertion of Membrane Proteins. EcoSal Plus 7. https://doi.org/10.1128/ecosalplus.ESP-0012-2016

Kumar, P., Arora, K., Lloyd, J.R., Lee, I.Y., Nair, V., Fischer, E., Boshoff, H.I.M., Barry, C.E., 2012. Meropenem inhibits D,D-carboxypeptidase activity in *Mycobacterium tuberculosis*: Peptidoglycan of *M. tuberculosis*. Mol. Microbiol. 86, 367–381. https://doi.org/10.1111/j.1365-2958.2012.08199.x

Kurosu, M., Mahapatra, S., Narayanasamy, P., Crick, D.C., 2007. Chemoenzymatic synthesis of Park's nucleotide: toward the development of high-throughput screening for MraY inhibitors. Tetrahedron Lett. 48, 799–803. https://doi.org/10.1016/j.tetlet.2006.11.160

Lanéelle, M.-A., Schiffler, B., Gounon, P., Bayan, N., Benz, R., Daffé, M., Puech, V., Chami, M., Lemassu, A., 2001. Structure of the cell envelope of corynebacteria: importance of the non-covalently bound lipids in the formation of the cell wall permeability barrier and fracture plane. Microbiology 147, 1365–1382. https://doi.org/10.1099/00221287-147-5-1365

Lavollay, M., Arthur, M., Fourgeaud, M., Dubost, L., Marie, A., Veziris, N., Blanot, D., Gutmann, L., Mainardi, J.-L., 2008. The Peptidoglycan of Stationary-Phase Mycobacterium tuberculosis Predominantly Contains Cross-Links Generated by L,D-Transpeptidation. J. Bacteriol. 190, 4360–4366. https://doi.org/10.1128/JB.00239-08

Lea-Smith, D.J., Martin, K.L., Pyke, J.S., Tull, D., McConville, M.J., Coppel, R.L., Crellin, P.K., 2008. Analysis of a New Mannosyltransferase Required for the Synthesis of Phosphatidylinositol Mannosides and Lipoarbinomannan Reveals Two Lipomannan Pools in Corynebacterineae. J. Biol. Chem. 283, 6773–6782. https://doi.org/10.1074/jbc.M707139200

Lea-Smith, D.J., Pyke, J.S., Tull, D., McConville, M.J., Coppel, R.L., Crellin, P.K., 2007. The Reductase That Catalyzes Mycolic Motif Synthesis Is Required for Efficient Attachment of Mycolic Acids to Arabinogalactan. J. Biol. Chem. 282, 11000–11008. https://doi.org/10.1074/jbc.M608686200

Leeflang, B.R., Faber, E.J., Erbel, P., Vliegenthart, J.F.G., 2000. Structure elucidation of glycoprotein glycans and of polysaccharides by NMR spectroscopy. J. Biotechnol. 77, 115–122. https://doi.org/10.1016/S0168-1656(99)00212-6

Lemassu, A., Ortalo-Magne, A., Bardou, F., Silve, G., Lanéelle, M.-A., Daffé, M., 1996. Extracellular and surface-exposed polysaccharides of non-tuberculous mycobacteria. Microbiology 142, 1513–1520.

Lim, H.C., Sher, J.W., Rodriguez-Rivera, F.P., Fumeaux, C., Bertozzi, C.R., Bernhardt, T.G., 2019. Identification of new components of the RipC-FtsEX cell separation pathway of Corynebacterineae. PLOS Genet. 15, e1008284. https://doi.org/10.1371/journal.pgen.1008284

Linton, K.J., Higgins, C.F., 1998. The Escherichia coli ATP-binding cassette (ABC) proteins: E. coli ABC proteins. Mol. Microbiol. 28, 5–13. https://doi.org/10.1046/j.1365-2958.1998.00764.x

Liu, J., Barry, C.E., Besra, G.S., Nikaido, H., 1996. Mycolic acid structure determines the fluidity of the mycobacterial cell wall. J. Biol. Chem. 271, 29545–29551.

Locher, K.P., 2016. Mechanistic diversity in ATP-binding cassette (ABC) transporters. Nat. Struct. Mol. Biol. 23, 487–493. https://doi.org/10.1038/nsmb.3216

Loskill, P., Pereira, P.M., Jung, P., Bischoff, M., Herrmann, M., Pinho, M.G., Jacobs, K., 2014. Reduction of the Peptidoglycan Crosslinking Causes a Decrease in Stiffness of the Staphylococcus aureus Cell Envelope. Biophys. J. 107, 1082–1089. https://doi.org/10.1016/j.bpj.2014.07.029

Ludwiczak, P., Gilleron, M., Bordat, Y., Martin, C., Gicquel, B., Puzo, G., 2002. Mycobacterium tuberculosis phoP mutant: lipoarabinomannan molecular structure. Microbiology 148, 3029–3037.

Mahapatra, S., Crick, D.C., Brennan, P.J., 2000. Comparison of the UDP-N-Acetylmuramate: l-Alanine Ligase Enzymes from Mycobacterium tuberculosis andMycobacterium leprae. J. Bacteriol. 182, 6827–6830.

Mahapatra, S., Scherman, H., Brennan, P.J., Crick, D.C., 2005. N Glycolylation of the Nucleotide Precursors of Peptidoglycan Biosynthesis of Mycobacterium spp. Is Altered

by Drug Treatment. J. Bacteriol. 187, 2341–2347. https://doi.org/10.1128/JB.187.7.2341-2347.2005

Maloney, E., Madiraju, S.C., Rajagopalan, M., Madiraju, M., 2011. Localization of acidic phospholipid cardiolipin and DnaA in mycobacteria. Tuberculosis 91, S150–S155. https://doi.org/10.1016/j.tube.2011.10.025

Martin, A., Daniel, J., 2018. The ABC transporter Rv1272c of Mycobacterium tuberculosis enhances the import of long-chain fatty acids in Escherichia coli. Biochem. Biophys. Res. Commun. 496, 667–672. https://doi.org/10.1016/j.bbrc.2018.01.115

Matteelli, A., Sulis, G., Capone, S., D'Ambrosio, L., Migliori, G.B., Getahun, H., 2017. Tuberculosis elimination and the challenge of latent tuberculosis. Presse Médicale 46, e13–e21. https://doi.org/10.1016/j.lpm.2017.01.015

McNeil, M., Daffe, M., Brennan, P.J., 1990. Evidence for the nature of the link between the arabinogalactan and peptidoglycan of mycobacterial cell walls. J. Biol. Chem. 265, 18200–18206.

Méndez, S.-T., Castillo-Villanueva, A., Martínez-Mayorga, K., Reyes-Vivas, H., Oria-Hernández, J., 2019. Structure-based identification of a potential non-catalytic binding site for rational drug design in the fructose 1,6-biphosphate aldolase from Giardia lamblia. Sci. Rep. 9, 11779. https://doi.org/10.1038/s41598-019-48192-3

Mikusova, K., Belanova, M., Kordulakova, J., Honda, K., McNeil, M.R., Mahapatra, S., Crick, D.C., Brennan, P.J., 2006. Identification of a Novel Galactosyl Transferase Involved in Biosynthesis of the Mycobacterial Cell Wall. J. Bacteriol. 188, 6592–6598. https://doi.org/10.1128/JB.00489-06

Mikusova, K., Huang, H., Yagi, T., Holsters, M., Vereecke, D., D'Haeze, W., Scherman, M.S., Brennan, P.J., McNeil, M.R., Crick, D.C., 2005. Decaprenylphosphoryl Arabinofuranose,

the Donor of the D-Arabinofuranosyl Residues of Mycobacterial Arabinan, Is Formed via a Two-Step Epimerization of Decaprenylphosphoryl Ribose. J. Bacteriol. 187, 8020–8025. https://doi.org/10.1128/JB.187.23.8020-8025.2005

Mills, J.A., Motichka, K., Jucker, M., Wu, H.P., Uhlik, B.C., Stern, R.J., Scherman, M.S., Vissa, V.D., Pan, F., Kundu, M., Ma, Y.F., McNeil, M., 2004. Inactivation of the Mycobacterial Rhamnosyltransferase, Which Is Needed for the Formation of the Arabinogalactan-Peptidoglycan Linker, Leads to Irreversible Loss of Viability. J. Biol. Chem. 279, 43540–43546. https://doi.org/10.1074/jbc.M407782200

Minnikin, D.E., Patel, P.V., Alshamaony, L., Goodfellow, M., 1977. Polar Lipid Composition in the Classification of Nocardia and Related Bacteria. Int. J. Syst. Bacteriol. 27, 104–117. https://doi.org/10.1099/00207713-27-2-104

Mishra, A.K., Alderwick, L.J., Rittmann, D., Tatituri, R.V.V., Nigou, J., Gilleron, M., Eggeling, L., Besra, G.S., 2007. Identification of an ?(1?6) mannopyranosyltransferase (MptA), involved in Corynebacterium glutamicum lipomanann biosynthesis, and identification of its orthologue in Mycobacterium tuberculosis. Mol. Microbiol. 65, 1503–1517. https://doi.org/10.1111/j.1365-2958.2007.05884.x

Mishra, A.K., Alderwick, L.J., Rittmann, D., Wang, C., Bhatt, A., Jacobs Jr, W.R., Takayama, K., Eggeling, L., Besra, G.S., 2008a. Identification of a novel α(1→6) mannopyranosyltransferase MptB from *Corynebacterium glutamicum* by deletion of a conserved gene, *NCgl1505* , affords a lipomannan- and lipoarabinomannan-deficient mutant. Mol. Microbiol. 68, 1595–1613. https://doi.org/10.1111/j.1365-2958.2008.06265.x

Mishra, A.K., Klein, C., Gurcha, S.S., Alderwick, L.J., Babu, P., Hitchen, P.G., Morris, H.R., Dell, A., Besra, G.S., Eggeling, L., 2008b. Structural characterization and functional

properties of a novel lipomannan variant isolated from a Corynebacterium glutamicum pimB' mutant. Antonie Van Leeuwenhoek 94, 277–287. https://doi.org/10.1007/s10482-008-9243-1

Mishra, A.K., Krumbach, K., Rittmann, D., Appelmelk, B., Pathak, V., Pathak, A.K., Nigou, J., Geurtsen, J., Eggeling, L., Besra, G.S., 2011. Lipoarabinomannan biosynthesis in Corynebacterineae: the interplay of two α(1→2)-mannopyranosyltransferases MptC and MptD in mannan branching: Identification and characterization of novel α(1→2)-mannopyranosyltransferases. Mol. Microbiol. 80, 1241–1259. https://doi.org/10.1111/j.1365-2958.2011.07640.x

Mishra, A.K., Krumbach, K., Rittmann, D., Batt, S.M., Lee, O.Y.-C., De, S., Frunzke, J., Besra, G.S., Eggeling, L., 2012. Deletion of manC in Corynebacterium glutamicum results in a phospho-myo-inositol mannoside- and lipoglycan-deficient mutant. Microbiology 158, 1908–1917. https://doi.org/10.1099/mic.0.057653-0

Mohammadi, T., Sijbrandi, R., Lutters, M., Verheul, J., Martin, N.I., den Blaauwen, T., de Kruijff, B., Breukink, E., 2014. Specificity of the Transport of Lipid II by FtsW in Escherichia coli. J. Biol. Chem. 289, 14707–14718. https://doi.org/10.1074/jbc.M114.557371

Morita, Y.S., Fukuda, T., Sena, C.B.C., Yamaryo-Botte, Y., McConville, M.J., Kinoshita, T., 2011. Inositol lipid metabolism in mycobacteria: Biosynthesis and regulatory mechanisms. Biochim. Biophys. Acta BBA - Gen. Subj. 1810, 630–641. https://doi.org/10.1016/j.bbagen.2011.03.017

Morita, Y.S., Sena, C.B.C., Waller, R.F., Kurokawa, K., Sernee, M.F., Nakatani, F., Haites, R.E., Billman-Jacobe, H., McConville, M.J., Maeda, Y., Kinoshita, T., 2006. PimE Is a Polyprenol-phosphate-mannose-dependent Mannosyltransferase That Transfers the

Fifth Mannose of Phosphatidylinositol Mannoside in Mycobacteria. J. Biol. Chem. 281, 25143–25155. https://doi.org/10.1074/jbc.M604214200

Morita, Y.S., Yamaryo-Botte, Y., Miyanagi, K., Callaghan, J.M., Patterson, J.H., Crellin, P.K., Coppel, R.L., Billman-Jacobe, H., Kinoshita, T., McConville, M.J., 2010. Stress-induced Synthesis of Phosphatidylinositol 3-Phosphate in Mycobacteria. J. Biol. Chem. 285, 16643–16650. https://doi.org/10.1074/jbc.M110.119263

Movahedzadeh, F., Smith, D.A., Norman, R.A., Dinadayala, P., Murray-Rust, J., Russell, D.G., Kendall, S.L., Rison, S.C.G., McAlister, M.S.B., Bancroft, G.J., McDonald, N.Q., Daffe, M., Av-Gay, Y., Stoker, N.G., 2004. The Mycobacterium tuberculosis ino1 gene is essential for growth and virulence: M. tuberculosis ino1 gene. Mol. Microbiol. 51, 1003–1014. https://doi.org/10.1046/j.1365-2958.2003.03900.x

Moynihan, P.J., Cadby, I.T., Veerapen, N., Jankute, M., Crosatti, M., Mukamolova, G.V., Lovering, A.L., Besra, G.S., 2019. The hydrolase LpqI primes mycobacterial peptidoglycan recycling. Nat. Commun. 10. https://doi.org/10.1038/s41467-019-10586-2

Murray, J.F., Schraufnagel, D.E., Hopewell, P.C., 2015. Treatment of Tuberculosis. A Historical Perspective. Ann. Am. Thorac. Soc. 12, 1749–1759. https://doi.org/10.1513/AnnalsATS.201509-632PS

Nigou, J., Gilleron, M., Brando, T., Puzo, G., 2004. Structural analysis of mycobacterial lipoglycans. Appl. Biochem. Biotechnol. 118, 253–267.

Nikitushkin, V.D., Demina, G.R., Shleeva, M.O., Guryanova, S.V., Ruggiero, A., Berisio, R., Kaprelyants, A.S., 2015. A product of RpfB and RipA joint enzymatic action promotes the resuscitation of dormant mycobacteria. FEBS J. 282, 2500–2511. https://doi.org/10.1111/febs.13292

Ortalo-Magne, A., Andersen, \AAse B., Daffé, M., 1996. The outermost capsular arabinomannans and other mannoconjugates of virulent and avirulent tubercle bacilli. Microbiology 142, 927–935.

Ortalo-Magne, A., Dupont, M.-A., Lemassu, A., Andersen, A.B., Gounon, P., Mamadou, D., 1995. Molecular composition of the outermost capsular material of the tubercle bacillus. Microbiology 141, 1609–1620. https://doi.org/10.1099/13500872-141-7-1609

Ortalo-Magné, A., Lemassu, A., Lanéelle, M.A., Bardou, F., Silve, G., Gounon, P., Marchal, G., Daffé, M., 1996. Identification of the surface-exposed lipids on the cell envelopes of Mycobacterium tuberculosis and other mycobacterial species. J. Bacteriol. 178, 456–461. https://doi.org/10.1128/JB.178.2.456-461.1996

Pandey, A., Shin, K., Patterson, R.E., Liu, X.-Q., Rainey, J.K., 2016. Current strategies for protein production and purification enabling membrane protein structural biology. Biochem. Cell Biol. 94, 507–527. https://doi.org/10.1139/bcb-2015-0143

Pandey, S.D., Pal, S., Kumar N, G., Bansal, A., Mallick, S., Ghosh, A.S., 2018. Two DD-carboxypeptidases from *Mycobacterium smegmatis* affect cell surface properties through regulation of peptidoglycan cross-linking and glycopeptidolipids. J. Bacteriol. JB.00760-17. https://doi.org/10.1128/JB.00760-17

Patel, Y.S., Mistry, N., Mehra, S., 2019. Repurposing artemisinin as an anti-mycobacterial agent in synergy with rifampicin. Tuberculosis 115, 146–153. https://doi.org/10.1016/j.tube.2019.03.004

Pawar, A., Jha, P., Konwar, C., Chaudhry, U., Chopra, M., Saluja, D., 2019. Ethambutol targets the glutamate racemase of Mycobacterium tuberculosis—an enzyme involved in

peptidoglycan biosynthesis. Appl. Microbiol. Biotechnol. 103, 843–851. https://doi.org/10.1007/s00253-018-9518-z

Piccazzo, R., Paparo, F., Garlaschi, G., 2014. Diagnostic Accuracy of Chest Radiography for the Diagnosis of Tuberculosis (TB) and Its Role in the Detection of Latent TB Infection: a Systematic Review. J. Rheumatol. Suppl. 91, 32–40. https://doi.org/10.3899/jrheum.140100

Pieters, J., 2008. Mycobacterium tuberculosis and the Macrophage: Maintaining a Balance. Cell Host Microbe 3, 399–407. https://doi.org/10.1016/j.chom.2008.05.006

Pisabarro, A.G., de Pedro, M.A., Vázquez, D., 1985. Structural modifications in the peptidoglycan of Escherichia coli associated with changes in the state of growth of the culture. J. Bacteriol. 161, 238–242.

Pitarque, S., Herrmann, J.-L., Duteyrat, J.-L., Jackson, M., Stewart, G., Lecointe, F., Payre, B., Schwartz, O., Young, D., Marchal, G., Lagrange, P., Puzo, G., Gicquel, B., Nigou, J., Neyrolles, O., 2005. Deciphering the molecular bases of *Mycobacterium tuberculosis* binding to the lectin DC-SIGN reveals an underestimated complexity. Biochem. J. 392, 615–624. https://doi.org/10.1042/BJ20050709

Pitarque, S., Larrouy-Maumus, G., Payré, B., Jackson, M., Puzo, G., Nigou, J., 2008. The immunomodulatory lipoglycans, lipoarabinomannan and lipomannan, are exposed at the mycobacterial cell surface. Tuberculosis 88, 560–565. https://doi.org/10.1016/j.tube.2008.04.002

Plath, K., Mothes, W., Wilkinson, B.M., Stirling, C.J., Rapoport, T.A., 1998. Signal Sequence Recognition in Posttranslational Protein Transport across the Yeast ER Membrane. Cell 94, 795–807. https://doi.org/10.1016/S0092-8674(00)81738-9

Portevin, D., de Sousa-D'Auria, C., Houssin, C., Grimaldi, C., Chami, M., Daffé, M., Guilhot, C., 2004. A polyketide synthase catalyzes the last condensation step of mycolic acid biosynthesis in mycobacteria and related organisms. Proc. Natl. Acad. Sci. 101, 314–319.

Porvaznik, I., Solovič, I., Mokrý, J., 2016. Non-Tuberculous Mycobacteria: Classification, Diagnostics, and Therapy, in: Pokorski, M. (Ed.), Respiratory Treatment and Prevention. Springer International Publishing, Cham, pp. 19–25. https://doi.org/10.1007/5584_2016_45

Postis, V., Rawson, S., Mitchell, J.K., Lee, S.C., Parslow, R.A., Dafforn, T.R., Baldwin, S.A., Muench, S.P., 2015. The use of SMALPs as a novel membrane protein scaffold for structure study by negative stain electron microscopy. Biochim. Biophys. Acta BBA - Biomembr. 1848, 496–501. https://doi.org/10.1016/j.bbamem.2014.10.018

Prabudiansyah, I., Kusters, I., Caforio, A., Driessen, A.J.M., 2015. Characterization of the annular lipid shell of the Sec translocon. Biochim. Biophys. Acta BBA - Biomembr. 1848, 2050–2056. https://doi.org/10.1016/j.bbamem.2015.06.024

Pushpakom, S., Iorio, F., Eyers, P.A., Escott, K.J., Hopper, S., Wells, A., Doig, A., Guilliams, T., Latimer, J., McNamee, C., Norris, A., Sanseau, P., Cavalla, D., Pirmohamed, M., 2019. Drug repurposing: progress, challenges and recommendations. Nat. Rev. Drug Discov. 18, 41–58. https://doi.org/10.1038/nrd.2018.168

Quentin, Y., Fichant, G., Denizot, F., 1999. Inventory, assembly and analysis of Bacillus subtilis ABC transport systems. J. Mol. Biol. 287, 467–484. https://doi.org/10.1006/jmbi.1999.2624

Radmacher, E., 2005. Ethambutol, a cell wall inhibitor of Mycobacterium tuberculosis, elicits L-glutamate efflux of Corynebacterium glutamicum. Microbiology 151, 1359–1368. https://doi.org/10.1099/mic.0.27804-0

Rawlings, A.E., 2016. Membrane proteins: always an insoluble problem? Biochem. Soc. Trans. 44, 790–795. https://doi.org/10.1042/BST20160025

Raynaud, C., Etienne, G., Peyron, P., Laneelle, M.-A., Daffe, M., 1998. Extracellular enzyme activities potentially involved in the pathogenicity of Mycobacterium tuberculosis. Microbiology 144, 577–587. https://doi.org/10.1099/00221287-144-2-577

Rees, D.C., Johnson, E., Lewinson, O., 2009. ABC transporters: the power to change. Nat. Rev. Mol. Cell Biol. 10, 218–227. https://doi.org/10.1038/nrm2646

Renner, L.D., Weibel, D.B., 2011. Cardiolipin microdomains localize to negatively curved regions of Escherichia coli membranes. Proc. Natl. Acad. Sci. 108, 6264–6269. https://doi.org/10.1073/pnas.1015757108

Reynolds, P.E., 1989. Structure, biochemistry and mechanism of action of glycopeptide antibiotics. Eur. J. Clin. Microbiol. Infect. Dis. 8, 943–950. https://doi.org/10.1007/BF01967563

Rolinson, G.N., 1994. A Review of the Microbiology of Amoxycillin/Clavulanic Acid Over the 15 Year Period 1978-1993. J. Chemother. 6, 283–318. https://doi.org/10.1080/1120009X.1994.11741165

Rose, N.L., Completo, G.C., Lin, S.-J., McNeil, M., Palcic, M.M., Lowary, T.L., 2006. Expression, Purification, and Characterization of a Galactofuranosyltransferase Involved in *Mycobacterium t uberculosis* Arabinogalactan Biosynthesis. J. Am. Chem. Soc. 128, 6721–6729. https://doi.org/10.1021/ja058254d

Rothnie, A.J., 2016. Detergent-Free Membrane Protein Purification, in: Mus-Veteau, I. (Ed.), Heterologous Expression of Membrane Proteins. Springer New York, New York, NY, pp. 261–267. https://doi.org/10.1007/978-1-4939-3637-3_16

Ruiz, 2016. Lipid Flippases for Bacterial Peptidoglycan Biosynthesis. Lipid Insights 21. https://doi.org/10.4137/LPI.S31783

Ruiz, N., 2008. Bioinformatics identification of MurJ (MviN) as the peptidoglycan lipid II flippase in Escherichia coli. Proc. Natl. Acad. Sci. 105, 15553–15557.

Rule, C.S., Patrick, M., Sandkvist, M., 2016. Measuring In Vitro ATPase Activity for Enzymatic Characterization. J. Vis. Exp. 54305. https://doi.org/10.3791/54305

Russell, N.J., Sandercock, S.P., 1980. The regulation of bacterial membrane fluidity by modification of phospholipid fatty acyl chain length, in: Kates, M., Kuksis, A. (Eds.), Membrane Fluidity: Biophysical Techniques and Cellular Regulation. Humana Press, Totowa, NJ, pp. 181–190. https://doi.org/10.1007/978-1-4612-6120-9_14

Safarpour, H., Banadkoki, S.B., Keshavarzi, Z., Morowvat, M.H., Soleimanpour, M., Pourmolaei, S., Shirazi, F.H., 2017. Expression analysis and ATR-FTIR characterization of the secondary structure of recombinant human TNF-α from Escherichia coli SHuffle ® T7 Express and BL21 (DE3) cells. Int. J. Biol. Macromol. 99, 173–178. https://doi.org/10.1016/j.ijbiomac.2017.02.052

Safi, H., Sayers, B., Hazbon, M.H., Alland, D., 2008. Transfer of embB Codon 306 Mutations into Clinical Mycobacterium tuberculosis Strains Alters Susceptibility to Ethambutol, Isoniazid, and Rifampin. Antimicrob. Agents Chemother. 52, 2027–2034. https://doi.org/10.1128/AAC.01486-07

Saleh, M.T., Belisle, J.T., 2000. Secretion of an Acid Phosphatase (SapM) by Mycobacterium tuberculosis That Is Similar to Eukaryotic Acid Phosphatases. J. Bacteriol. 182, 6850–6853. https://doi.org/10.1128/JB.182.23.6850-6853.2000

Salman, M., Lonsdale, J.T., Besra, G.S., Brennan, P.J., 1999. Phosphatidylinositol synthesis in mycobacteria. Biochim. Biophys. Acta BBA - Mol. Cell Biol. Lipids 1436, 437–450. https://doi.org/10.1016/S0005-2760(98)00151-9

Sancho-Vaello, E., Albesa-Jové, D., Rodrigo-Unzueta, A., Guerin, M.E., 2017. Structural basis of phosphatidyl-myo-inositol mannosides biosynthesis in mycobacteria. Biochim. Biophys. Acta BBA - Mol. Cell Biol. Lipids 1862, 1355–1367. https://doi.org/10.1016/j.bbalip.2016.11.002

Sanders, A.N., Wright, L.F., Pavelka, M.S., 2014. Genetic characterization of mycobacterial L,D-transpeptidases. Microbiology 160, 1795–1806. https://doi.org/10.1099/mic.0.078980-0

Sathappa, M., Alder, N.N., 2016. The ionization properties of cardiolipin and its variants in model bilayers. Biochim. Biophys. Acta BBA - Biomembr. 1858, 1362–1372. https://doi.org/10.1016/j.bbamem.2016.03.007

Sauvage, E., Kerff, F., Terrak, M., Ayala, J.A., Charlier, P., 2008. The penicillin-binding proteins: structure and role in peptidoglycan biosynthesis. FEMS Microbiol. Rev. 32, 234–258. https://doi.org/10.1111/j.1574-6976.2008.00105.x

Schaeffer, M.L., Khoo, K.-H., Besra, G.S., Chatterjee, D., Brennan, P.J., Belisle, J.T., Inamine, J.M., 1999. The pimB gene of Mycobacterium tuberculosis encodes a mannosyltransferase involved in lipoarabinomannan biosynthesis. J. Biol. Chem. 274, 31625–31631.

Schäfer, A., Tauch, A., Jäger, W., Kalinowski, J., Thierbachb, G., Pühler, A., 1994. Small mobilizable multi-purpose cloning vectors derived from the Escherichia coli plasmids pK18 and pK19: selection of defined deletions in the chromosome of Corynebacterium glutumicum 5.

Schlegel, S., Genevaux, P., de Gier, J.-W., 2015. De-convoluting the Genetic Adaptations of E. coli C41(DE3) in Real Time Reveals How Alleviating Protein Production Stress Improves Yields. Cell Rep. 10, 1758–1766. https://doi.org/10.1016/j.celrep.2015.02.029

Schroeder, B.G., Barry, C.E., 2001. The Specificity of Methyl Transferases Involved in trans Mycolic Acid Biosynthesis in Mycobacterium tuberculosis and Mycobacterium smegmatis. Bioorganic Chem. 29, 164–177. https://doi.org/10.1006/bioo.2001.1207

Seeger, M.A., 2018. Membrane transporter research in times of countless structures. Biochim. Biophys. Acta BBA - Biomembr. 1860, 804–808. https://doi.org/10.1016/j.bbamem.2017.08.009

Seidel, M., Alderwick, L.J., Birch, H.L., Sahm, H., Eggeling, L., Besra, G.S., 2007a. Identification of a Novel Arabinofuranosyltransferase AftB Involved in a Terminal Step of Cell Wall Arabinan Biosynthesis in Corynebacterianeae, such as *Corynebacterium glutamicum* and *Mycobacterium tuberculosis*. J. Biol. Chem. 282, 14729–14740. https://doi.org/10.1074/jbc.M700271200

Seidel, M., Alderwick, L.J., Sahm, H., Besra, G.S., Eggeling, L., 2007b. Topology and mutational analysis of the single Emb arabinofuranosyltransferase of Corynebacterium glutamicum as a model of Emb proteins of Mycobacterium tuberculosis. Glycobiology 17, 210–219. https://doi.org/10.1093/glycob/cwl066

Sham, L.-T., Butler, E.K., Lebar, M.D., Kahne, D., Bernhardt, T.G., Ruiz, N., 2014. MurJ is the flippase of lipid-linked precursors for peptidoglycan biogenesis. Science 345, 220–222. https://doi.org/10.1126/science.1254522

Shi, D., Li, L., Zhao, Y., Jia, Q., Li, H., Coulter, C., Jin, Q., Zhu, G., 2011. Characteristics of embB mutations in multidrug-resistant Mycobacterium tuberculosis isolates in Henan, China. J. Antimicrob. Chemother. 66, 2240–2247. https://doi.org/10.1093/jac/dkr284

Shi, L., Berg, S., Lee, A., Spencer, J.S., Zhang, J., Vissa, V., McNeil, M.R., Khoo, K.-H., Chatterjee, D., 2006. The Carboxy Terminus of EmbC from *Mycobacterium smegmatis* Mediates Chain Length Extension of the Arabinan in Lipoarabinomannan. J. Biol. Chem. 281, 19512–19526. https://doi.org/10.1074/jbc.M513846200

Shi, W., Zhang, X., Jiang, X., Yuan, H., Lee, J.S., Barry, C.E., Wang, H., Zhang, W., Zhang, Y., 2011. Pyrazinamide Inhibits Trans-Translation in Mycobacterium tuberculosis. Science 333, 1630–1632. https://doi.org/10.1126/science.1208813

Shimizu, K., Cao, W., Saad, G., Shoji, M., Terada, T., 2018. Comparative analysis of membrane protein structure databases. Biochim. Biophys. Acta BBA - Biomembr. 1860, 1077–1091. https://doi.org/10.1016/j.bbamem.2018.01.005

Sievers, F., Wilm, A., Dineen, D., Gibson, T.J., Karplus, K., Li, W., Lopez, R., McWilliam, H., Remmert, M., Söding, J., Thompson, J.D., Higgins, D.G., 2011. Fast, scalable generation of high-quality protein multiple sequence alignments using Clustal Omega. Mol. Syst. Biol. 7, 539. https://doi.org/10.1038/msb.2011.75

Singer-Leshinsky, S., 2016. Pulmonary tuberculosis: Improving diagnosis and management. J. Am. Acad. Physician Assist. 29, 20–25. https://doi.org/10.1097/01.JAA.0000476207.96819.a7

Singh, A., Somvanshi, P., Grover, A., 2019. Drug repurposing against arabinosyl transferase (EmbC) of Mycobacterium tuberculosis: Essential dynamics and free energy minima based binding mechanics analysis. Gene 693, 114–126. https://doi.org/10.1016/j.gene.2019.01.029

Singh, A., Varela, C., Bhatt, K., Veerapen, N., Lee, O.Y.C., Wu, H.H.T., Besra, G.S., Minnikin, D.E., Fujiwara, N., Teramoto, K., Bhatt, A., 2016. Identification of a Desaturase Involved in Mycolic Acid Biosynthesis in Mycobacterium smegmatis. PLOS ONE 11, e0164253. https://doi.org/10.1371/journal.pone.0164253

Singh, H., Velamakanni, S., Deery, M.J., Howard, J., Wei, S.L., van Veen, H.W., 2016. ATP-dependent substrate transport by the ABC transporter MsbA is proton-coupled. Nat. Commun. 7, 12387. https://doi.org/10.1038/ncomms12387

Singh, R., Kraft, C., Jaiswal, R., Sejwal, K., Kasaragod, V.B., Kuper, J., Bürger, J., Mielke, T., Luirink, J., Bhushan, S., 2014. Cryo-electron Microscopic Structure of SecA Protein Bound to the 70S Ribosome. J. Biol. Chem. 289, 7190–7199. https://doi.org/10.1074/jbc.M113.506634

Skalic, M., Sabbadin, D., Sattarov, B., Sciabola, S., De Fabritiis, G., 2019. From Target to Drug: Generative Modeling for Multimodal Structure-Based Ligand Design. Mol. Pharm. acs.molpharmaceut.9b00634. https://doi.org/10.1021/acs.molpharmaceut.9b00634

Škovierová, H., Larrouy-Maumus, G., Pham, H., Belanová, M., Barilone, N., DasGupta, A., Mikušová, K., Gicquel, B., Gilleron, M., Brennan, Patrick.J., Puzo, G., Nigou, J., Jackson, M., 2010. Biosynthetic Origin of the Galactosamine Substituent of Arabinogalactan in *Mycobacterium tuberculosis*. J. Biol. Chem. 285, 41348–41355. https://doi.org/10.1074/jbc.M110.188110

Škovierová, H., Larrouy-Maumus, G., Zhang, J., Kaur, D., Barilone, N., Korduláková, J., Gilleron, M., Guadagnini, S., Belanová, M., Prevost, M.-C., Gicquel, B., Puzo, G., Chatterjee, D., Brennan, P.J., Nigou, J., Jackson, M., 2009. AftD, a novel essential arabinofuranosyltransferase from mycobacteria. Glycobiology 19, 1235–1247. https://doi.org/10.1093/glycob/cwp116

Smyth, D.R., Mrozkiewicz, M.K., McGrath, W.J., Listwan, P., Kobe, B., 2003. Crystal structures of fusion proteins with large-affinity tags. Protein Sci. 12, 1313–1322. https://doi.org/10.1110/ps.0243403

Srivastava, S., Ayyagari, A., Dhole, T.N., Nyati, K.K., Dwivedi, S.K., 2009. emb nucleotide polymorphisms and the role of embB306 mutations in Mycobacterium tuberculosis resistance to ethambutol. Int. J. Med. Microbiol. 299, 269–280. https://doi.org/10.1016/j.ijmm.2008.07.001

Stoop, E.J.M., Mishra, A.K., Driessen, N.N., van Stempvoort, G., Bouchier, P., Verboom, T., van Leeuwen, L.M., Sparrius, M., Raadsen, S.A., van Zon, M., van der Wel, N.N., Besra, G.S., Geurtsen, J., Bitter, W., Appelmelk, B.J., van der Sar, A.M., 2013. Mannan core branching of lipo(arabino)mannan is required for mycobacterial virulence in the context of innate immunity: Mannosyltransferase affects granuloma initiation. Cell. Microbiol. 15, 2093–2108. https://doi.org/10.1111/cmi.12175

Strahl, H., Errington, J., 2017. Bacterial Membranes: Structure, Domains, and Function. Annu. Rev. Microbiol. 71, 519–538. https://doi.org/10.1146/annurev-micro-102215-095630

Takayama, K., Kilburn, J.O., 1989. Inhibition of synthesis of arabinogalactan by ethambutol in Mycobacterium smegmatis. Antimicrob. Agents Chemother. 33, 1493–1499. https://doi.org/10.1128/AAC.33.9.1493

Takayama, K., Wang, C., Besra, G.S., 2005. Pathway to Synthesis and Processing of Mycolic Acids in Mycobacterium tuberculosis. Clin. Microbiol. Rev. 18, 81–101. https://doi.org/10.1128/CMR.18.1.81-101.2005

Takeya K., Hisatsune K., 1963. Mycobacterial cell walls I. Methods of preparation and treatment with various chemicals. J. Bacteriol. 85.

Tang, P., Johnston, J., 2017. Treatment of Latent Tuberculosis Infection. Curr. Treat. Options Infect. Dis. 9, 371–379. https://doi.org/10.1007/s40506-017-0135-7

Tanne, A., Ma, B., Boudou, F., Tailleux, L., Botella, H., Badell, E., Levillain, F., Taylor, M.E., Drickamer, K., Nigou, J., Dobos, K.M., Puzo, G., Vestweber, D., Wild, M.K., Marcinko, M., Sobieszczuk, P., Stewart, L., Lebus, D., Gicquel, B., Neyrolles, O., 2009. A murine DC-SIGN homologue contributes to early host defense against *Mycobacterium tuberculosis*. J. Exp. Med. 206, 2205–2220. https://doi.org/10.1084/jem.20090188

Tassoni, R., Blok, A., Pannu, N.S., Ubbink, M., 2019. New Conformations of Acylation Adducts of Inhibitors of β-Lactamase from *Mycobacterium tuberculosis*. Biochemistry 58, 997–1009. https://doi.org/10.1021/acs.biochem.8b01085

Tatituri, Alderwick, L.J., Mishra, A.K., Nigou, J., Gilleron, M., Krumbach, K., Hitchen, P., Giordano, A., Morris, H.R., Dell, A., Eggeling, L., Besra, G.S., 2007a. Structural characterization of a partially arabinosylated lipoarabinomannan variant isolated from a Corynebacterium glutamicum ubiA mutant. Microbiology 153, 2621–2629. https://doi.org/10.1099/mic.0.2007/008078-0

Tatituri, Illarionov, P.A., Dover, L.G., Nigou, J., Gilleron, M., Hitchen, P., Krumbach, K., Morris, H.R., Spencer, N., Dell, A., Eggeling, L., Besra, G.S., 2007b. Inactivation of *Corynebacterium glutamicum* NCgl0452 and the Role of MgtA in the Biosynthesis of a

Novel Mannosylated Glycolipid Involved in Lipomannan Biosynthesis. J. Biol. Chem. 282, 4561–4572. https://doi.org/10.1074/jbc.M608695200

Teo, A.C.K., Lee, S.C., Pollock, N.L., Stroud, Z., Hall, S., Thakker, A., Pitt, A.R., Dafforn, T.R., Spickett, C.M., Roper, D.I., 2019. Analysis of SMALP co-extracted phospholipids shows distinct membrane environments for three classes of bacterial membrane protein. Sci. Rep. 9. https://doi.org/10.1038/s41598-018-37962-0

Thwaites, G., 2014. Tuberculosis, in: Manson's Tropical Infectious Diseases. Elsevier, pp. 468-505.e3. https://doi.org/10.1016/B978-0-7020-5101-2.00041-8

Tommassen, J., 2010. Assembly of outer-membrane proteins in bacteria and mitochondria. Microbiology 156, 2587–2596. https://doi.org/10.1099/mic.0.042689-0

Touchette, M.H., Seeliger, J.C., 2017. Transport of outer membrane lipids in mycobacteria. Biochim. Biophys. Acta BBA - Mol. Cell Biol. Lipids. https://doi.org/10.1016/j.bbalip.2017.01.005

Tsirigotaki, A., De Geyter, J., Šoštaric´, N., Economou, A., Karamanou, S., 2017. Protein export through the bacterial Sec pathway. Nat. Rev. Microbiol. 15, 21–36. https://doi.org/10.1038/nrmicro.2016.161

Tsukamura, M., 1965. Resistance Pattern of Mycobacterium tuberculosis and Mycobacterium bovis to Etham butol. Acta Tuberc. Pneumol. Scand. 46, 89–92.

Turnbull, W.B., Shimizu, K.H., Chatterjee, D., Homans, S.W., Treumann, A., 2004. Identification of the 5-Methylthiopentosyl Substituent inMycobacterium tuberculosis Lipoarabinomannan. Angew. Chem. Int. Ed. 43, 3918–3922. https://doi.org/10.1002/anie.200454119

van der Laan, M., Bechtluft, P., Kol, S., Nouwen, N., Driessen, A.J.M., 2004. $F_1 F_0$ ATP synthase subunit c is a substrate of the novel YidC pathway for membrane protein biogenesis. J. Cell Biol. 165, 213–222. https://doi.org/10.1083/jcb.200402100

van der Laan, M., Houben, E.N.G., Nouwen, N., Luirink, J., Driessen, A.J.M., 2001. Reconstitution of Sec-dependent membrane protein insertion: nascent FtsQ interacts with YidC in a SecYEG-dependent manner. EMBO Rep. 2, 519–523. https://doi.org/10.1093/embo-reports/kve106

Vergne, I., Chua, J., Deretic, V., 2003. Tuberculosis Toxin Blocking Phagosome Maturation Inhibits a Novel Ca^{2+} /Calmodulin-PI3K hVPS34 Cascade. J. Exp. Med. 198, 653–659. https://doi.org/10.1084/jem.20030527

Vergne, I., Chua, J., Lee, H.-H., Lucas, M., Belisle, J., Deretic, V., 2005. Mechanism of phagolysosome biogenesis block by viable Mycobacterium tuberculosis. Proc. Natl. Acad. Sci. 102, 4033–4038. https://doi.org/10.1073/pnas.0409716102

Vollmer, W., Blanot, D., De Pedro, M.A., 2008. Peptidoglycan structure and architecture. FEMS Microbiol. Rev. 32, 149–167. https://doi.org/10.1111/j.1574-6976.2007.00094.x

von Heijne, G., 1994. *Sec* -independent protein insertion into the inner *E. coli* membrane A phenomenon in search of an explanation. FEBS Lett. 346, 69–72. https://doi.org/10.1016/0014-5793(94)00296-7

Wagner, R.M., Kricks, L., Lopez, D., 2017. Functional Membrane Microdomains Organize Signaling Networks in Bacteria. J. Membr. Biol. 250, 367–378. https://doi.org/10.1007/s00232-016-9923-0

Walburger, A., 2004. Protein Kinase G from Pathogenic Mycobacteria Promotes Survival Within Macrophages. Science 304, 1800–1804. https://doi.org/10.1126/science.1099384

Walter, C., Wilken, S., Schneider, E., 1992. Characterization of side-directed mutations in conserved domains of MalK, a bacterial member of the ATP-binding cassette (ABC) family. FEBS Lett. 303, 41–44. https://doi.org/10.1016/0014-5793(92)80473-T

Wang, S., Yang, C.-I., Shan, S., 2017. SecA mediates cotranslational targeting and translocation of an inner membrane protein. J. Cell Biol. 216, 3639–3653. https://doi.org/10.1083/jcb.201704036

Wang, T., Kunze, C., Dunlop, M.J., 2019. Salicylate Increases Fitness Cost Associated with MarA-Mediated Antibiotic Resistance. Biophys. J. 117, 563–571. https://doi.org/10.1016/j.bpj.2019.07.005

Wang, Y., Cui, T., Zhang, C., Yang, M., Huang, Y., Li, W., Zhang, L., Gao, C., He, Y., Li, Y., Huang, F., Zeng, J., Huang, C., Yang, Q., Tian, Y., Zhao, C., Chen, H., Zhang, H., He, Z.-G., 2010. Global Protein−Protein Interaction Network in the Human Pathogen *Mycobacterium tuberculosis* H37Rv. J. Proteome Res. 9, 6665–6677. https://doi.org/10.1021/pr100808n

World Health Organization, 2018. Global tuberculosis report 2018.

Xie, X.L., Li, C.H., Yang, Y.X., Jin, L., Tan, J.J., Zhang, X.Y., Su, J.G., Wang, C.X., 2015. Allosteric transitions of ATP-binding cassette transporter MsbA studied by the adaptive anisotropic network model: Allosteric Transitions of Transporter MsbA. Proteins Struct. Funct. Bioinforma. 83, 1643–1653. https://doi.org/10.1002/prot.24850

Yamaguchi, H., Mano, N., 2019. Analysis of membrane transport mechanisms of endogenous substrates using chromatographic techniques. Biomed. Chromatogr. 33, e4495. https://doi.org/10.1002/bmc.4495

Zhang, D., Wang, C., Hou, X., Yan, C., 2019. Structural characterization and osteoprotective effects of a polysaccharide purified from Achyranthes bidentata. Int. J. Biol. Macromol. 139, 1063–1073. https://doi.org/10.1016/j.ijbiomac.2019.08.013

Zhang, N., Torrelles, J.B., McNeil, M.R., Escuyer, V.E., Khoo, K.-H., Brennan, P.J., Chatterjee, D., 2003. The Emb proteins of mycobacteria direct arabinosylation of lipoarabinomannan and arabinogalactan via an N-terminal recognition region and a C-terminal synthetic region: Two functional domains in Emb proteins. Mol. Microbiol. 50, 69–76. https://doi.org/10.1046/j.1365-2958.2003.03681.x

Zhang, Y., 2003. Mode of action of pyrazinamide: disruption of Mycobacterium tuberculosis membrane transport and energetics by pyrazinoic acid. J. Antimicrob. Chemother. 52, 790–795. https://doi.org/10.1093/jac/dkg446

Zumla, A., Nahid, P., Cole, S.T., 2013. Advances in the development of new tuberculosis drugs and treatment regimens. Nat. Rev. Drug Discov. 12, 388–404. https://doi.org/10.1038/nrd4001

Appendix 1:

Prediction of number and position of transmembrane helices.

Transmembrane helix predictions of MsbA and Mycobacterial and corynebacterial homologs.

TMPred output of *E. coli* MsbA:

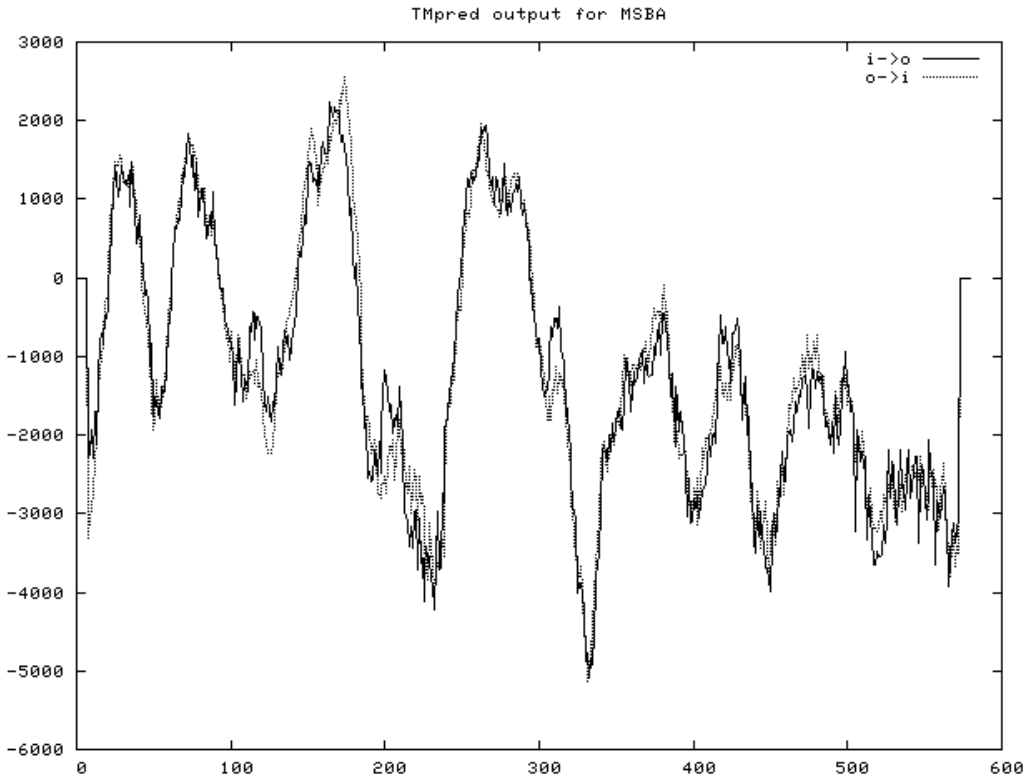

TMHMM output for *E. coli* MsbA:

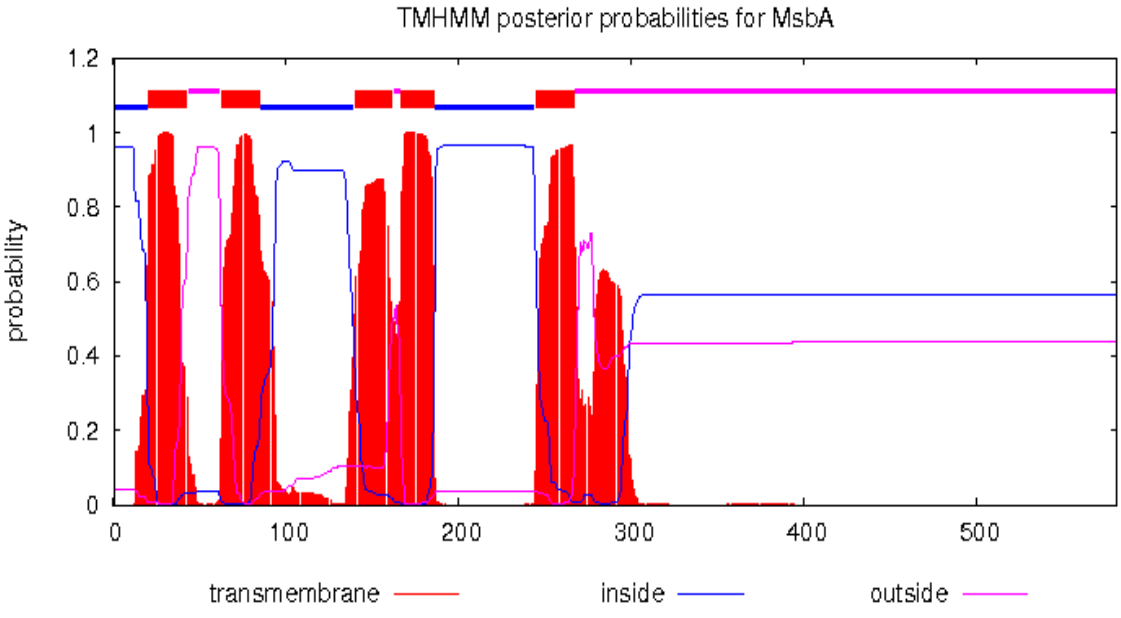

TMPred output for *M. tuberculosis* Rv1272c:

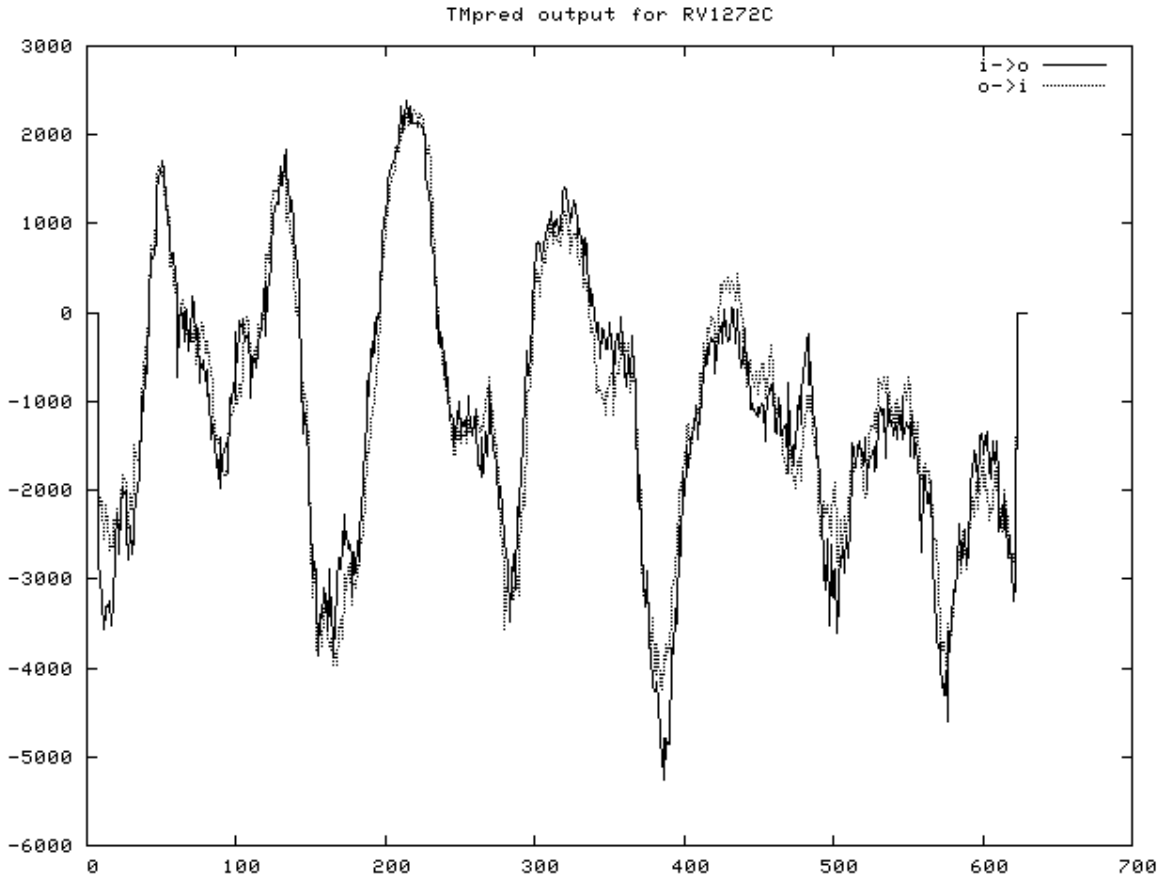

TMHMM output for *M. tuberculosis* Rv1273c:

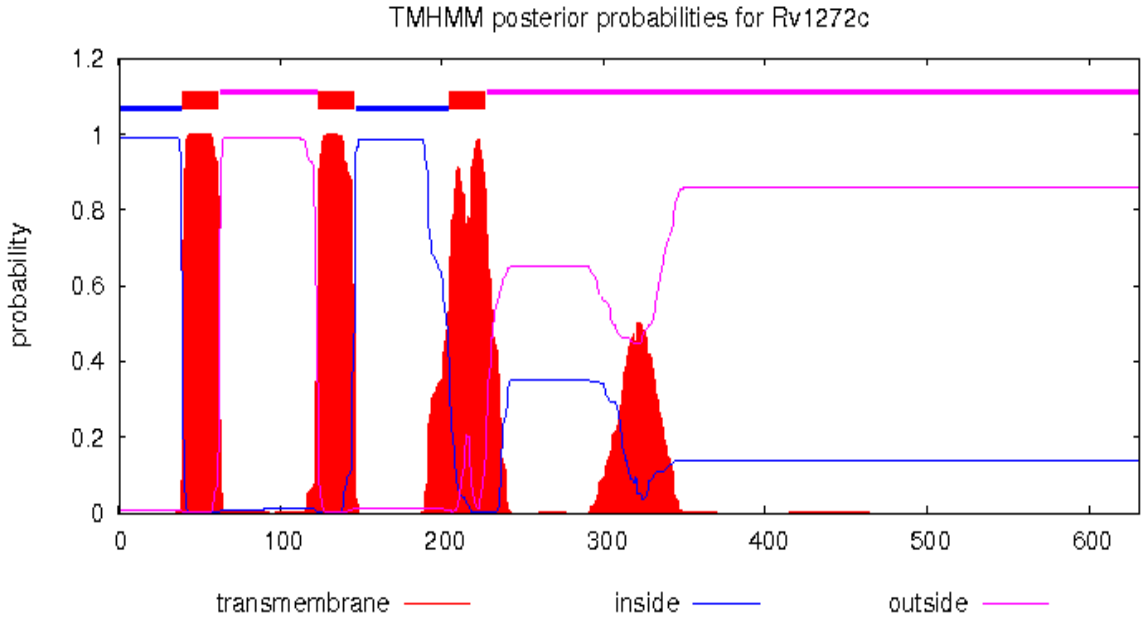

TMPred output for *M. tuberculosis* Rv1273c:

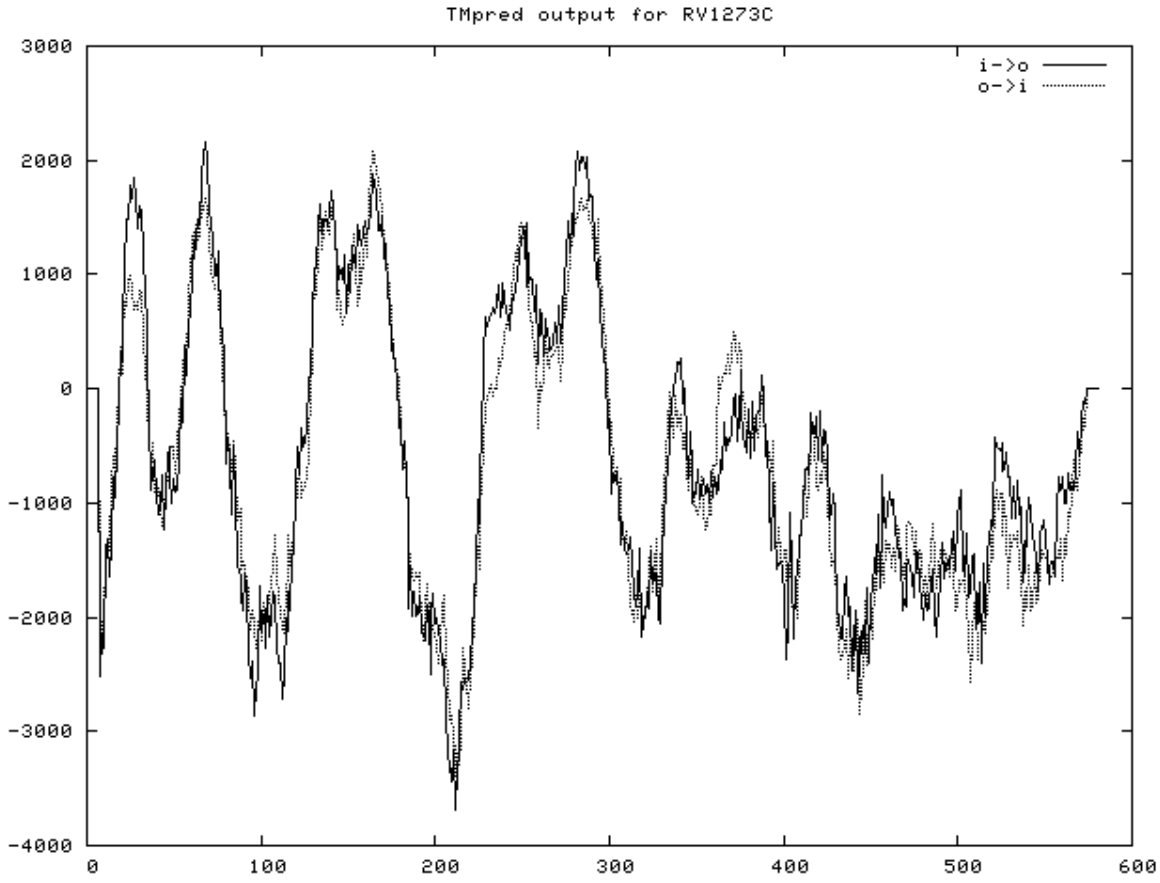

TMHMM output for Rv1273c:

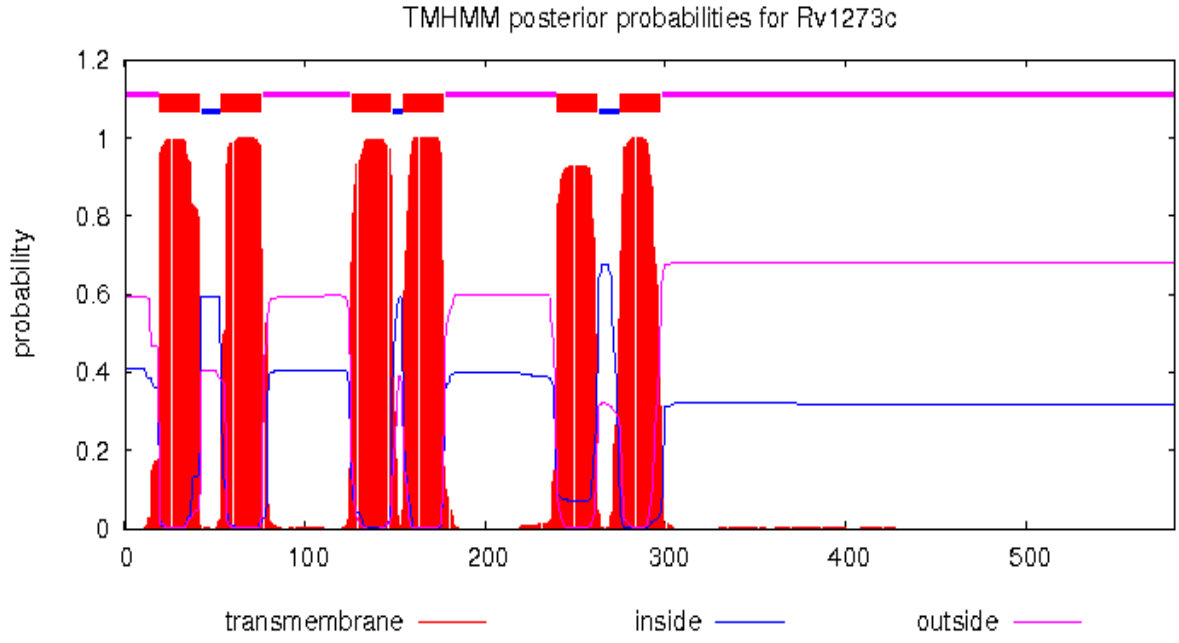

TMPred output for *M. bovis* Mb1303c:

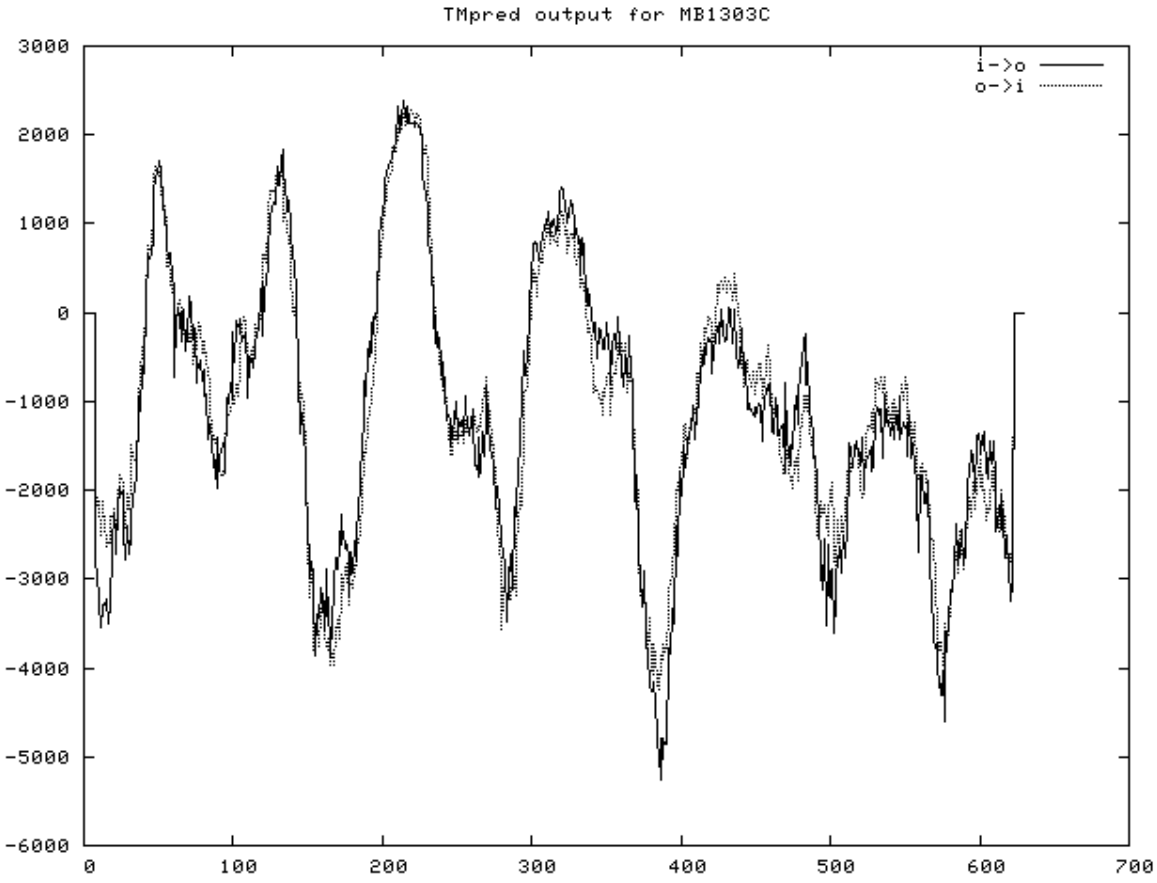

TMHMM output for *M. bovis* Mb1303c:

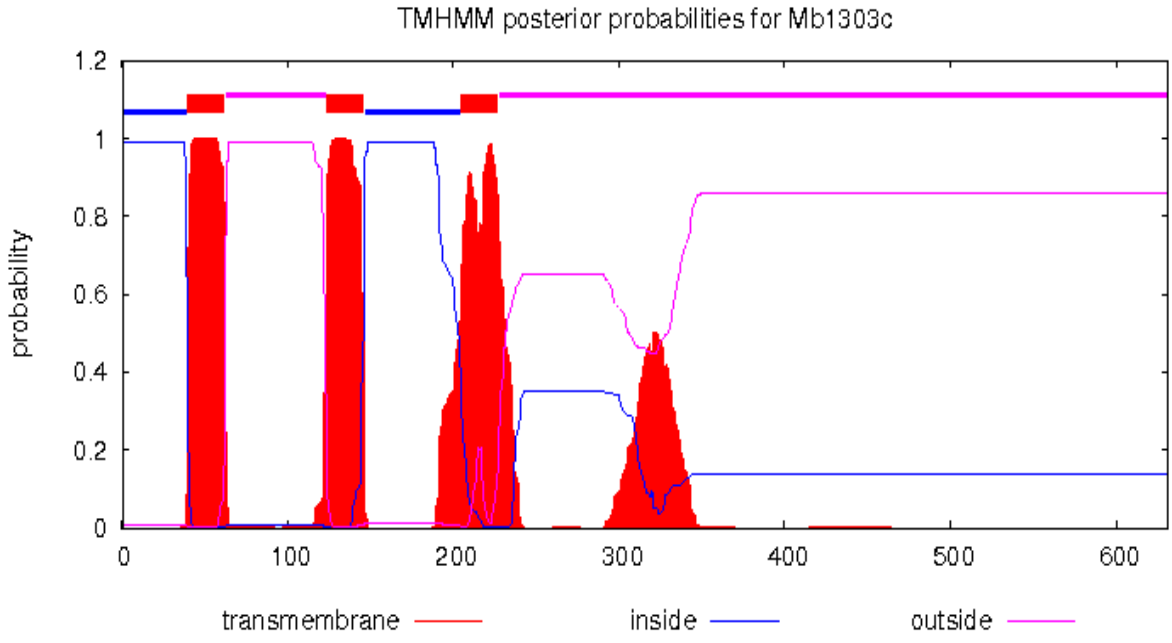

TMPred output for *M. bovis* Mb1304c:

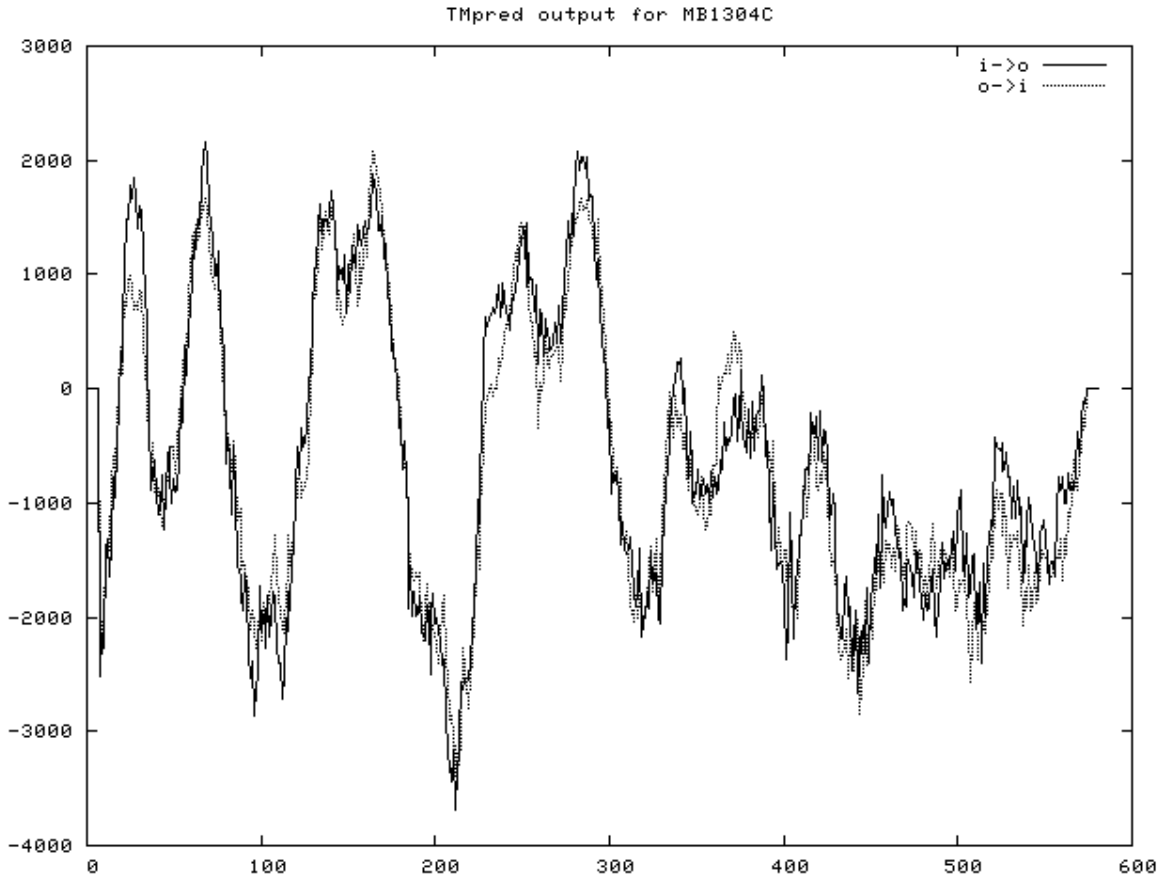

TMHMM output for *M. bovis* Mb1304c:

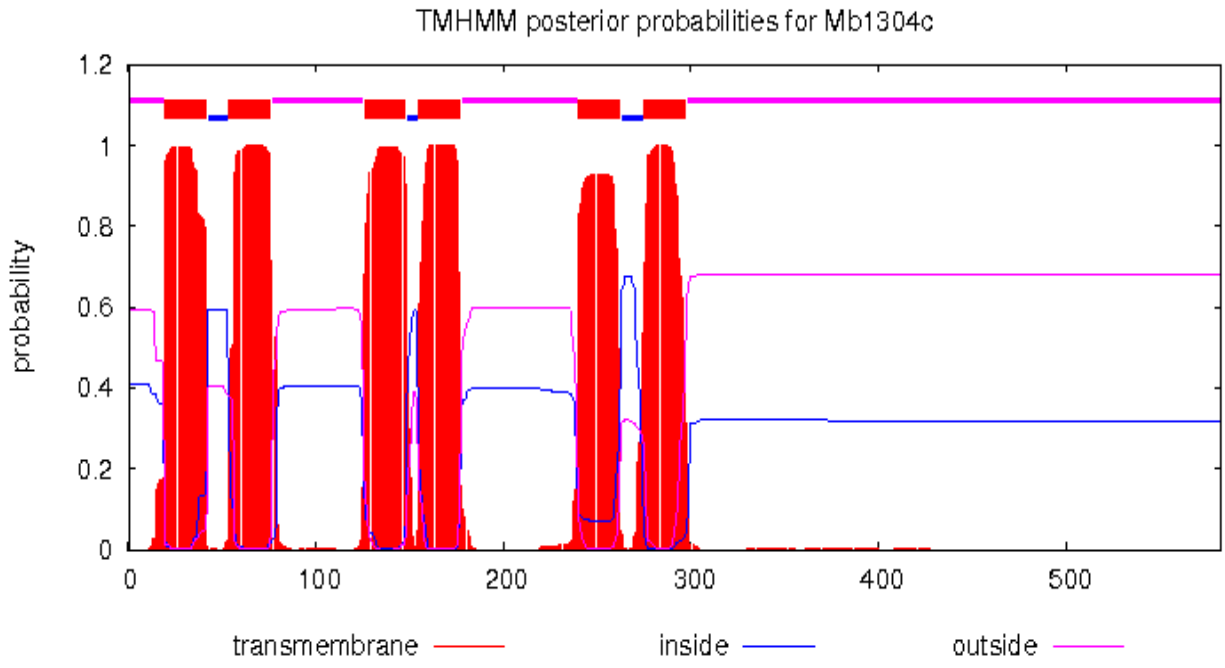

TMPred output for *M. leprae* ML1113c:

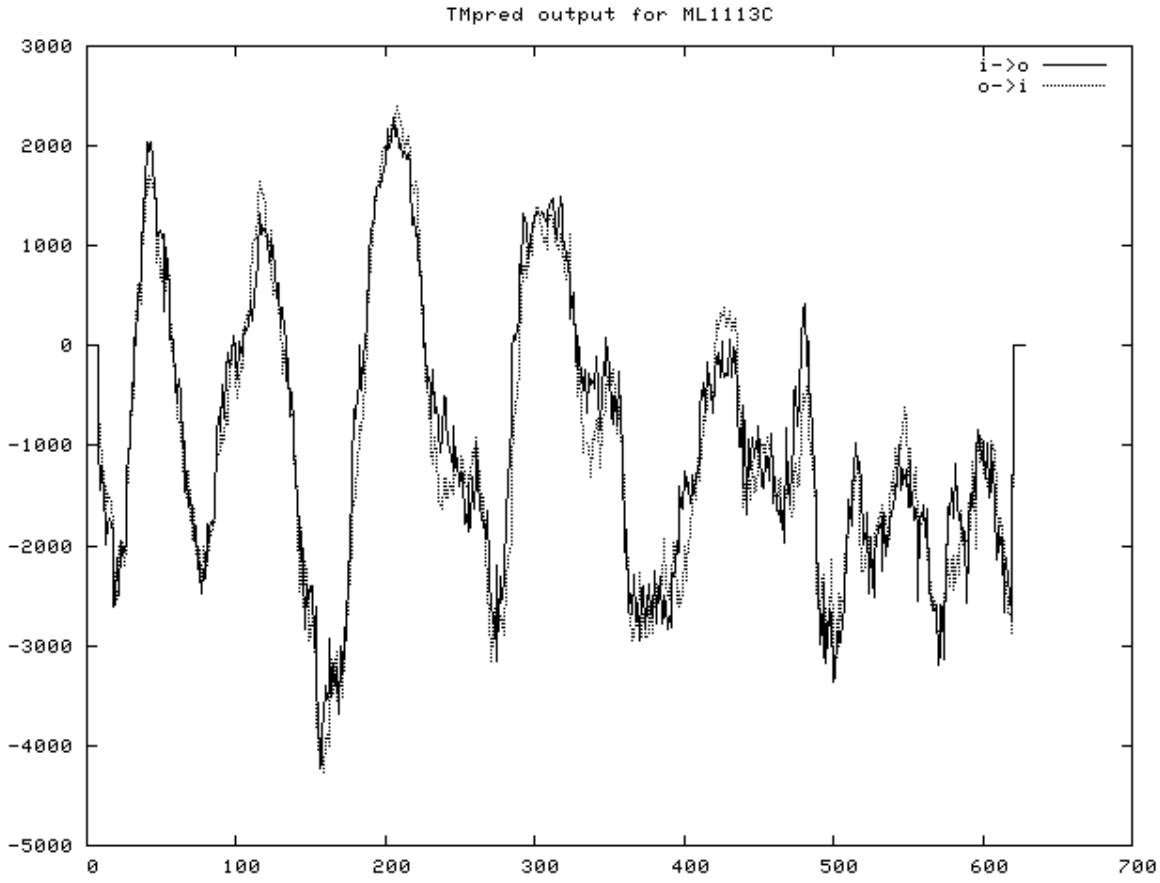

TMHMM output for *M. leprae* ML1113c:

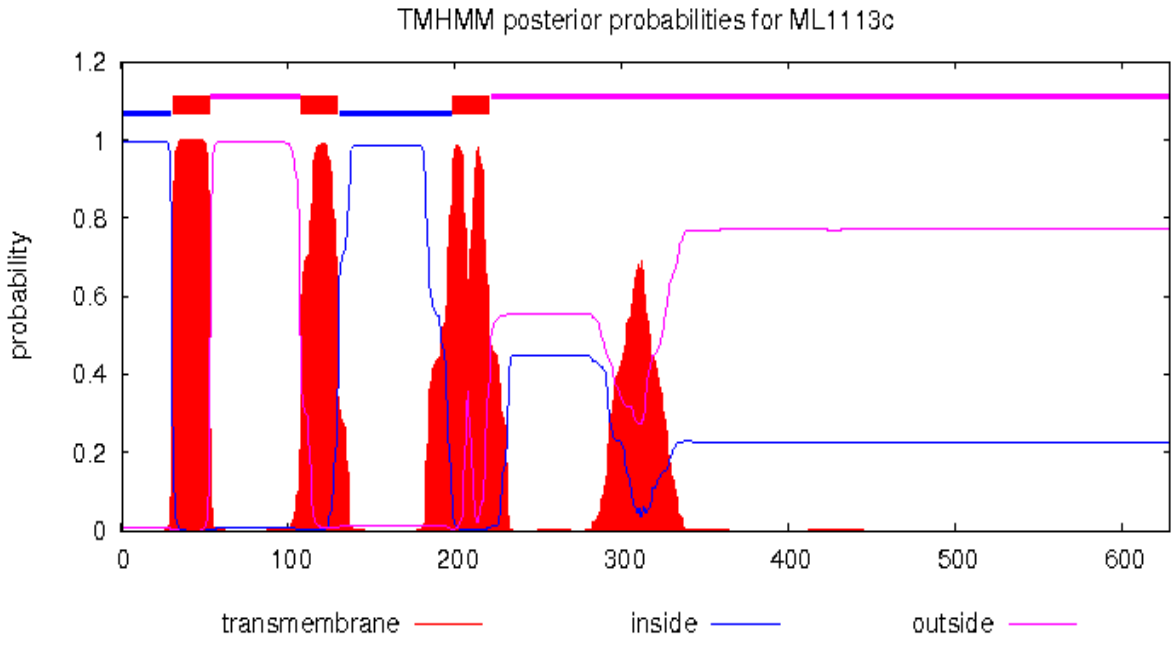

TMPred output for *M. leprae* ML1114c:

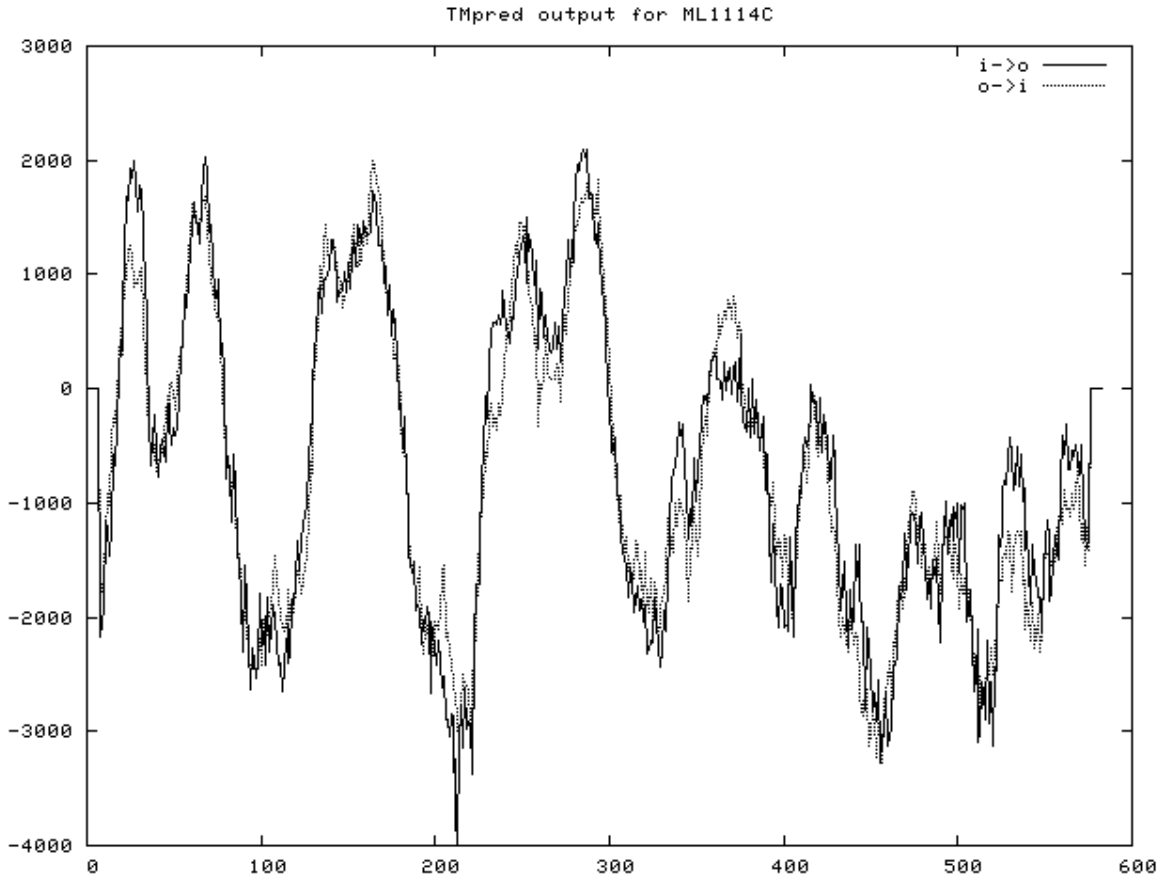

TMHMM output for *M. leprae* ML1114c:

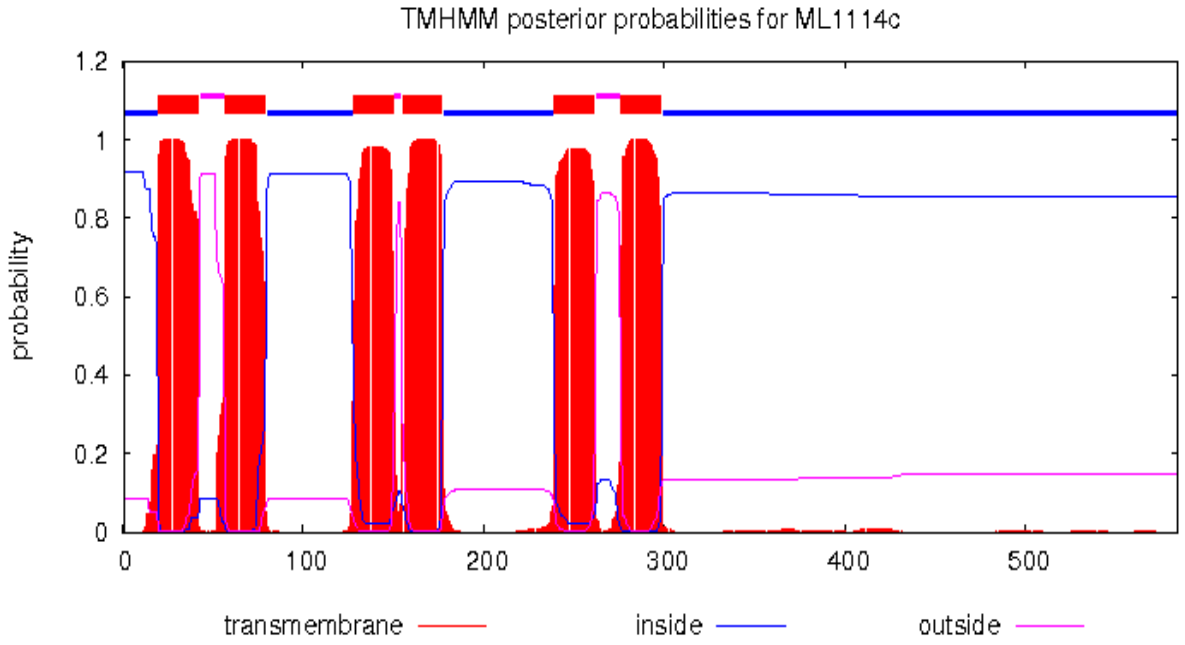

TMPred output for *M. marinum* MMAR_4147:

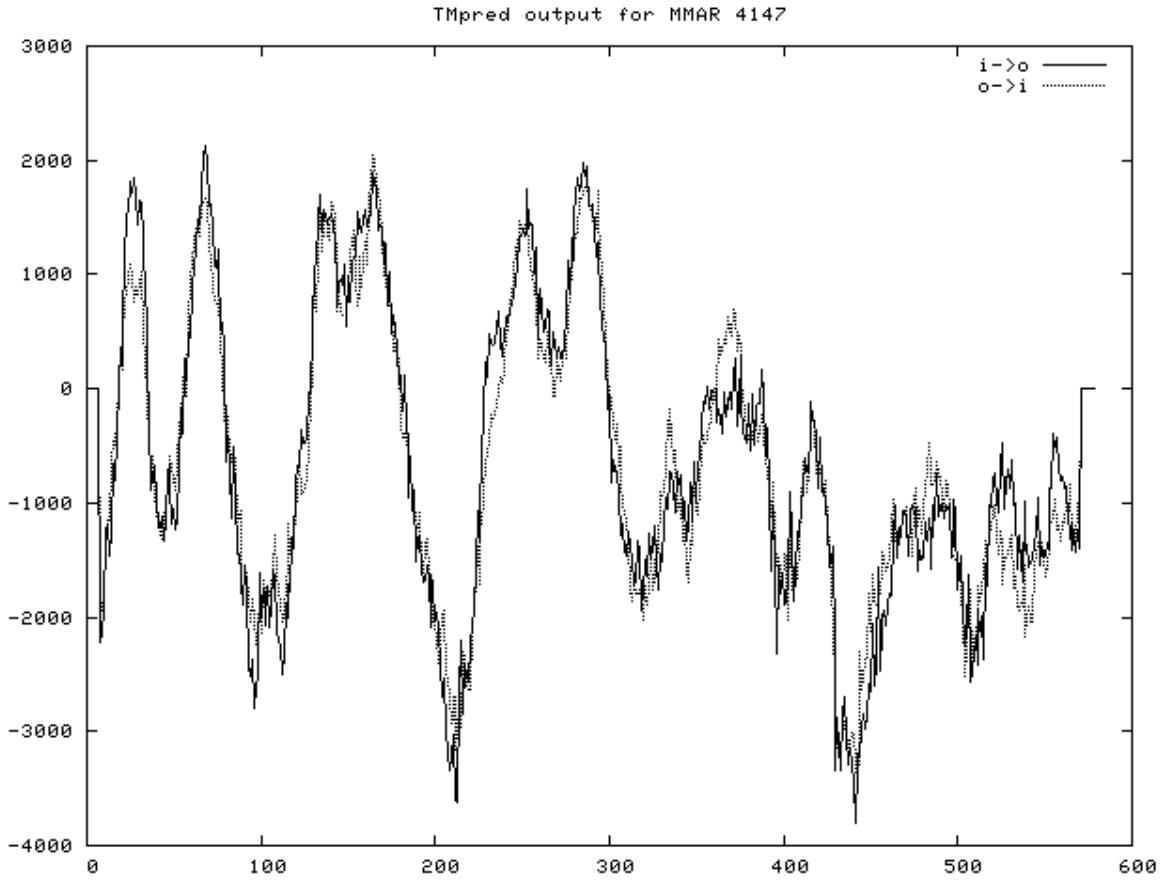

TMHMM output for *M. marinum* MMAR_4147:

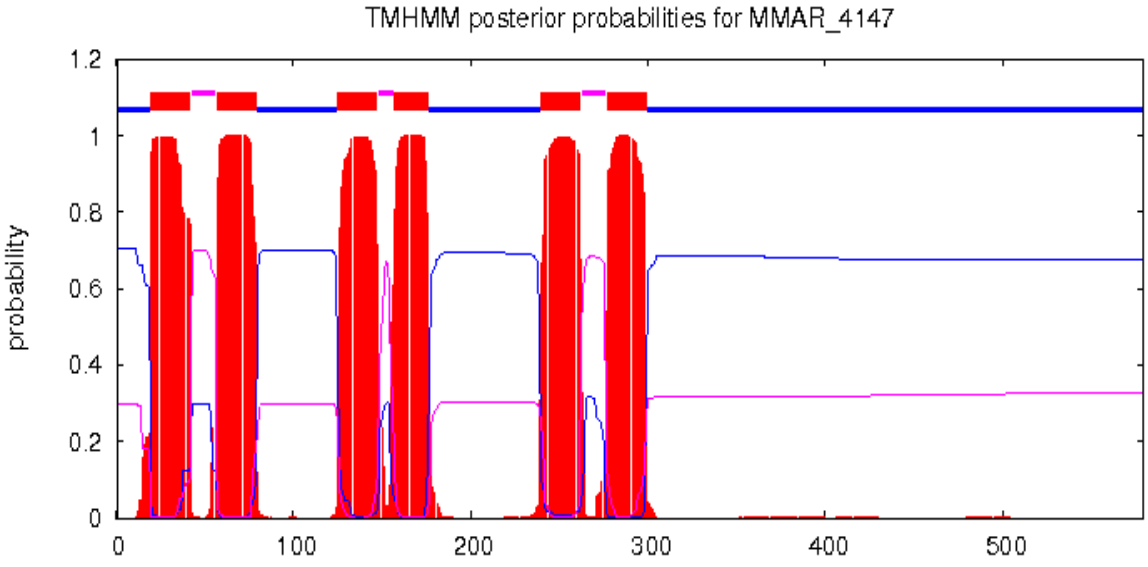

TMPred output for *M. marinum* MMAR_4148:

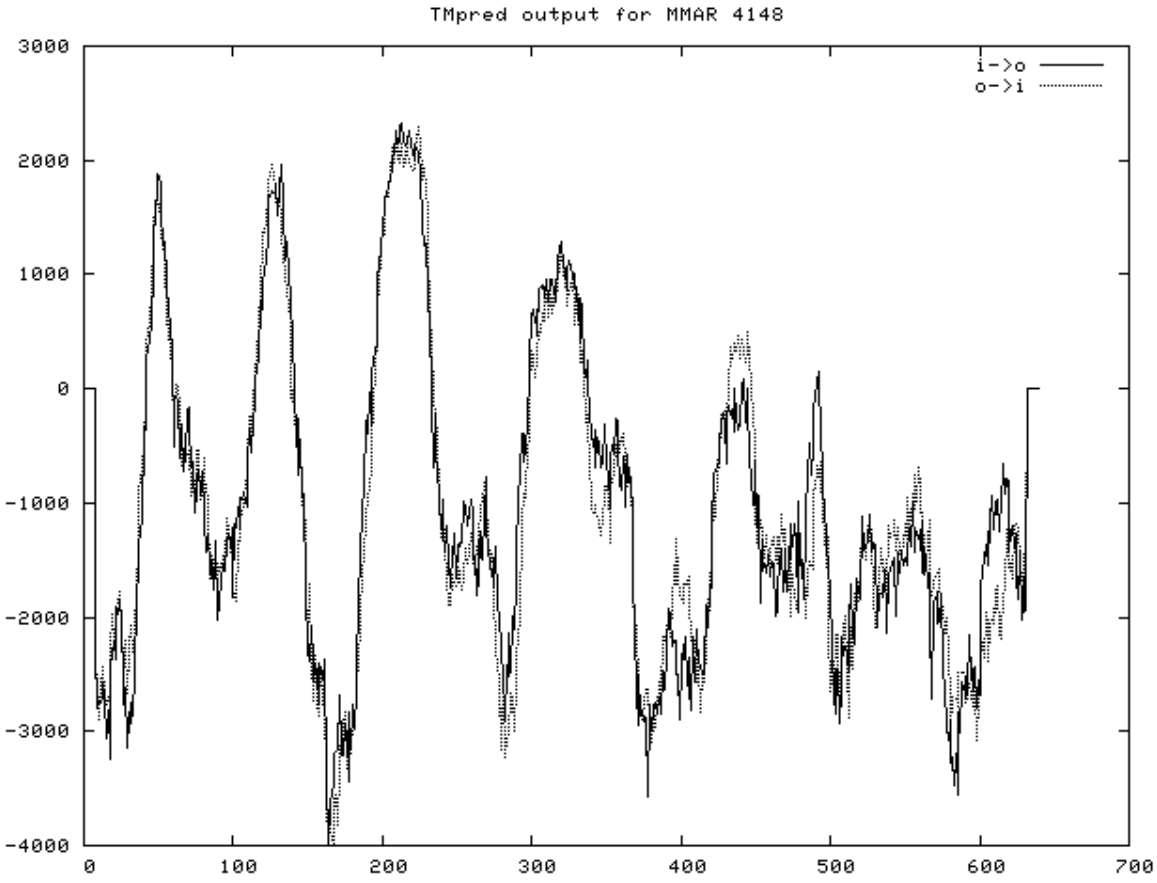

TMHMM output for *M. marimum* MMAR_4148:

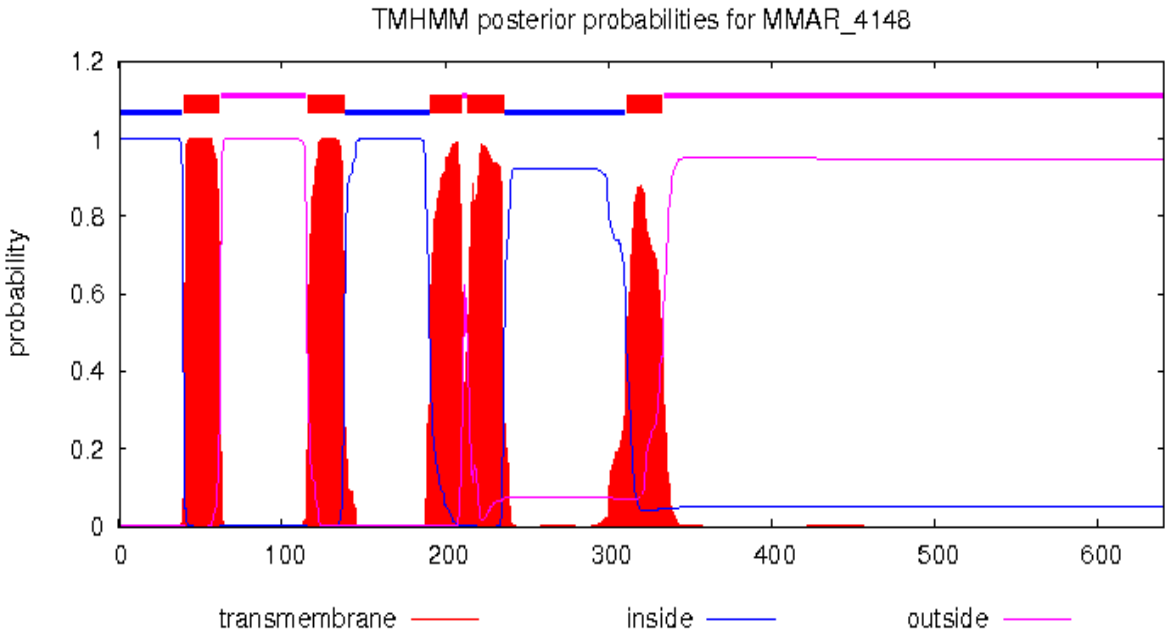

TMPred output for *M. smegmatis* MSMEG_5008:

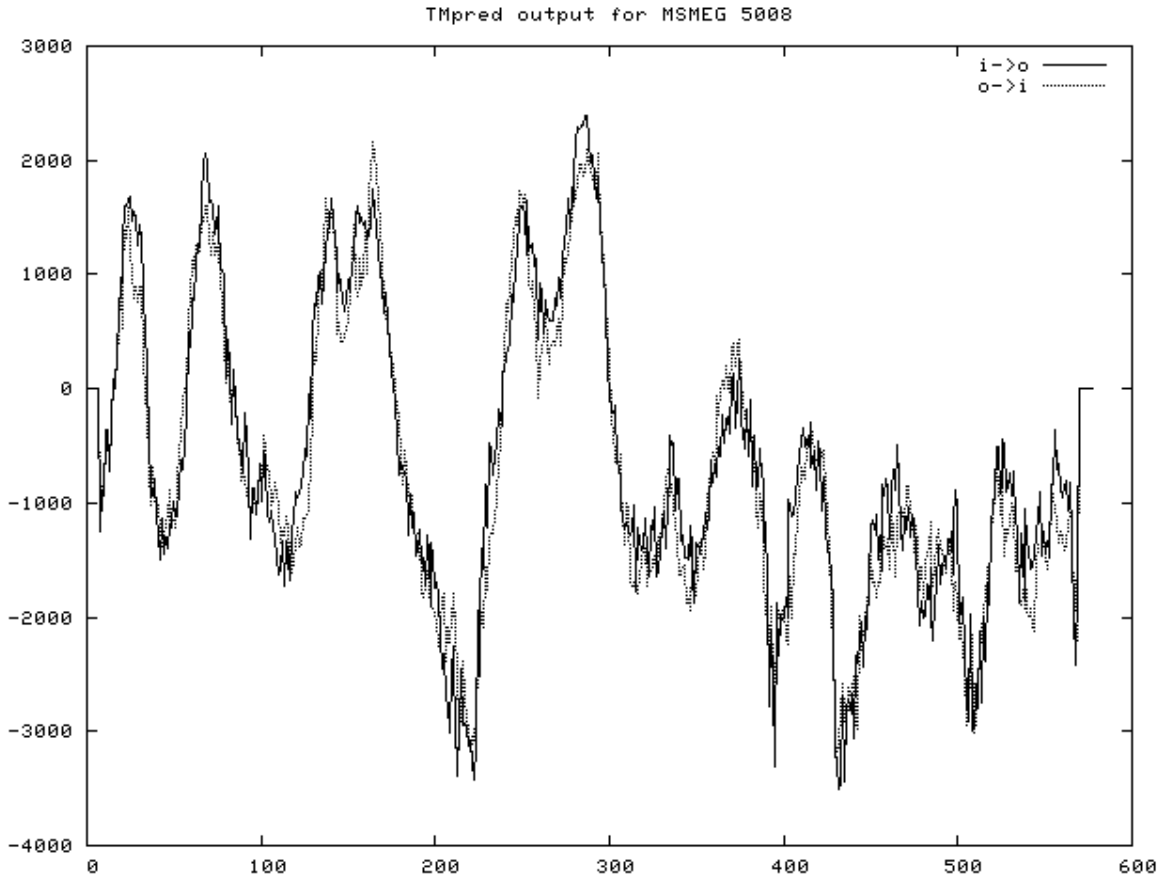

TMHMM output for *M. smegmatis* MSMEG_5008:

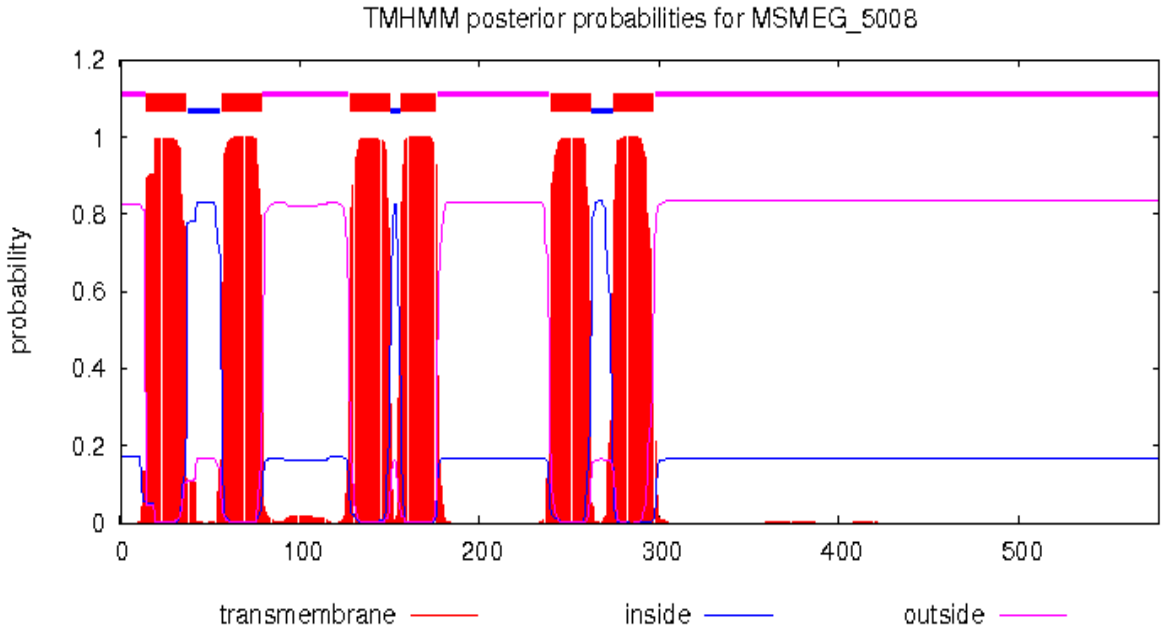

TMPred output for *M. smegmatis* MSMEG_5009:

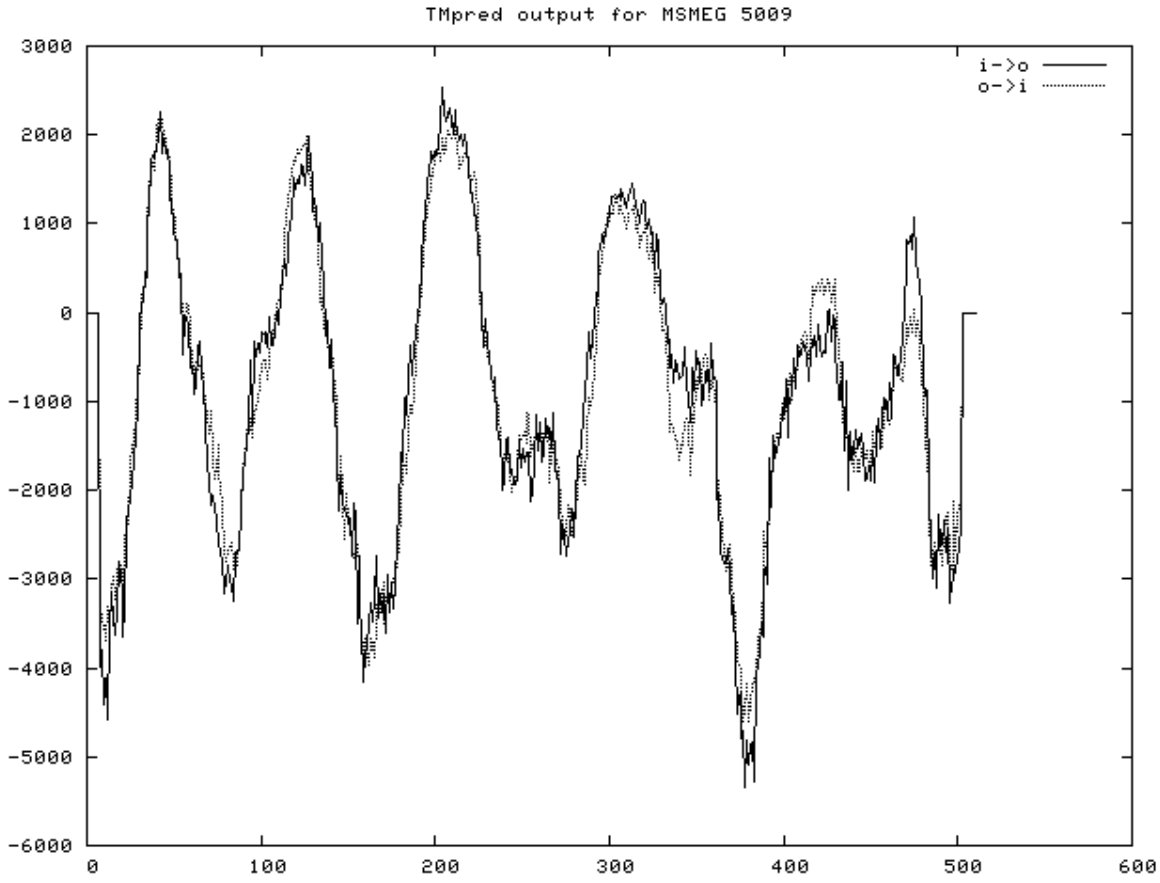

TMHMM output for *M. smegmatis* MSMEG_5009:

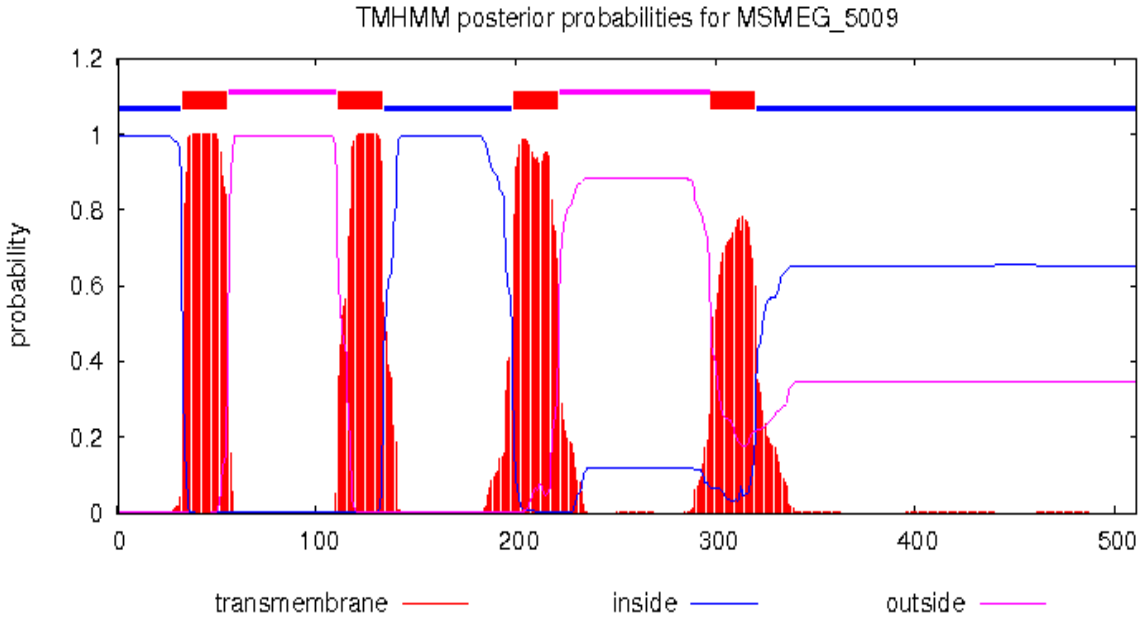

TMPred output for *C. glutamicum* NCgl0925:

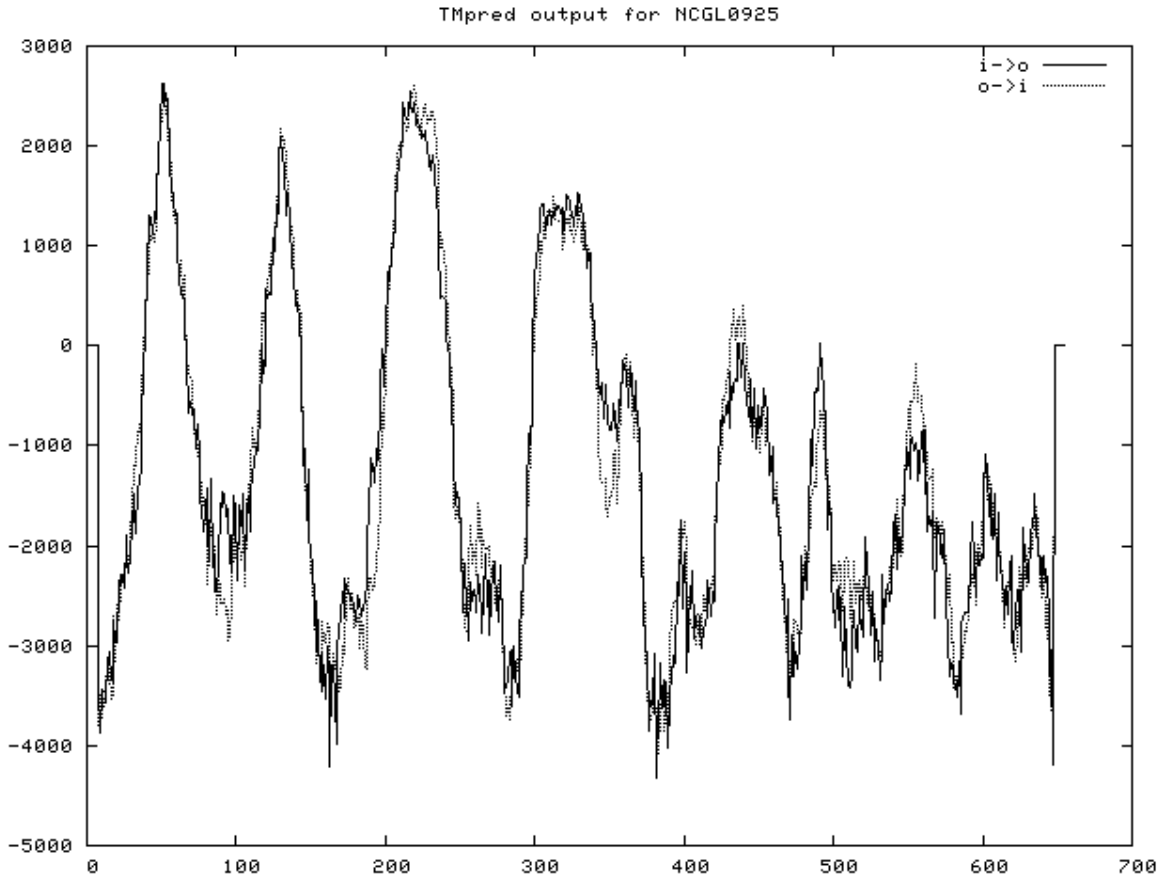

TMHMM output for *C. glutamicum* NCgl0925:

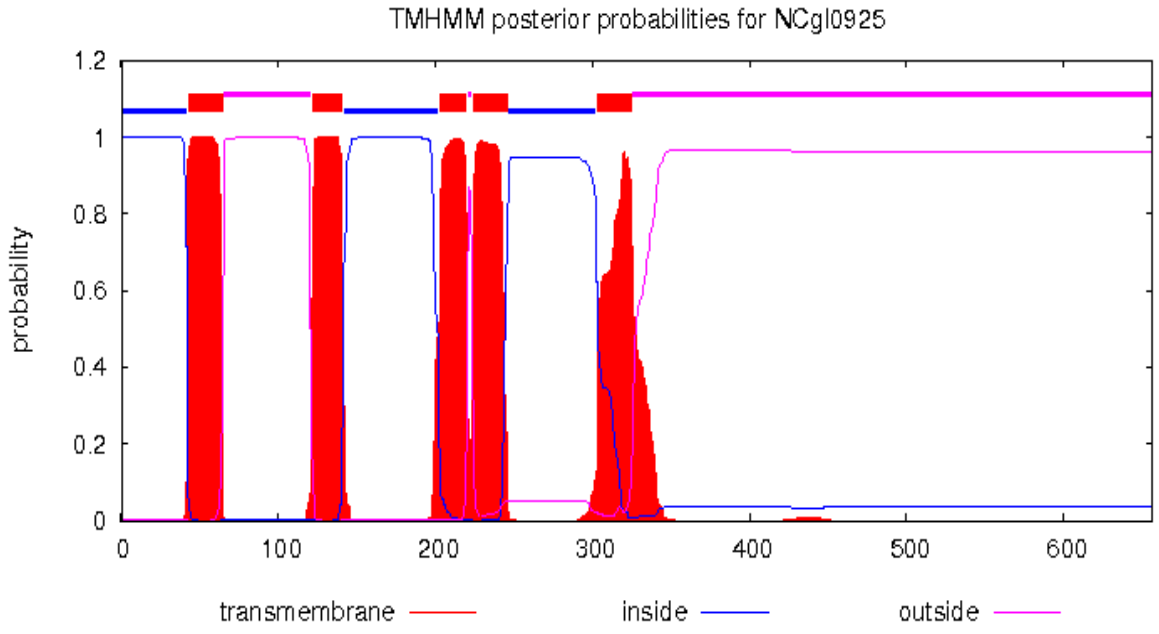

TMPred output from *C. glutamicum* NCgl0926:

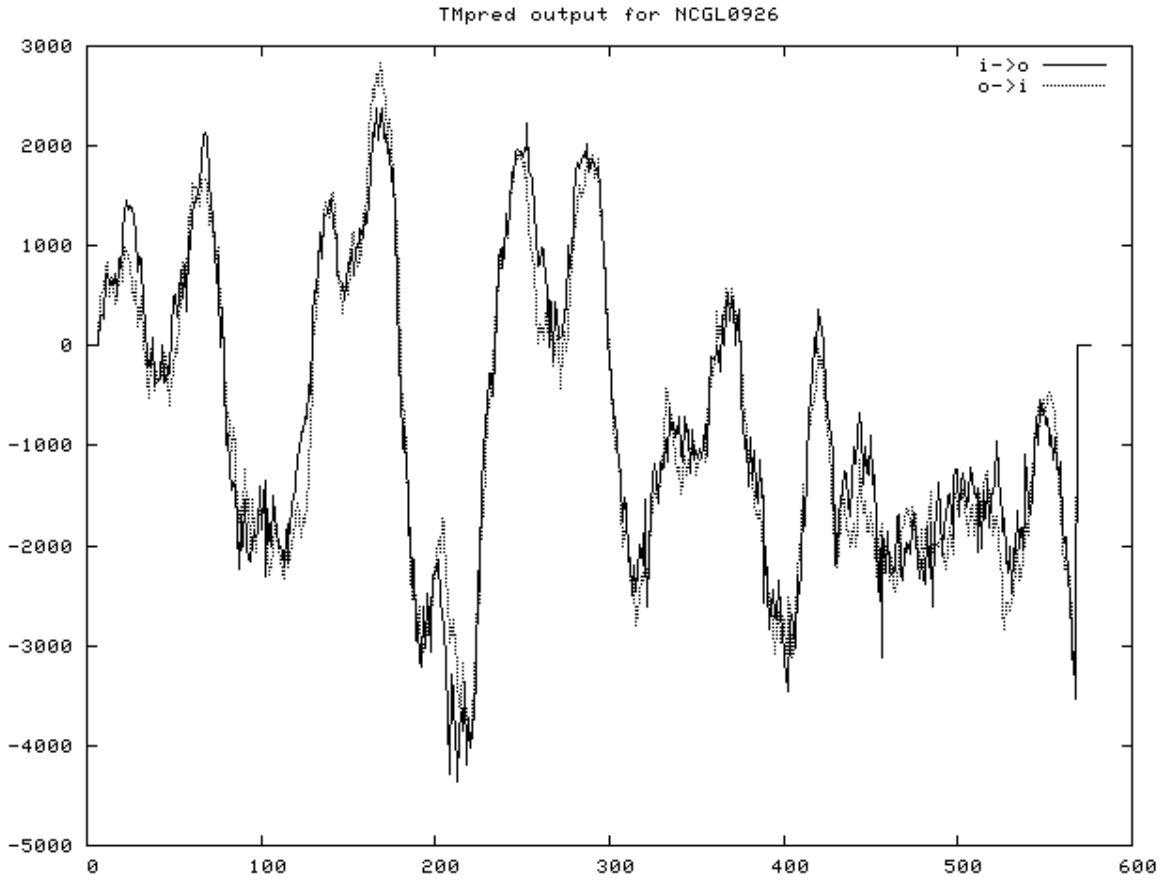

TMHMM output from *C. glutamicum* NCgl0926:

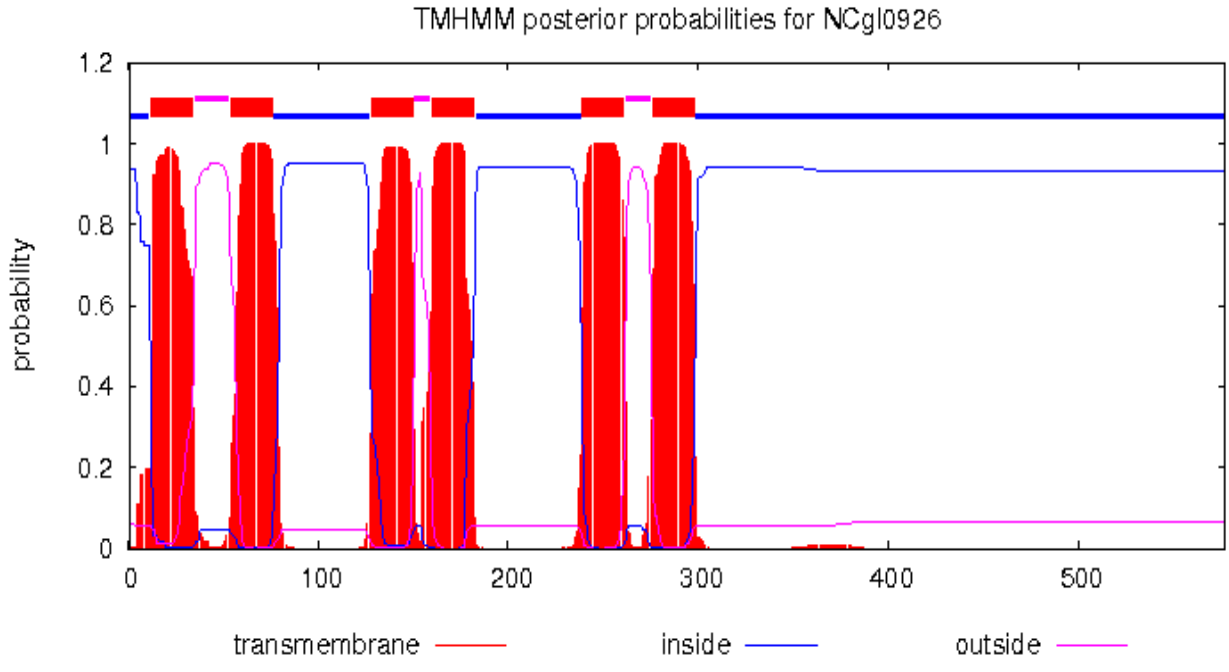

Transmembrane predictions of predicted galactan ABC-transporter proteins.

TMPred output of *M. tuberculosis* Rv3783:

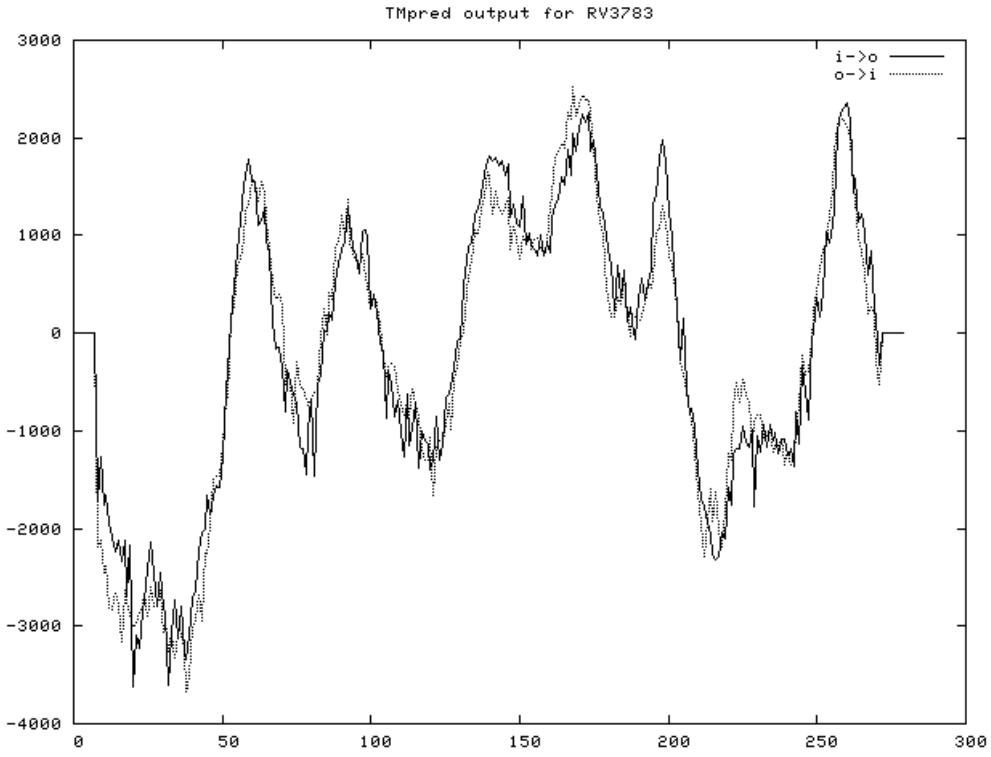

TMHMM output of *M. tuberculosis* Rv3783:

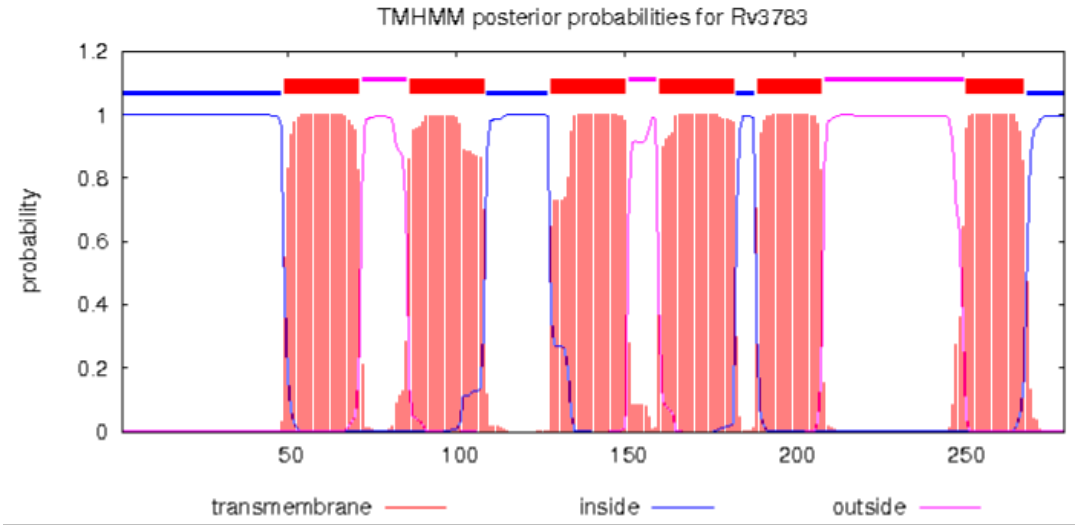

TMPred output of *M. smegmatis* MSMEG_6369:

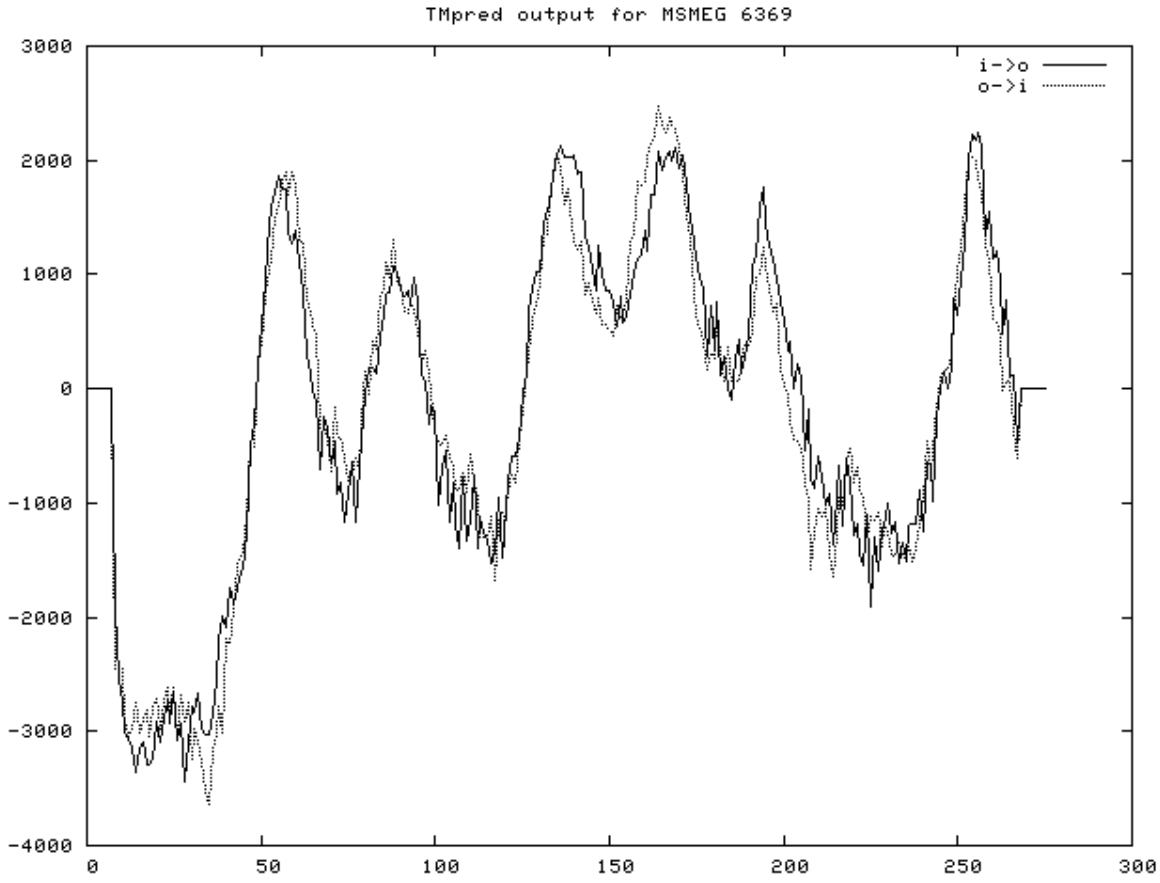

TMHMM output of *M. smegmatis* MSMEG_6369:

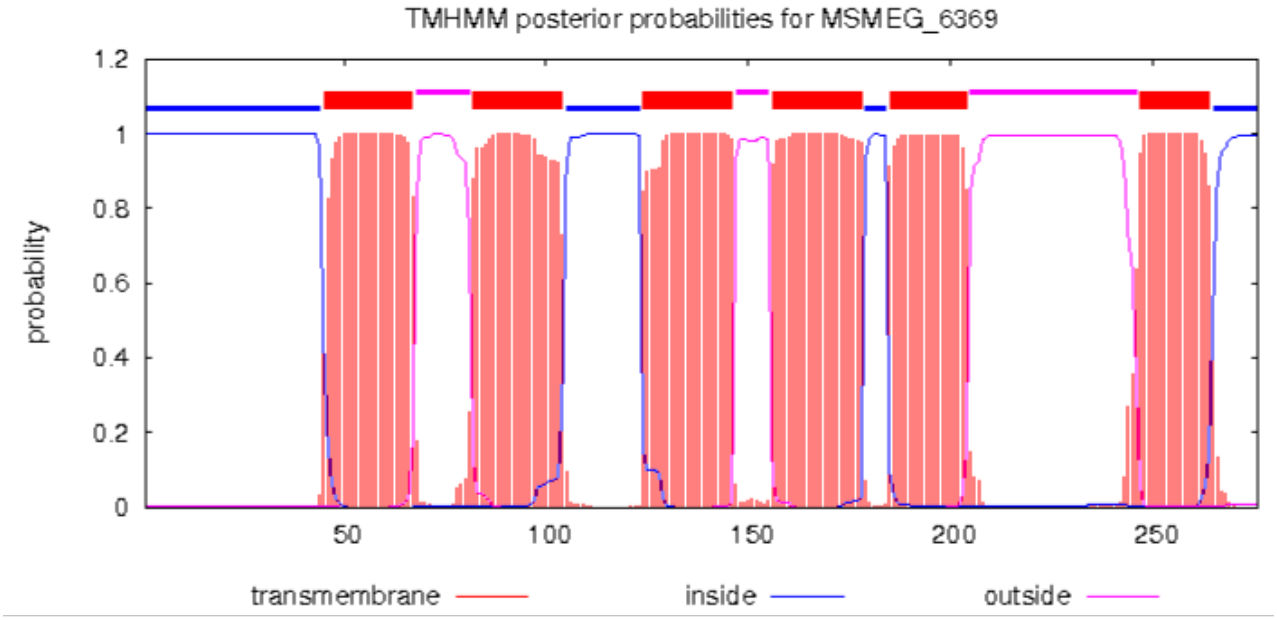

TMPred output of *M. tuberculosis* Rv3781:

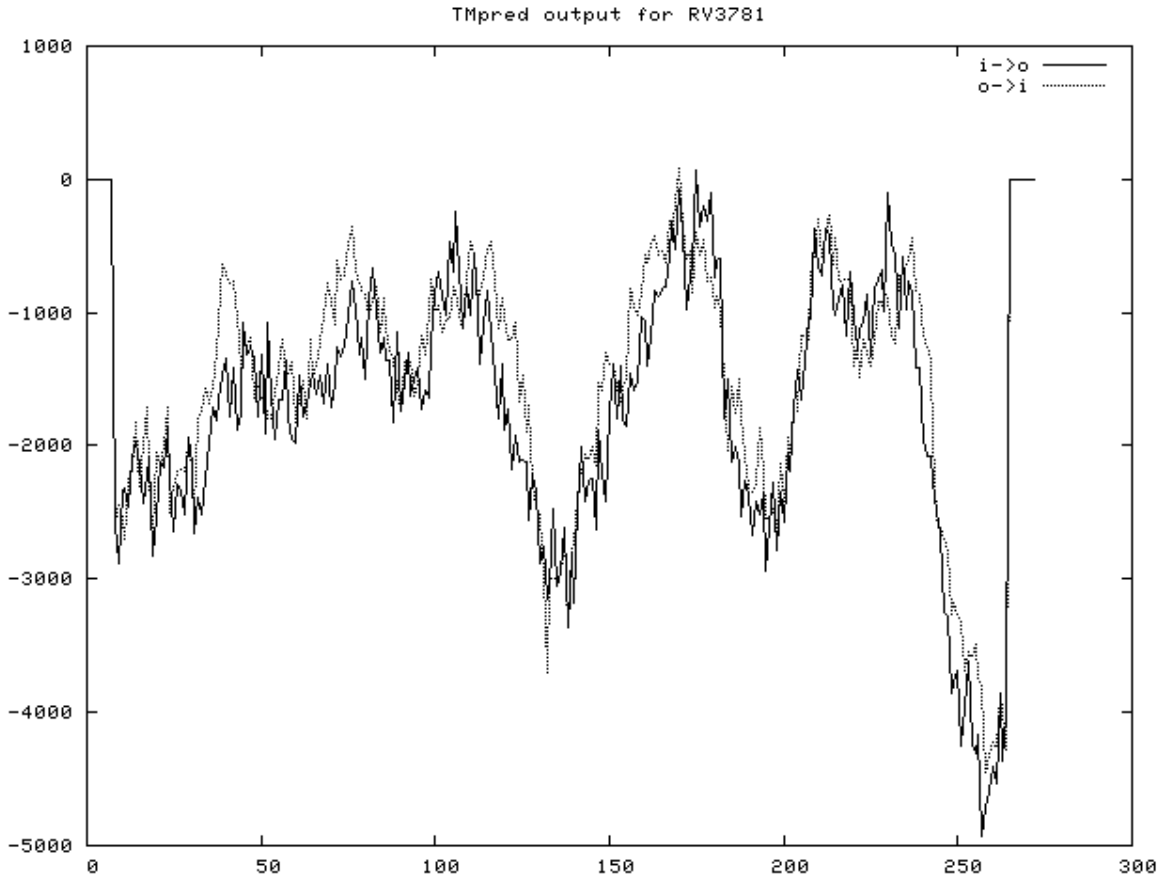

TMHMM output of *M. tuberculosis* Rv3781:

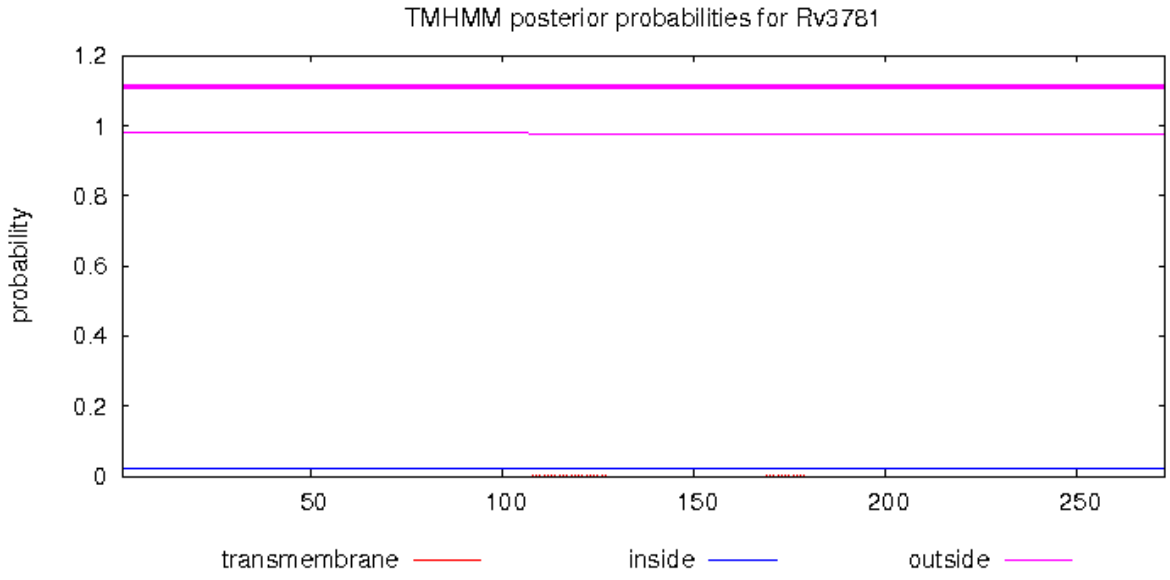

TMPred output of *M. smegmatis* MSMEG_6366:

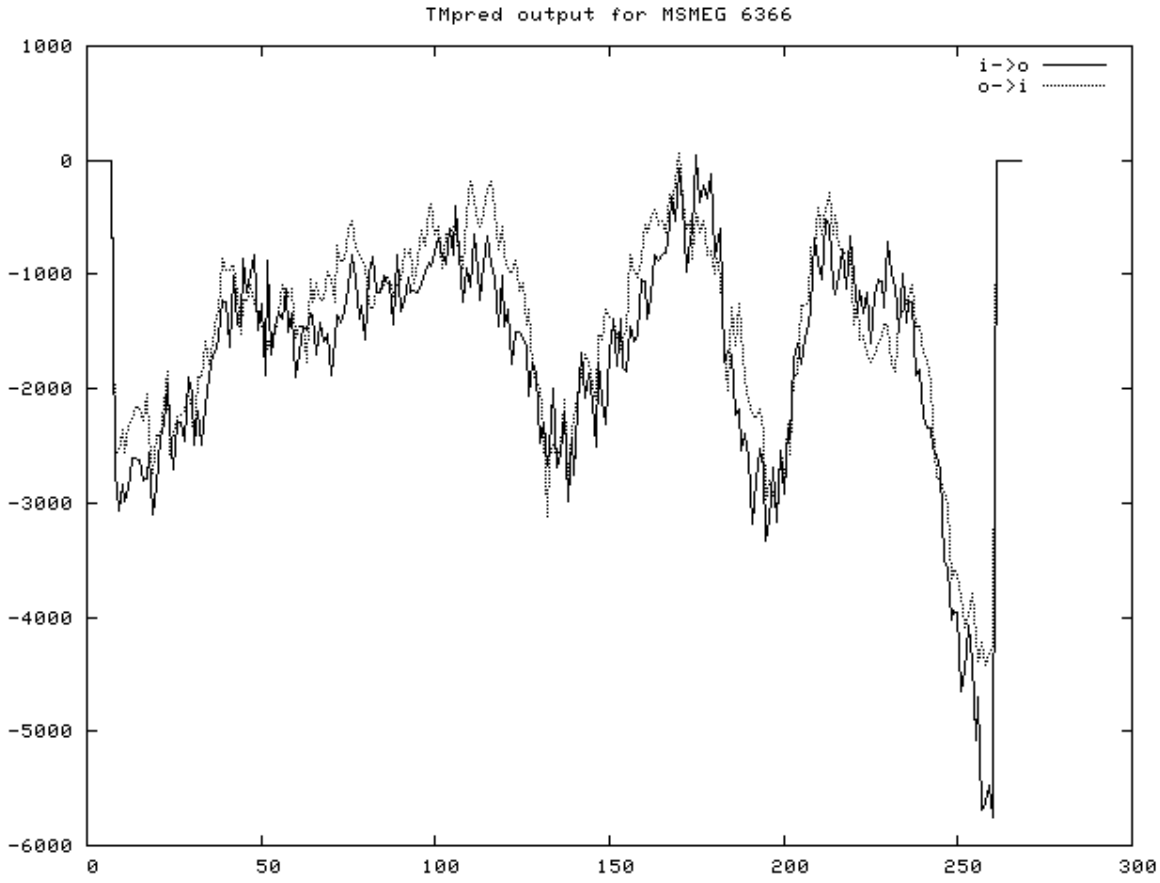

TMHMM output of *M.smegmatis* MSMEG_6366:

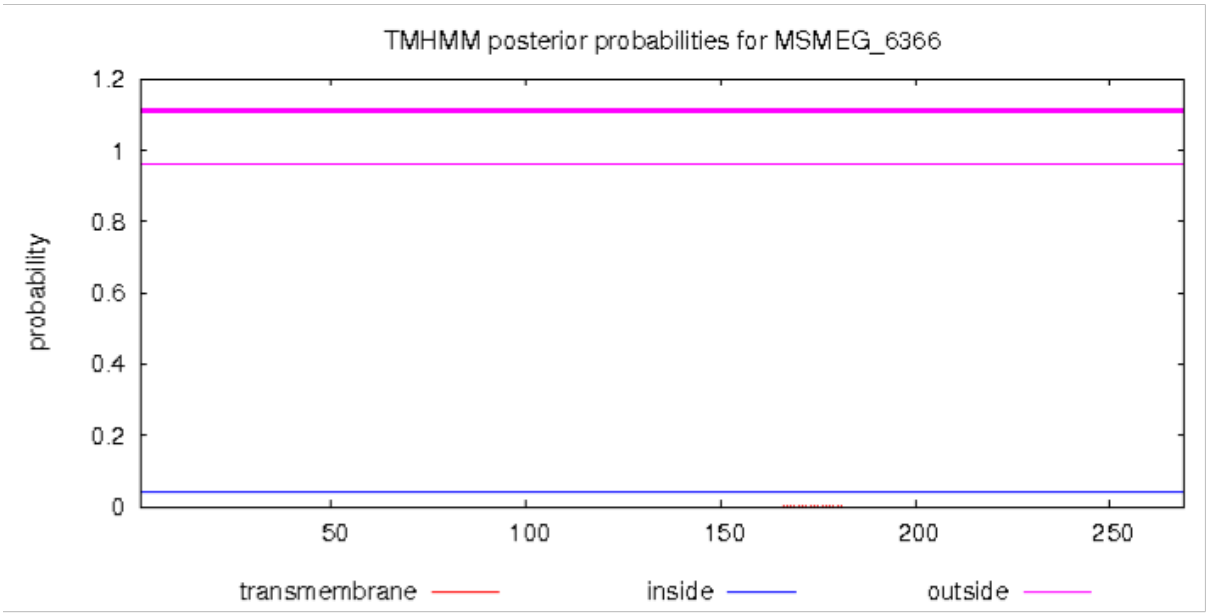

Appendix 2: Antibiotic sensitivity of *C. glutamicum* strains

Results from Chapter 2: Characterization of a PIM transporter system in *C. glutamicum*:

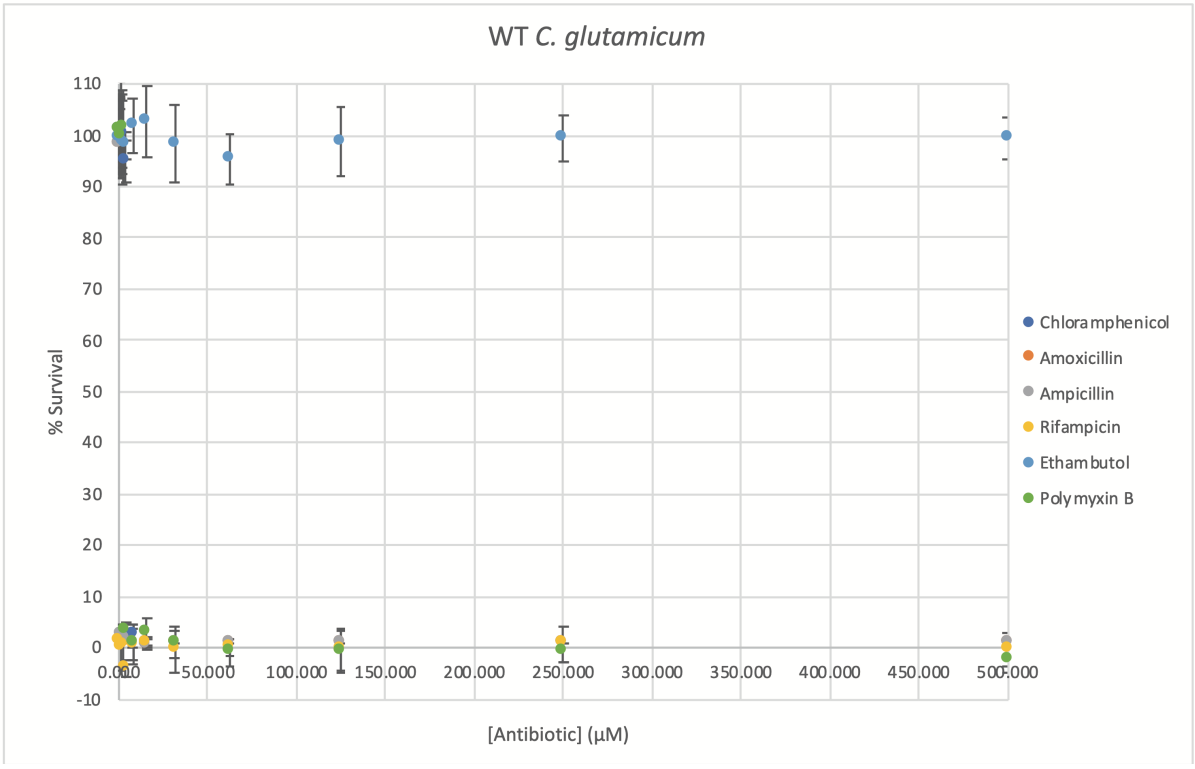

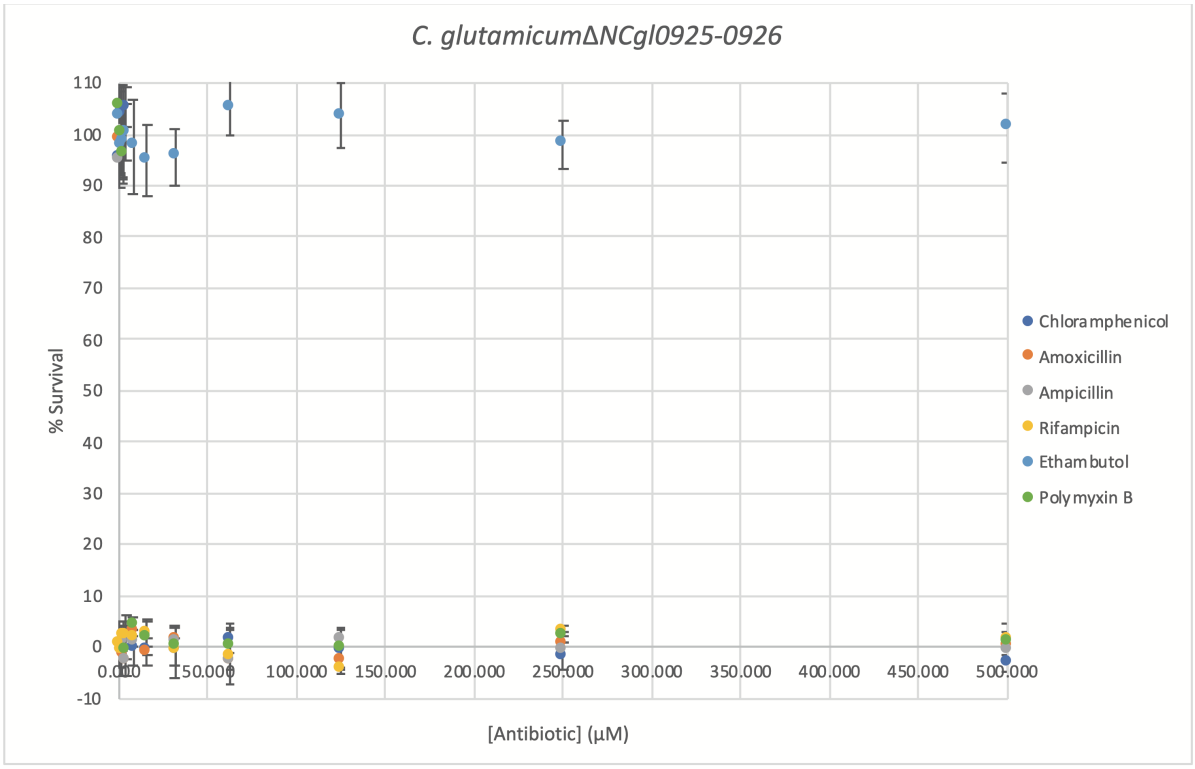

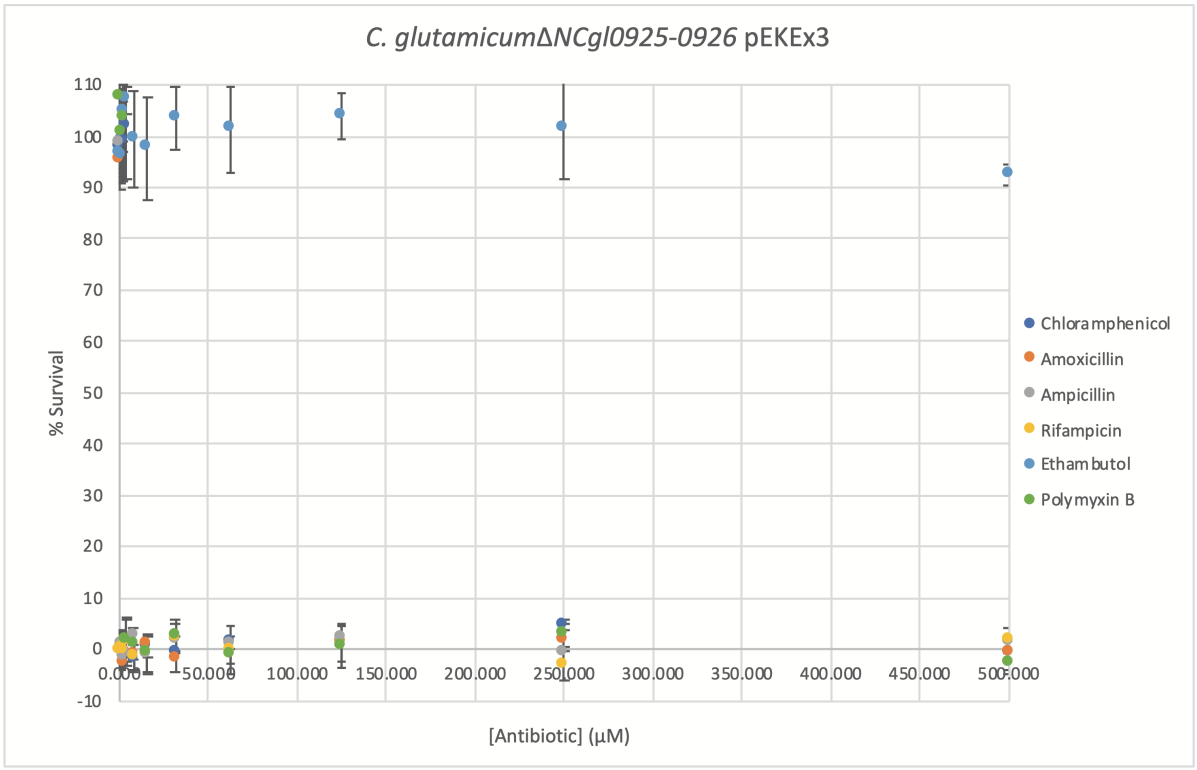
*C. glutamicum*ΔNCgl0925-0926 pEKEx3
% Survival
[Antibiotic] (µM)
Chloramphenicol
Amoxicillin
Ampicillin
Rifampicin
Ethambutol
Polymyxin B

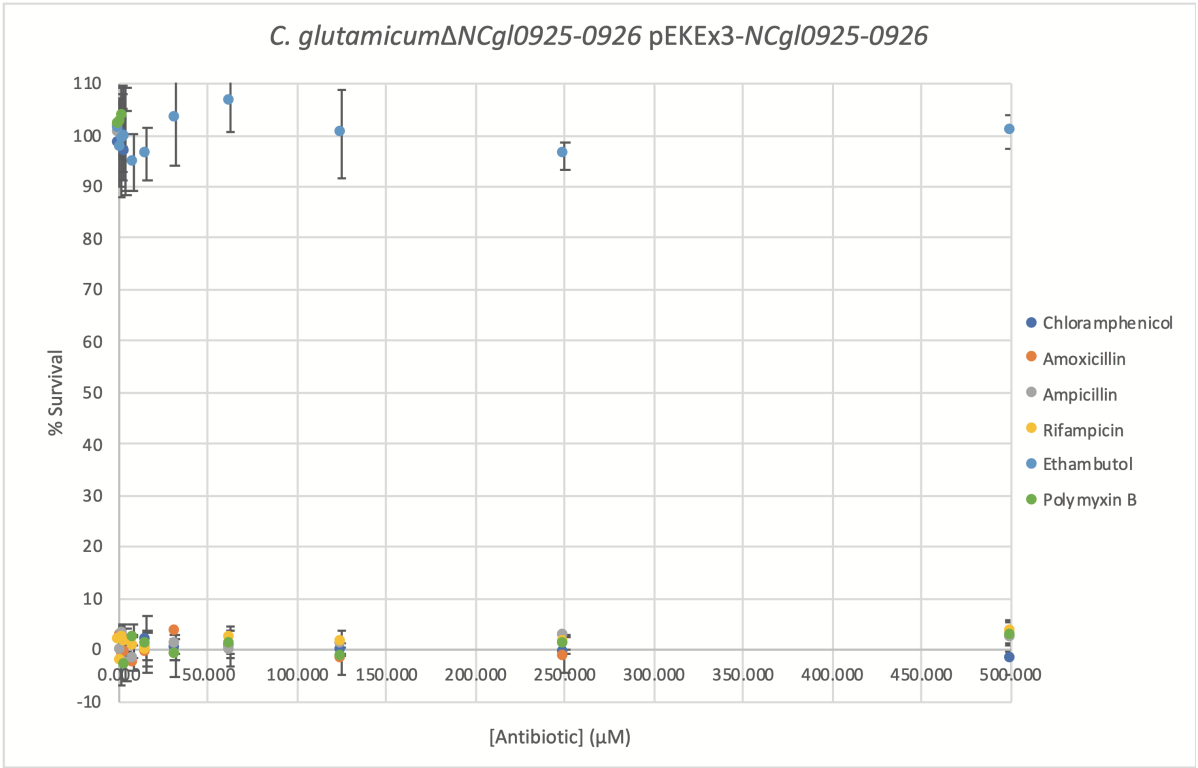
*C. glutamicum*ΔNCgl0925-0926 pEKEx3-NCgl0925-0926
% Survival
[Antibiotic] (µM)
Chloramphenicol
Amoxicillin
Ampicillin
Rifampicin
Ethambutol
Polymyxin B

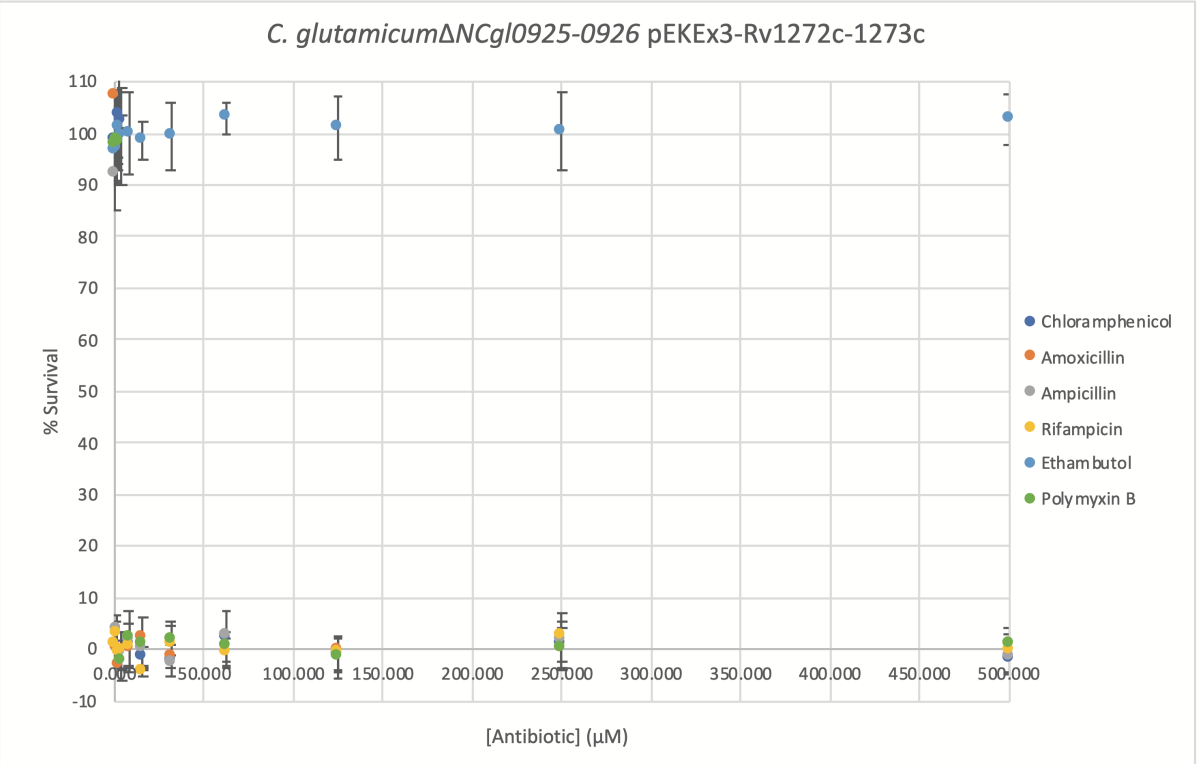
*C. glutamicum*ΔNCgl0925-0926 pEKEx3-Rv1272c-1273c
% Survival
[Antibiotic] (µM)
Chloramphenicol
Amoxicillin
Ampicillin
Rifampicin
Ethambutol
Polymyxin B

Appendix 3: Gas chromatography spectra of derivatized *C. glutamicum* lipoglycan extracts.

Aditol acetate derivatized lipoglycan extract from WT *C. glutamicum*:

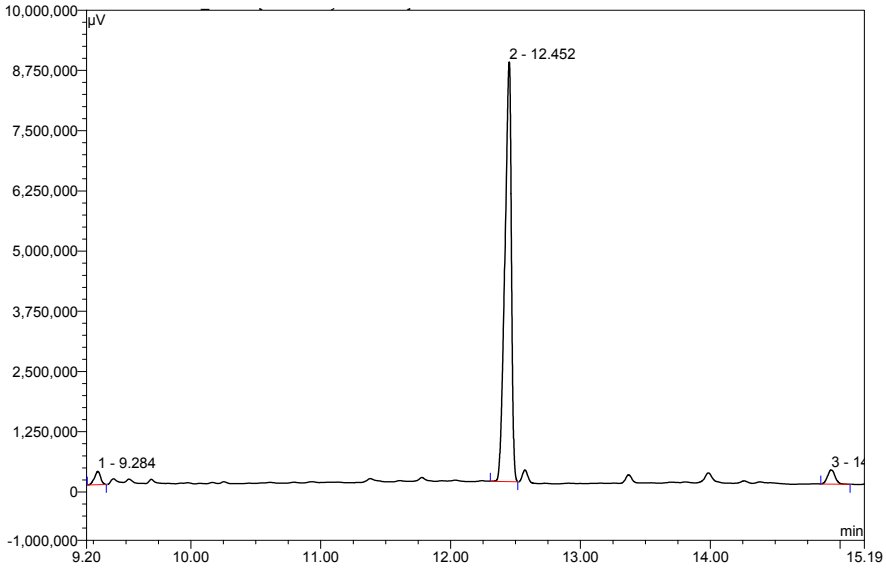

No.	Ret.Time min	Peak Name	Height µV	Area µV*min	Rel.Area %	Amount
1	9.28	n.a.	275857.00	15041.3	2.66	n.a.
2	12.45	n.a.	8709729.00	502606.2	89.03	n.a.
3	14.93	n.a.	293524.00	19818.6	3.51	n.a.

Aditol acetate derivatized lipoglycan extract from *C. glutamicumΔNCgl0925-NCgl0926*:

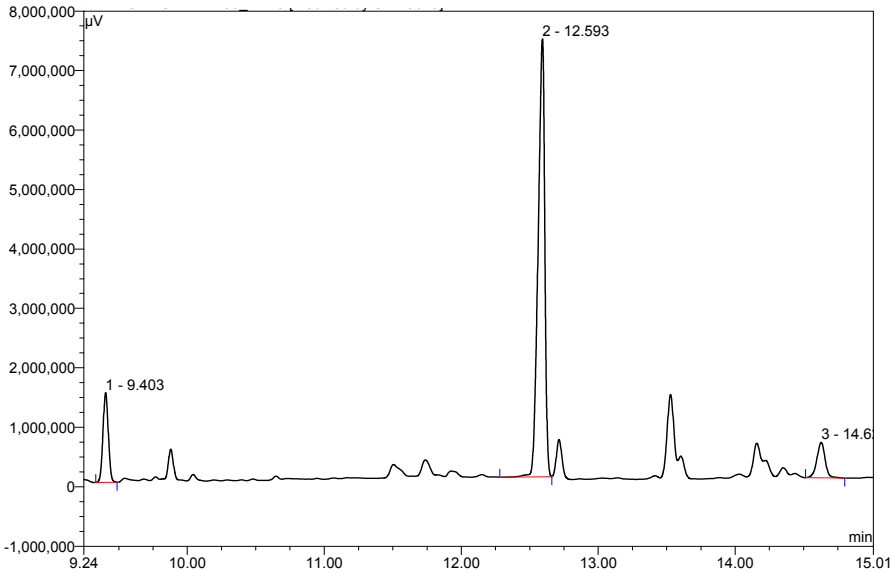

No.	Ret.Time min	Peak Name	Height µV	Area µV*min	Rel.Area %	Amount
1	9.40	n.a.	1507080.00	68623.7	9.31	n.a.
2	12.59	n.a.	7363614.00	415524.3	56.39	n.a.
3	14.63	n.a.	597322.00	41675.8	5.66	n.a.

Aditol acetate derivatized lipoglycan extract from *C. glutamicum ΔNCgl0925-NCgl0926* pEKEx3:

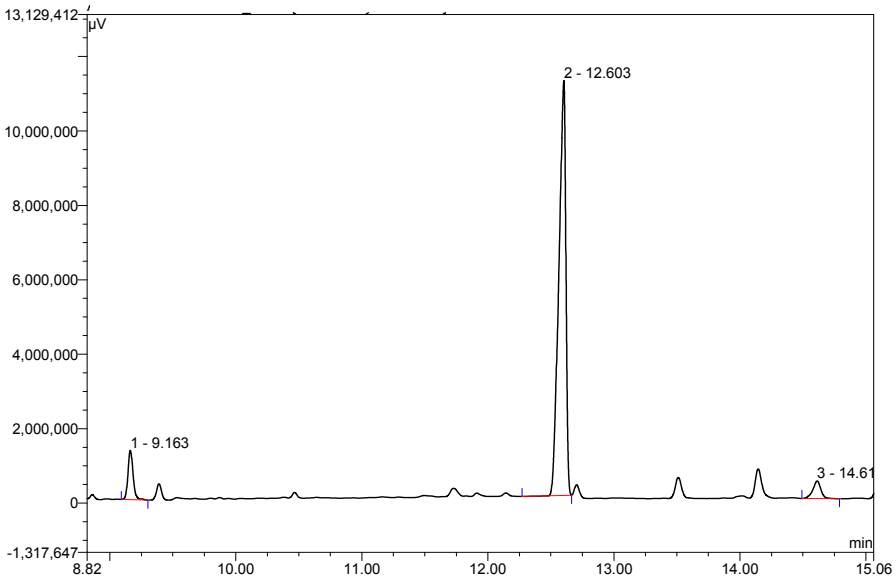

No.	Ret.Time min	Peak Name	Height µV	Area µV*min	Rel.Area %	Amount
1	9.16	n.a.	1322958.00	62789.3	7.68	n.a.
2	12.60	n.a.	11138419.00	719493.5	88.05	n.a.
3	14.61	n.a.	471535.00	34875.3	4.27	n.a.

Aditol acetate derivatized lipoglycan extract from *C. glutamicum ΔNCgl0925-NCgl0926* pEKEx3- *NCgl0925-NCgl0926*:

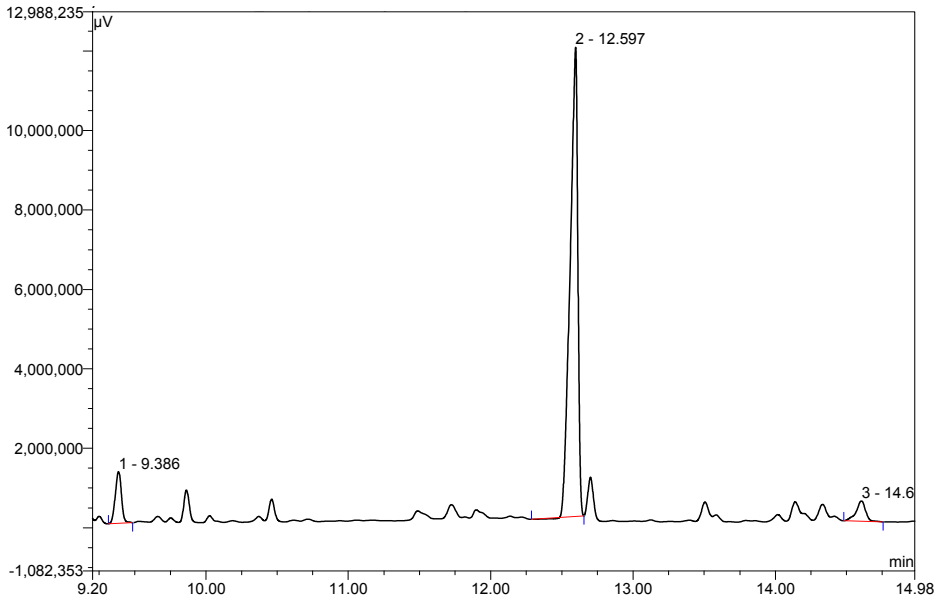

No.	Ret.Time min	Peak Name	Height µV	Area µV*min	Rel.Area %	Amount
1	9.39	n.a.	1302776.00	65615.0	7.76	n.a.
2	12.60	n.a.	11802907.00	739953.2	87.56	n.a.
3	14.61	n.a.	508142.00	39516.7	4.68	n.a.

Aditol acetate derivatized lipoglycan extract from *C. glutamicum ΔNCgl0925-NCgl0926* pEKEx3- *rv1272c-rv1273c*

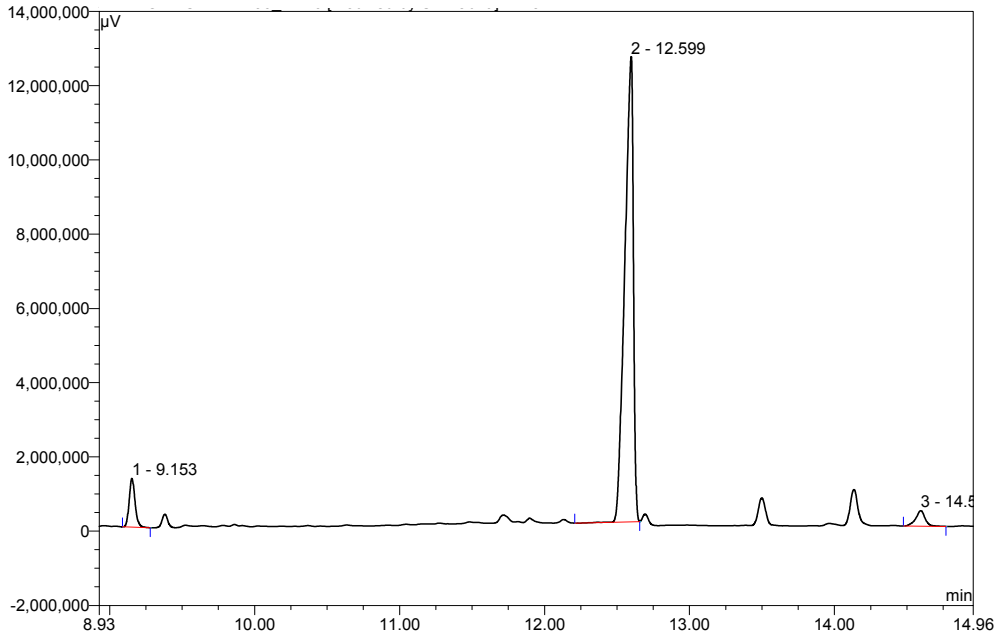

No.	Ret.Time min	Peak Name	Height µV	Area µV*min	Rel.Area %	Amount
1	9.15	n.a.	1310824.00	61915.8	6.13	n.a.
2	12.60	n.a.	12527413.00	859781.8	85.07	n.a.
3	14.60	n.a.	415909.00	31493.0	3.12	n.a.

Aditol acetate derivatized lipoglycan extract from *C. glutamicumΔsteAΔripA*:

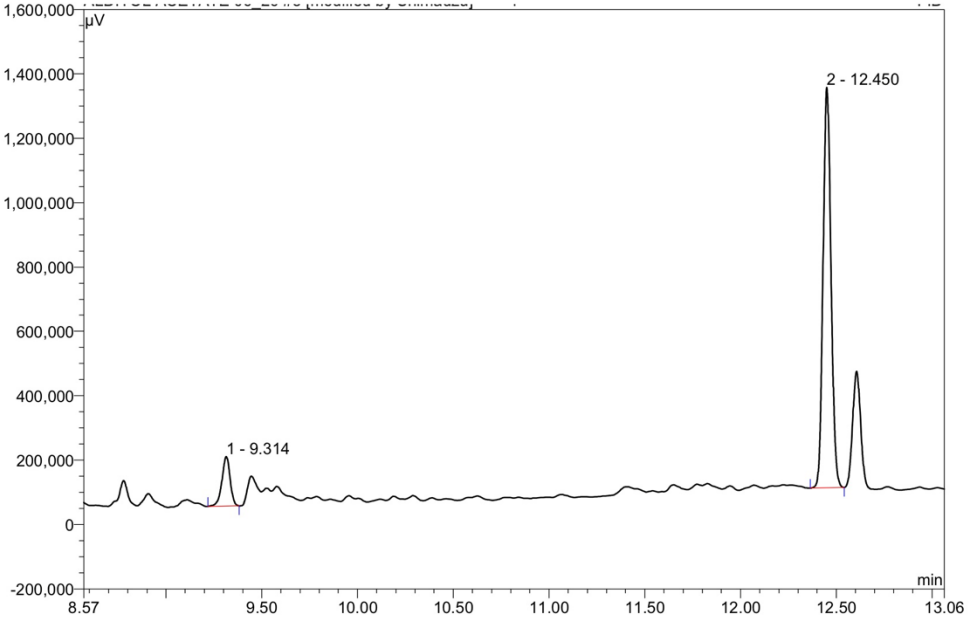

No.	Ret.Time min	Peak Name	Height µV	Area µV*min	Rel.Area %	Amount
1	9.31	n.a.	153230.00	7637.5	6.62	n.a.
2	12.45	n.a.	1243826.00	60022.3	52.05	n.a.

Aditol acetate derivatized lipoglycan extract from *C. glutamicum*Δ*steA*Δ*ripA* Emb^{G411S}:

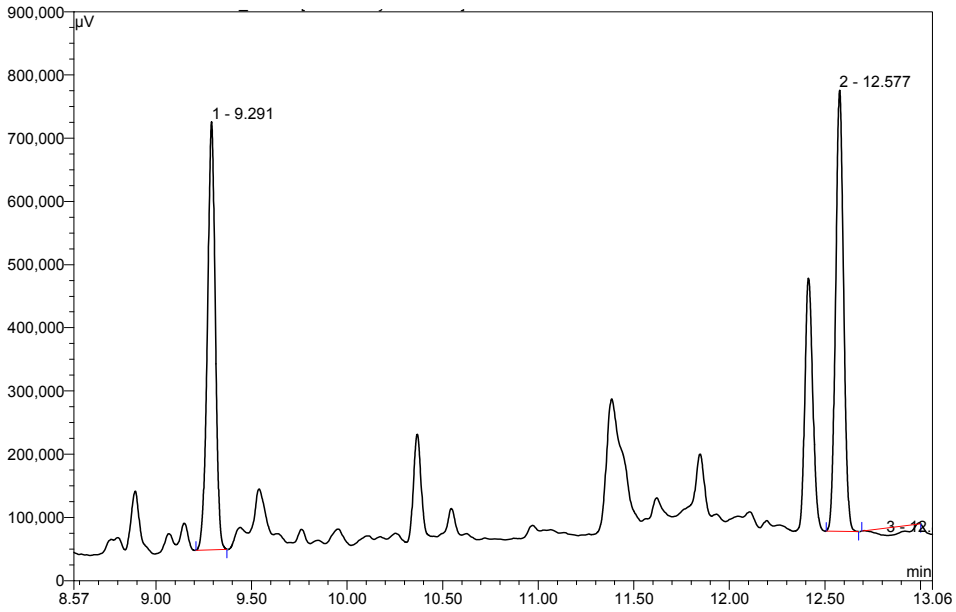

No.	Ret.Time min	Peak Name	Height μV	Area μV*min	Rel.Area %	Amount
1	9.29	n.a.	676948.00	32449.4	20.68	n.a.
2	12.58	n.a.	697604.00	33654.4	21.45	n.a.

Aditol acetate derivatized lipoglycan extract from *C. glutamicum*Δ*steA*Δ*ripA* Emb^{P414T}:

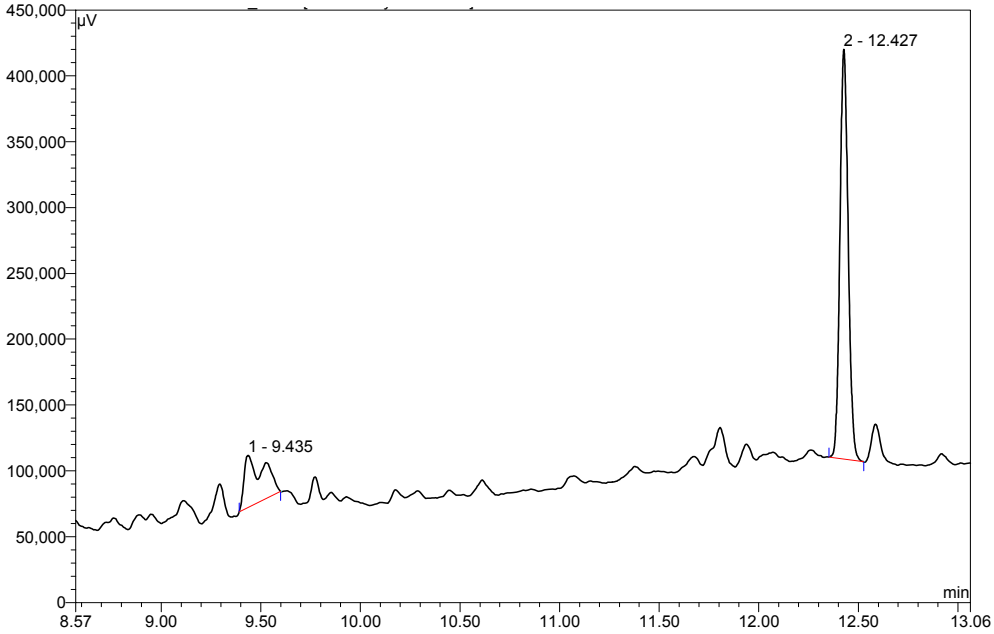

No.	Ret.Time min	Peak Name	Height μV	Area μV*min	Rel.Area %	Amount
1	9.44	n.a.	39586.00	4269.2	11.91	n.a.
2	12.43	n.a.	311231.00	14998.1	41.84	n.a.

Aditol acetate derivatized lipoglycan extract from *C. glutamicum*Δ*steA*Δ*ripA* Emb^{A453V}:

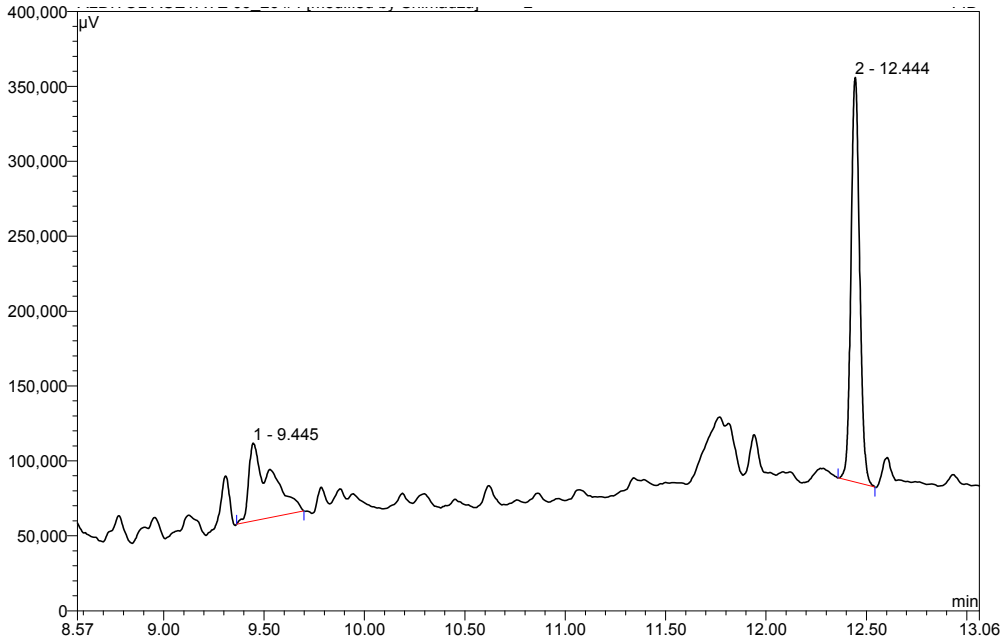

No.	Ret.Time min	Peak Name	Height µV	Area µV*min	Rel.Area %	Amount
1	9.45	n.a.	51867.00	6710.5	16.75	n.a.
2	12.44	n.a.	270032.00	13508.7	33.72	n.a.

Aditol acetate derivatized lipoglycan extract from *C. glutamicum*Δ*steA*Δ*ripA* Emb^{A453E}:

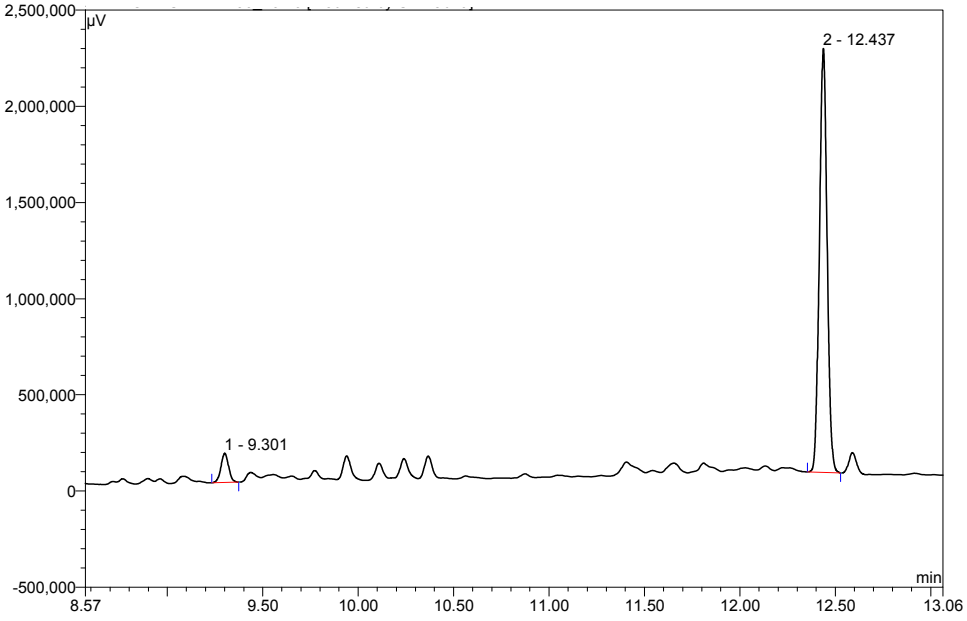

No.	Ret.Time min	Peak Name	Height µV	Area µV*min	Rel.Area %	Amount
1	9.30	n.a.	152044.00	7070.0	3.08	n.a.
2	12.44	n.a.	2204270.00	103448.6	45.08	n.a.

Aditol acetate derivatized lipoglycan extract from *C. glutamicum*Δ*steA*Δ*ripA* Emb^{P505L}:

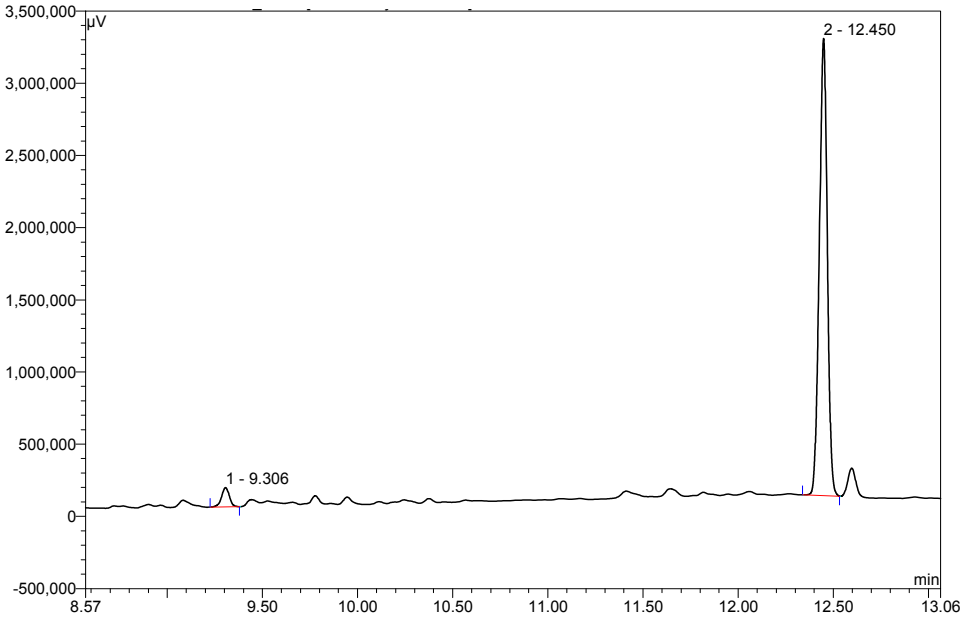

No.	Ret.Time min	Peak Name	Height µV	Area µV*min	Rel.Area %	Amount
1	9.31	n.a.	134110.00	6430.0	2.65	n.a.
2	12.45	n.a.	3165353.00	154533.8	63.63	n.a.

Aditol acetate derivatized lipoglycan extract from *C. glutamicum*Δ*steA*Δ*ripA* Emb^{S528A}:

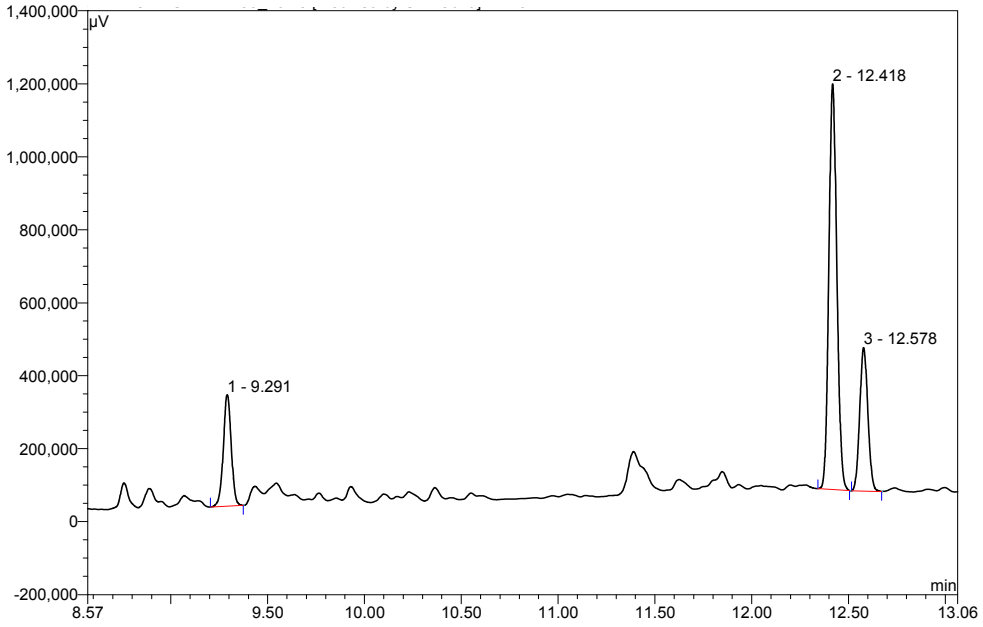

No.	Ret.Time min	Peak Name	Height µV	Area µV*min	Rel.Area %	Amount
1	9.29	n.a.	305067.00	14606.4	9.30	n.a.
2	12.42	n.a.	1111650.00	53371.7	33.98	n.a.